

UNIVERSITY OF TASMANIA

***N*-Heterocyclic Carbene-Based Pd and Ni Complexes and Their Applications to the Activation of Alkyl nitriles**

By

Tanita S. Wierenga, BSc (Hons)

A thesis submitted in partial fulfilment of the requirements for the degree of
Doctor of Philosophy in Chemistry at the University of Tasmania

School of Natural Sciences – Chemistry

University of Tasmania

April 2019

Declaration

To the best of my knowledge, this thesis contains no copy or paraphrase of material previously published or written except where due reference is included in the text.

Tanita S. Wierenga

April 2019

Acknowledgements

Firstly, I would like to thank and dedicate this to my partner James for the support and encouragement I have received throughout this journey.

Secondly, I would like to thank my supervisor Associate Professor Michael Gardiner for his endless ideas, help, support, encouragement and supervision throughout this journey as well as collection of X-ray crystallographic data at the Australian Synchrotron. I would also like to thank my secondary supervisor Dr Alex Bissember for his endless help and support.

Additionally I would like to thank Dr Alireza Ariaferd for the DFT calculations performed that have been presented in this thesis and Dr James Horne for the NMR spectroscopy assistance in particular for the help in relation to VT and 2D NMR spectra which have supported the experimental work performed.

I also wish to extend my gratitude to the support of Dr Curtis Ho for his help, ideas and strength when necessary. Additionally I would like to thank the rest of the Gardiner group and the synthetic super group for their many ideas and support.

Finally I couldn't have done it without the support from my mother, father, sister, family and friends who have helped me get through my PhD.

Abstract

α -Cyanocarbanion complexes are an interesting class of complexes that contain a nitrile ligand featuring a deprotonated α -carbon. Chapter 1 gives an overview of the various synthetic methods, bonding modes and applications that have been established in the literature. Of particular interest is the role these complexes have as intermediates in the formation of various different compounds including the synthetically versatile β -hydroxynitriles.

One example of a catalyst that can be used to synthesise a range of β -hydroxynitriles from the corresponding aldehydes under base free conditions is the POCOP pincer complex $[[2,6-(iPr_2PO)_2C_6H_3]Ni(CH_2CN)]$. DFT calculations outlined in Chapter 2 indicated some of the key features of the complex in relation to its catalytic performance. These were that the $-CH_2CN$ ligand isomerises to yield the active *N*-bound catalyst in solution, the trans donation effect of the phenyl ring lowers the energy of the transition state of the reaction and the rate determining transition state involves a 5 coordinate intermediate and therefore the steric hindrance of the phosphine substituent influences the performance.

Chapter 3 describes a series of bis(NHC) palladium(II) complexes (NHC = *N*-heterocyclic carbene) of the type $[[RIm)_2CH_2]Pd(NCMe)_2][PF_6]_2$ with different *N*-substituents which were reacted with NaOH in CH_3CN . Two different products were formed under similar conditions. $[[RIm)_2CH_2]Pd(CH_2CN)_2]$ was observed for both the $R = Me$ and 2,4,6-trimethylphenyl (Mes) substituent while $[[RIm)_2CH_2]Pd(\mu-CH_2CN)_2][PF_6]_2$ was observed for both the $R = Mes$ and 2,6-diisopropylphenyl substituent. The two initial products that were not formed under these conditions could be synthesised under modified conditions. Complexes of the type $[[MesIm)_2CH_2]Pd(NCR)_2][PF_6]_2$ where $R = CH_2CH_3$ and $CH_2CH_2CH_3$ were also synthesised, however, subsequent conversion to the corresponding $[[RIm)_2CH_2]Pd(CHRCN)_2]$ was not successful.

In Chapter 4 a range of NHC-containing pincer complexes were synthesised due to their close structural similarity to the successful POCOP complex and therefore may result in successful catalytic applications under similar reaction conditions. These complexes contain two NHC ligands bridged by either a pyridine or phenyl ring. $[\text{CNC}^{\text{Pr}}\text{Pd}(\text{CH}_2\text{CN})][\text{SbF}_6]$ was synthesised from the corresponding NCMe complex following the same method used for the bis(NHC) complexes. $[\text{C}^{\wedge}\text{C}^{\wedge}\text{C}^{\text{Me}}\text{Pd}(\text{NCMe})][\text{SbF}_6]$ was prepared from the previously reported Br complex. However attempts to form the corresponding $-\text{CH}_2\text{CN}$ complex were not fruitful.

A number of alternative synthetic approaches were attempted for the desired non methylene linked phenyl based complex using various ligand modifications. Initially reactions were based on the pro-ligands of the type $[1,3-\{(\text{R})\text{ImH}\}_2\text{Ph}]\text{X}_2$ where $\text{R} = \text{CH}_3$ and $\text{X} = \text{I}$ or $\text{R} = n\text{Bu}$ and $\text{X} = \text{Br}$ were reacted in various approaches, however, due to the difficulty of the three C–H metallations an alternative pathway was pursued. This strategy investigated the preparation of a phenyl–OTf based pro-ligand, however, due to difficulties in synthesising the pro-ligand an alternative approach was needed.

A series of pro-ligands of the type $[2,6-(\text{RImH})_2\text{1-BrPh}]\text{X}_2$ where $\text{R} = \text{CH}_3$ and $\text{X} = \text{I}$ or $\text{R} = n\text{Bu}$, Ad and $\text{X} = \text{Br}$ were synthesised from 2-bromo-1,3-difluorobenzene. The desired $[\text{CCC}^{n\text{Bu}}\text{PdBr}]$ was then successfully prepared from the corresponding pro-ligand in good yield. This provided an alternative synthetic pathway to that previously developed for these complexes, although the yield was lower, the lack of a zirconium transfer reagent and the use of air-stable starting materials and higher atom efficiency make this method advantageous to previous literature methods. The catalytically relevant $-\text{NCMe}$ derivative was synthesised, however, the attempted formation of the $-\text{CH}_2\text{CN}$ ligated complex was not successful. $[\text{CCC}^{n\text{Bu}}\text{NiCl}]$ was also synthesised from the corresponding pro-ligand which then was reacted further to form the catalytically relevant NiNCMe complex.

The catalytic studies described in Chapter 5 explored the C–C coupling of benzaldehyde and CH₃CN to yield 3-hydroxy-3-phenylpropionitrile. Various bis(NHC) and NHC containing pincer –CH₂CN complexes were tested, however, no reaction was observed. For the pincer complexes in which the –CH₂CN complex could not be successfully synthesised, the –NCMe complex was used as a pre-catalyst in solution with a catalytic amount of NaOH to prepare the required complex *in situ*. However, the yield of the product was identical to the background reaction performed in the absence of the transition metal catalyst.

Table of Contents

Acknowledgements	i
Abstract	ii
Abbreviations	x
Chapter 1: Introduction	1
1.1 Introduction to α -Cyanocarbanion Complexes:	1
1.2 Synthesis of α -Cyanocarbanion Complexes:	1
1.2.1 Oxidative Addition:	2
1.2.2 Salt Metathesis:	4
1.2.3 Base-assisted Deprotonation of Nitriles:	4
1.3 Bonding of α -Cyanocarbanions:	7
1.3.1 Crystallographic and Spectroscopic Data for Binding Modes I–IV	8
1.3.2 Relationship Between the Binding Modes:	13
1.4 Reactivity of α -Cyanocarbanions:	18
1.4.1 Coupling of Deprotonated Nitrile Ligands:	18
1.4.2 Acrylonitrile Coupling Reactions:	22
1.4.3 C-C Activation of Acetonitrile:	24
1.4.4 Synthesis of Alkyl nitrile Compounds:	25
1.5 Summary and Outlook:	29
1.6 Project Scope:	29
1.7 References:	32
Chapter 2: Ni POCOP complexes	41

2.1 Introduction to POCOP Complexes:	41
2.2.1 DFT Calculations on Guan's Catalysis:	42
2.2.2 Attempted Synthesis of $[\{2,6-(iPr_2PO)_2C_6H_3\}Ni(CH_2CN)]$:	49
2.3 Experimental:	52
2.3.1 General Considerations:	52
2.3.2 Instrumentation:	53
2.3.3 Preparation of $[\{2,6-(iPr_2PO)_2C_6H_3\}Ni(NCMe)][SbF_6]$ (I):	54
2.4 References:	55
Chapter 3: Synthesis of bis(NHC) α-Cyanocarbanion Complexes	57
3.1 Introduction to bis(NHC) α-Cyanocarbanion Complexes:	57
3.2 Results and Discussion:	59
3.2.1 Synthesis of $[\{(MesIm)_2CH_2\}Pd(CH_2CN)_2]$ (IIa) and $[\{([MesIm]_2CH_2)Pd(\mu-CH_2CN)\}_2][PF_6]_2$ (IIIa):	59
3.2.2 Synthesis of $[\{(Melm)_2CH_2\}Pd(CH_2CN)_2]$ (IIb):	73
3.2.3 Synthesis of $[\{([DipIm]_2CH_2)Pd(\mu-CH_2CN)\}_2][PF_6]_2$:	79
3.2.4 Synthesis of $[\{(MesIm)_2CH_2\}Pd(NCR)_2][PF_6]_2$:	86
3.3 Conclusion:	91
3.4 Experimental:	93
3.4.1 General Considerations:	93
3.4.2 Instrumentation:	93
3.4.3 Preparation of $[\{(MesIm)_2CH_2\}Pd(CH_2CN)_2]$ (IIa):	95
3.4.4 Preparation of $[\{([MesIm]_2CH_2)Pd(\mu-CH_2CN)\}_2][PF_6]_2$ (IIIa):	96

3.4.5 Preparation of $\{[(\text{MesIm})_2\text{CH}_2]\text{Pd}(\mu\text{-CH}_2\text{CN})\}_2[\text{BF}_4]_2$:	97
3.4.6 Preparation of 3-Aminocrotononitrile (IV) and 4-Amino-2,6-dimethylpyrimidine (V):	98
3.4.7 Preparation of $\{[(\text{Melm})_2\text{CH}_2]\text{Pd}(\text{CH}_2\text{CN})_2\}$ (IIb):	98
3.4.8 Preparation of $\{[(\text{Melm})_2\text{CH}_2]\text{Pd}(\mu\text{-CH}_2\text{CN})\}_2[\text{BF}_4]_2$ (IIb):	99
3.4.9 Preparation of $\{[(\text{DipIm})_2\text{CH}_2]\text{Pd}(\mu\text{-CH}_2\text{CN})\}_2[\text{PF}_6]_2$ (IIIc):	100
3.4.10 Preparation of $\{[(\text{DipIm})_2\text{CH}_2]\text{Pd}(\text{CH}_2\text{CN})_2\}$ (IIc):	100
3.4.11 Preparation of $\{[(\text{MesIm})_2\text{CH}_2]\text{Pd}(\text{NCCH}_2\text{CH}_3)_2\}[\text{PF}_6]_2$ (VI):	101
3.4.12 Preparation of $\{[(\text{MesIm})_2\text{CH}_2]\text{Pd}(\text{NCCH}_2\text{CH}_2\text{CH}_3)_2\}[\text{PF}_6]_2$ (VII):	102
3.5 References:	103
Chapter 4: Synthesis of NHC Containing Pincer Complexes	105
4.1 Introduction to NHC Containing Pincer Complexes:	105
4.2 Results and Discussion:	108
4.2.1 Synthesis of $[(\text{CNC}^{\text{Pr}})\text{Pd}(\text{CH}_2\text{CN})][\text{SbF}_6]$:	108
4.2.2 Synthesis of $[(\text{C}^{\wedge}\text{C}^{\wedge}\text{C}^{\text{Me}})\text{Pd}(\text{NCMe})][\text{SbF}_6]$:	113
4.2.3 Synthesis Attempt for CCC Complex Using Unsubstituted Ligand: ...	118
4.2.4 Attempted Synthesis of CCC Complex using Triflate Functionality on Central Carbon:	122
4.2.5 Synthesis of $[2,6\text{-}(\text{ImHR})_2\text{1-BrPh}]\text{X}_2$:	125
4.2.6 Synthesis of $[(\text{CCC}^{\text{R}})\text{Pd}(\text{NCMe})][\text{SbF}_6]$:	130
4.2.7 Synthesis of $[(\text{CCC}^{\text{nBu}})\text{PdL}]$ Complexes:	143
4.2.8 Synthesis of Other $[(\text{CCC}^{\text{nBu}})\text{M}(\text{NCMe})][\text{SbF}_6]$ Group 10 Metal Complexes:	147

4.3 Conclusion:	152
4.4 Experimental:	154
4.4.1 General Considerations:	154
4.4.2 Instrumentation:	155
4.4.3: Preparation of [(CNC^{iPr})PdBr]Br (VIII):	156
4.4.4 Preparation of [(CNC^{iPr})Pd(NCMe)][SbF₆]₂ (IX):	157
4.4.5 Preparation of [(CNC^{iPr})Pd(CH₂CN)][SbF₆] (X):	157
4.4.6 Preparation of 2,6-(CH₂Br)₂-1-BrPh (XI):	158
4.4.7 Preparation of [2,6-(MelmHCH₂)₂-1-BrPh]Br₂ (XII):	158
4.4.8 Preparation of [(C[^]C[^]C^{Me})PdBr] (XIII):	159
4.4.9 Preparation of [(C[^]C[^]C^{Me})Pd(NCMe)][SbF₆] (XIV):	159
4.4.10 Preparation of 1,3-Im₂Ph (XV):	160
4.4.11 Preparation of [1,3-(MelmH)₂Ph]I₂ (XVIa):	161
4.4.12 Preparation of [1,3-(<i>n</i>BulmH)₂Ph]Br₂ (XVIb):	161
4.4.13 Preparation of 2,6-Br₂1-OHPh (XVII):	161
4.4.14 Preparation of 2,6-Br₂1-OBnPh (XVIII):	162
4.4.15 Preparation of 2,6-Im₂1-OBnPh (XIXa) and 2,6-Im₂1-OHPh (XIXb):	163
4.4.16 Preparation of 2,6-Im₂1-OHPh (XIXb):	164
4.4.17 Preparation of 2,6-Im₂1-BrPh (XX):	164
4.4.18 Preparation of [2,6-(MelmH)₂1-BrPh]I₂ (XXIa):	165
4.4.19 Preparation of [2,6-(<i>n</i>BulmH)₂1-BrPh]Br₂ (XXIb):	165
4.4.20 Preparation of [2,6-(AdlmH)₂1-BrPh]Br₂ (XXIc):	166

4.4.21 Preparation of [(CCC ^{nBu})PdBr] (XXIIa):	167
4.4.22 Preparation of [(3-(<i>n</i> Bulm _a H),1-(<i>n</i> Bulm _b PdBr ₃)Ph)] (XXIII):	168
4.4.23 Preparation of [(2,6-(<i>n</i> BulmH) ₂ Ph)PdBr ₃] (XXIV):	169
4.4.24 Preparation of [(CCC ^{nBu})Pd(NCMe)][SbF ₆] (XXVa):	169
4.4.25 Preparation of [(CCC ^{nBu})Pd(ONO ₂)] (XXVI):	170
4.4.26 Preparation of [(CCC ^{nBu})PdCl] (XXIIb):	171
4.4.27 Preparation of [NaO ₂ CCH ₂ CN] (XXVII):	171
4.4.28 Preparation of [AgO ₂ CCH ₂ CN] (XXVIII):	172
4.4.29 Preparation of [(CCC ^{nBu})NiCl] (XXIIc):	172
4.4.30 Preparation of [(CCC ^{nBu})Ni(NCMe)][SbF ₆] (XXVb):	173
4.5 References:	174
Chapter 5: Catalytic Synthesis of β-Hydroxynitriles	179
5.1 Introduction:	179
5.2 Results and Discussion:	180
5.3 Conclusion:	186
5.4 Experimental:	187
5.4.1 General Considerations:	187
5.4.2 Instrumentation:	187
5.4.3 Synthesis of β-hydroxynitriles and other by-products:	187
5.5 References	189

Abbreviations

Å	Ångström, 10^{-10} m
acac	acetylacetonate
acetone- d_6	deuterated acetone
Ar	aryl
Ad	adamantyl
BINAP	2,2'-bis(diphenylphosphino)-1,1'-binaphthalene
bs	broad singlet (NMR)
Bn	benzyl
cat.	catalyst
C_6D_6	deuterated benzene
CCC	RImPhImR ligand
CCC _a	normal-abnormal RImPhImR ligand
C [^] C [^] C	RImCH ₂ PhCH ₂ ImR Ligand
CCDC	the Cambridge Crystallographic Data Centre
CDCl ₃	deuterated chloroform
CD ₃ CN	deuterated acetonitrile
CEC	RImArImR ligand
C [^] E [^] C	RImCH ₂ ArCH ₂ ImR ligand

CF	compact fluorescent
CNC	RImPyImR ligand
C [^] N [^] C	RImCH ₂ PyCH ₂ ImR ligand
COD	1,4-cyclooctadiene
Cp	cyclopentadienyl
Cp*	1,2,3,4,5-pentamethylcyclopentadienyl
cyanoNacNac	α-cyano-β-diketiminate
d	doublet (NMR)
dba	dibenzylideneacetone
DBU	1,8-diazabicyclo(5.4.0)undec-7-ene
dd	doublet of doublets (NMR)
DFT	density functional theory
Dipp	2,6-diisopropylphenyl
DiPrPF	1,1'-bis(di-isopropylphosphino)ferrocene
DMAc	dimethylacetamide
DMAP	4-dimethylaminopyridine
DMF	dimethylformamide
DMSO	dimethyl sulfoxide
DMSO-d ₆	deuterated dimethyl sulfoxide

DOSY	Diffusion Ordered Spectroscopy
DPPBz	1,2-bis(diphenylphosphino)benzene
E	electron donating substituent
ee	enantiomeric excess
EI-MS	electron ionisation-mass spectrometry
ESI-MS	electrospray ionisation-mass spectrometry
GC	gas chromatography
GC-MS	gas chromatography-mass spectrometry
Im	imidazole
IMes	1,3-dimesitylimidazol-2-ylidene
ImH	imidazolium
<i>i</i> Pr	isopropyl
IR	infrared
L	ligand
LDA	lithium diisopropylamide
M	metal
m	multiplet (NMR)
<i>m</i> -	<i>meta</i>
Me	methyl

Mes	mesityl; 2,4,6-trimethylphenyl
MW	microwave
NaHMDS	sodium hexamethyldisilazide
<i>n</i> Bu	<i>n</i> -butyl
NHC	<i>N</i> -heterocyclic carbene
NMR	nuclear magnetic resonance
NOESY	Nuclear Overhauser Effect Spectroscopy
<i>n</i> Oe	nuclear Overhauser effect
<i>o</i> -	<i>ortho</i>
OTf	trifluoromethanesulfonate
<i>p</i>	pentet (NMR)
<i>p</i> -	<i>para</i>
PCP	2,6-(R ₂ PCH ₂) ₂ C ₆ H ₃
Ph	phenyl
PNP	(<i>i</i> Pr ₂ P){MePh} ₂ N
POCOP	2,6-(R ₂ PO) ₂ C ₆ H ₃
ppm	parts per million
psi	pounds per square inch
Py	pyridine

R	alkyl substituent
(R) DTBM-SEGPHOS	(<i>R</i>)-(-)-5,5'-bis[di(3,5-di- <i>t</i> -butyl-4-methoxyphenyl)phosphino]-4,4'-bi-1,3-benzodioxole
rpm	revolutions per minute
rt	room temperature
s	singlet (NMR)
sep	septet (NMR)
sex	sextet (NMR)
t	triplet (NMR)
<i>t</i> Bu	<i>t</i> -butyl
THF	tetrahydrofuran
THF- <i>d</i> ₈	deuterated tetrahydrofuran
TLC	thin layer chromatography
TMEDA	tetramethylethylenediamine
TMS	trimethylsilyl
Tp	hydrotris(pyrazolyl)borate
Tp ^{Me}	tris(3,5-dimethylpyrazolyl)borate
TS	transition state

X	halide, Br/I
Xantphos	4,5-bis(diphenylphosphino)-9,9-dimethylxanthene

Chapter 1: Introduction

1.1 Introduction to α -Cyanocarbanion Complexes:

α -Cyanocarbanion complexes represent an interesting class of complexes that contain a nitrile ligand featuring a deprotonated α -carbon. The interest is due to the various synthetic methods, bonding modes and applications that have been established in the literature. Since the first crystal structure of an α -cyanocarbanion complex was reported in 1970^[1] applications for these complexes have mostly surrounded the development of catalysts for the synthesis of nitrile-based small molecules.^[2] These complexes have also been observed as key intermediates in the reaction of acrylonitrile with various substrates in phosphination, amination and copolymerisation processes amongst others.^[3] Due to the often distinct synthetic approaches and applications of cyanoanions where a negative charge on the α -carbon is stabilised by further conjugation, such complexes will not be discussed in the introduction.^[4]

1.2 Synthesis of α -Cyanocarbanion Complexes:

A wide variety of methods for the synthesis of α -cyanocarbanion complexes have been developed. However, the most common strategies employed are: (i) the oxidative addition of an α -halogenated nitrile to a metal complex; (ii) the salt metathesis of a preformed α -cyanocarbanion metal complex onto the corresponding desired metal halide complex and (iii) the reaction of a transition metal complex,

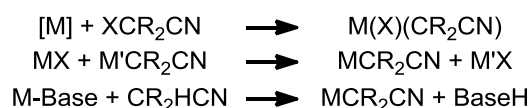


Figure 1.1: Three of the most common methods for the synthesis of α -cyanocarbanions.

base and alkyl nitrile (Figure 1.1). Synthesis *via* decarboxylation will also be discussed.

A number of less common synthetic approaches that will not be specifically discussed^[5] include electrochemical generation of the desired ligand from BrCH_2CN ,^[6] the use of O_2 as a C-H bond cleavage mediator,^[7] acrylonitrile insertion into a metal–ligand bond^[3d, 8] and crystal isomerisation *via* heat or light with the alkyl ligand isomerising between different carbons on the alkyl chain to form the α -cyanocarbanion.^[9]

1.2.1 Oxidative Addition:

Oxidative addition was the first method developed for the synthesis of α -cyanocarbanions with the addition of ICH_2CN to $\text{Pd}(\text{PPh}_3)_4$.^[10] This oxidative addition can proceed from XCH_2CN where X is a halide^[10, 11] or hydrogen.^[12] A 4-coordinate rhodium(I) complex was used to synthesise the desired 6-coordinate rhodium(III) complex by oxidative addition of ICH_2CN in CH_2Cl_2 (Figure 1.2).^[11a]

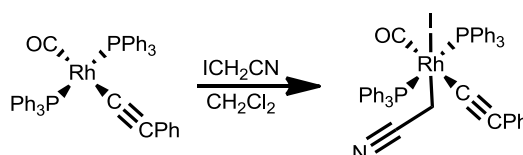


Figure 1.2: Oxidative addition of ICH_2CN .

A rhodium(III) complex that readily undergoes reductive elimination was used as a starting material to form the desired rhodium(III) α -cyanocarbanion.^[13] These rhodium starting material complexes (**1** & **2**) have been shown to readily reductively eliminate to form the corresponding unsaturated rhodium(I) fragment $[\text{Tp}^{\text{Me}}\text{Rh}(\text{PR}_3)]$ (**3**). Thus, **1** & **2** were reacted with acetonitrile allowing C–H activation to form the desired rhodium(III) complex (Figure 1.3).^[13a]

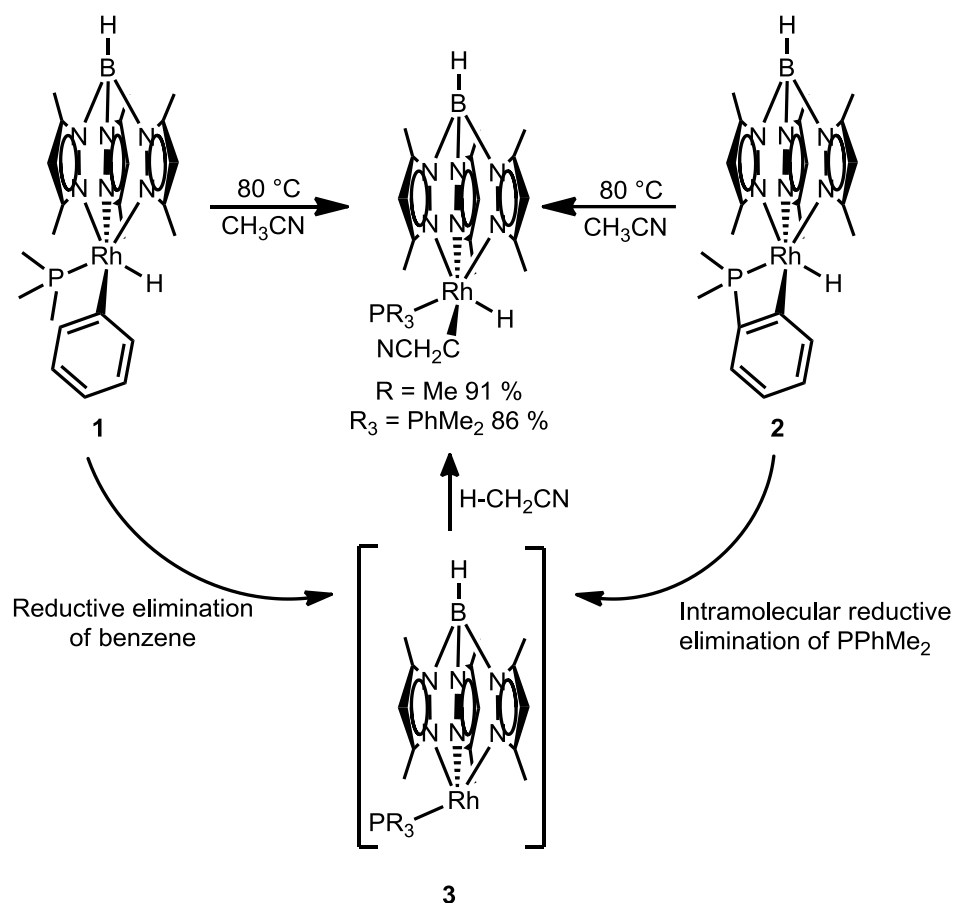


Figure 1.3: Synthesis of Rh complexes *via* oxidative addition from a complex that readily undergoes reductive elimination.

Oxidative addition has been shown to have applications with metal clusters.^[11b, 11c, 11e] Typically, in these reactions the halide and CR₂CN segments ultimately bind to different metals in the cluster increasing their oxidation state by one. An example is using Br-CH₂CN to oxidatively add to a digold(I) ylide to form the corresponding gold(II) ylide (Figure 1.4).^[11e]

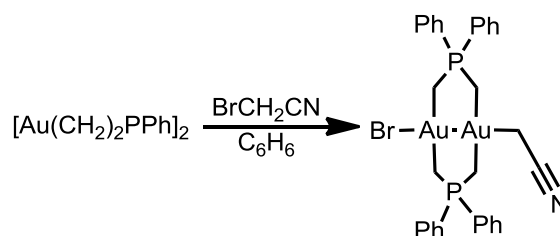


Figure 1.4: Synthesis of a gold(II) ylide *via* oxidative addition of bromoacetonitrile in benzene.

1.2.2 Salt Metathesis:

The second fundamental synthesis strategy^[14] is salt metathesis, which involves the reaction of a preformed alkali metal salt with the corresponding metal halide to form the desired α -cyanocarbanion complex. Typically the alkali metal salt are not characterised,^[14, 15] however, lithium ketenimine salts were characterised (a structural isomer of the CH_2CN ligands presented in Section 1.2.1, the binding modes of these complexes will subsequently be discussed, *vide infra*) from the reaction of diphenyl acetonitrile with $n\text{BuLi}$. Salt metathesis was then performed with the corresponding indium(III) and gallium(III) halide complexes (Figure 1.5).^[16]

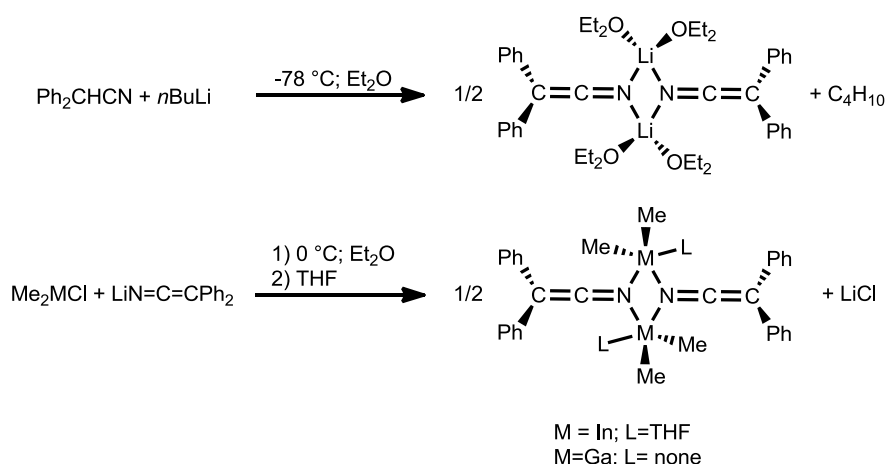


Figure 1.5: Transmetalation of ketenimine salt from the corresponding lithium salt.

1.2.3 Base-assisted Deprotonation of Nitriles:

The most common of these approaches feature the reaction of a metal complex with a base and a nitrile. Variants of the metal precursor complex have been used with the base,^[17] parent nitrile^[15b, 18] or halogen^[18a, 18b, 19] bound to the metal centre. A wide selection of bases have been used for these reactions including milder bases like preformed $\text{M}-\text{OH}$,^[17a-d, 18a] NaOH ^[20] and KO^tBu ^[18b, 18c, 19a-c, 21] and stronger bases such as NaH ^[19e] and $n\text{BuLi}$.^[18d] The α -hydrogen can also be removed utilising bulky free carbenes.^[22]

Initial work using base-assisted deprotonation involved the use of stronger pre-coordinated bases. This was first utilised by Boche and co-workers^[23] while analysing the mechanism for the reaction of LDA with phenylacetonitrile in which they observed a monoketenimine intermediate (Figure 1.6).

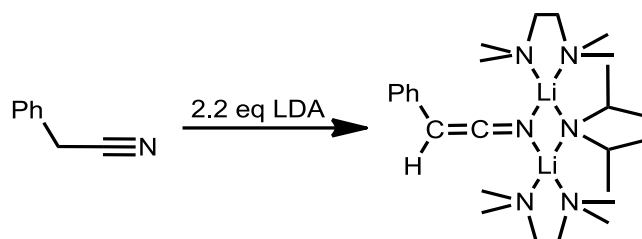


Figure 1.6: Synthesis of a monoketenimine from phenylacetonitrile.

However, an unexpected property of these complexes is the ability of NaOH and other weak bases to deprotonate unactivated nitriles, such as acetonitrile, despite their high pK_a . This is likely due to activation of the nitrile *via* coordination on the metal. Although the pK_a of acetonitrile is 31.3 in DMSO^[24] and 25 in water,^[25] NaOH and KO t Bu have been successfully utilised as bases.^[18b, 18c, 19a-c, 20, 21] K_2CO_3 can be used to activate nitriles like methyl cyanoacetate.^[26]

Tolman and co-workers demonstrated the formation of α -cyanocarbanion complexes **4** from either the corresponding Cu–OH or Ni–OH complexes in CH_3CN (Figure 1.7).^[17a] Three possible reaction mechanisms were proposed for the deprotonation of the nitrile ligand, all which were consistent with the kinetic data,

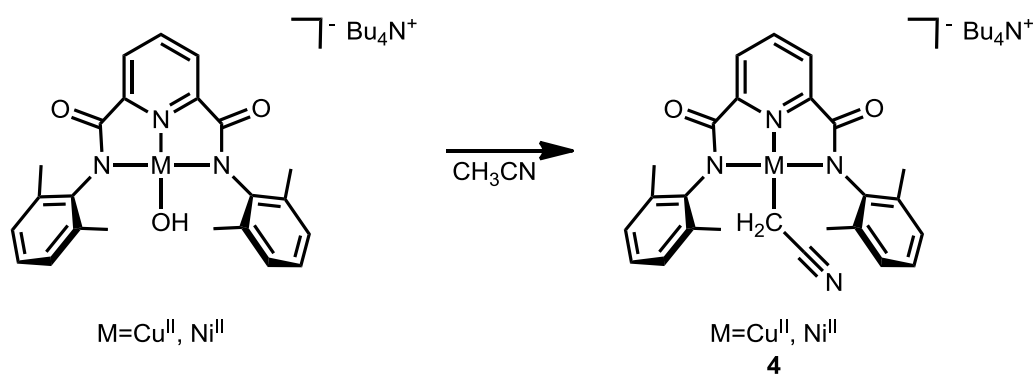


Figure 1.7: Synthesis of Cu– and Ni– CH_2CN complexes **4** from the corresponding M–OH complexes in CH_3CN .

however, no DFT studies were performed to support which mechanism is operative for this deprotonation (Figure 1.8).

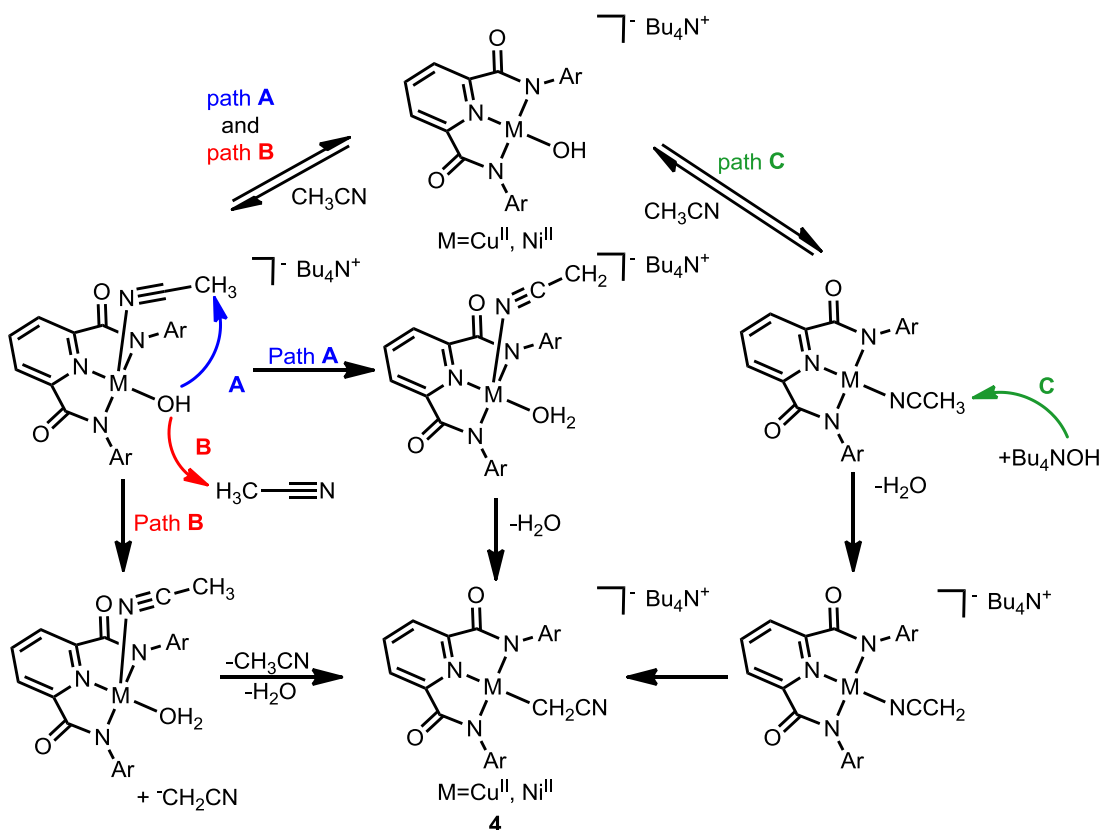


Figure 1.8: Possible reaction mechanisms for the synthesis of **4**.

The hydration of nitriles to form carboxamides in the presence of hydroxides has also been observed.^[27] Ir-OH complexes have been employed in a similar manner, however, the resulting nitrile-derived organometallic products were shown to be dependent on the nitrile substituent (Figure 1.9). When R is an aromatic group the carboxamide product **5** is formed exclusively. However, when R = methyl a mixture of both hydration product **5** and α -deprotonated product **6** were formed. Additionally, when R = CHPh₂ ketenimine complex **7** was the sole product. The hydrolysis versus deprotonation products are believed to be competing reactions with the deprotonation only possible with an α -hydrogen while the hydrolysis reaction is not preferential with the large steric bulk of R = CHPh₂. For the formation of complex **7**,

the corresponding iridium triflate catalyst was shown to accelerate the rate of the reaction.^[17c]

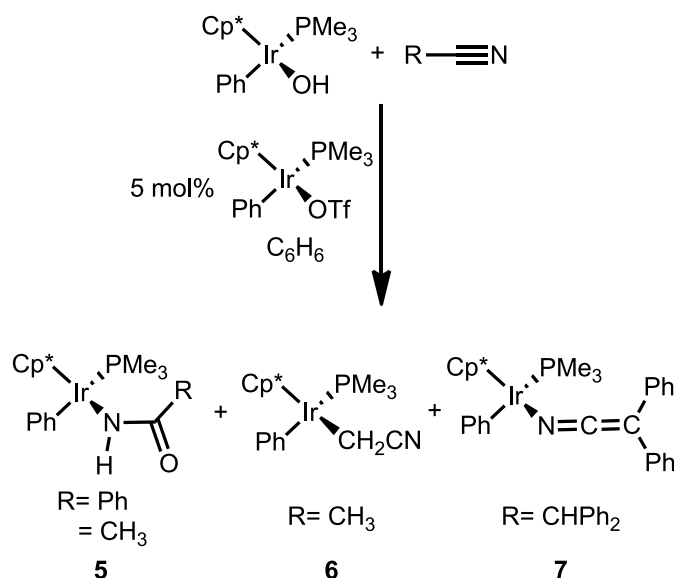


Figure 1.9: Synthesis of various nitrile products, R = CHPh₂, CH₃ and Ph.

1.2.4 Synthesis *via* Decarboxylation of Cyanoacetate:

Complexes of α -cyanocarbanions can also be formed *via* decarboxylation.^[28] Cyanomethylcopper(I) was synthesised from the corresponding copper(I) and copper(II) cyanoacetates. When copper(II) was used, in addition to the formation of cyanomethylcopper(I) and the evolution of CO₂, succinonitrile was also observed.^[28b]

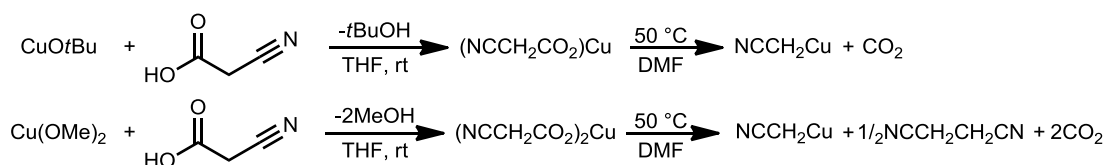


Figure 1.10: Synthesis of copper α -cyanocarbanion *via* decarboxylation.

1.3 Bonding of α -Cyanocarbanions:

Various bonding modes have been observed for complexes bearing α -deprotonated alkylnitrile ligands (Figure 1.11). The most common are M-CR₂CN (**I**) and M-NCCR₂ (**III**). These bonding modes can be distinguished *via* X-ray

crystallography, and in some cases NMR and IR spectroscopic techniques due to their unique characteristics.

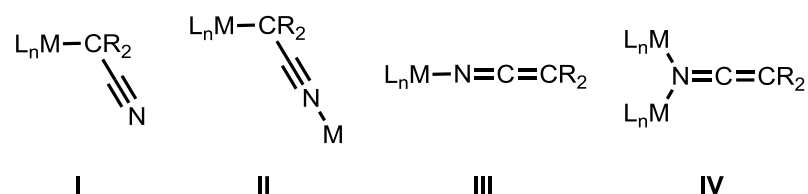


Figure 1.11: Predominant different bonding modes of α -cyanocarbene.

1.3.1 Crystallographic and Spectroscopic Data for Binding Modes I–IV:

Studies have been performed on these complexes in attempt to assign bonding modes, however, without X-ray crystal structure analysis often the nature of the binding cannot conclusively be assigned.^[29] Representative spectroscopic data for complexes displaying each of the four predominant bonding modes **I–IV** (Figure 1.11) is presented in Table 1.1. These complexes were selected due to the availability of complete characterisation data.

$[\text{Ni}(\text{IMes})(\text{CH}_2\text{CN})\text{Cp}]$ adopts bonding mode **I** (Figure 1.12)^[18c] displaying a $\text{C}-\text{C}_\alpha$ bond length of 1.429(3) Å typical of a $\text{C}(sp)-\text{C}(sp^3)$ single bond and the $\text{C}-\text{N}$ bond length of 1.147(3) Å is as expected of a $\text{C}\equiv\text{N}$ bond. Similarly, the example of bonding mode **II**, $[\text{Cp}(\text{OC})_2\text{Fe}(\text{CH}_2\text{CN})\text{Re}(\text{CO})_5][\text{BF}_4]$,^[30] has bond lengths typical of a $\text{C}\equiv\text{N}$ bond and a $\text{C}(sp)-\text{C}(sp^3)$ single bond (Figure 1.13).

	M–CR₂CN (I)	M–CR₂CN–M (II)	M–N=C=CR₂ (III)	M₂–N=C=CR₂ (IV)
Example used	[Ni(IMes)(CH ₂ CN)Cp] ^[18c]	[Cp(OC) ₂ Fe(CH ₂ CN)Re(CO) ₅]BF ₄ ^[30]	[Cp*(PMe ₃)Ir{N=C=C(Ph) ₂ }Ph] ^[17c]	{[Ph] ₂ C=C=N}InMe ₂ (THF) ₂ ^[16]
Bond lengths				
C_α–C (Å)	1.429(3)	1.447 ^a	1.377(7)	1.350(5)-1.358(5)
C–N (Å)	1.147(3)	1.144 ^a	1.168(6)	1.188(5)-1.201(5)
Bond angles				
C_α–C–N (°)	178.5(6)	178.9(10)	178.9(5)	178.5(4)-179.4(4)
M–C_α–C (°)	112.5(2)	111.7(7)		
C–N–M (°)		178.2(7)	163.5(4)	124.6(3)-129.2(3)
M–N–M (°)				103.4(1)-106.1(1)
NMR and IR spectroscopy				
¹H NMR resonance (ppm)	–0.08 ^b	1.59 ^c		
¹³C NMR resonance C_α (ppm)	–42.0 ^b	–31.9 ^c	142.6 ^d	55.0 ^e
¹³C NMR resonance C (ppm)	132.7 ^b	140.2 ^c	129.5 ^d	141.2 ^e
IR band (cm⁻¹)	2188	2251	2105	2167

Table 1.1: Key spectroscopic data for binding modes **I-IV**. ^a incorrectly reported in original paper, values were obtained from CCDC. ^b in CDCl₃.

^c in acetone-*d*₆. ^d in C₆D₆. ^e in THF-*d*₈.

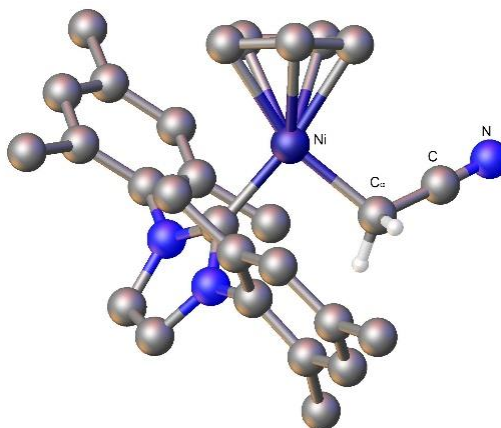


Figure 1.12: Molecular structure of $[\text{Ni}(\text{IMes})(\text{CH}_2\text{CN})\text{Cp}]$, hydrogen atoms not on the nitrile ligand have been omitted for clarity.

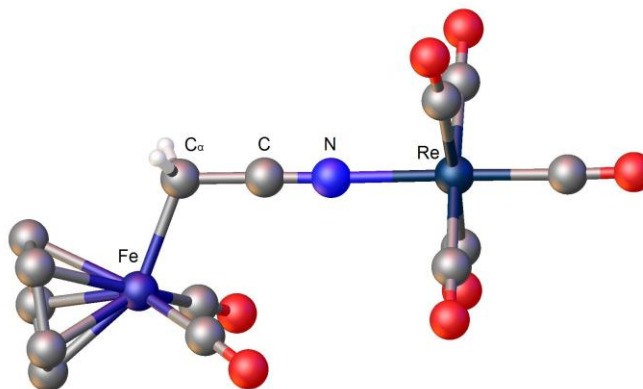


Figure 1.13: Molecular structure of $[\text{Cp}(\text{OC})_2\text{Fe}(\text{CH}_2\text{CN})\text{Re}(\text{CO})_5][\text{BF}_4]$, hydrogen atoms not on the nitrile ligand have been omitted for clarity.

Most complexes featuring binding mode **II** are bi- and tri-nuclear species^[3d, 15a, 31] and a variety of homo- and hetero-metallic examples are known. When the bridging ligand is involved in metallocyclic ring formation, the geometries of the complexes are distorted from that noted in $[\text{Cp}(\text{OC})_2\text{Fe}(\text{CH}_2\text{CN})\text{Re}(\text{CO})_5][\text{BF}_4]$ as discussed in Table 1.1 to accommodate the influence of the ring formation. An example of this effect is $\{[(\text{ONO}^t\text{Bu})\text{Ir}(\text{PPh}_3)(\mu\text{-CH}_2\text{CN})_2]\}^{[32c]}$ ($\text{ONO}^t\text{Bu} = 2,2'-(4-t\text{-butyl-}2,6\text{-pyridinediyl})\text{bis}(4,6\text{-bis}(t\text{-butyl})\text{phenoxide})$) with a N-C-C_α angle of $171.7(2)^\circ$, an average C-N-M angle of 157.1° and a $\text{M-C}_\alpha\text{-C}$ angle of $105.13(16)^\circ$.

In contrast, for bonding mode **III** the X-ray crystal structure of $[\text{Cp}^*(\text{PMe}_3)\text{Ir}\{\text{N}=\text{C}=\text{C}(\text{Ph})_2\}\text{Ph}]^{[17\text{c}]}$ (Figure 1.15) reveals a systematic shift in the bond lengths of the ligand with a lengthening of the C–N bond and a shortening of the C–C_α bond in comparison to binding mode **I**. This is consistent with a greater contribution of the ketenimine resonance form of the ligand (Figure 1.14). The C–N bond length is lengthened to 1.168(6) Å, still within the range of a typical CN triple bond, while the C–C_α bond length is substantially shorter at 1.377(7) Å. These lengths are consistent with other complexes displaying binding mode **III**.^[5f, 15c, 32] Similarly, for bonding mode **IV**, the X-ray crystal structure of $\{([\text{Ph}]_2\text{C}=\text{C}=\text{N})\text{InMe}_2(\text{THF})\}_2^{[16\text{f}]}$ (Figure 1.16) contains further characteristics of the ketenimine resonance form in comparison to bonding mode **III** (Figure 1.14).



Figure 1.14: Resonance forms of ketenimine ligand.

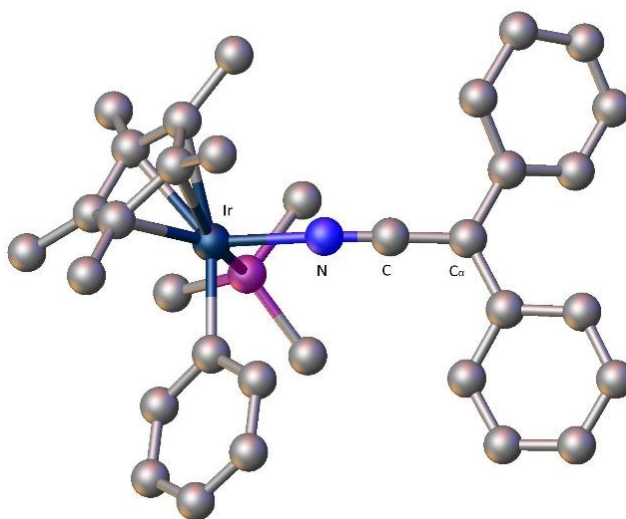


Figure 1.15: Molecular structure of $[\text{Cp}^*(\text{PMe}_3)\text{Ir}\{\text{N}=\text{C}=\text{C}(\text{Ph})_2\}\text{Ph}]$, hydrogen atoms removed for clarity

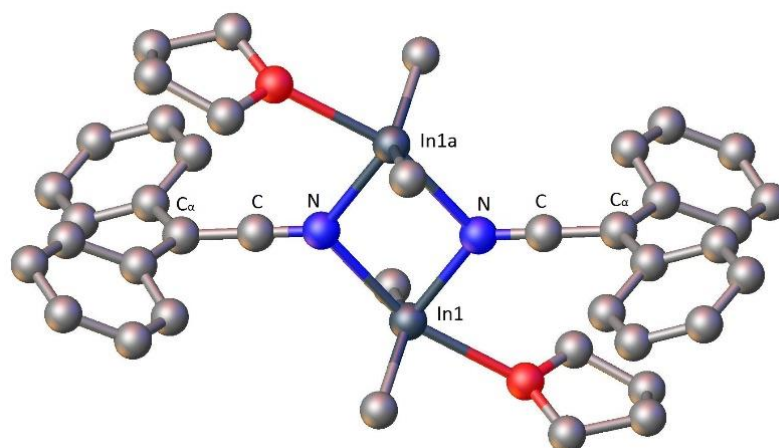


Figure 1.16: Molecular structure of $\{[(\text{Ph})_2\text{C}=\text{C}=\text{N})\text{InMe}_2(\text{THF})]_2\}$, hydrogen atoms removed for clarity.

There is only one non aromatic nitrile ligand of binding mode **III** as observed by Hartwig for $[\text{Pd}(\text{DiPrPF})\{\text{NCC}(\text{Me}_2)\}(\text{C}_6\text{H}_4\text{-4-}t\text{Bu})]$.^[15a] The N–C bond distance of 1.21 Å is lengthened and the C–C bond distance of 1.35 Å is shortened in comparison with the aromatic ketenimine ligand $[\text{Cp}^*(\text{PMe}_3)\text{Ir}\{\text{N}=\text{C}=\text{C}(\text{Ph})_2\}\text{Ph}]$, possibly indicating greater contribution of the ketenimine resonance form (Figure 1.14).

The ^1H NMR resonances of the C_α protons of complexes with binding modes **I** & **II** typically range between 0–2 ppm^[12a, 13a, 18c, 30, 33] while the few examples of bonding mode **III** with an α -hydrogen typically have a downfield shift in resonances to between 2.5–6 ppm.^[15c, 32a, 34] Similarly, the ^{13}C NMR resonances of the C_α are the most contrasting between the binding modes with the downfield shift in resonance for bonding modes **III** in comparison to **I**. The C_α resonance is typically between –40 and –21 ppm^[12a, 13a, 18c, 30, 33] for binding mode **I**. However, for binding mode **III** this signal is usually further downfield with resonances typically observed between 36.7–142.6 ppm.^[32a, 32b, 34] These downfield shifts in both the ^{13}C NMR and ^1H NMR spectra are consistent with an increased contribution from the ketenimine resonance form (Figure 1.14). The C–N IR band also is trending towards lower

wave numbers for bonding modes **III** & **IV**, with the C_{α} -C bands typically not assigned for these complexes. These spectroscopic data are consistent with greater contribution from the ketenimine resonance for complexes of binding modes **III** and **IV** (Figure 1.14).

Although rare, a few other bonding modes have been observed due to the involvement of the various π -bonds and lone pairs in the ligand system. One was discovered with lanthanum and cerium, which appears to be a hybrid between bonding mode **II** and **III** with the lanthanide coordinated to both the α -carbon atom and the nitrogen while the bond distances for the $C-C_{\alpha}$ and the $C-N$ bonds are similar to that observed with bonding mode **III**.^[35] Utilising an α -stabilised carbanion, a sodium ketenimine complex was formed (bonding mode **III**), however due to the propensity of sodium to aggregate it also interacted with both the nitrogen atom and the α -carbon atom of other nitrile ligands (Figure 1.17).^[36] Deprotonated malononitrile with conjugation across both nitrile substituents similarly binds *via* binding mode **I**,^[37] **III**^[17d] and **III**^[38] depending on the complex. However, when conjugation is increased to tricyanomethane, bonding is exclusively seen on the nitrogen due to the increased conjugation.^[4]

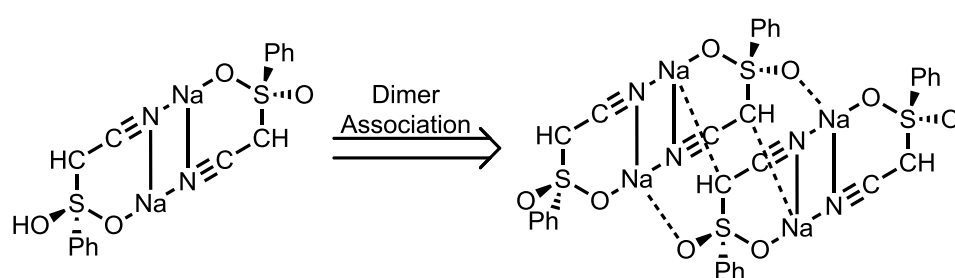


Figure 1.17: Bonding of the sodium aggregate $[(\text{PhSO}_2\text{CHCN})\text{Na}\cdot\text{THF}]$.

1.3.2 Relationship Between the Binding Modes:

The relationship between bonding mode **I** and **III** was first observed by Naota and co-workers who synthesised a series of ruthenium complexes. They introduced an

electron withdrawing α -sulfonyl group that has minimal resonance influence onto the nitrile ligand and successfully observed both bonding modes **I** and **III** with a series of ruthenium complexes. Some of these complexes were then shown to interconvert between the two binding modes upon heating in benzene (Figure 1.18).^[39]

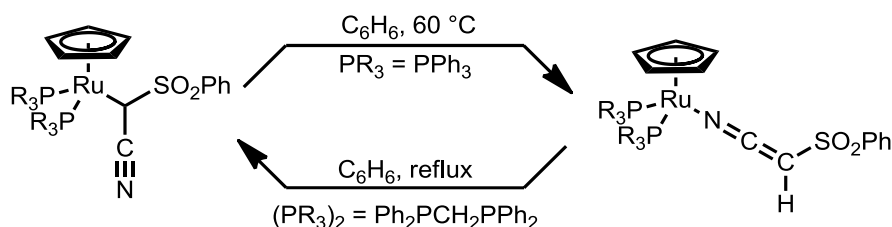


Figure 1.18: Interconversion between binding mode **I** and **III**.

An intermediate of bonding mode **III** was later postulated in the synthesis of a molybdenum α -cyanocarbanion complex as supported by IR spectroscopy (Figure 1.19). The presence of ketenimine intermediate **8** was assigned due to the presence of two strong ν_{CO} bands and a weak band at 2178 cm^{-1} assigned to the ketenimine ligand.^[15e]

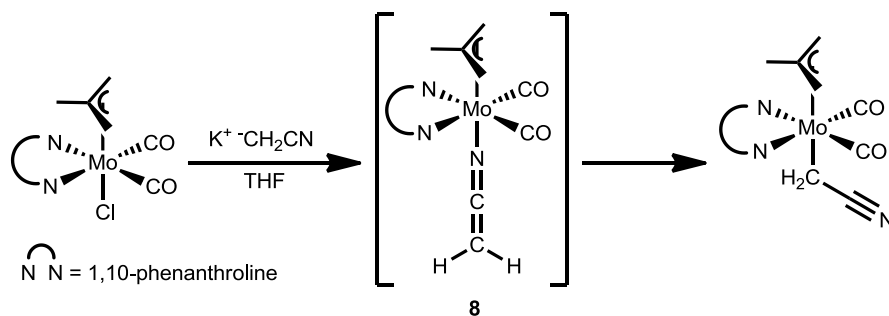


Figure 1.19: Isomerisation of α -cyanocarbanion as supported by IR spectroscopy.

Mechanistic data^[31a, 39b] and DFT studies^[39b, 40] indicate that the transformation between isomers of type **III** and **I** occurs *via* two different mechanisms with an intramolecular slippage process occurring for both the *C*- to *N*- and *N*- to *C*-interconversions while a self assembly intermolecular process has also been observed for the *C*- to *N*-interconversion (Figure 1.20). The presence of a complex of binding mode **II** as an intermediate was verified by NMR spectroscopic

studies.^[31a, 39b] DFT calculations performed on the formation of a nickel α -cyanocarbanion complex from the reaction of the corresponding acetonitrile salt with KO^tBu, proposed that the reaction also proceeded *via* a ketenimine intermediate before isomerising to the related carbanion of bonding mode I.^[18c]

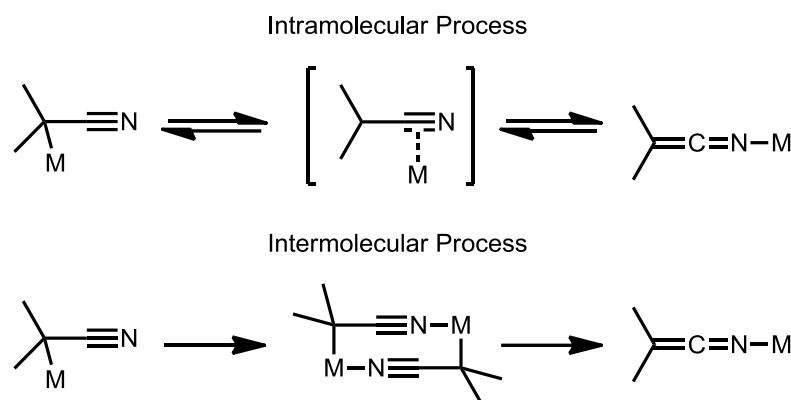


Figure 1.20: Isomerisation of α -cyanocarbanion nitrile ligand.

The preference for the various bonding modes that are observed ultimately seems to depend on a number of factors. Bonding mode **IV** has been exclusively observed with Group 1 and 13 metals.^[16, 23, 41] Group 1 metals also form complexes of bonding mode **III** depending on the co-ligands.^[42] The rationalisation for other classes of complexes can be more complicated. Recent work has suggested that the electronegativity of the metal preferences the formation of the *N*- versus *C*-bound ligand.^[43] Although complexes of bonding mode **I** typically contain metals with higher electronegativity,^[7, 8, 11b, 13a, 15e, 17a, 18a, 18d, 19a, 19b, 33, 44] there are also complexes of metals with lower electronegativity (< 1.8 on the Pauling scale)^[45] that exhibit binding mode **I**.^[15d, 17e] Similarly, complexes of bonding mode **III** typically have lower electronegativity,^[5f, 15c, 16, 32a, 46] however, complexes with this binding mode have been observed for metals with higher electronegativities (> 2.0 on the Pauling scale^[45]).^[15a, 17c, 34]

Steric effects influence the binding modes observed for α -cyanocarbanion complexes with binding modes **I** and **III** typically featuring different steric bulk of the

R-substituents. Generally, nitriles featuring low steric bulk, often with at least one α -substituent being hydrogen, favour bonding mode **I**.^[9a, 15a, 18a, 47] While ligands in which at least one α -substituent is a phenyl group prefer bonding mode **III**.^[15a, 15c, 32a]

Bonding mode **II** aggregation typically occurs when bonding *via* the α -carbon atom is preferential and there is an open coordination site on the metal allowing aggregation to arise by bridging, or when an additional metal complex is present that has propensity to bind to *N*-donors. This is supported by work done by Piers and co-workers where bonding mode **II** was initially observed, however, upon the addition of PPh₃ or PMe₃, bonding mode **I** was observed with a break-up of the aggregate.^[3d] Conversely, the reaction of a palladium complex of bonding mode **I** containing a chloride co-ligand with Ag[BF₄] leading to the formation of a dinuclear complex having bonding mode **II**.^[48]

Naota and co-workers observed the impact of the steric hindrance of the ancillary ligand on the binding mode. A range of ruthenium complexes with phosphine co-ligands of various cone angles were synthesised.^[39] Bonding mode **I** was observed with phosphine co-ligands featuring smaller cone angles while for phosphine ligands with larger cone angles bonding mode **III** was exclusively observed. The authors also noticed a solvent effect on the reaction; when the reaction was performed in EtOH/toluene (1:1) the complex of bonding mode **III** was exclusively formed. However, when the reaction was undertaken in EtOH/hexane (1:1) a 59:41 mixture of bonding mode **I:III** was observed.^[39a]

This work was supported by the synthesis of a series of palladium complexes with hydrotris(pyrazolyl)borato (Tp) ligands. The presence of an *i*Pr substituent on the Tp ligand, favoured bonding mode **III** exclusively. However, with a Me substituent on the Tp ligand, complexes of both bonding modes **III** and **I** were formed. Experiments showed that bonding mode **III** is the kinetic product while bonding mode **I** is the thermodynamic product of this reaction, as discussed earlier.^[49]

Hartwig and co-workers subsequently synthesised a series of phosphine-ligated palladium complexes and reacted them with a potassium nitrile complex *via* salt metathesis (Figure 1.21). Due to the steric bulk and electronic variation of the phosphine and nitrile ligand they successfully observed complexes of the three different bonding modes I–III. The variation in bonding modes between complex **13** and **14** could be due to electronic stabilisation by the Ph substituents of **13**, however, this is inconsistent with other R substituents. Thus, the difference in binding mode is likely due to the increased steric hindrance of the second R substituent. The preference in binding is also impacted by the variation in ancillary ligand consistent with those discussed above.^[15a]

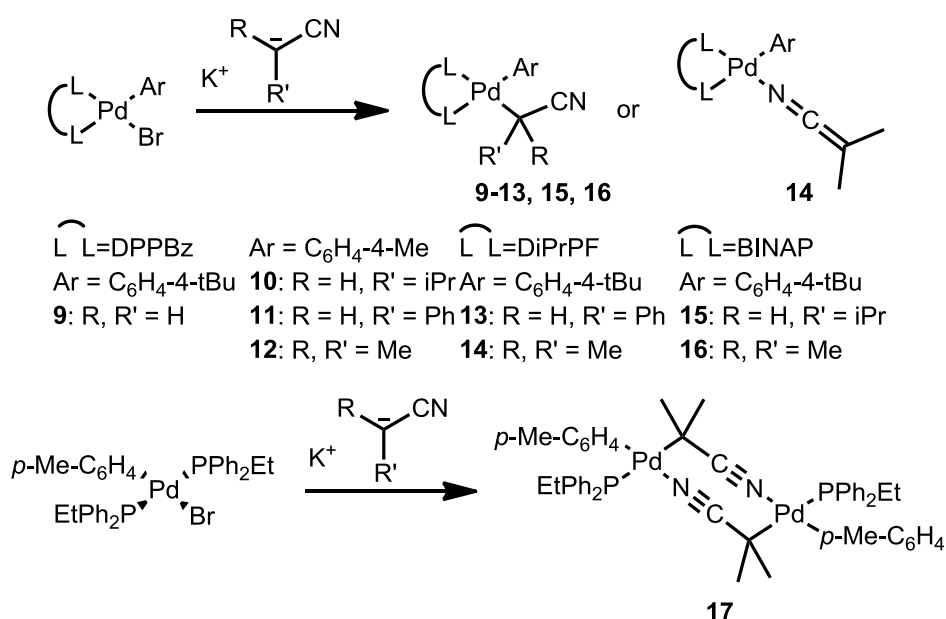


Figure 1.21: Synthesis of Pd complexes with various binding modes.

In cases where the binding mode of complexes where the C_α substituents are hydrogens and crystallographically identified disorder or high thermal motion limits accurate bonding mode determination, the M-X-C angle can be used to differentiate between bonding mode I and III due to the near linear M-N-C angle and the close to ideal tetrahedral M-C-C angle (Table 1.1).

1.4 Reactivity of α -Cyanocarbanions:

α -Cyanocarbanion complexes have been utilised for three primary modes of reactivity. The first is the formation of alkylnitriles *via* catalytic C–C bond formation reactions, developed by the pioneering work by Murahashi and co-workers in the late 1980s. These researchers identified various aldol and Michael reactions of nitriles,^[3c, 50] while this Introduction will focus on recently discovered applications. Alkylnitriles are useful compounds in organic synthesis due to the nitrile moiety, which can be functionalised further. α -Cyanocarbanion ligands are also interesting due to their propensity to react with other ligands including nitriles on the metal to form novel C–C coupling products. These complexes are also key intermediates in the reaction of acrylonitrile with various substrates including polymerisation and hydrophosphination reactions and thus have been studied to understand more about these reactions, their catalytic cycles and to improve yields. There are also a number of less common applications that won't be focused on, such as α -cyanocarbanion complexes reacting with CO_2 to form the cyanoacetate,^[51] enantioselective alkylation of an α -cyanocarbanion ligand,^[52] organocobaloxime complexes which have applications as Vitamin B₁₂ mimics and undergo crystalline state reactions^[9a, 53] and the application in the activation of O_2 .^[7]

1.4.1 Coupling of Deprotonated Nitrile Ligands:

The cyclotrimerisation of nitriles to form 6-membered heterocyclic rings have been observed affording various heterocycles depending on the conditions. It is well established that the reaction of KOMe ^[54] or KOtBu (Figure 1.22)^[55] with neat CH_3CN forms 4-amino-2,6-dimethylpyrimidine.

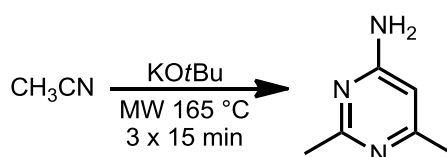


Figure 1.22: Synthesis of 4-amino-2,6-dimethylpyrimidine.

However, in addition to the formation of pyrimidines, $[\text{Pd}(\text{TMEDA})(\text{C}_6\text{H}_5)(\text{OH})]$ ^[17b] and $[\{(\text{C}_6\text{F}_5)_2\text{Pd}(\mu\text{-OH})\}_2]$ ^[2-17d] have been used to catalyse the formation of 4,6-diamino-2-cyanomethyl-3,5-pyridinedicarbonitrile from malononitrile (Figure 1.23).

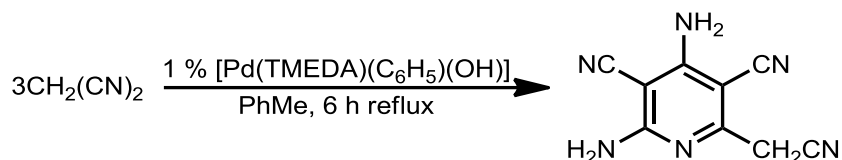


Figure 1.23: Cyclotrimerisation of malononitrile with $[\text{Pd}(\text{TMEDA})(\text{C}_6\text{H}_5)(\text{OH})]$.

Acetonitrile can also be trimerised with gallium and indium complexes in the presence of CsF ^[56] or *via* a $\text{Rh}-\text{CH}_2\text{CN}$ bond^[44a] to form a 6-membered metallacycle (Figure 1.24). The rhodium metallacycle is thought to be formed by the insertion of two equivalents of acetonitrile into the $\text{Rh}-\text{CH}_2\text{CN}$ bond and tautomerisation of the cyanomethylene protons to form a cyanoNacNac ligand.^[44a]

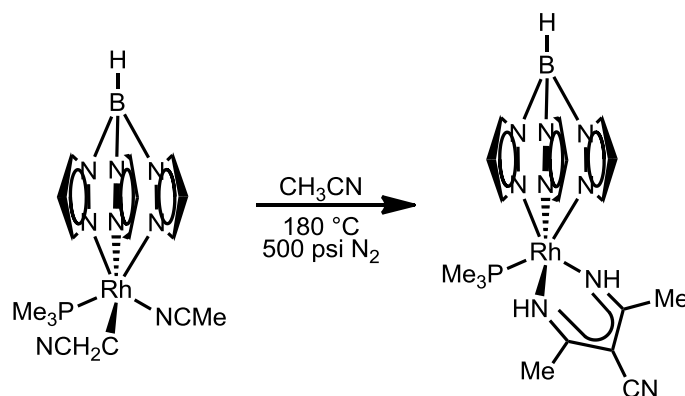


Figure 1.24: Trimerisation of acetonitrile on a rhodium complex.

In addition, there are a number of complexes where dimerisation of α -cyanocarbanion ligands occurs. In one example, by Rosenthal and co-workers, it is suggested that the reaction proceeded *via* a ketenimine intermediate to form a compound containing two zirconocene units which are connected by 5-membered bridges which occur *via* the C–C coupling of two nitrile ligands, one bound through the α -carbon atom and the second bound through the nitrile carbon atom (Figure

1.25).^[15c] Analogous dimerisation was also observed in an intramolecular fashion with a zirconium adiponitrile complex.^[57]

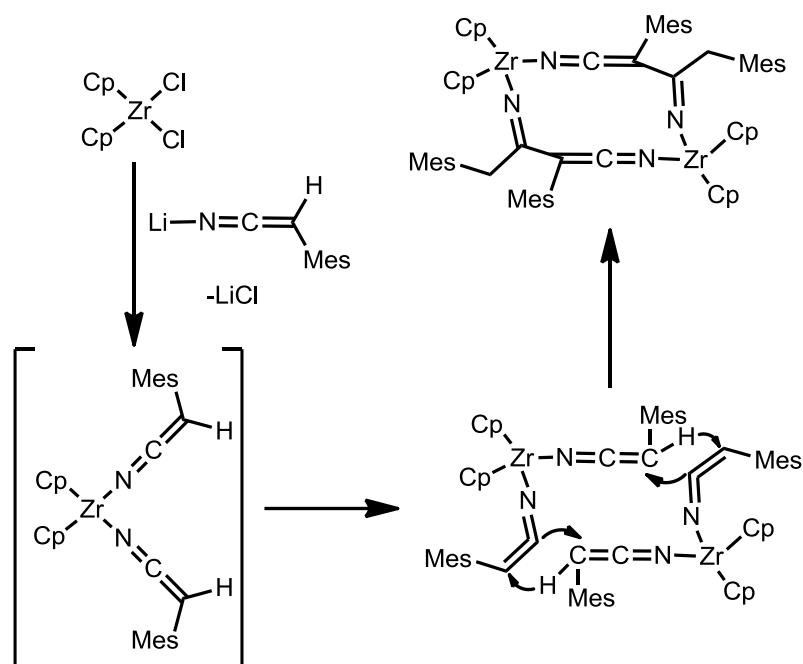


Figure 1.25: C–C coupling *via* an α -cyanocarbanion intermediate.

The dimerisation of α -cyanocarbanion ligands *via* C–C coupling of the α -carbon atom and the carbon atom of the nitrile has also formed an alternative isomer of that observed by Rosenthal.^[5f, 46b, 49] Intermediate **18** is postulated as analogous products were observed for the reaction of barium and magnesium with diphenylacetonitrile. Complex **19** was isolated and its structure confirmed *via* X-ray crystallography. Hydrolysis of **19** was observed in the NMR sample yielding 3-aminocrotonitrile (Figure 1.26).^[46b]

In addition to dimerisation between the α -carbon atom and nitrile carbon atom, dimerisation between two α -carbon atoms has been observed with platinum clusters^[11b] and *via* reductive elimination from a nickel phosphine complex under an atmosphere of O_2 (Figure 1.27).^[15f]

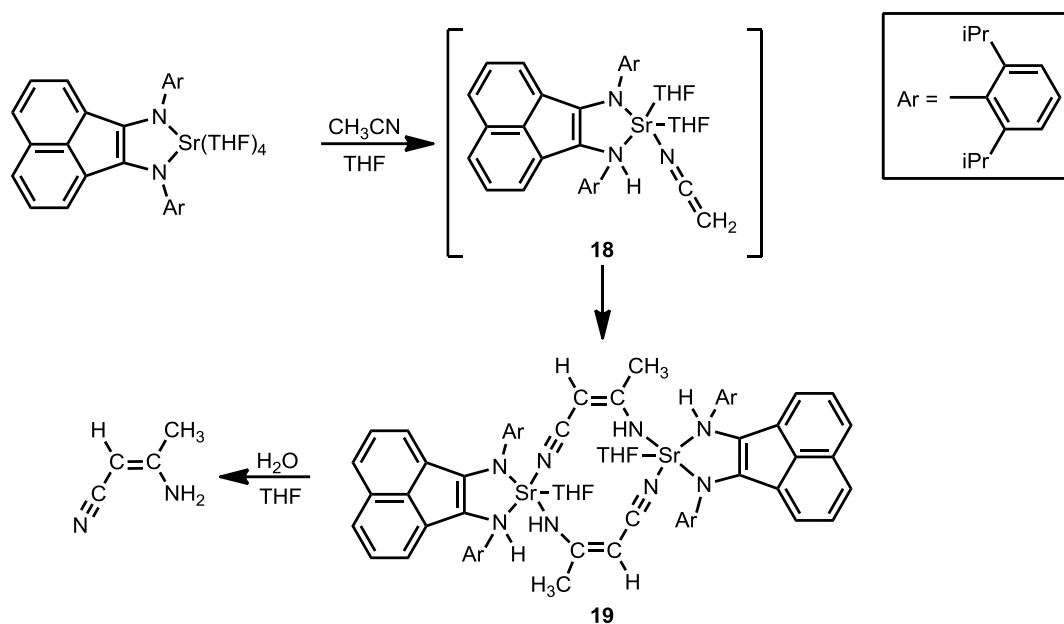


Figure 1.26: Synthesis of 3-aminocrotononitrile *via* a strontium complex.

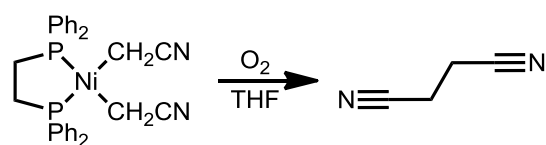


Figure 1.27: Generation of succinonitrile from a Ni phosphine complex.

A zinc α -cyanocarbanion complex was synthesised by reacting a Zn alkoxide with acetonitrile. Given the lower pK_a of acetone compared to acetonitrile (20^[58] vs 25^[25]) the authors attempted to react the alkoxide with acetone, however, no reaction was observed. An alternative synthetic method was attempted for deprotonation where they reacted the cyanocarbanion complex with acetone. Unexpectedly, this ligand coupled with the acetone to form the β -ketoiminate complex (Figure 1.28).^[17e]

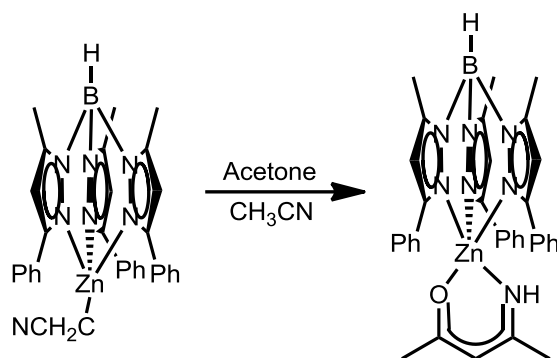


Figure 1.28: Synthesis of ketoiminate zinc complex.

1.4.2 Acrylonitrile Coupling Reactions:

Acrylonitrile is a useful starting material for various transition metal-catalysed reactions including hydrophosphination and copolymerisation and it is believed that many of these reactions proceed *via* α -cyanocarbanion complex intermediates. In this section, a number of papers are highlighted which observed these intermediates and used this information to understand the reaction mechanisms and optimise yields.

Metallacycle **21** was synthesised from the addition of alkenes from the precursor **20**. This key intermediate and studies that indicated that the Ru–C bond can be broken

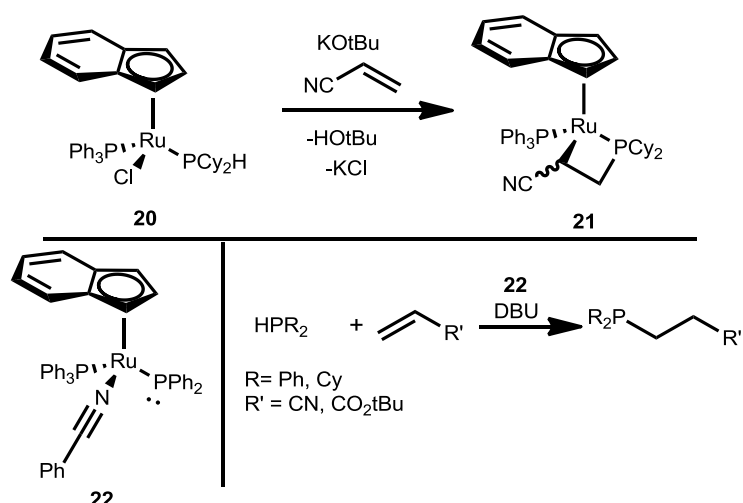


Figure 1.29: Hydrophosphination of alkenes

in the presence of a base were used to develop a related catalyst (**22**). **22** was shown to be effective in synthesising the linear hydrophosphination product exclusively, a specificity that has not previously been obtained (Figure 1.29).^[3a]

Nickel and platinum PCP-type complexes (PCP = 2,6-(R₂PCH₂)₂C₆H₃, R = Ph, Cy) have applications in the hydroamination of acrylonitrile. In 2002, the mechanism for the formation of the hydroamination product using catalyst **23** was analysed. Due to the slow reaction rate the reaction was monitored by ³¹P{¹H}NMR spectroscopy and two species (**24** & **25**) were observed (15 and 45 % yield in 2 days at 45 °C). Their identities were confirmed by independent syntheses. In addition to this, to elucidate

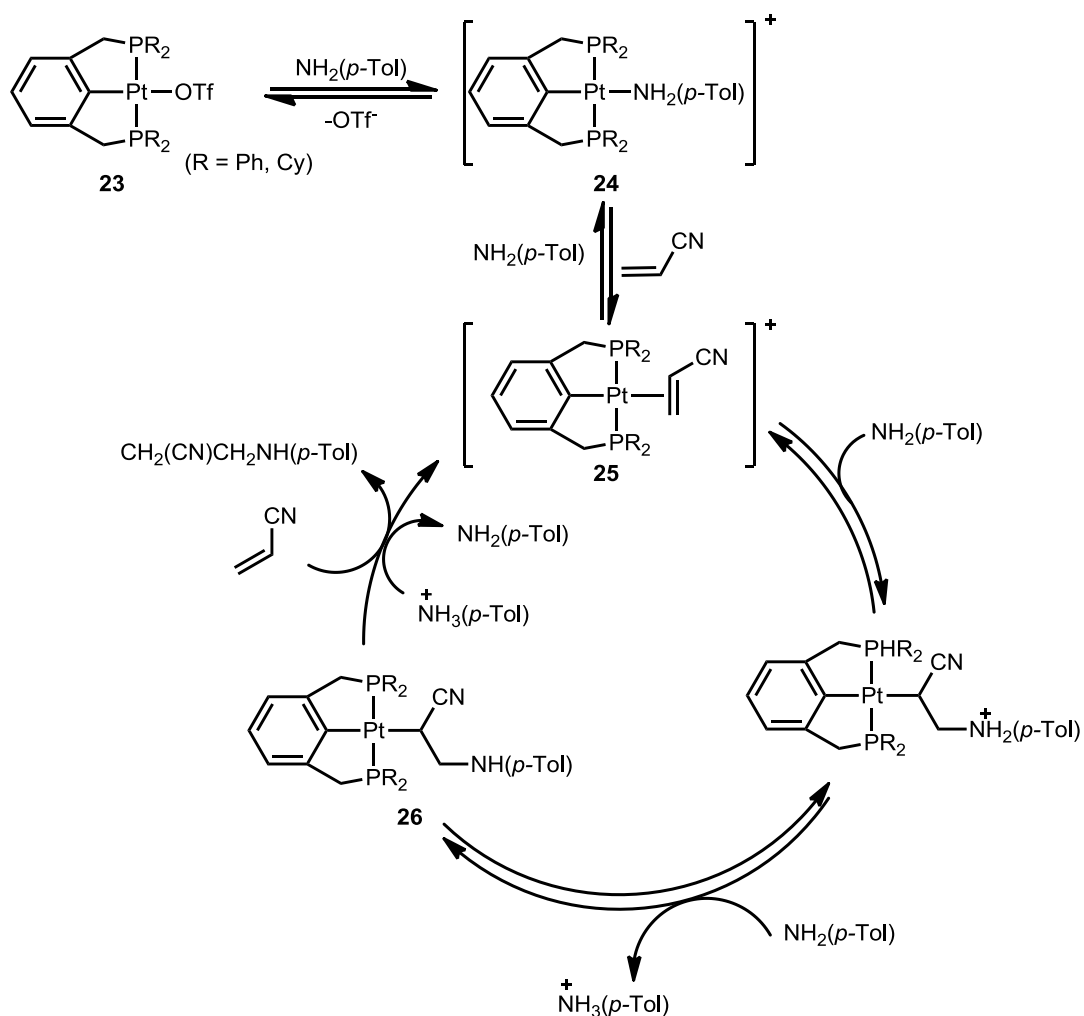


Figure 1.30: Proposed catalytic cycle of the hydroamination of acrylonitrile.

the possible mechanism for the liberation of the product, intermediate **26** was synthesised and possible reaction pathways were analysed. In addition, the liberation of the by-product $[\text{NH}_3(p\text{-Tol})]\text{BPh}_4$ was observed supporting the mechanism proposed in Figure 1.30.^[3b] Since then further work has utilised a range of Ni–PCP and Ni–POCOP ligands (POCOP = 2,6- $(i\text{Pr}_2\text{PO})_2\text{C}_6\text{H}_3$) also producing the same hydroamination product.^[59] However, further work is required to support the mechanism as this work proposes an alternative mechanism in which the nickel acts a Lewis acid.^[60]

Piers and co-workers^[3d] investigated the insertion of acrylonitrile into palladium methyl bonds and the importance of this work in understanding the mechanism of polymer formation using polar monomers. Previously, polymers and copolymers integrating polar monomers were prepared *via* less controlled methods than transition metal catalysis such as radical-initiated polymerisations.^[61] The authors studied the factors that affected the formation of acrylonitrile-based polymers and found that the barriers to insertion are not the issue but the dominance of coordination of polar functional groups must be overcome to enable more effective polymerisation. Due to this dominance of the coordination of the polar functional group, they reported no success in the reaction of it with ethylene or carbon monoxide, a key reaction step to form the desired polymers.^[3d] However, since then subsequent work employing alternative catalysts has overcome these problems.^[62]

1.4.3 C-C Activation of Acetonitrile:

In addition to C–H activation of acetonitrile there are a number of complexes that then further react *via* C–CN bond activation to form nitrile and methyl ligands by C–C bond cleavage.^[5h, 13] One example employs a rhodium complex to achieve the selective cleavage of C–H and C–C bonds.^[13b] Both were observed with acetonitrile depending on the reaction conditions (Figure 1.31). However, in the case of

benzonitrile C–C bond activation occurred exclusively due to the lack of α -hydrogen atoms.^[13b]

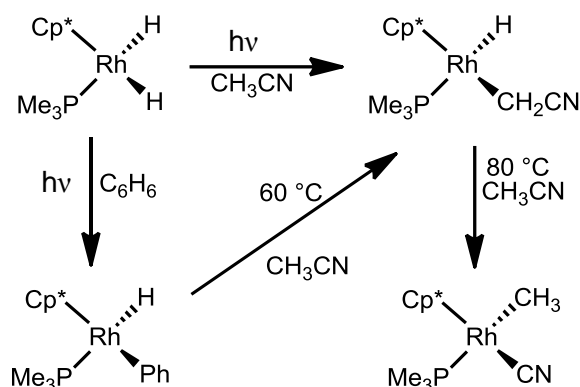


Figure 1.31: C-CN activation of acetonitrile with a rhodium catalyst.

1.4.4 Synthesis of Alkyl nitrile Compounds:

The applications of α -cyanocarbanion complexes in catalysis to form alkyl nitrile compounds were covered in a recent review by Palomo *et al.*^[2] and are an important class of complexes that are found as structural motifs in a number of natural products^[63] and pharmaceuticals,^[64] as well as being synthetically useful intermediates. These compounds are typically α -aryl nitriles or β -hydroxy, β -amino and β -ketonitriles.

Alkyl nitriles have been successfully synthesised *via* organic methodologies using a strong base to deprotonate the α -position,^[65] substituting an electron withdrawing group onto the α -substituted aromatic ring, reducing the pK_a of the α -carbon^[66] or the use of synthetic equivalents most commonly TMSCH₂CN^[67] and silyl ketenimines.^[68] However, the metal-catalysed formation of alkyl nitriles provides synthetic advantages due to the high functional group tolerance and atom efficiency that has not been achieved under organic reaction conditions.

Hartwig and co-workers developed a palladium-catalysed arylation of alkyl nitriles.^[15a] Their work tolerated a variety of aryl bromides and was compatible

with secondary nitriles. When R'' = hydrogen disubstitution of the aryl substituent was exclusively observed over 16 h in 60 % yield (Figure 1.32). By using a trimethylsilyl functionality on the α -carbon further studies enabled the monoarylation of compounds where R' and/or R'' are hydrogen.^[69] Since then, the reaction was performed using a chiral palladium catalyst yielding asymmetric α -arylated alkylnitriles in 80–95 % ee.^[70]

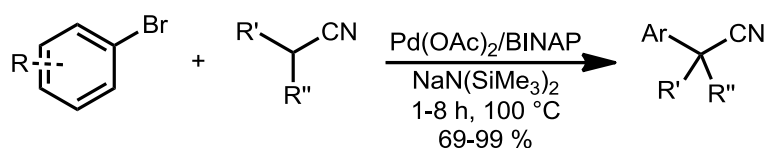


Figure 1.32: Synthesis of α -arylnitriles

There are a number of synthetic methods for the formation of β -substituted nitriles. Based off Hartwig's work, a range of β -ketonitriles were synthesised using an *in situ* generated palladium catalyst under a CO atmosphere (Figure 1.33).^[71]

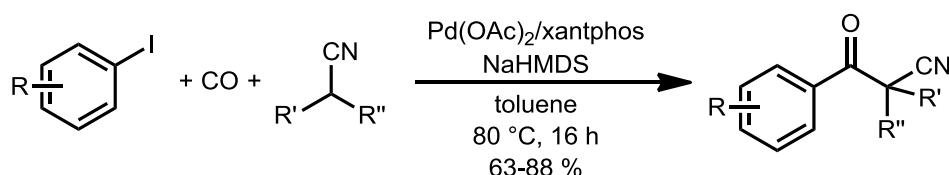


Figure 1.33: Synthesis of β -aryl- β -ketonitriles

Decarboxylative Mannich-type reactions are one synthetic method used to generate β -aminonitriles. Initial reactions looked at the performance with and without an α -substitution of a carboxylic acid and showed that this substitution greatly increased the diastereomeric ratio and ee of the product observed (Figure 1.34).^[72]

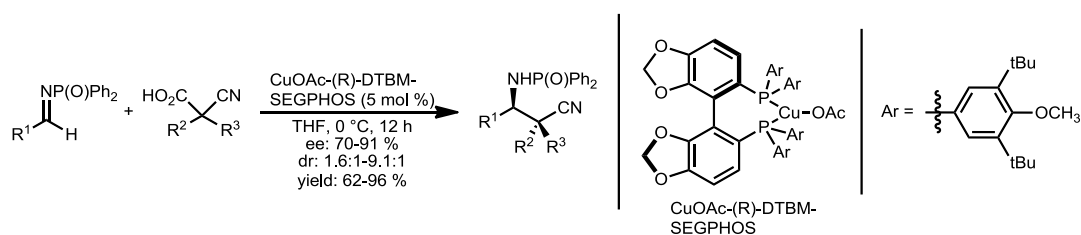


Figure 1.34: Synthesis of β -aminonitriles from imines

β -Hydroxy, β -amino and β -ketonitriles have also been successfully synthesised from the corresponding ketone or imine and a non-activated nitrile. There are a number of these reports in the literature and some of the most promising examples will be presented below. Both β -hydroxy^[73] and β -aminonitriles^[74] have been successfully synthesised asymmetrically with the use of chiral catalysts. Previously, the synthesis of chiral α,α -dichloro- β -aminonitriles has been challenging due to the low thermal stability of α,α -dichlorocarbanions. These compounds were successfully formed by reaction dichloroacetonitrile with a variety of imines in high yields and enantioselectivities (Figure 1.35). The proposed catalytic cycle involves an α -cyanocarbanion complex of bonding mode III.^[75]

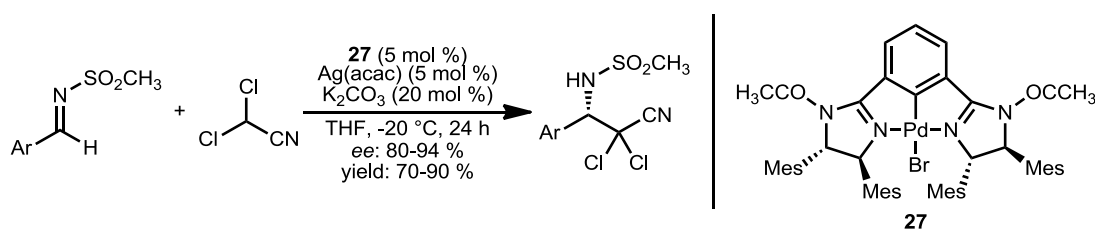


Figure 1.35: Synthesis of α,α -dichloro- β -aminonitriles using a chiral palladium catalyst

A nickel PNP type complex was used to catalyse the formation of a range of β -hydroxynitrile compounds using a $-\text{OTf}$ based catalyst in the presence of DBU (Figure 1.36, **28**). The authors proposed a mechanism involving a ketenimine intermediate. Interestingly, when the corresponding $\text{Ni}-\text{CH}_2\text{CN}$ complex was used no reaction was observed suggesting that this species is not a competent catalyst. The authors postulated that this was due to either the ketenimine isomer being

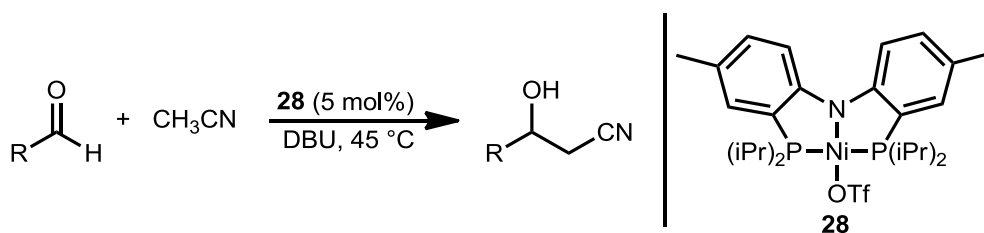


Figure 1.36: Preparation of β -hydroxynitriles *via* a PNP catalyst

stabilised in the reaction mixture *via* hydrogen-bonding with the protonated DBU, (DBUH)⁺, or that the reaction of the ketenimine with the aldehyde is much faster than the isomerisation to the –CH₂CN ligand.^[76]

The synthesis of alkylnitrile compounds *via* catalytic processes typically requires the addition of a base, which can lower the functional group tolerance of the methodology. Notably, Guan and co-workers utilised a preformed α -cyanocarbanion complex to catalyse the formation of β -hydroxynitriles from aldehydes without the addition of a base (Figure 1.37). The proposed catalytic cycle (Figure 1.38) involves the reversible addition of the aldehyde to the carbon-bound α -cyanocarbanion complex **29** forming the alkoxide intermediate **30**. It is claimed that a $\sigma\pi$ - $\pi\pi$

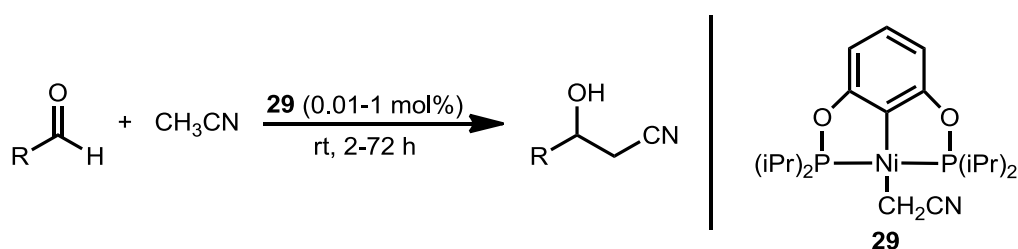


Figure 1.37: Synthesis of β -hydroxynitrile compounds *via* a Ni-POCOP catalyst

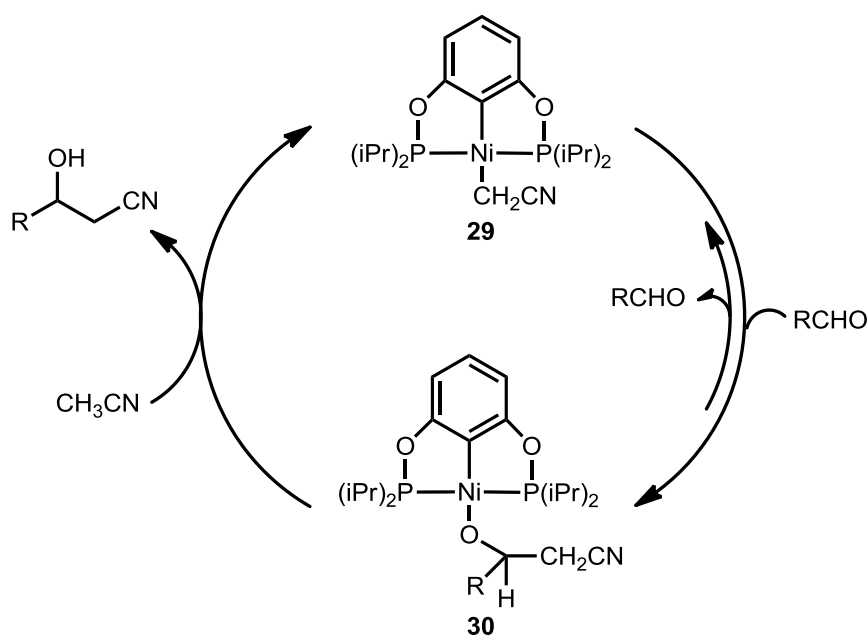


Figure 1.38: Proposed mechanism for β -hydroxynitrile synthesis *via* catalyst **29**

repulsion of the Ni–O bond promotes the reformation of the active catalyst despite the fact that it is energetically unfavourable.^[15b] The mechanism proposed is further examined in Chapter 2 accompanied by DFT calculations.

1.5 Summary and Outlook:

α -Cyanocarbanion complexes are key intermediates for the synthesis of a range of small molecules from β -hydroxynitriles to reactions such as hydrophosphination reactions. These complexes can be synthesised using a variety of methods primarily *via* the use of a base to deprotonate a nitrile, oxidative addition and salt metathesis. DFT studies indicate that transformations between the two main binding modes occur *via* an intramolecular or a metal slippage process and the binding mode observed is influenced by the steric hindrance of the ligands.

1.6 Project Scope:

Ongoing studies on α -cyanocarbanion complexes highlight these species as key intermediates in various synthetic processes with recent promising examples including the base-free synthesis of β -hydroxynitriles. Further work is needed to understand the mechanisms for the formation and isomerisation of these complexes and the roles of the binding modes in catalysis.

The project scope is based on previous work in which members of the Gardiner group serendipitously synthesised palladium bis(NHC) α -cyanocarbanion complexes of bonding mode I and II (Figure 1.39).^[77] This finding, combined with the applications of α -cyano carbanion complexes in the synthesis of β -hydroxynitriles^[2] and the extensive applications that palladium NHC complexes have in carbon-carbon cross reactions^[78] formed the basis of potential catalytic applications of these compounds.

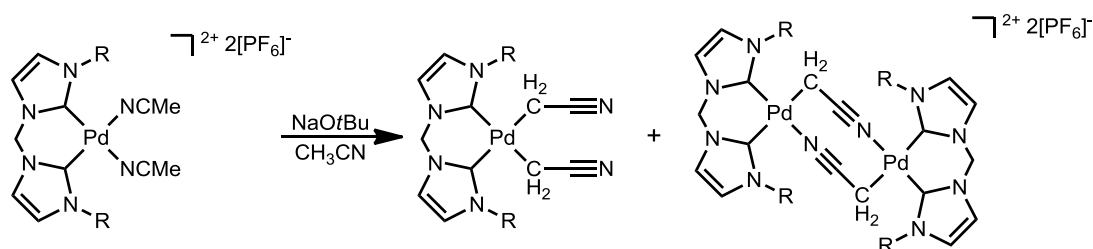


Figure 1.39: Synthesis of α -cyanocarbanion complexes from the corresponding acetonitrile complex

Areas of interest of NHC based α -cyanocarbanion complexes to the scope of the project include:

1. Chapter 2 will focus on the most promising published system for the synthesis of β -hydroxynitriles^[15b], outlining the DFT calculations performed as part of this study as well as the synthesis of some related complexes (**31**, Figure 1.40).
2. A range of bis(NHC) complexes with α -cyanocarbanion ligands will be discussed in Chapter 3.
3. A range of NHC containing pincer complexes based on the information discussed in Chapters 2 & 3 will be discussed in Chapter 4 including a new synthetic pathway for the formation of complexes of the type **33** (Figure 1.40, **32**, **33**).
4. Chapter 5 outlines catalyst screening employing the complexes described in

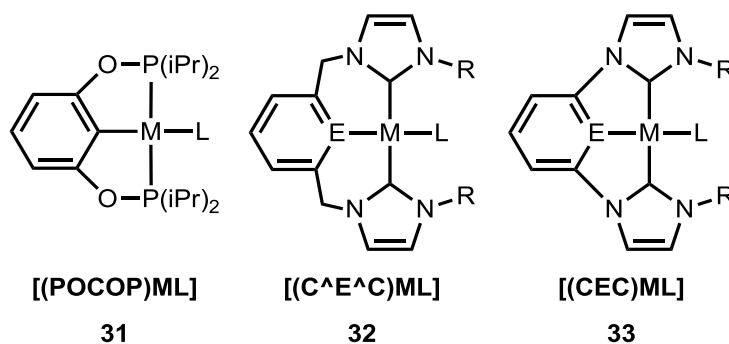


Figure 1.40: General classes of complexes to be studied E = N/C

Chapters 2-4 for the synthesis of β -hydroxynitriles.

1.7 References:

- [1] M. Cesari, C. Neri, G. Pergo, E. Perroti, A. Zazzetta, *J. Chem. Soc., Chem. Commun.* **1970**, 276–277.
- [2] R. Lopez, C. Palomo, *Angew. Chem. Int. Ed.* **2015**, *54*, 13170–13184.
- [3] a) R. G. Belli, K. M. E. Burton, S. A. Rufh, R. McDonald, L. Rosenberg, *Organometallics* **2015**, *34*, 5637–5646; b) J. M. Seul, S. Park, *Dalton Trans.* **2002**, 1153–1158; c) S. Murahashi, T. Naota, H. Taki, M. Mizuno, H. Takaya, S. Komiya, Y. Mizuho, N. Oyasato, M. Hiraoka, M. Hirano, A. Fukuoka, *J. Am. Chem. Soc.* **1995**, *117*, 12436–12451; d) L. F. Groux, T. Weiss, D. N. Reddy, P. A. Chase, W. E. Piers, T. Ziegler, M. Parvez, J. Benet-Buchholz, *J. Am. Chem. Soc.* **2005**, *127*, 1854–1869.
- [4] D. R. Turner, A. S. Chesman, K. S. Murray, G. B. Deacon, S. R. Batten, *Chem. Commun.* **2011**, *47*, 10189–10210.
- [5] a) L. Busetto, F. Marchetti, S. Zacchini, V. Zanotti, *Eur. J. Inorg. Chem.* **2005**, 3250–3260; b) M. Maekawa, M. Munakata, T. Kuroda-Sowa, K. Hachiya, *Inorg. Chim. Acta* **1995**, *230*, 249–252; c) M. I. Bruce, P. J. Low, F. Hartl, P. A. Humphrey, F. d. Montigny, M. Jevric, C. Lapinte, G. J. Perkins, R. L. Roberts, B. W. Skelton, A. H. White, *Organometallics* **2005**, *24*, 5241–5255; d) R. B. Osborne, J. A. Ibers, *J. Organomet. Chem.* **1982**, *232*, 371–385; e) Y. Wakatsuki, T. Sakurai, H. Yamazaki, *J. Chem. Soc., Dalton Trans.* **1982**, 1923–1927; f) C. Wang, X. Zhang, M. Xue, Y. Zhang, Q. Shen, *Organometallics* **2013**, *32*, 3618–3624; g) J. H. MacNeil, A. W. Roszak, M. C. Baird, K. F. Preston, A. L. Rheingold, *Organometallics* **1993**, *12*, 4402–4412; h) T. A. Atesin, T. Li, S. Lachaize, W. W. Brennessel, J. J. Garcia, W. D. Jones, *J. Am. Chem. Soc.* **2007**, *129*, 7562–7569; i) B. T. Sterenberg, R. W. Hilts, G. Moro, R. McDonald, M. Cowie, *J. Am. Chem. Soc.* **1995**, *117*, 245–

- 258; j) M. B. Chambers, S. Groysman, D. Villagran, D. G. Nocera, *Inorg. Chem.* **2013**, *52*, 3159–3169.
- [6] T. J. Zerk, P. V. Bernhardt, *Inorg. Chem.* **2017**, *56*, 5784–5792.
- [7] A. I. Nguyen, R. G. Hadt, E. I. Solomon, T. D. Tilley, *Chem. Sci.* **2014**, *5*, 2874–2878.
- [8] a) M. W. Johnson, S. L. Shevick, F. D. Toste, R. G. Bergman, *Chem. Sci.* **2013**, *4*, 1023–1027; b) B. Nekoueshahraki, S. P. Sarish, H. W. Roesky, D. Stern, C. Schulzke, D. Stalke, *Angew. Chem. Int. Ed.* **2009**, *48*, 4517–4520; c) J. J. Ko, T. M. Bockman, J. K. Koch, *Organometallics* **1990**, *9*, 1833–1842; d) R. L. Cowan, W. C. Trogler, *J. Am. Chem. Soc.* **1989**, *111*, 4750–4761; e) K. M. E. Burton, D. A. Pantazis, R. G. Belli, R. McDonald, L. Rosenberg, *Organometallics* **2016**, *35*, 3970–3980; f) M. Lenarda, G. Nardin, G. Pellizer, E. Braye, M. Graziani, *J. Chem. Soc., Chem. Commun.* **1985**, *713*, 1536–1538; g) D. L. Reger, D. G. Garza, L. Lebioda, *Organometallics* **1992**, *11*, 4285–4292.
- [9] a) H. Yamagiwa, A. Sekine, *Bull. Chem. Soc. Jpn.* **2013**, *86*, 1028–1034; b) C. Vithana, H. Uekusa, A. Sekine, Y. Ohashi, *Acta Crystallogr. Sect. B: Struct. Sci.* **2002**, *58*, 986–997.
- [10] K. Suzuki, H. Yamamoto, *J. Organomet. Chem.* **1973**, *54*, 385–390.
- [11] a) C.-C. Lee, Y.-C. Lin, Y.-H. Liu, Y. Wang, *Organometallics* **2005**, *24*, 136–143; b) Z. Beni, R. Ros, A. Tassan, R. Scopelliti, R. Roulet, *Dalton Trans.* **2005**, 315–325; c) F. Ragaini, F. Porta, A. Fumagalli, F. Demartin, *Organometallics* **1991**, *10*, 3785–3789; d) F. Porta, F. Ragaini, S. Cenini, F. Demartin, *Organometallics* **1990**, *9*, 929–935; e) H. H. Murray, J. John P. Fackler, A. M. Mazany, L. C. Porter, J. Shain, L. R. Falvello, *Inorg. Chim. Acta* **1986**, *114*, 171–178; f) L. Canovese, F. Visentin, C. Biz, T. Scattolin, C.

- Santo, V. Bertolasi, *Polyhedron* **2015**, *102*, 94–102; g) H. A. Burkill, R. Vilar, A. J. P. White, *Inorg. Chim. Acta* **2006**, *359*, 3709–3722.
- [12] a) M. G. Crestani, A. Steffen, A. M. Kenwright, A. S. Batsanov, J. A. K. Howard, T. B. Marder, *Organometallics* **2009**, *28*, 2904–2914; b) A. J. Vetter, R. D. Rieth, W. D. Jones, *Proc. Natl. Acad. Sci. U.S.A.* **2007**, *104*, 6957–6962.
- [13] a) T. Tanabe, M. E. Evans, W. W. Brennessel, W. D. Jones, *Organometallics* **2011**, *30*, 834–843; b) M. E. Evans, T. Li, W. D. Jones, *J. Am. Chem. Soc.* **2010**, *132*, 16278–16284.
- [14] J. G. Davidson, E. K. Barefield, D. G. V. Derveer, *Organometallics* **1985**, *4*, 1178–1184.
- [15] a) D. A. Culkin, J. F. Hartwig, *J. Am. Chem. Soc.* **2002**, *124*, 9330–9331; b) S. Chakraborty, Y. J. Patel, J. A. Krause, H. Guan, *Angew. Chem. Int. Ed.* **2013**, *52*, 7523–7526; c) L. Becker, M. Haehnel, A. Spannenberg, P. Arndt, U. Rosenthal, *Chem. Eur. J.* **2015**, *21*, 3242–3248; d) K. C. MacLeod, J. L. Conway, B. O. Patrick, K. M. Smith, *J. Am. Chem. Soc.* **2010**, *132*, 17325–17334; e) D. Morales, M. E. N. Clemente, J. Perez, L. Riera, V. Riera, D. Miguel, *Organometallics* **2003**, *22*, 4124–4128; f) P. R. Albuquerque, A. R. Pinhas, J. A. K. Bauer, *Inorg. Chim. Acta* **2000**, *298*, 239–244; g) T. Koike, T. Ikariya, *J. Organomet. Chem.* **2007**, *692*, 408–419; h) M. Baya, P. Crochet, M. A. Esteruelas, E. Onate, *Organometallics* **2001**, *20*, 240–253.
- [16] E. Irvani, B. Neumuller, *Organometallics* **2003**, *22*, 4129–4135.
- [17] a) J. Tehranchi, P. J. Donoghue, C. J. Cramer, W. B. Tolman, *Eur. J. Inorg. Chem.* **2013**, 4077–4084; b) J. Ruiz, M. T. Martinez, V. Rodriguez, G. Lopez, J. Perez, P. A. Chaloner, P. B. Hitchcock, *Dalton Trans.* **2004**, 3521–3527; c) D. M. Tellers, J. C. M. Ritter, R. G. Bergman, *Inorg. Chem.* **1999**, *38*, 4810–4818; d) J. Ruiz, V. Rodriguez, G. Lopez, J. Casabo, E. Molins, C. Miravittles,

- Organometallics* **1999**, *18*, 1177–1184; e) H. Brombacher, H. Vahrenkamp, *Inorg. Chem.* **2004**, *43*, 6054–6060.
- [18] a) R. A. Arthurs, M. Ismail, C. C. Prior, V. S. Oganessian, P. N. Horton, S. J. Coles, C. J. Richards, *Chem. Eur. J.* **2016**, *22*, 3065–3072; b) A. M. Oertel, J. Freudenreich, J. Gein, V. Ritleng, L. F. Veiros, M. J. Chetcuti, *Organometallics* **2011**, *30*, 3400–3411; c) A. M. Oertel, V. Ritleng, M. J. Chetcuti, L. F. Veiros, *J. Am. Chem. Soc.* **2010**, *132*, 13588–13589; d) V. G. Albano, L. Busetto, F. Marchetti, M. Monari, V. Zanotti, *J. Organomet. Chem.* **2002**, *649*, 64–69.
- [19] a) Q. Liu, H. Li, X. Zhao, S. Ge, M. Shi, G. Shen, Y. Zang, X. Wang, *Inorg. Chim. Acta* **2011**, *376*, 437–445; b) Q. Liu, A. Chen, X. Zhao, Y. Zang, X. Wu, X. Wang, J. Guo, *Cryst. Eng. Comm.* **2011**, *13*, 293–305; c) J. L. Portscher, H. C. Malinakova, *Org. Lett.* **2002**, *4*, 3679–3681; d) D. Emeljanenko, A. Peters, V. Vitske, E. Kaifer, H. Himmel, *Eur. J. Inorg. Chem.* **2010**, 4783–4789; e) C. Lee, Y. Chuang, C. Chiang, G. Lee, W. Liaw, *Inorg. Chem.* **2006**, *45*, 10895–10904; f) N. B. Pahor, S. Geremia, C. Lopez, L. Randaccio, E. Zangrando, *Inorg. Chem.* **1990**, *20*, 1043–1049; g) E. Zangrando, N. Bresciani-Pahor, L. Randaccio, *Organometallics* **1986**, *5*, 1938–1944; h) M. F. Summers, L. G. Marzilli, N. Bresciani-Pahor, L. Randaccio, *J. Am. Chem. Soc.* **1984**, *106*, 4478–4485; i) Y. Chang, K. Takeuchi, M. Wakioka, F. Ozawa, *Organometallics* **2015**, *34*, 1957–1962; j) D. Huang, L. Deng, J. Sun, R. H. Holm, *Inorg. Chem.* **2009**, *48*, 6159–6166.
- [20] a) R. A. Arthurs, C. J. Richards, *Org. Lett.* **2017**, *19*, 702–705; b) R. A. Arthurs, P. N. Horton, S. J. Coles, C. J. Richards, *Chem. Commun.* **2016**, *52*, 7024–7027.
- [21] a) E. J. Derrah, K. E. Giesbrecht, R. McDonald, L. Rosenberg, *Organometallics* **2008**, *27*, 5025–5032; b) M. I. Bruce, M. A. Buntine, K.

- Costuas, B. G. Ellis, J. Halet, P. J. Low, B. W. Skelton, A. H. White, *J. Organomet. Chem.* **2004**, 689, 3308–3326.
- [22] A. M. Oertel, V. Ritleng, L. Burr, M. J. Chetcuti, *Organometallics* **2011**, 30, 6685–6691.
- [23] W. Zarges, M. Marsch, K. Harms, G. Boche, *Angew. Chem., Int. Ed. Engl.* **1989**, 28, 1392–1394.
- [24] F. G. Bordwell, *Acc. Chem. Res.* **1988**, 21, 456–463.
- [25] R. G. Pearson, R. L. Dillon, *J. Am. Chem. Soc.* **1953**, 75, 2439–2443.
- [26] A. Panunzi, G. Roviello, F. Ruffo, *Inorg. Chem. Commun.* **2003**, 6, 1282–1286.
- [27] V. Y. Kukushkin, A. J. L. Pombeiro, *Inorg. Chim. Acta* **2005**, 358, 1–21.
- [28] a) J. Li, G. N. Khairallah, V. Steinmetz, P. Maitred, R. A. J. O’Hair, *Dalton Trans.* **2015**, 44, 9230–9240; b) T. Tsuda, T. Nakatsuka, T. Hirayama, T. Saegu, *J. Chem. Soc., Chem. Commun.* **1974**, 557–558.
- [29] M. Purzycki, W. Liu, G. Hilmersson, F. F. Fleming, *Chem. Commun.* **2013**, 49, 4700–4702.
- [30] M. Wieser, C. Missling, C. Robl, W. Beck, *J. Organomet. Chem.* **1994**, 479, 227–235.
- [31] a) T. Naota, A. Tannna, S. Kamuro, S.-I. Murahashi, *J. Am. Chem. Soc.* **2002**, 124, 6842–6843; b) J. Vela, S. Vaddadi, T. R. Cundari, J. M. Smith, E. A. Gregory, R. J. Lachicotte, C. J. Flaschenriem, P. L. Holland, *Organometallics* **2004**, 23, 5226–5239; c) R. Fu, J. E. Bercaw, J. A. Labinger, *Organometallics* **2011**, 30, 6751–6765; d) J. Fernández-Cestau, N. Giménez, E. Lalinde, P. Montaña, M. T. Moreno, S. Sánchez, *Organometallics* **2015**, 34, 1766–1778;

- e) B. M. Schmidt, J. T. Engle, M. Zhang, I. Babahan, C. J. Ziegler, L. Jia, *J. Organomet. Chem.* **2016**, *805*, 94–99.
- [32] a) W. Yi, J. Zhang, F. Zhang, Y. Zhang, Z. Chen, X. Zhou, *Chem. Eur. J.* **2013**, *19*, 11975–11983; b) L. Becker, V. V. Burlakov, P. Arndt, A. Spannenberg, W. Baumann, H. Jiao, U. Rosenthal, *Chem. Eur. J.* **2013**, *19*, 4230–4237; c) J. Zhao, S. Zhang, W. Zhang, Z. Xi, *Organometallics* **2012**, *31*, 8370–8374; d) J. Zhao, S. Zhang, W. Zhang, Z. Xi, *Organometallics* **2011**, *30*, 3464–3467.
- [33] C. C. Comanescu, V. M. Iluc, *Organometallics* **2015**, *34*, 4684–4692.
- [34] J. R. Fulton, S. Sklenak, M. W. Bouwkamp, R. G. Bergman, *J. Am. Chem. Soc.* **2002**, *124*, 4722–4737.
- [35] H. J. Heeres, A. Meetsma, J. H. Teuben, *Angew. Chem., Int. Ed. Engl.* **1990**, *29*, 420–422.
- [36] K. W. Henderson, A. R. Kennedy, D. J. MacDougall, *Inorg. Chem.* **2003**, *42*, 2736–2741.
- [37] N. A. Bailey, B. M. Higson, E. D. McKenzie, *J. Chem. Soc., Dalton Trans.* **1975**, 1105–1108.
- [38] W. Hiller, S. Frey, J. Strahle, G. Boche, W. Zarges, K. Harms, M. Marsch, R. Wollert, K. Dehnicke, *Chem. Ber.* **1992**, *125*, 87–92.
- [39] a) T. Naota, A. Tanna, S.-I. Murahashi, *J. Am. Chem. Soc.* **2000**, *122*, 2960–2961; b) T. Naota, A. Tanna, S. Kamuro, M. Hieda, K. Ogata, S. Murahashi, H. Takaya, *Chem. Eur. J.* **2008**, *14*, 2482–2498.
- [40] A. Ariafard, H. Ghari, Y. Khaledi, A. Hossein Bagi, T. S. Wierenga, M. G. Gardiner, A. J. Canty, *ACS Catal.* **2016**, *6*, 60–68.

- [41] J. Barker, N. D. R. Barnett, D. Barr, W. Clegg, R. E. Muhey, P. A. O'Neil, *Angew. Chem., Int. Ed. Engl.* **1993**, *32*, 1366–1368.
- [42] a) D. Förster, M. Nieger, D. Gudat, *Organometallics* **2011**, *30*, 2628–2631; b) L. Braun, G. Kehr, T. Blömker, R. Fröhlich, G. Erker, *Eur. J. Inorg. Chem.* **2007**, 3083–3090; c) I. Langlotz, M. Marsch, K. Harms, G. Boche, *Z. Kristallogr. - New Cryst. Struct.* **1999**, *214*, 509–510.
- [43] W. Qin, S. Long, A. Bongini, M. Panunzio, *Eur. J. Org. Chem.* **2015**, 3495–3505.
- [44] a) N. A. Foley, T. B. Gunnoe, T. R. Cundari, P. D. Boyle, J. L. Petersen, *Angew. Chem. Int. Ed.* **2008**, *47*, 726–730; b) D. J. Darensbourg, J. A. Joyce, A. Rheingold, *Organometallics* **1991**, *10*, 3407–3410.
- [45] L. Pauling, *The Nature of the Chemical Bond*, 3d ed., Cornell University Press, Ithaca, N.Y., **1960**.
- [46] a) I. L. Fedushkin, A. G. Morozov, V. A. Chudakova, G. K. Fukin, V. K. Cherkasov, *Eur. J. Inorg. Chem.* **2009**, 4995–5003; b) I. L. Fedushkin, A. G. Morozov, O. V. Rassadin, G. K. Fukin, *Chem. Eur. J.* **2005**, *11*, 5749–5757.
- [47] M. Henrion, A. M. Oertel, V. Ritleng, M. J. Chetcuti, *Chem. Commun.* **2013**, *49*, 6424–6426.
- [48] N. Ishio, Y. Nakamura, S. Okeya, *Bull. Chem. Soc. Jpn.* **1984**, *57*, 1012–1020.
- [49] M. Kujime, S. Hikichi, M. Akita, *Organometallics* **2001**, *20*, 4049–4060.
- [50] a) T. Naota, H. Taki, M. Mizuno, S.-I. Murahashi, *J. Am. Chem. Soc.* **1989**, *111*, 5954–5955; b) T. Naota, A. Tannna, S.-I. Murahashi, *Chem. Commun.* **2001**, 63–64.

- [51] G. L. Monica, M. A. Angaroni, G. A. Ardizzoia, *J. Organomet. Chem.* **1988**, *348*, 279–284.
- [52] a) G. L. Crocco, K. E. Lee, J. A. Gladysz, *Organometallics* **1990**, *9*, 2819–2831; b) G. L. Crocco, J. A. Gladysz, *J. Am. Chem. Soc.* **1985**, *107*, 4103–4104.
- [53] a) Y. Ohashi, *Crystallogr. Rev.* **2013**, *19*, 2–146; b) J.-P. Charland, W. M. Attia, L. Randaccio, L. G. Marzi, *Organometallics* **1990**, *9*, 1367–1375.
- [54] A. R. Ronzio, W. B. Cook, *Org. Synth.* **1944**, *24*, 6.
- [55] I. R. Baxendale, S. V. Ley, *J. Comb. Chem.* **2005**, *7*, 483–489.
- [56] a) M. R. Kopp, T. Krauter, A. Dashti-Mommertz, B. Neumuller, *Organometallics* **1998**, *17*, 4226–4231; b) M. R. Kopp, B. Neumuller, *Z. Anorg. Allg. Chem.* **1999**, *625*, 1246–1248; c) M. R. Kopp, B. Neumuller, *Z. Anorg. Allg. Chem.* **1999**, *625*, 739–745.
- [57] L. Becker, A. Spannenberg, P. Arndt, U. Rosenthal, *Acta Crystallogr., Sect. E: Struct. Rep. Online* **2015**, *71*, m219–m220.
- [58] E. Tapuhi, W. P. Jencks, *J. Am. Chem. Soc.* **1982**, *104*, 5758–5765.
- [59] A. Castonguay, D. M. Spasyuk, N. Madern, A. L. Beauchamp, D. Zargarian, *Organometallics* **2009**, *28*, 2134–2141.
- [60] S. Lapointe, D. Zargarian, *Dalton Trans.* **2016**, *45*, 15800–15810.
- [61] M. Kopeć, P. Kryś, R. Yuan, K. Matyjaszewski, *Macromolecules* **2016**, *49*, 5877–5883.
- [62] B. P. Carrow, K. Nozaki, *J. Am. Chem. Soc.* **2012**, *134*, 8802–8805.
- [63] F. F. Fleming, *Nat. Prod. Rep.* **1999**, *16*, 597–606.

- [64] F. F. Fleming, L. Yao, P. C. Ravikumar, L. Funk, B. C. Shook, *J. Med. Chem.* **2010**, *53*, 7902–7917.
- [65] P. Kisanga, D. McLeod, B. D'Sa, J. Verkade, *J. Org. Chem.* **1999**, *64*, 3090–3094.
- [66] M. B. Cid, S. Duce, S. Morales, E. Rodrigo, J. L. Garcia Ruano, *Org. Lett.* **2010**, *12*, 3586–3589.
- [67] Y. Fan, G. Du, W. Sun, W. Kang, L. He, *Tetrahedron Lett.* **2012**, *53*, 2231–2233.
- [68] A. H. Mermerian, G. C. Fu, *Angew. Chem. Int. Ed.* **2005**, *44*, 949–952.
- [69] L. Wu, J. F. Hartwig, *J. Am. Chem. Soc.* **2005**, *127*, 15824–15832.
- [70] Z. Jiao, K. W. Chee, J. S. Zhou, *J. Am. Chem. Soc.* **2016**, *138*, 16240–16243.
- [71] J. Schranck, M. Burhardt, C. Bornschein, H. Neumann, T. Skrydstrup, M. Beller, *Chem. Eur. J.* **2014**, *20*, 9534–9538.
- [72] L. Yin, M. Kanai, M. Shibasaki, *J. Am. Chem. Soc.* **2009**, *131*, 9610–9611.
- [73] Y. Suto, R. Tsuji, M. Kanai, M. Shibasaki, *Org. Lett.* **2005**, *7*, 3757–3760.
- [74] Y. Kawato, N. Kumagai, M. Shibasaki, *Chem. Commun.* **2013**, *49*, 11227–11229.
- [75] M. Kondo, M. Sugimoto, S. Nakamura, *Chem. Commun.* **2016**, *52*, 13604–13607.
- [76] L. Fan, O. V. Ozerov, *Chem. Commun.* **2005**, 4450–4452.
- [77] M. Tucker, Honours thesis, University of Tasmania (Hobart Tasmania), **2014**.
- [78] E. A. Kantchev, C. J. O'Brien, M. G. Organ, *Angew. Chem. Int. Ed.* **2007**, *46*, 2768–2813

Chapter 2: Ni POCOP complexes

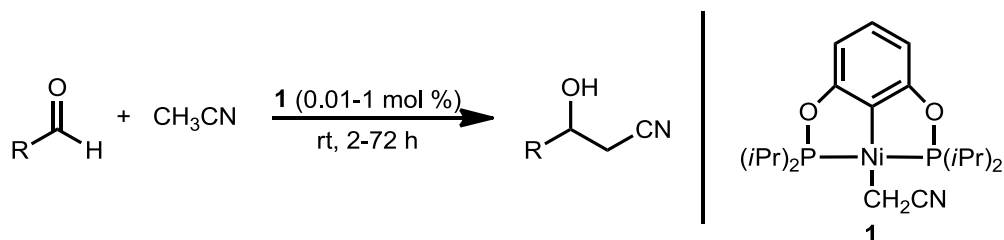
2.1 Introduction to POCOP Complexes:

The phosphine-based pincer complexes of the type PCP have been studied extensively and have been shown to have applications in various areas of catalysis including Mizoroki–Heck and Suzuki–Miyaura coupling reactions.^[1] POCOP style complexes were developed in 2000^[2] after noticing that phosphite ligands were much more active in Mizoroki–Heck reactions than the corresponding phosphine ligands.^[3] These replaced the methylene linker of the PCP complexes with an electron withdrawing alkoxy group substituted to the phosphine ligand. These complexes were shown to be effective in the Mizoroki–Heck reaction and can be synthesised in two steps from commercially available starting materials in an 86% overall yield.^[2]

Since then the POCOP complexes have found applications in a wide variety of catalytic applications. These include Kharasch additions,^[4] hydrosilylation of aldehydes,^[5] homocoupling of benzyl halides,^[6] dimerisation of terminal alkynes,^[7] aromatic C–H borylation^[8] and alkane dehydrogenation.^[9]

In addition to this, α -cyanocarbanions have been proposed as an intermediate for a number of POCOP catalysis reactions. This includes the hydroamination reaction discussed in Chapter 1^[10] and Michael addition reactions.^[4] However, at this stage, no DFT calculations have been performed on these complexes to support the bonding mode of the intermediate.

The most interesting work from the perspective of this study is work published by Guan *et al.*^[11] featuring a preformed α -cyanocarbanion complex in the catalytic formation of β -hydroxynitriles (Scheme 2.1). A discussion on the mechanism proposed by these authors is detailed in Chapter 1.



Scheme 2.1: Synthesis of β -hydroxynitrile compounds via a Ni-POCOP catalyst.

2.2 Results and Discussion:

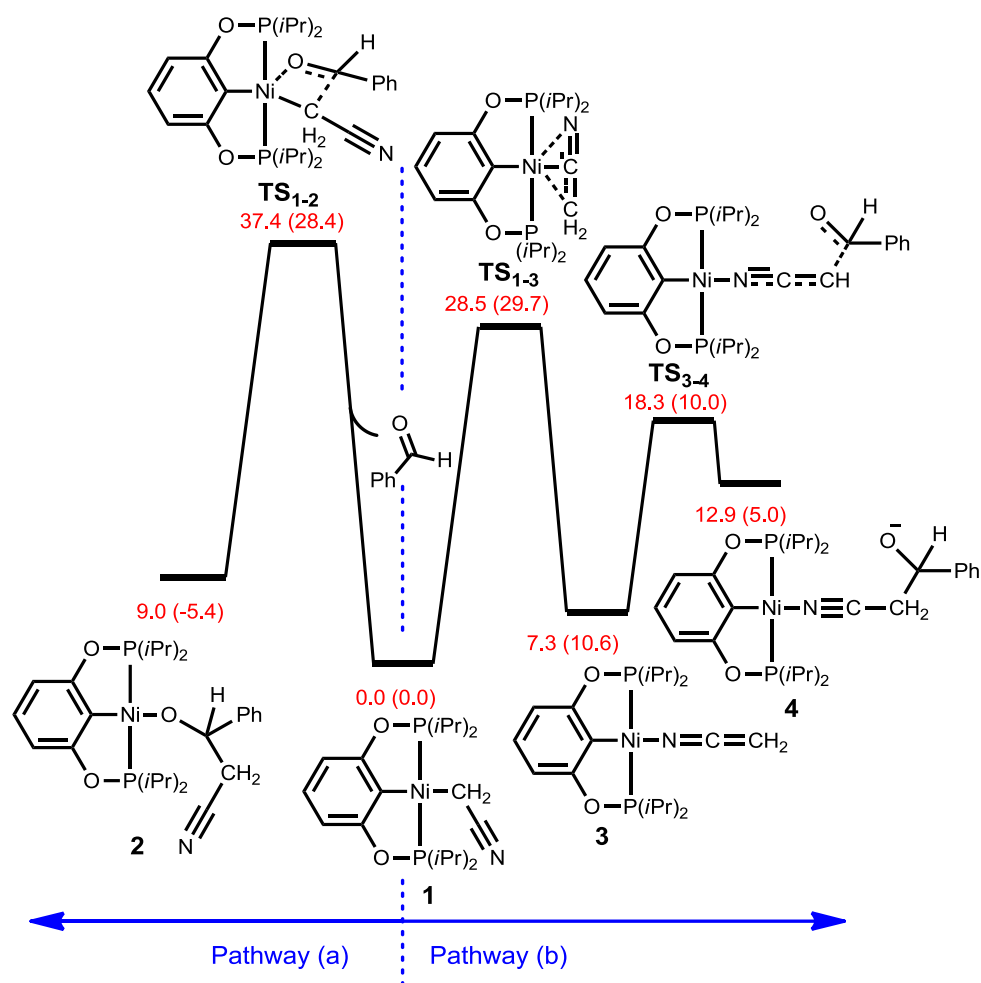
2.2.1 DFT Calculations on Guan's Catalysis:

Since the work performed by Guan and co-workers, collaborators Alireza Ariafard and Allan Canty performed DFT studies to better understand the reaction and the impact of steric and electronic variations of the supporting ligands had on the catalytic cycle. This information was vital for the subsequent development of complexes presented later in this thesis and is thus discussed in detail here. The DFT methodology will not be discussed in detail but more information can be found in the paper.^[12]

Guan proposed that the $-\text{CH}_2\text{CN}$ ligated complex was the active catalyst while other similar reactions proposed the isomerised ligand of $-\text{NCCH}_2$ as the active catalyst.^[13] Therefore, the energies of the two were compared for the addition of the aldehyde.

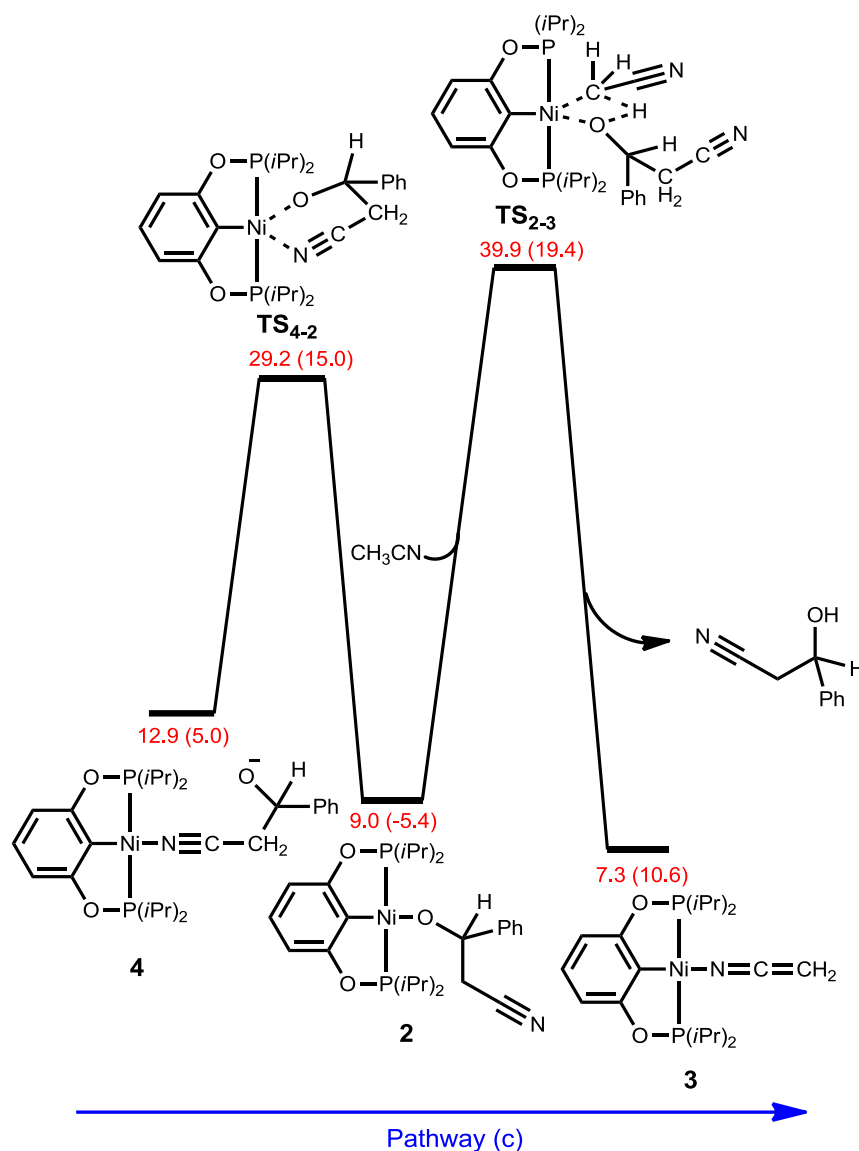
Two initial mechanisms were investigated for the insertion of the aldehyde. Pathway (a) was that proposed by Guan *et al.* with complex **1** representing the active catalyst and **2** being the intermediate. However, the energy for TS_{1-2} makes this path not favoured relative to the alternative pathways investigated. Thus, an alternative mechanism (b) was proposed. The proposed mechanism involves the intramolecular slippage process as described by Naota *et al.*^[14] (discussed in detail in chapter 1.3.2) that transforms the ligand from bonding mode **I** to **III**. This is

followed by the addition of the alkoxide to the α -carbon to form the remote alkoxide intermediate **4** (Scheme 2.2).



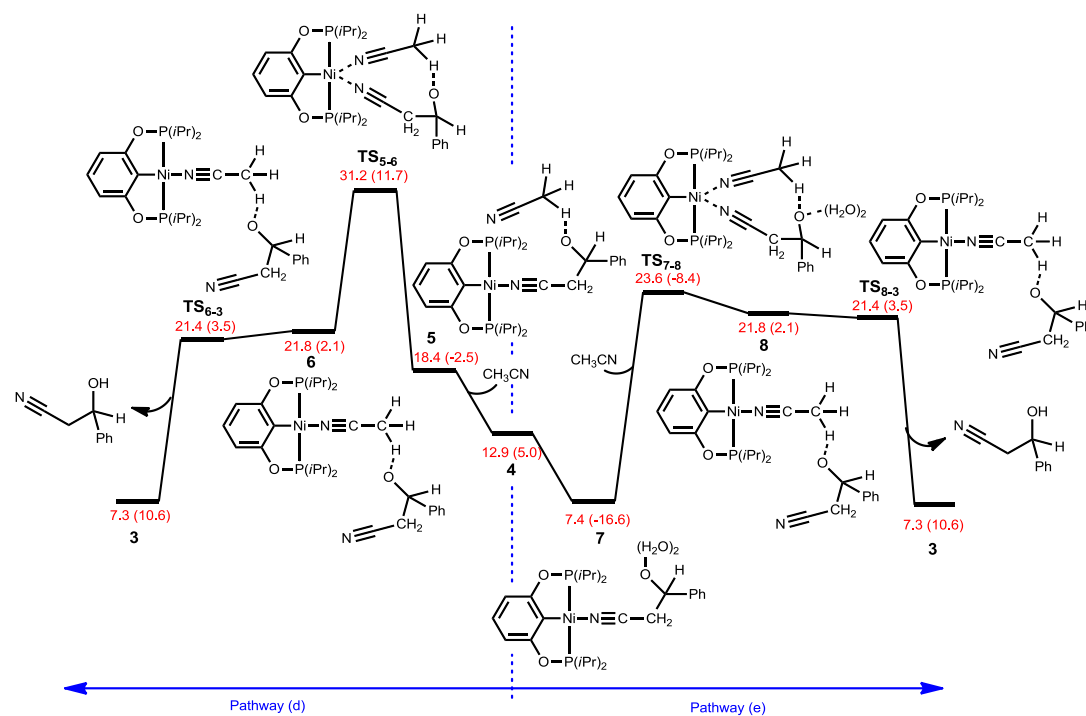
Scheme 2.2: Computed energy profile for pathway a and b of proposed mechanism.

As **2** is a common proposed intermediate by Guan and related catalysis papers^[13c, 15] the catalytic cycle pathway (c) was analysed with the rearrangement from the N-bound remote alkoxide intermediate (**4**) to the proposed O-bound alkoxide intermediate **2**. However, the energy for the TS_{2-3} makes this path unfeasible. Thus, it appears that the O-bound alkoxide is not an intermediate in the reaction and that the reaction instead proceeds by the N-bound remote alkoxide intermediate **4** (Scheme 2.3).



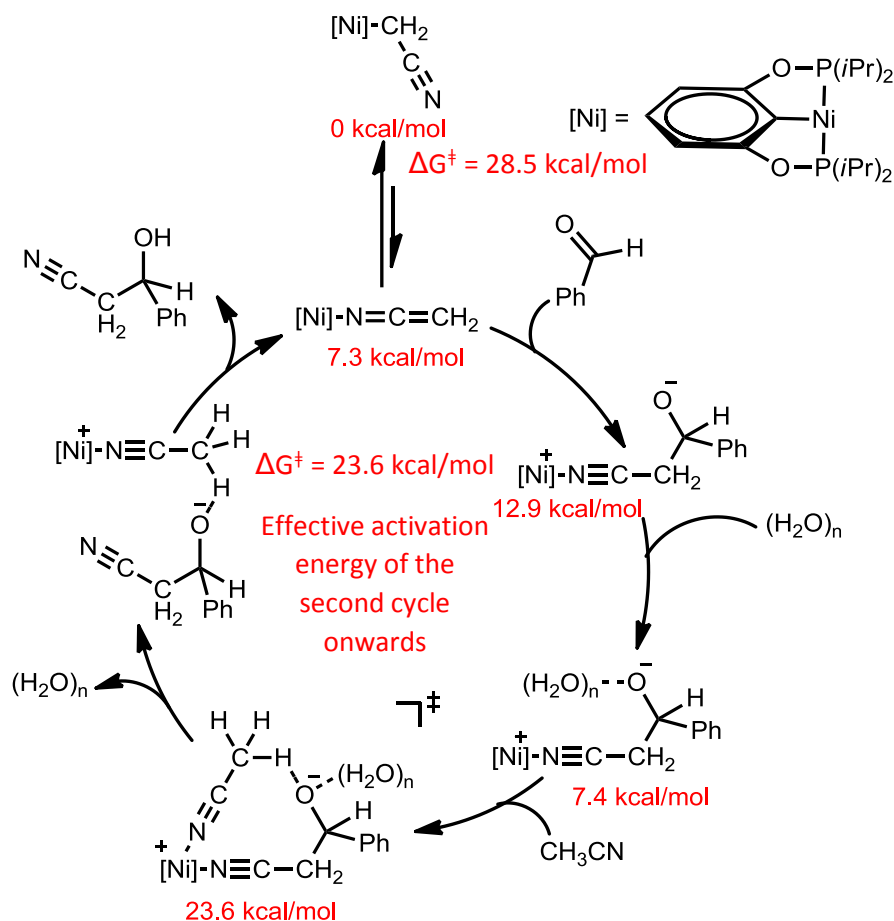
Scheme 2.3: Computed energy profile for pathway c of proposed mechanism.

The initial calculations were performed for the transformation of the alkoxide intermediate to the active ketenimine catalyst *via* pathway (d). As Guan *et al.* suggested that they did not scrupulously exclude water from the reaction, the calculations were also performed with the incorporation of a H₂O dimer. This was shown to reduce the energy of the five coordinate transition state **TS₅₋₆** and **TS₇₋₈** from 31.2 to 23.6 kcal/mol. The calculations then showed a reformation of the active catalyst **3** and the β -hydroxynitrile product (Scheme 2.4).



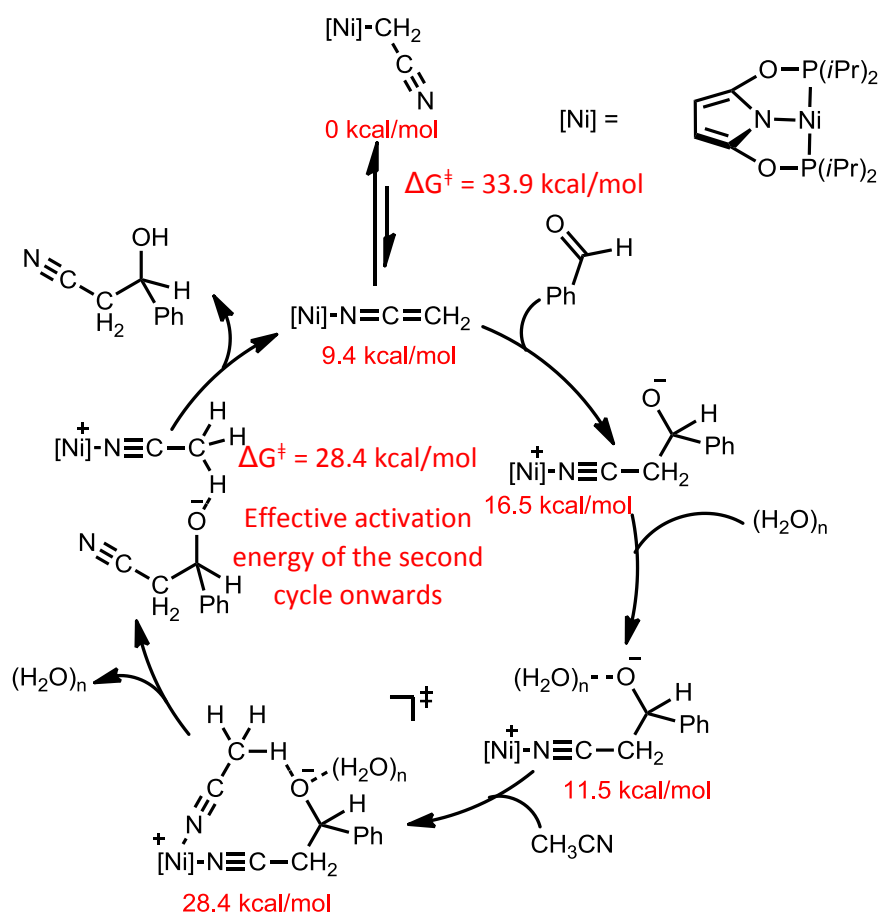
Scheme 2.4: Computed energy profile for pathway d and e of proposed mechanism.

Thus, the overall catalytic cycle is proposed below. An activation energy of 28.5 kcal/mol for the first formation of the product was calculated, however, the effective activation energy for the second cycle onwards is 23.6 kcal/mol. This is because the activation energy of 28.5 kcal/mol is required to form the active catalyst however, this complex is reformed at the end of the catalytic cycle and therefore TS_{7-8} is the highest energy for subsequent cycles (Scheme 2.5).



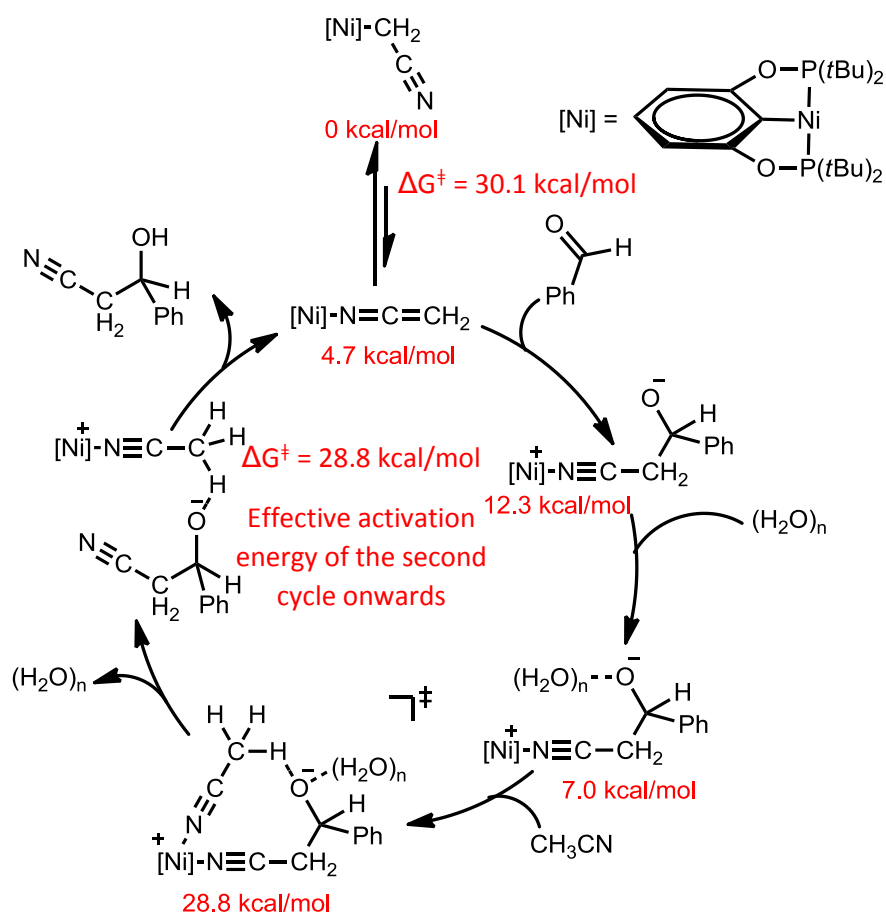
Scheme 2.5: Catalytic cycle proposed for the formation of β -hydroxynitriles using catalyst 1.

Steric and electronic influences of the ligand on the activation energy of the catalytic cycle were then investigated by modification of the POCOP catalyst to give insight into some of the important characteristics of these complexes. The first modification performed was changing the central phenyl ring to a pyrrole ring. Due to the weaker *trans* influence the energetics for both the intramolecular isomerisation and the five-coordinate transition state is higher than that observed for the corresponding phenyl ring (Scheme 2.6).



Scheme 2.6: Catalytic cycle when central phenyl is replaced with a pyrrole.

The catalytic cycle was also modified to look at the effect of increasing the steric bulk to *t*Bu from *i*Pr. When Guan *et al.* used the corresponding *t*Bu ligand no conversion was observed. The calculations indicate that the 5-coordinate transition state energy is increased to 28.8 kcal/mol, which may account for the observation that no reaction was observed (Scheme 2.7).^[11]



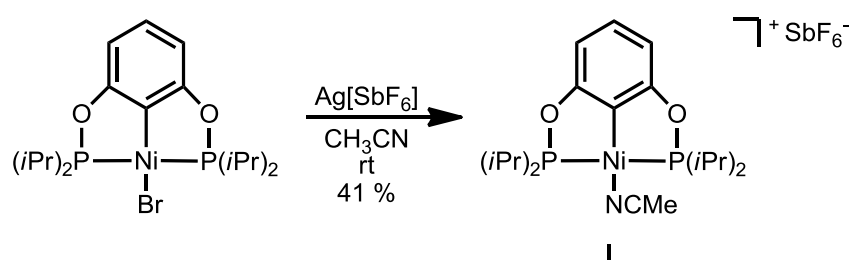
Scheme 2.7: Catalytic cycle when the steric bulk is increased from *i*Pr to *t*Bu.

The important conclusions from the DFT calculations performed which may assist in understanding the effect that the pincer ligand has on the catalytic cycle are summarised below;

- The C-bound isomer is not the active catalyst and instead the N-bound catalyst is the active catalyst.
- The *trans* donor effect of the phenyl ring is important in lowering the energy of the transition state of the isomerisation to the N-bound active catalyst and the 5-coordinate transition state.
- Due to the presence of the 5-coordinate transition state, increasing the steric bulk to a *t*Bu ligand prevents the reaction from proceeding.

2.2.2 Attempted Synthesis of $[\{2,6-(iPr_2PO)_2C_6H_3\}Ni(CH_2CN)]:$

A series of catalytically relevant Ni POCOP complexes were synthesised to compare their catalytic activity to previously known catalysts (as discussed in Chapter 5). $[\{2,6-(iPr_2PO)_2C_6H_3\}Ni(NCMe)][SbF_6]$ (**I**) was synthesised following a modified published procedure^[10] by reacting $[\{2,6-(iPr_2PO)_2C_6H_3\}NiBr]$ and $Ag[SbF_6]$ in CH_3CN at room temperature for 17 h with the exclusion of light (Scheme 2.8). The structure was confirmed by X-ray crystallography and supported by 1H and ^{13}C NMR spectroscopy with a 1H NMR resonance at 2.20 ppm consistent with the CH_3 from the formation of the $-NCMe$ ligand.



Scheme 2.8: Synthesis of $[\{2,6-(iPr_2PO)_2C_6H_3\}Ni(NCMe)][SbF_6]$ (**I**).

The metrics of the crystal structure of $[\{2,6-(iPr_2PO)_2C_6H_3\}Ni(NCMe)][SbF_6]$ is consistent with the previously published $[\{2,6-(iPr_2PO)_2C_6H_3\}Ni(NCMe)][OTf]$ complex which had Ni–C bond distances of 1.881(2)–1.883(2) Å and Ni–N bond distances of 1.874(2)–1.884(2) Å (Figure 2.1).^[4]

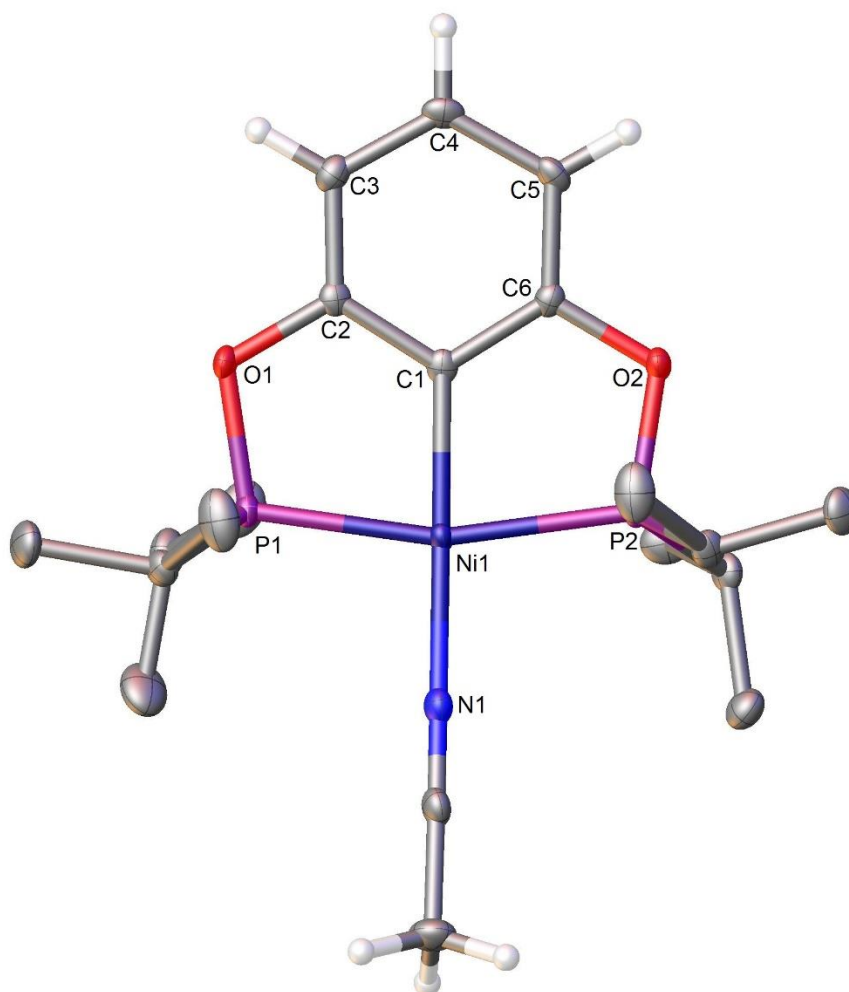


Figure 2.2: X-ray molecular structure of cation $[(2,6-(iPr_2PO)_2C_6H_3)Ni(NCMe)]^+$ of **I**.

Thermal ellipsoids are shown at the 50 % probability level. Only one of the three $[(2,6-(iPr_2PO)_2C_6H_3)Ni(NCMe)]$ complexes in the asymmetric unit is displayed and all phosphine substituent hydrogen atoms and $[SbF_6]$ counter anions are removed for clarity. Range of selected bond lengths (Å) and angles (°): Ni–C 1.885(3)–1.888(3), Ni–P 2.1635(8)–2.1755(8), Ni–N 1.876(2)–1.884(2), P–Ni–P 162.92(3)–164.32(3), N–Ni–P 95.34(7)–101.30(7), N–Ni–C 173.89(11)–174.01(11), C–Ni–P 81.81(8)–82.24(8).

One of the three crystallographically independent complexes in the lattice had a distorted geometry with N–Ni–P angles of 95.34(7) and 101.30(7) ° in contrast to 97.32(7)–98.70(7) ° observed for the other two complexes. This is consistent with a

distortion of the –NCMe ligand due to the steric bulk of the *i*Pr₂P substituent (Figure 2.2).

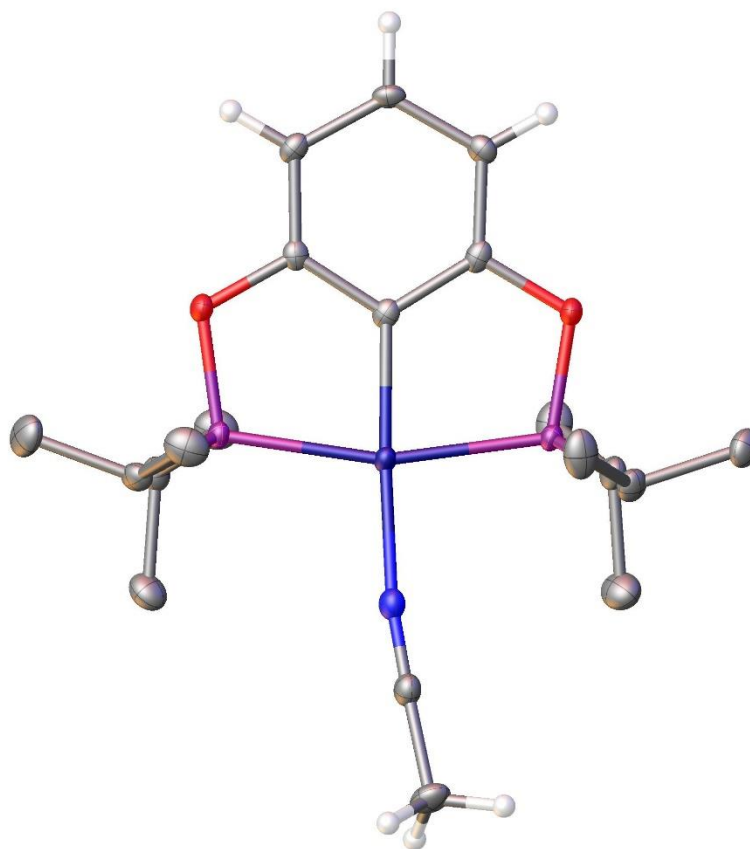


Figure 2.2: X-ray molecular structure of cation [(2,6-(*i*Pr₂PO)₂C₆H₃)Ni(NCMe)]⁺ of **1**.

Thermal ellipsoids are shown at the 50 % probability level. The one complex of three in the lattice with a distorted geometry is shown.

A number of approaches were explored in an attempt to prepare Guan's catalyst [(2,6-(*i*Pr₂PO)₂C₆H₃)Ni(CH₂CN)] (**1**). The previously reported two synthetic methods were attempted under modified conditions.^[11] **1** was reported to be an air stable complex both as a solid and as a solution in toluene.

[(2,6-(*i*Pr₂PO)₂C₆H₃)Ni(NCMe)][SbF₆] was reacted with [LiN(SiMe₃)₂] in THF. When the ¹H NMR spectrum was recorded in CDCl₃ the resonances were consistent with [(2,6-(*i*Pr₂PO)₂C₆H₃)NiCl] indicating decomposition in the presence of CDCl₃. Similarly, when the product was purified on the bench top the product decomposed

from one major product to various products by ^1H NMR spectroscopy. When the purification was performed in a glove box, various products were observed by ^1H NMR spectroscopy and thus purification was not possible. An alternative method was pursued in a desire to synthesise the reported complex.

Alternatively, $[\{2,6-(i\text{Pr}_2\text{PO})_2\text{C}_6\text{H}_3\}\text{Ni}(\text{NCMe})][\text{SbF}_6]$ was reacted with NaOH in CH_3CN . Although initially a yellow powder was observed, when the powder was left standing over the weekend exposed to air the product had decomposed to a green solid with multiple products observed by ^1H NMR spectroscopy. Thus this synthesis method, discussed further in Chapter 3 used for the formation of the bis(NHC)– CH_2CN complexes is not suitable here.

$[\{2,6-(i\text{Pr}_2\text{PO})_2\text{C}_6\text{H}_3\}\text{NiBr}]$ was reacted with *in situ* generated $[\text{LiCH}_2\text{CN}]$ in THF however recrystallisation attempts did not yield the desired product as judged by ^1H NMR spectroscopy. Similarly, $[\{2,6-(i\text{Pr}_2\text{PO})_2\text{C}_6\text{H}_3\}\text{NiCl}]$ was reacted with *in situ* generated $[\text{LiCH}_2\text{CN}]$ in THF forming an inseparable mixture.

Due to the difficulty in synthesising the desired $[\{2,6-(i\text{Pr}_2\text{PO})_2\text{C}_6\text{H}_3\}\text{Ni}(\text{CH}_2\text{CN})]$ (**1**) catalyst, $[\{2,6-(i\text{Pr}_2\text{PO})_2\text{C}_6\text{H}_3\}\text{NiCl}]$ and $[\{2,6-(i\text{Pr}_2\text{PO})_2\text{C}_6\text{H}_3\}\text{NiBr}]$ were both reacted with NaOH in THF in an attempt to form $[\{2,6-(i\text{Pr}_2\text{PO})_2\text{C}_6\text{H}_3\}\text{Ni}(\text{OH})]$ following a modified published procedure developed for the related PCP complexes.^[16] This complex would have been used for the synthesis of β -hydroxynitriles as an alternative to **1**, however, a range of products were observed by ^1H NMR spectroscopy and purification was not possible.

2.3 Experimental:

2.3.1 General Considerations:

All air sensitive reactions were performed under an atmosphere of high purity argon using standard Schlenk techniques. Glassware was heated under vacuum and back-filled with argon to ensure the exclusion of oxygen and moisture in the

reactions. $\text{Ag}[\text{SbF}_6]$ was purchased from Sigma-Aldrich and used as received. NaOH was purchased from Chem Supply and dried under vacuum at $200\text{ }^\circ\text{C}$. $[\text{LiN}(\text{SiMe}_3)_2]$ (1.0 M in THF) was purchased from Aldrich and stored in an ampoule. Anhydrous CH_3CN was obtained by passage through an Innovative Technologies Solvent Purifier and stored in an ampoule over 3 \AA molecular sieves. All other anhydrous solvents were obtained by passage through an Innovative Technologies Solvent Purifier and stored in an ampoule over a mirror of sodium. $[\{2,6-(i\text{Pr}_2\text{PO})_2\text{C}_6\text{H}_3\}\text{NiBr}]$,^[4] $[\{2,6-(i\text{Pr}_2\text{PO})_2\text{C}_6\text{H}_3\}\text{NiCl}]$ ^[4] and $[\text{LiCH}_2\text{CN}]$ ^[11] were all synthesised according to literature procedures.

2.3.2 Instrumentation:

NMR spectroscopic studies were carried out on a Bruker Avance III HD 400 MHz Wide Bore Spectrometer with a 5 mm BBFO probe at room temperature (293 K) or $120\text{ }^\circ\text{C}$ (393 K) where indicated or a Bruker Avance III HD 600 MHz spectrometer with a 5 mm TCI-cyprobeat 300 K, in $\text{DMSO-}d_6$. $\text{DMSO-}d_6$ was used as received. ^1H NMR spectra were obtained at 399.58 MHz, ^{13}C NMR spectra were recorded at 150.89 MHz and ^{31}P NMR spectra were recorded at 161.75 MHz. ^1H NMR spectra were referenced to the residual ^1H resonance of the residual solvent peak while ^{13}C NMR spectra were referenced to a deuterated ^{13}C resonance.

Elemental analyses were conducted by Dr. Thomas Rodemann at the Central Science Laboratory at the University of Tasmania using a Carlo Erba EA1108 Elemental Analyser.

X-ray crystallographic data for **I** was collected at $-173\text{ }^\circ\text{C}$ on crystals mounted on a Hampton Scientific cryoloop on a Bruker AXS D8 Quest with a $\text{Cu K}\alpha$ source. The structure was solved by direct methods with SHELXT, refined using full-matrix least-squares routines against F^2 with SHELXL-97,^[17] and visualised using Olex2.^[18] All non-hydrogen atoms were refined anisotropically. All hydrogen atoms were placed in calculated positions and refined using a riding model with fixed C–H distances of

0.95 Å (sp^2CH), 1.00 Å (sp^3CH) and 0.98 Å (CH_3). The thermal parameters of all hydrogen atoms were estimated as $U_{iso}(H) = 1.2U_{eq}(C)$, except for CH_3 where $U_{iso}(H) = 1.5U_{eq}(C)$. Cif file available on request.

2.3.3 Preparation of $[\{2,6-(iPr_2PO)_2C_6H_3\}Ni(NCMe)][SbF_6]$ (I):

A modified published procedure was employed.^[10] $[\{2,6-(iPr_2PO)_2C_6H_3\}NiBr]$ (0.098 g, 2.04×10^{-4} mol), $Ag[SbF_6]$ (0.087 g, 2.54×10^{-4} mol) and CH_3CN (5 mL) were combined in a Schlenk flask and stirred overnight at room temperature with the exclusion of light for 17 h. CH_3CN was removed under vacuum and the product was dissolved in CH_3CN and filtered through a glass fibre filter pipette. The ensuing solid was then recrystallised *via* vapour diffusion of diethyl ether into a near saturated solution in CH_3CN yielding orange crystals (41 % yield, 0.057 g).

1H NMR (400 MHz, d_6 -DMSO): δ 7.03 (t, 1H, $J = 8.0$ Hz, p -CH), 6.44 (d, 2H, $J = 8.0$ Hz, m -CH), 2.55–2.58 (m, 4H, iPr CH), 2.20 (d, 3H, $J = 2.5$ Hz, NCMe), 1.28–1.40 ppm (m, 24H, iPr CH_3).

^{13}C NMR (150 MHz, d_6 -DMSO): δ 169.0 (t, $J_{PC} = 8.9$ Hz, o -C), 131.0 (p -CH), 122.6 (bs, as defined by HMBC, NCMe), 117.8 (bs, confirmed by HMBC, Ni–C), 106.3 (t, $J_{PC} = 5.7$ Hz, m -CH), 28.1 (t, $J_{PC} = 11.9$ Hz, iPr CH), 17.7 (iPr CH_3), 16.9 (iPr CH_3), 2.2 ppm (NCMe).

^{31}P NMR (161.8 MHz, d_6 -DMSO): δ 186.7 ppm

Anal. Calc. for $C_{20}NH_{34}O_2P_2NiSbF_6$: C, 35.49; H, 5.06; N, 2.07; Found: C, 35.01; H, 5.21; N, 1.89 %

2.4 References:

- [1] M. E. v. d. Boom, D. Milstein, *Chem. Rev.* **2003**, *103*, 1759–1792.
- [2] D. Morales-Morales, C. Grause, K. Kasaoka, R. Redon, R. E. Cramer, C. M. Jensen, *Inorg. Chim. Acta* **2000**, *300–302*, 958–963.
- [3] M. Beller, A. Zapf, *Synlett.* **1998**, 792–793.
- [4] V. Pandarus, D. Zargarian, *Organometallics* **2007**, *26*, 4321–4334.
- [5] S. Chakraborty, J. A. Krause, H. Guan, *Organometallics* **2009**, *28*, 582–586.
- [6] T. Chen, L. Yang, L. Li, K.-W. Huang, *Tetrahedron* **2012**, *68*, 6152–6157.
- [7] C. J. Pell, O. V. Ozerov, *ACS Catal.* **2014**, *4*, 3470–3480.
- [8] L. P. Press, A. J. Kosanovich, B. J. McCulloch, O. V. Ozerov, *J. Am. Chem. Soc.* **2016**, *138*, 9487–9497.
- [9] Y. Zhang, H. Fang, W. Yao, X. Leng, Z. Huang, *Organometallics* **2016**, *35*, 181–188.
- [10] A. Castonguay, D. M. Spasyuk, N. Madern, A. L. Beauchamp, D. Zargarian, *Organometallics* **2009**, *28*, 2134–2141.
- [11] S. Chakraborty, Y. J. Patel, J. A. Krause, H. Guan, *Angew. Chem. Int. Ed.* **2013**, *52*, 7523–7526.
- [12] A. Ariafard, H. Ghari, Y. Khaledi, A. Hossein Bagi, T. S. Wierenga, M. G. Gardiner, A. J. Canty, *ACS Catal.* **2016**, *6*, 60–68.
- [13] a) L. Fan, O. V. Ozerov, *Chem. Commun.* **2005**, 4450–4452; b) M. Kondo, M. Sugimoto, S. Nakamura, *Chem. Commun.* **2016**, *52*, 13604–13607; c) Y. Suto, R. Tsuji, M. Kanai, M. Shibasaki, *Org. Lett.* **2005**, *7*, 3757–3760.

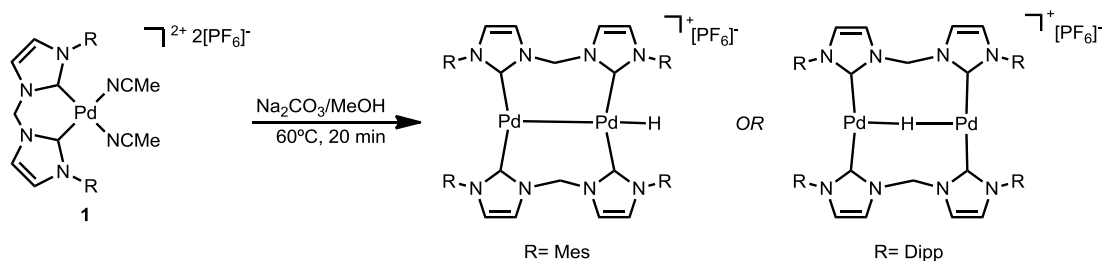
- [14] a) T. Naota, A. Tanna, S. Kamuro, S. Murahashi, *J. Am. Chem. Soc.* **2002**, *124*, 6842–6843; b) T. Naota, A. Tanna, S. Kamuro, M. Hieda, K. Ogata, S. Murahashi, H. Takaya, *Chem. Eur. J* **2008**, *14*, 2482–2498.
- [15] a) N. Kumagai, S. Matsunaga, M. Shibasaki, *J. Am. Chem. Soc.* **2004**, *126*, 13632–13633; b) N. Kumagai, S. Matsunaga, M. Shibasaki, *Chem. Commun.* **2005**, 3600–3602.
- [16] J. Cámpora, P. Palma, D. d. Río, E. Álvarez, *Organometallics* **2004**, *23*, 1652–1655.
- [17] G. M. Sheldrick, in *SHELX97, Programs for Crystal Structure Analysis*, Universität Göttingen: Germany, **1998**.
- [18] O. V. Dolomanov, L. J. Bourhis, R. J. Gildea, J. A. K. Howard, H. Puschmann, *J. Appl. Cryst.* **2009**, *42*, 339–341.

Chapter 3: Synthesis of bis(NHC) α -Cyanocarbanion Complexes

Complexes

3.1 Introduction to bis(NHC) α -Cyanocarbanion Complexes:

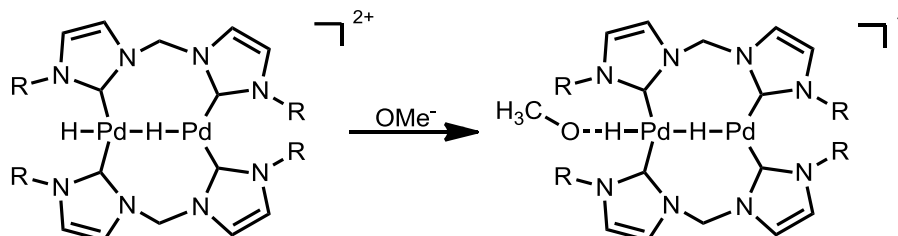
Bis(NHC) (bis *N*-heterocyclic carbene) complexes of type **1** have been shown to be active in the copolymerisation of CO and ethene to form polyketones.^[1] However, the yields and TON are much lower than that observed with the comparable bisphosphine palladium(II) catalysts used for the previously commercialised Shell process.^[2] Thus, previous work by the Gardiner group studied these complexes under catalytically relevant conditions to understand if the performance of these catalysts can be improved. Reacting the [bis(NHC)Pd(NCMe)₂][PF₆]₂ complex (**1**) with Na₂CO₃ in MeOH led to the generation of two novel Pd₂(I) hydride species (Scheme 3.1).^[3]



Scheme 3.1: Synthesis of Pd₂(I) hydride species under catalytically relevant conditions.

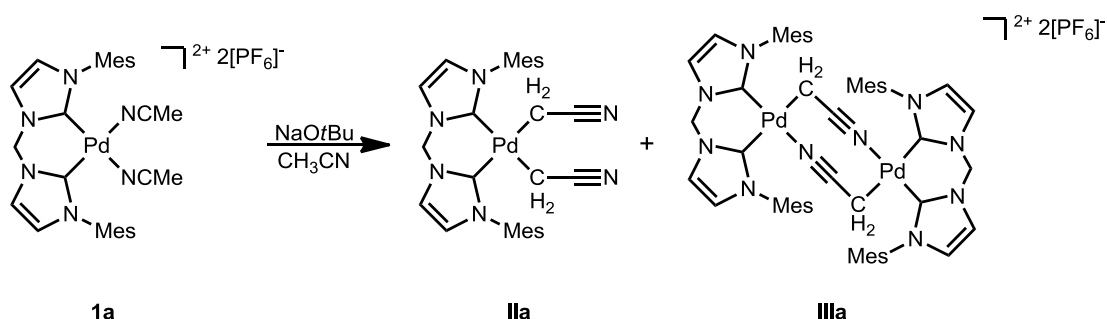
In the initial DFT calculations of the reaction in Scheme 3.1 a key proposed reaction step was the abstraction and reductive elimination of a hydride from Pd₂(II) dihydride intermediate by methoxide (Scheme 3.2) yielding the observed Pd₂(I) hydride complexes. Palladium(II) hydride species have been proposed as intermediates for the synthesis of polyketones,^[2] however, they have been very infrequently observed under catalytically relevant conditions. Attempts were made to

trap some of the reactive Pd(II) hydride intermediates via the reaction of **1** with a more sterically hindered alkoxide and the corresponding alcohol as a solvent.^[4]



Scheme 3.2: Deprotonation and reductive elimination step of the mechanism from the dipalladium(II) hydride complex to the dipalladium(I) hydride complex.

During this work,^[4] an unexpected product was observed when the solvent was changed from the corresponding alcohol of the base to CH_3CN due to the practical issues of the melting point of $t\text{BuOH}$ being $25\text{ }^\circ\text{C}$. When **1a**, NaOtBu and CH_3CN were reacted, the deprotonation of the acetonitrile ligand was observed forming two different complexes (Scheme 3.3). These two complexes are related; complex **IIa** involves two deprotonated acetonitrile molecules per Pd bis(NHC) motif, while complex **IIIa** is a dinuclear complex with a 1:1 ratio of the deprotonated acetonitrile molecule and Pd bis(NHC) motif. These complexes were shown to exhibit bonding



Scheme 3.3: Synthesis of bis(NHC) supported α -cyanocarbanion complexes of different binding modes.

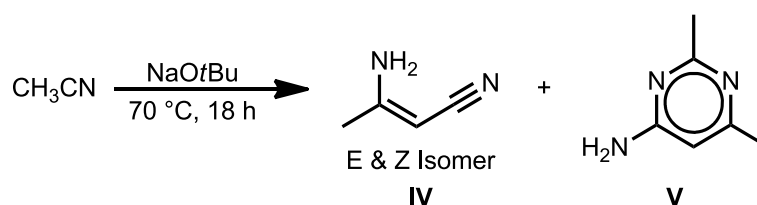
modes **I** and **II** (See Figure 1.11, Chapter 1) by X-ray crystallography but were not further characterised prior to this project commencing (bonding modes are discussed in depth in the introduction in Section 1.3).

Interest in further studying these complexes was prompted by their potential catalytic applications in the formation of β -hydroxynitriles^[5] and to understand more about the unexpected synthesis of these complexes given the high pK_a of acetonitrile. With a pK_a of 31.3 in DMSO^[6] and 25 in water,^[7] acetonitrile was not expected to readily react with NaOtBu under these conditions.

3.2 Results and Discussion:

3.2.1 Synthesis of $\{[(\text{MesIm})_2\text{CH}_2]\text{Pd}(\text{CH}_2\text{CN})_2\}$ (**IIa**) and $\{[(\text{MesIm})_2\text{CH}_2]\text{Pd}(\mu\text{-CH}_2\text{CN})_2\}[\text{PF}_6]_2$ (**IIIa**):

The use of NaOtBu for the synthesis of **IIa** and **IIIa** was identified as an issue due to the formation of an unexpected by-product. A background reaction was observed when NaOtBu was stirred with CH₃CN at 70°C for 16 h yielding three products: the *E* & *Z* isomer of 3-aminocrotononitrile (**IV**) and 4-amino-2,6-dimethylpyrimidine (**V**) (Scheme 3.4). The formation of **IV** was supported by ¹H NMR spectroscopy which displayed resonances at 4.85 and 4.99 ppm consistent with the formation of the amine and previous literature values.^[8] The ¹H NMR resonance at 6.07 ppm supported the formation of **V** and was consistent with previous literature reports.^[9]

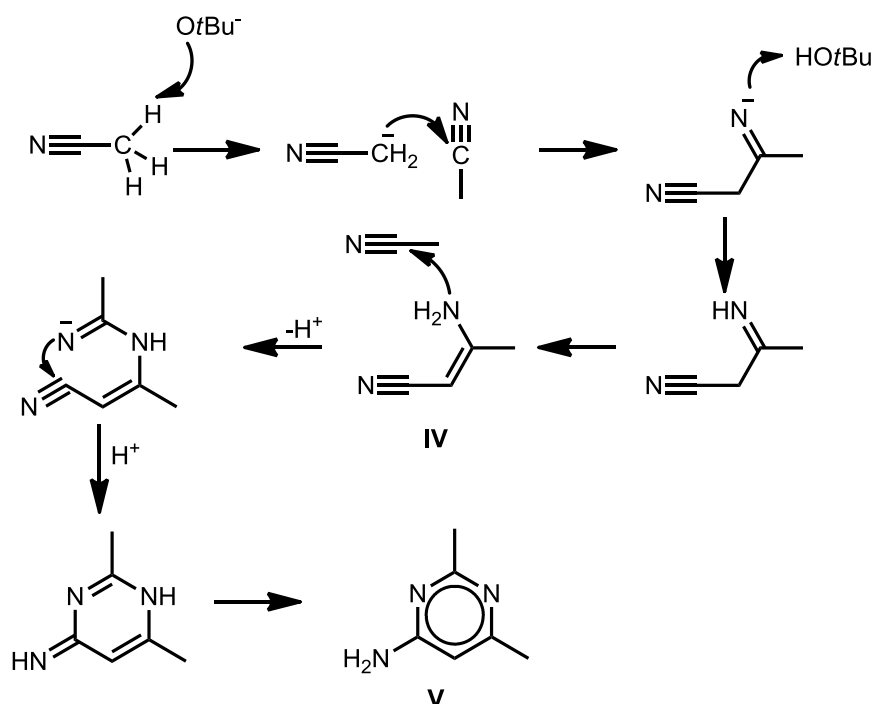


Scheme 3.4: Unintended synthesis of 3-aminocrotononitrile **IV** and 4-amino-2,6-dimethylpyrimidine **V**.

The formation of the *E*- and *Z*-isomer of 3-aminocrotononitrile is thought to result from the dimerisation of acetonitrile which had been observed under similar

conditions.^[8] This dimer is suggested as an intermediate in the formation of **V**, a trimerisation product from acetonitrile, with previous studies involving the reaction of **IV** with $\text{Me}_4\text{NOH}\cdot 5\text{H}_2\text{O}$ in CH_3CN yielding 4-amino-2,6-dimethylpyrimidine (**V**).^[10] The synthesis of 4-amino-2,6-dimethylpyrimidine (**V**), has been previously observed from acetonitrile^[9, 11] using KOtBu at 165 °C in a microwave.^[9] These milder conditions have not previously been recorded and are interesting due to the previous reports for the synthesis of **V** requiring elevated temperatures.^[9, 11]

The mechanism proposed for the dimerisation and trimerisation of acetonitrile is modified from that proposed by Murahashi who observed dimerisation of acetonitrile with NaOtBu acting as a catalyst instead of iridium (Scheme 3.5).^[12]

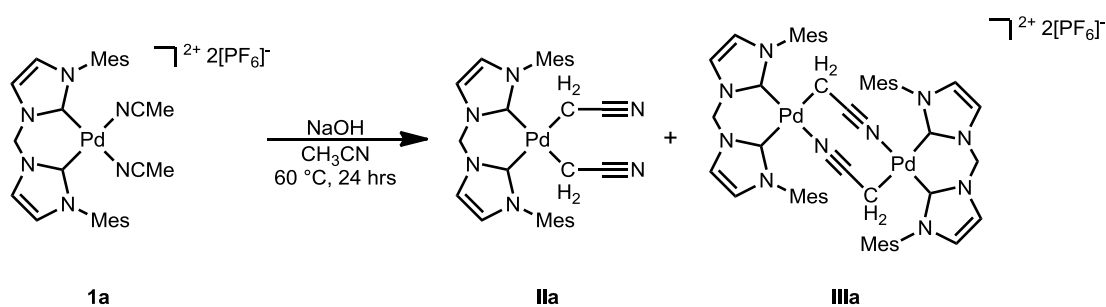


Scheme 3.5: Proposed reaction mechanism for the synthesis of 3-aminocrotononitrile **IV** and 4-amino-2,6-dimethylpyrimidine **V**.

Due to the success that was observed with copper,^[13] nickel^[13] and iridium^[14] hydroxide complexes in the synthesis of α -cyanocarbanions discussed in Chapter 1, NaOH was chosen as an alternative base for the reaction.

NaOH was shown to have the same performance as NaOtBu forming the desired $-\text{CH}_2\text{CN}$ product with no formation of a carboxamide product which has been observed under similar conditions.^[14-15]

Reacting $\{[(\text{MesIm})_2\text{CH}_2]\text{Pd}(\text{NCMe})_2\}[\text{PF}_6]_2$ with NaOH in CH_3CN at $60\text{ }^\circ\text{C}$ for 24 h yielded $\{[(\text{MesIm})_2\text{CH}_2]\text{Pd}(\text{CH}_2\text{CN})_2\}$ (**IIa**) or $\{[(\text{MesIm})_2\text{CH}_2]\text{Pd}(\mu\text{-CH}_2\text{CN})_2\}[\text{PF}_6]_2$ (**IIIa**) depending on the reaction conditions (Scheme 3.6). The specificity between the two products **IIa** and **IIIa** will be discussed later in the Chapter when other *N*-substituents have been considered.



Scheme 3.6: Synthesis of two different α -cyanocarbanion complexes $\{[(\text{MesIm})_2\text{CH}_2]\text{Pd}(\text{CH}_2\text{CN})_2\}$ (**IIa**) and $\{[(\text{MesIm})_2\text{CH}_2]\text{Pd}(\mu\text{-CH}_2\text{CN})_2\}[\text{PF}_6]_2$ (**IIIa**).

When 6.3 equiv. of NaOH was used **IIa** was synthesised in a quantitative yield. There are a number of possible reasons for the high yield obtained. This could be due to the contamination with **IIIa** which was difficult to separate from **IIa**. The identity of $\{[(\text{MesIm})_2\text{CH}_2]\text{Pd}(\text{CH}_2\text{CN})_2\}$ (**IIa**) was supported by ^1H NMR spectroscopy with a resonance at 0.36 ppm consistent with the formation of an α -cyanocarbanion of bonding mode **I**. The product was spectroscopically identical to

that previously reported in the Gardiner group.^[4] An ESI-MS was obtained of the product with a m/z consistent with the formation of **IIa**.

When 3.5 equiv of NaOH was used **IIIa** was synthesised in a 45 % yield. The formation of the desired product was supported by ^1H NMR spectroscopy in d_6 -DMSO at 120 °C with a resonance at 0.31 ppm corresponding to the CH_2CN ligand and 4 inequivalent imidazol-2-ylidene resonances. This is consistent with the two imidazol-2-ylidene rings becoming inequivalent due to two different *trans* ligands consistent with a Pd–C and Pd–N bond from the μ - CH_2CN ligands. At room temperature there are two resonances at 6.29 and 6.52 ppm consistent with the methylene linker of the bis(NHC) ligand observed as a AB spin system which is consistent with the retention of a boat conformation for the $\text{C}_3\text{N}_2\text{Pd}$ ring with ring flipping that is slow on the NMR time scale.^[16]

The X-ray crystal structure of $\{[(\text{MesIm})_2\text{CH}_2)\text{Pd}(\mu\text{-CH}_2\text{CN})\}_2[\text{PF}_6]_2$ (**IIIa**) is consistent with that reported for similar complexes, including the starting material $\{[(\text{MesIm})_2\text{CH}_2)\text{Pd}(\text{NCMe})_2\}[\text{PF}_6]_2$. A boat shape geometry is observed for the $\text{C}_3\text{N}_2\text{Pd}$ ring with Pd– C_{NHC} distances of 1.991(5) Å for the ligand *trans* to the nitrogen and 2.050(5) Å for the ligand *trans* to the carbon and angles of the NHC plane to the PdL_4 plane at 24.60(10) and 33.28(10) °. Consistent with other complexes of binding mode **II** as discussed in the introduction, the bond order of the two deprotonated nitrile ligands are consistent with a N–C triple bond with a length of 1.143(6) Å and a C–C bond length of 1.422(6) Å consistent with a single bond between a sp and sp^3 centre. There is also a C(8)–N(5)–Pd(1) angle of 163.0(4) ° distorted from the ideal linear angle to accommodate the formation of the $\text{Pd}_2\text{N}_2\text{C}_4$ metallocyclic ring of the dinuclear species. The C(8)–C(9)–Pd(1) angle of 109.8(3) ° is close to the ideal tetrahedral angle (Figure 3.1, Table 3.1).

Complex:	1a ^[1, 17]	IIa ^[4]	IIIa	1b ^[1]	IIb	IIIb ^a	1c ^[18]	IIc ^a	IIIC
Pd-C_{carbene} distance (Å)	1.983(4), 1.984(4)	2.039(4)– 2.065(3)	1.991(5), 2.050(5)	1.966(2), 1.972(3)	2.023(9), 2.037(10)		1.979(3), 1.984(3)		2.065(3), 2.013(3)
C_{carbene}-Pd-C_{carbene} angle (°)	85.87(17)	86.59(14), 86.79(14)	87.5(2)	84.05(11)	85.4(4)		87.68(11)		88.28(11)
C_{carbene}-N-R angle (°)	127.2(3), 128.1(4)	125.7(3)– 126.7(3)	126.1(4), 126.6(4)	125.8(2), 126.3(3)	124.8(9), 126.6(9)		127.2(2), 129.6(2)		127.6(2), 130.5(2)
Im/PdC₂L₂ dihedral angle (°)	37.7(2), 35.92(14)	37.18(13)– 37.94(13)	34.8(4), 31.6(4)	42.4252(4), 42.7953(5)	40.6(4), 39.6(4)		27.59(9), 28.45(9)		24.60(10), 33.28(10)
Av. distance from Im plane for C_N-substituent and Pd (Å)	0.045	0.103	0.0538	0.0446	0.0648		0.083		0.230
Distance of CH₂ from PdC₂L₂ plane (Å)	1.537(7)	1.551(5)	1.394(8)	1.596030(14)	1.642(14)		1.255(4)		1.246(4)
Pd-C-C angle (°)		108.6(2)– 118.4(3)	109.8(3)		110.2(7), 110.3(7)				110.7(2)
Pd-N-C angle (°)	167.8(4), 168.4(4)		163.0(4)	172.8(2), 179.4(2)			165.6(2), 166.0(2)		164.9(2)
N≡C-C angle (°)	178.2(5), 179.1(5)	177.3(4), 179.5(4)	176.6(5)	178.8(3), 179.2(3)	175.4(11), 177.6(12)		178.2(3), 178.8(3)		175.3(3)
¹H NMR shift of CH_{2/3} (ppm)	2.49 ^b	0.36 ^c	0.31 ^b	2.08 ^b	1.04 ^c	1.26– 1.32 ^c	2.05 ^b	0.30 ^b	0.46 ^c
¹³C NMR shift of CH_{2/3} (ppm)	1.6 ^b	–15.0 ^c	–12.4 ^b	1.6 ^b	–13.5 ^c	–14.1 ^c	1.9 ^b	–10.5 ^b	–14.3 ^c

Table 3.1: Key crystallographic and NMR data for $\{[(\text{MesIm})_2\text{CH}_2]\text{Pd}(\text{NCMe})_2\}[\text{PF}_6]_2$ (**1a**), $\{[(\text{MesIm})_2\text{CH}_2]\text{Pd}(\text{CH}_2\text{CN})_2\}$ (**IIa**), $\{[(\text{MesIm})_2\text{CH}_2]\text{Pd}(\mu\text{-CH}_2\text{CN})_2\}[\text{PF}_6]_2$ (**IIIa**), $\{[(\text{MelIm})_2\text{CH}_2]\text{Pd}(\text{NCMe})_2\}[\text{BF}_4]_2$ (**1b**), $\{[(\text{MelIm})_2\text{CH}_2]\text{Pd}(\text{CH}_2\text{CN})_2\}$ (**IIb**), $\{[(\text{MelIm})_2\text{CH}_2]\text{Pd}(\mu\text{-CH}_2\text{CN})_2\}[\text{PF}_6]_2$ (**IIIb**), $\{[(\text{dipplm})_2\text{CH}_2]\text{Pd}(\text{NCMe})_2\}[\text{PF}_6]_2$ (**1c**), $\{[(\text{dipplm})_2\text{CH}_2]\text{Pd}(\text{CH}_2\text{CN})_2\}$ (**IIc**) and $\{[(\text{dipplm})_2\text{CH}_2]\text{Pd}(\mu\text{-CH}_2\text{CN})_2\}[\text{PF}_6]_2$ (**IIIC**). ^a X-ray crystal structure not obtained ^b NMR spectra performed in *d*₆-DMSO. ^c NMR spectra performed in CD₃CN.

A detailed comparison of all the compounds presented in Table 3.1 will be performed later in this Chapter when all the complexes presented in the Table have been discussed.

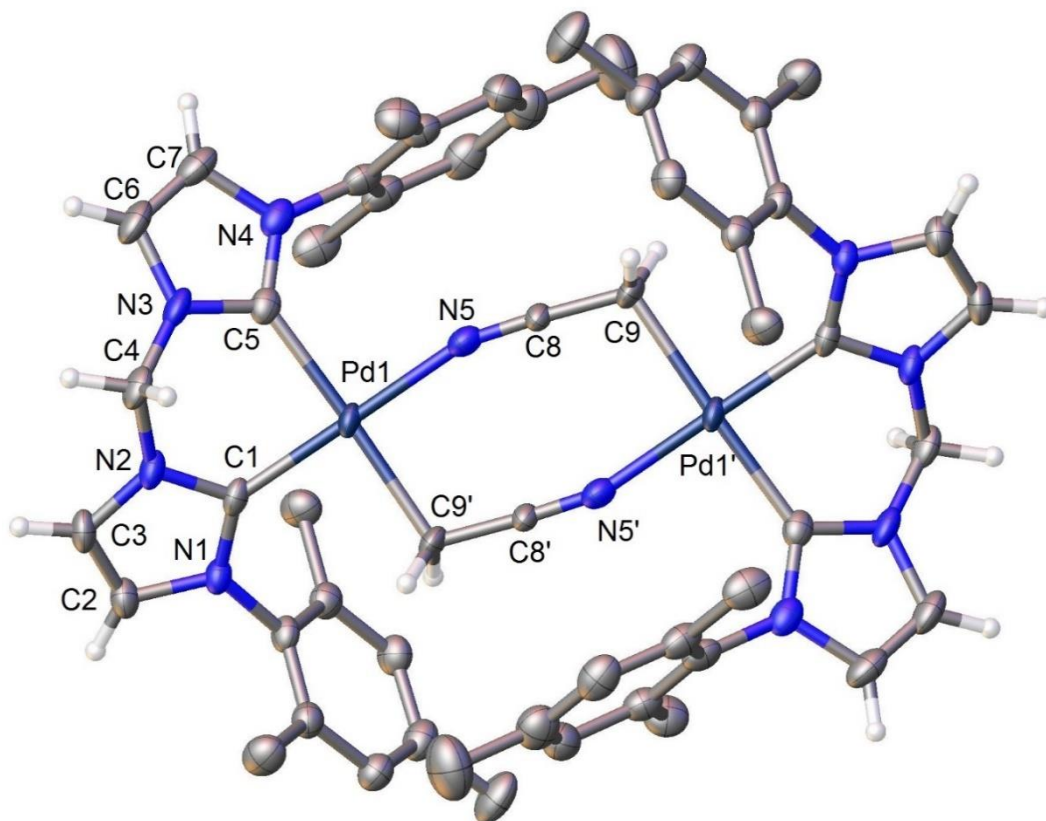


Figure 3.1: X-ray molecular structure of cation $\{([MesIm]_2CH_2)Pd(\mu-CH_2CN)\}_2^{2+}$ of **IIIa**. Thermal ellipsoids are shown at the 50% probability level. 2 $[PF_6]^-$ counter ions and 2 CH_3CN lattice solvent molecules omitted for clarity. All mesityl hydrogen atoms removed for clarity. Selected bond lengths (Å) and angles ($^\circ$): Pd(1)–N(5) 2.030(4), Pd(1)–C(1) 1.991(5), Pd(1)–C(5) 2.050(5), Pd(1)–C(9) 2.136(5), N(5)–C(8) 1.143(6), C(8)–C(9) 1.422(6), N(5)–Pd(1)–C(5) 92.07(18), N(5)–Pd(1)–C(9) 89.53(18), C(1)–Pd(1)–C(5) 87.5(2), C(1)–Pd(1)–C(9) 90.91(19), C(8)–N(5)–Pd(1) 163.0(4), N(5)–C(8)–C(9) 176.6(5), C(8)–C(9)–Pd(1) 109.8(3).

While in DMSO- d_6 the ^1H NMR spectroscopy of $\{([\text{MesIm}]_2\text{CH}_2)\text{Pd}(\mu\text{-CH}_2\text{CN})_2\}[\text{PF}_6]_2$ (**IIIa**) is consistent with the presence of the dinuclear complex with a 1:1 ratio of the deprotonated acetonitrile molecule and Pd bis(NHC) motif, as described above. Analysis of the ^1H NMR spectra of **IIIa** in CD_3CN provides insight into the different influence on solvent intervened monomer/dimer equilibria. At room temperature two products were observed, complexes A and B in a 1.8:1 ratio. The two species both exhibit ^1H NMR resonances characteristic of a bis(NHC) ligand bound to a palladium with the two NHC rings within each complex being inequivalent imidazol-2-ylidene rings due to the presence of two inequivalent *trans* ligands (Figure 3.2, Green). The integration ratios support both complex A and B having one CH_2CN ligand per Pd bis(NHC) motif. 2D NMR spectroscopy allowed the assignment of resonances for complex A and B. The NMR spectra were compared with **IIa** and **1a** suggesting that neither of these products were present in solution (Figure 3.2). The full assignment and behaviour in solution will be presented after the discussion of the identity of complexes A and B in solution.

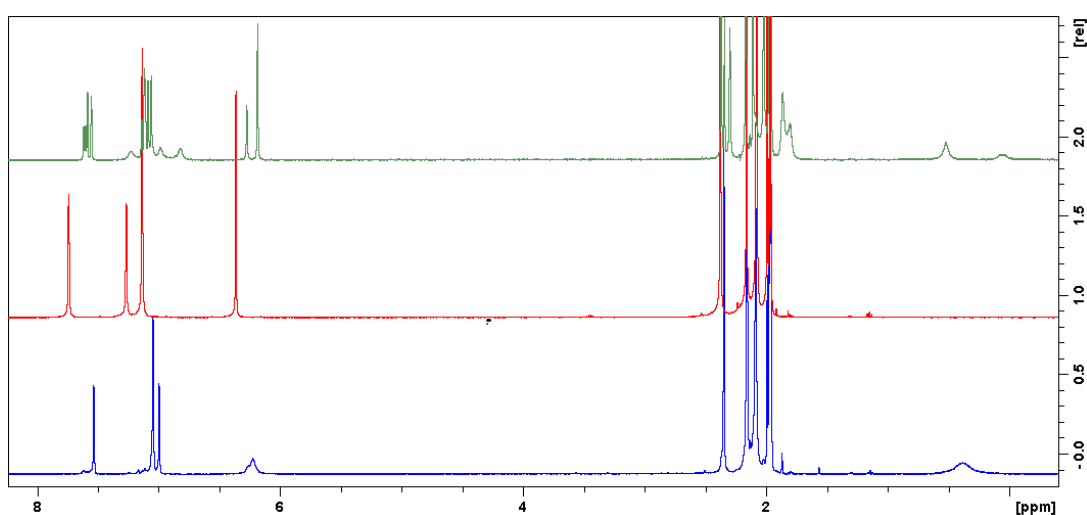


Figure 3.2: ^1H NMR spectra of $\{([\text{MesIm}]_2\text{CH}_2)\text{Pd}(\mu\text{-CH}_2\text{CN})_2\}[\text{PF}_6]_2$ (**IIIa**, green), $\{([\text{MesIm}]_2\text{CH}_2)\text{Pd}(\text{NCMe})_2\}[\text{PF}_6]_2$ (**1a**, red) and $\{([\text{MesIm}]_2\text{CH}_2)\text{Pd}(\text{CH}_2\text{CN})_2\}$ (**IIa**, blue).

In order to make partial structural assignment for the two complexes in solution a Diffusion Ordered Spectroscopy (DOSY) NMR experiment was recorded of a CD_3CN solution containing a mixture of **1a** and **IIIa**. The addition of $\{[(\text{MesIm})_2\text{CH}_2]\text{Pd}(\text{NCMe})_2\}[\text{PF}_6]_2$ (**1a**) in the solution served as an internal standard as the molecular weight, and thus diffusion coefficient of its cation $\{[(\text{MesIm})_2\text{CH}_2]\text{Pd}(\text{NCMe})_2\}^{2+}$ was roughly equivalent to the fragment of **IIIa** $\{[(\text{MesIm})_2\text{CH}_2]\text{Pd}(\text{CH}_2\text{CN})\}^+$ if the species was cleaved in solution. The NMR spectrum was recorded of the mixture of **1a** and **IIIa** suggesting that the complexes were unaltered in solution and that an equilibrium between the internal standard and the two complexes A and B in solution does not occur (Figure 3.3).

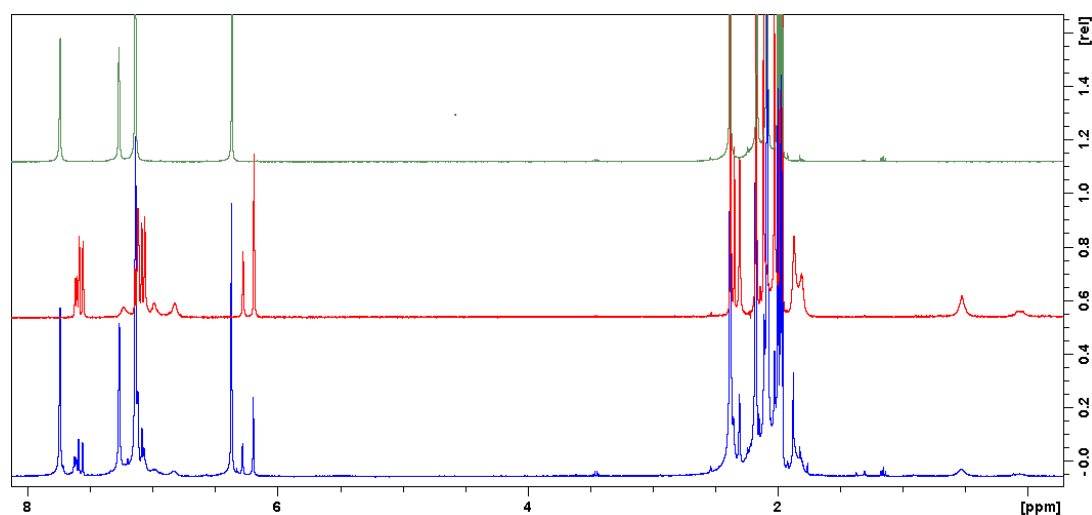


Figure 3.3: ^1H NMR spectra of $\{[(\text{MesIm})_2\text{CH}_2]\text{Pd}(\text{NCMe})_2\}[\text{PF}_6]_2$ (**1a**, green), $\{[(\text{MesIm})_2\text{CH}_2]\text{Pd}(\mu\text{-CH}_2\text{CN})_2\}[\text{PF}_6]_2$ (**IIIa**, red) and the solution of **1a** and **IIIa** combined (blue).

Analysis of the DOSY experiment (Figure 3.4) indicates that the diffusion coefficient of **1a** (black dots) and complex B (green dots) are close and thus have a similar molecular weight while the diffusion coefficient of complex A (red dots) is lower and thus it has a higher molecular weight.

It is proposed that complex A corresponds to the dimer observed in the crystal structure in solution while this species is also cleaved in solution to form complex B

with an NCMe ligand complexing to the open coordination site. The similarity in chemical shifts between complexes A and B support complex B having a CH₂CN ligand being of bonding mode I (Scheme 3.7). An ESI-MS was recorded of the solution of **IIIa** in an attempt to observe a molecular ion consistent with the assignment for complex B, however, due to the dissociation of Pd–N bonds under even mild conditions only the fragment $[\{(MesIm)_2CH_2\}Pd(CH_2CN)]^+$ was observed. This is consistent with the ESI-MS of $[\{(dipIm)_2CH_2\}Pd(NCMe)_2][PF_6]_2$ in which both $[\{(dipIm)_2CH_2\}Pd]^{2+}$ and $[\{(dipIm)_2CH_2\}Pd(NCMe)]^{2+}$ were observed.^[18]

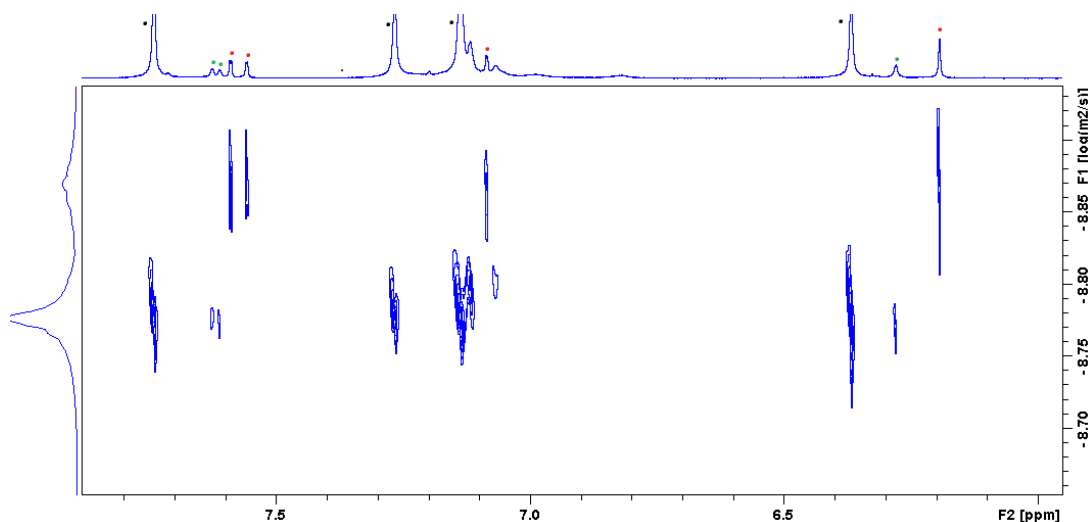
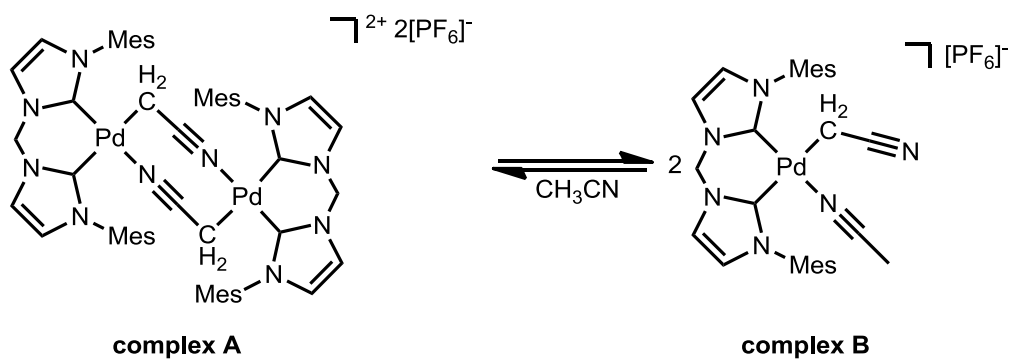


Figure 3.4: DOSY NMR spectra of a mixture of $[\{(MesIm)_2CH_2\}Pd(NCMe)_2][PF_6]_2$ (black dots) and $[\{([MesIm]_2CH_2)Pd(\mu-CH_2CN)\}_2][PF_6]_2$ (complex A red dots, complex B green dots).



Scheme 3.7: Proposed equilibrium of **IIIa** in CH₃CN.

To support the proposed equilibrium a ^1H NMR spectrum of **IIIa** was performed in $\text{DMSO-}d_6$ at room temperature and it was titrated with CD_3CN . The ^1H NMR spectrum of $[\{([\text{MesIm}]_2\text{CH}_2)\text{Pd}(\mu\text{-CH}_2\text{CN})\}_2][\text{PF}_6]_2$ in $\text{DMSO-}d_6$ at room temperature had broad signals, but was consistent with the pure **IIIa** sample previously recorded at $120\text{ }^\circ\text{C}$. The aromatic and methylene region of the ^1H NMR spectra were monitored with the progressive titration of CD_3CN into the solution. Two doublets were observed to appear both in the range of $7.85 - 7.95\text{ ppm}$ and $7.30 - 7.50\text{ ppm}$ (Figure 3.5, black dots). In addition, the integration ratio of the two methylene peaks between $6.20 - 6.60\text{ ppm}$ changed upon the addition of CD_3CN . In the $\text{DMSO-}d_6$ solution the integration ratio is 1:1, however, with $435\text{ }\mu\text{L}$ of CD_3CN added to the solution the peak at 6.5 ppm had increased in comparison to the peak at 6.2 ppm with a ratio of 1.6:1 (Figure 3.5, red dots). This supports the proposal above that the presence of acetonitrile affects the equilibrium with complex B only observed with CD_3CN in solution.

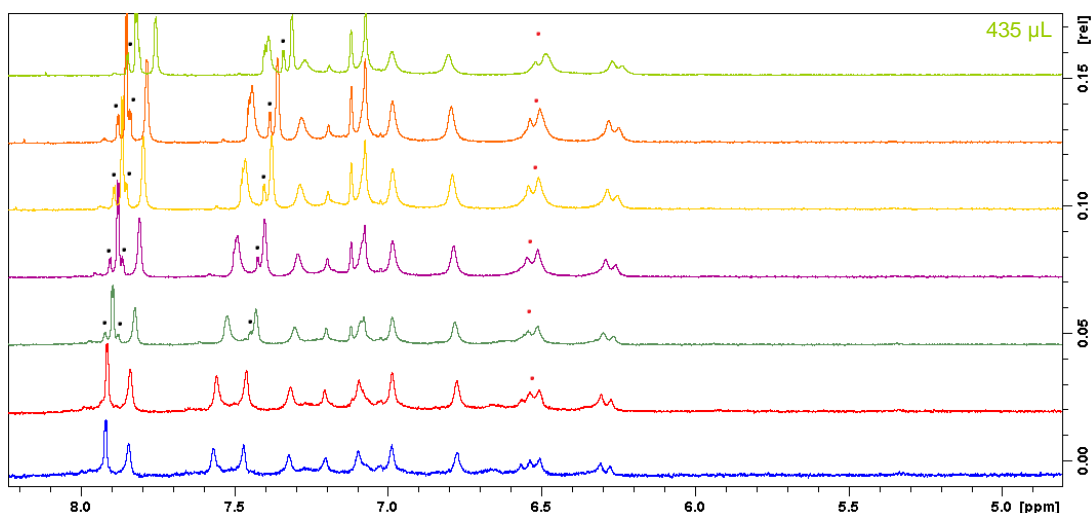


Figure 3.5: ^1H NMR spectra of $[\{([\text{MesIm}]_2\text{CH}_2)\text{Pd}(\mu\text{-CH}_2\text{CN})\}_2][\text{PF}_6]_2$ (**IIIa**) in $\text{DMSO-}d_6$ with titrated addition of CD_3CN . Titrated volume shown on right.

A NOESY NMR experiment was also recorded analysing the protons in exchange and protons that are close in distance to each other. In this case, cross peaks due

to chemical exchange (Figure 3.6, 3.7, blue) are opposite in phase to nOe crosspeaks (Figure 3.6–3.8, green). Analysis of the exchange peaks shows exchange between the CH₂ peaks for complexes A and B of both the methylene linker and CH₂CN ligand (Figure 3.6, 3.7 black dots); this indicates that the two complexes are in an equilibrium, which is slow on the NMR time scale at room temperature supporting what was described above. As expected, the aromatic mesityl peaks also exchange (Figure 3.7, red dots). From analysis of the nOe peaks it can be seen that the imidazol-2-ylidene ring proton resonances correlate with each other (Figure 3.7, green dots, Figure 3.9 a) in addition to the methylene linker (Figure 3.7, black dots, Figure 3.9 b). nOe interactions can be seen between the imidazol-2-ylidene and mesityl *m*-H peaks to the aliphatic mesityl peaks (Figure 3.8, Figure 3.9 c). In addition, a nOe correlation is observed between the mesityl *o*-CH₃ hydrogens and the CH₂CN peaks consistent with a H...H distance of 2.69(4) Å observed in the X-ray crystal structure (Figure 3.9 d).

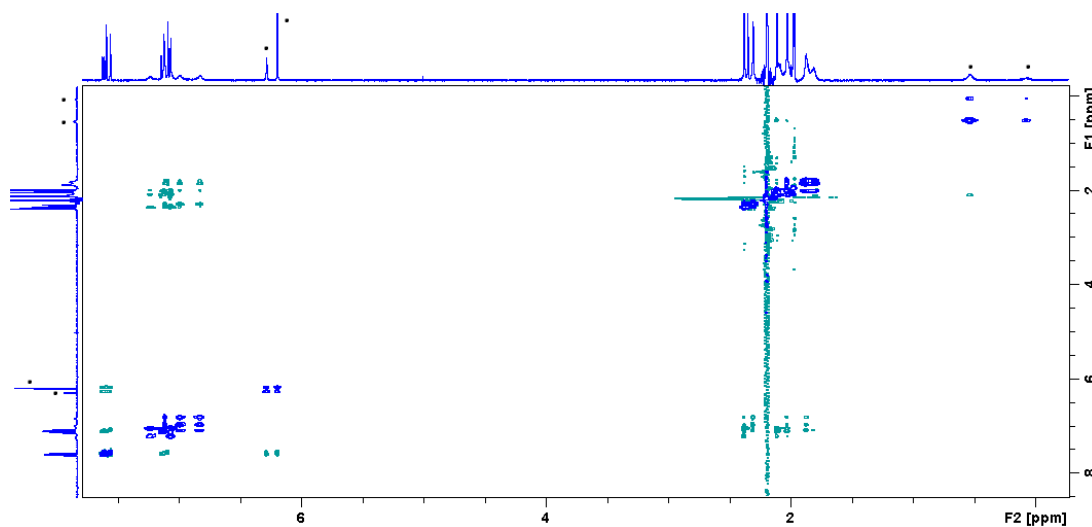


Figure 3.6: NOESY NMR spectra of **IIIa** (blue peaks exchange peaks, green peaks nOe peaks, black dots methylene and CH₂CN ligand CH₂ signals)

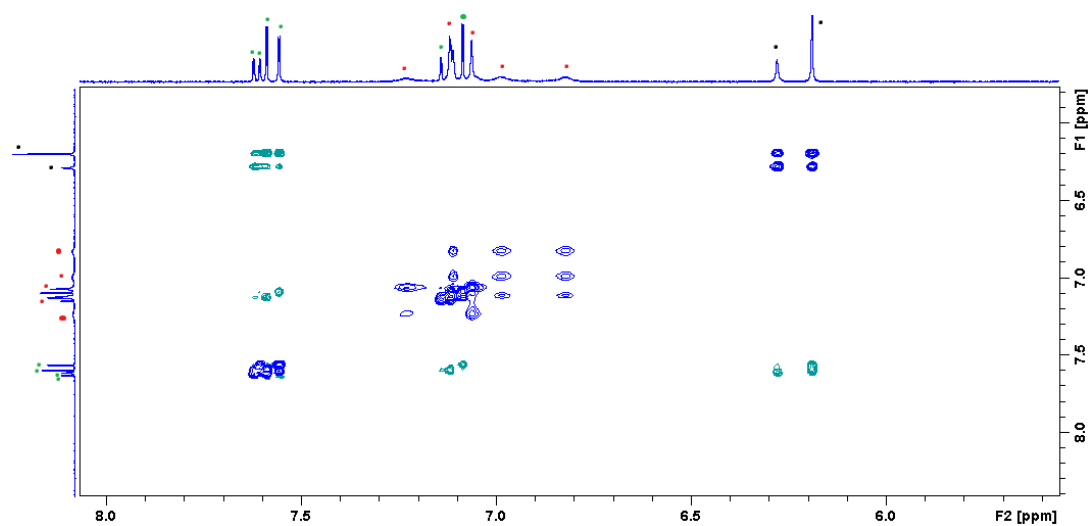


Figure 3.7: NOESY NMR spectra of **IIIa**, aromatic and methylene region (blue peaks exchange peaks, green peaks nOe peaks, black dots methylene, red dots aromatic mesityl, green dots imidazolium resonances).

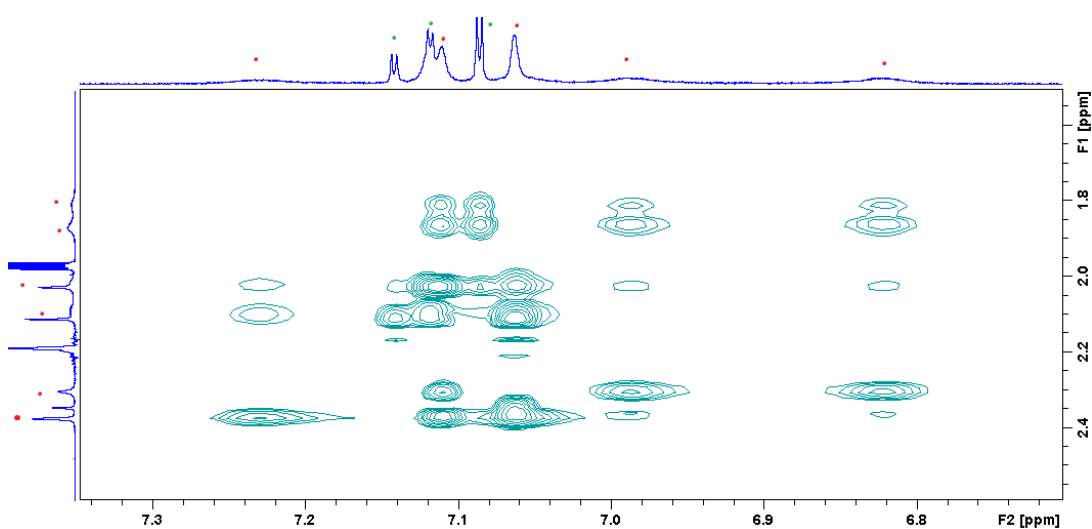


Figure 3.8: NOESY NMR spectra of **IIIa**, partial aromatic and aliphatic correlation region (green peaks nOe peaks, red dots mesityl, green dots imidazolium resonances).

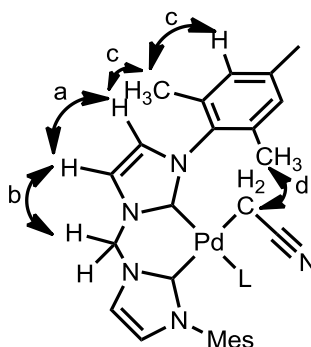


Figure 3.9: IIIa fragment highlighting nOe correlations.

VT NMR studies were undertaken to elucidate the equilibrium behaviour of the proposed two complexes in solution. The characteristic CH_2 peaks in the range of 6.1–6.4 ppm do not coalesce indicating the presence of complexes A and B at all temperatures in a slow exchange on the NMR time scale. The ratio of complexes A and B are influenced by temperature, with a ratio at $-10\text{ }^\circ\text{C}$ of 1:2.7 while at $70\text{ }^\circ\text{C}$ it is 1:1.3 (Figure 3.10, blue dots). This supports the presence of an equilibrium noted in the NOESY NMR spectra. At room temperature, the methylene bridge CH_2 protons are equivalent in both complex A and B, however, below $10\text{ }^\circ\text{C}$ the peaks become separated consistent with the formation of an AB spin system for each complex (Figure 3.10, blue dots). This is consistent with the locking of the boat conformation of the bis(NHC) chelate rings.^[16]

At room temperature, there are four *m*-H peaks consistent with both complex A and complex B having restricted motion, i.e. H_a and H_b were inequivalent by ^1H NMR spectroscopy (Figure 3.11). When the solution is heated above room temperature, the aryl peaks coalesce indicating rapid N–C rotation rendering H_a equivalent to H_b (Figure 3.10, red and black dots). The peaks in the -0.5 to 1 ppm region correspond to the CH_2CN ligands (Figure 3.10, green dots). When the temperature is $-5\text{ }^\circ\text{C}$ or below an AB spin system is observed consistent with the two protons becoming inequivalent due to restricted motion. At $-15\text{ }^\circ\text{C}$, a third product is apparent,

evidenced by the presence of a third set of CH₂CN peaks in the –0.5 to 1 ppm region.

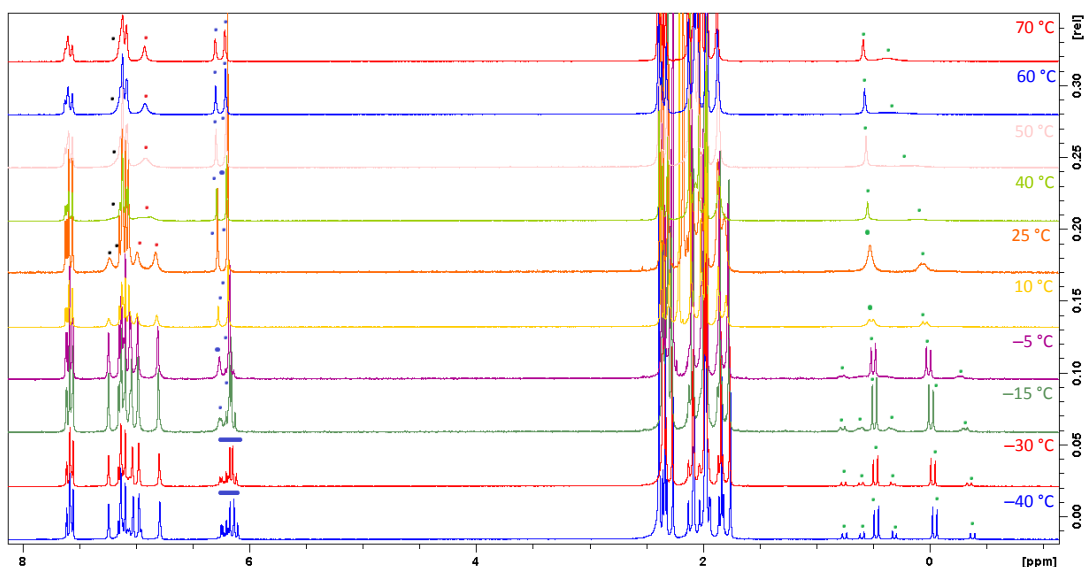


Figure 3.10: Overlay of the ¹H NMR spectra of **IIIa** in CD₃CN at various temperatures.

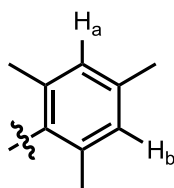
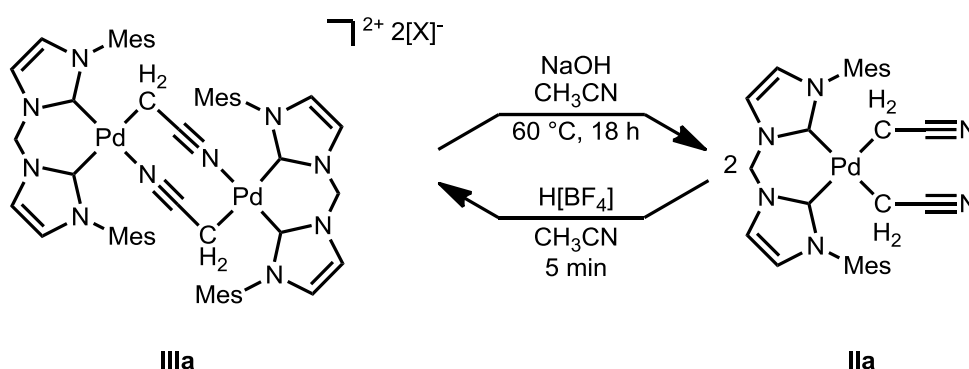


Figure 3.11: **IIIa** fragment highlighting restricted motion.

A DOSY NMR spectra was recorded at –40 °C to determine the diffusion coefficient of the third complex was inconclusive, which is likely due to increasing solvent viscosity and inability to resolve any differences in diffusion. Thus, the identity of the product formed is unclear and due to the difficulty in studying this product it was not pursued further.

To understand the relationship between $[\{(\text{MesIm})_2\text{CH}_2\}\text{Pd}(\text{CH}_2\text{CN})_2]$ (**IIa**) and $[\{([\text{MesIm}]_2\text{CH}_2)\text{Pd}(\mu\text{-CH}_2\text{CN})_2\}][\text{PF}_6]_2$ (**IIIa**) in their synthesis from $[\{(\text{MesIm})_2\text{CH}_2\}\text{Pd}(\text{NCMe})_2][\text{PF}_6]_2$ (**1a**) $[\{([\text{MesIm}]_2\text{CH}_2)\text{Pd}(\mu\text{-CH}_2\text{CN})_2\}][\text{PF}_6]_2$ (**IIIa**) was reacted with an excess of NaOH at 60 °C for 24 h in CH₃CN forming

$[\{(\text{MesIm})_2\text{CH}_2\}\text{Pd}(\text{CH}_2\text{CN})_2]$ (**IIa**) in 75% yield. When **IIa** was reacted with 1 equivalent of $\text{H}[\text{BF}_4]$ in CH_3CN for 5 minutes, the product $[\{[(\text{MesIm})_2\text{CH}_2]\text{Pd}(\mu\text{-CH}_2\text{CN})\}_2][\text{BF}_4]_2$ (**IIIa**) was reformed (Scheme 3.8). This means that the formation of **IIIa** is likely favoured when there is insufficient NaOH in the reaction mixture to allow complete reactivity. This is consistent with the fact that when 6.3 equivalents of NaOH were reacted with **1a**, **IIa** was observed as the sole product. However when 3.5 equivalents of NaOH was reacted with **1a**, **IIIa** was observed as the sole product.



Scheme 3.8: Interconversion between $[\{[(\text{MesIm})_2\text{CH}_2]\text{Pd}(\mu\text{-CH}_2\text{CN})\}_2][\text{X}]_2$ (**IIIa**) and $[\{(\text{MesIm})_2\text{CH}_2\}\text{Pd}(\text{CH}_2\text{CN})_2]$ (**IIa**).

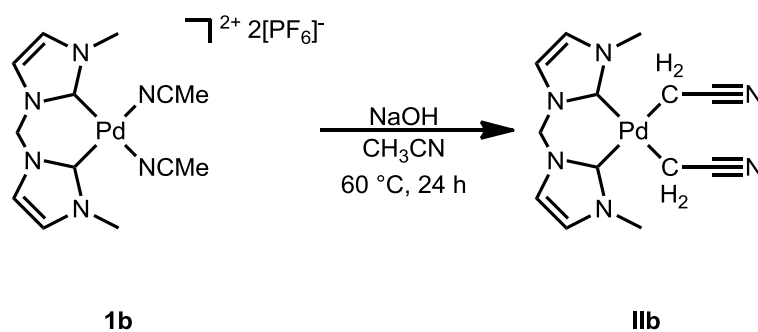
Similarly, upon the addition of excess $\text{H}[\text{BF}_4]$ to $[\{[(\text{MesIm})_2\text{CH}_2]\text{Pd}(\mu\text{-CH}_2\text{CN})\}_2][\text{BF}_4]_2$, $[\{(\text{MesIm})_2\text{CH}_2\}\text{Pd}(\text{NCMe})_2][\text{PF}_6]_2$ **1a** was observed.

Given the formation of both **IIa** and **IIIa** from **1a** under similar conditions and the solution phase equilibrium of **IIIa** observed, the effect of the steric bulk of the bis(NHC) ligands was investigated by decreasing the steric bulk to a methyl substituent and increasing the steric bulk to a diisopropylphenyl substituent in comparison to the initially studied mesityl substituent.

3.2.2 Synthesis of $[\{(\text{Melm})_2\text{CH}_2\}\text{Pd}(\text{CH}_2\text{CN})_2]$ (**IIb**):

$[\{(\text{Melm})_2\text{CH}_2\}\text{Pd}(\text{NCMe})_2][\text{PF}_6]_2$, **1b** was reacted with 9.4 equiv of NaOH in CH_3CN at $60 \text{ }^\circ\text{C}$ for 24 h. $[\{(\text{Melm})_2\text{CH}_2\}\text{Pd}(\text{CH}_2\text{CN})_2]$ (**IIb**) was isolated (Scheme 3.9, Figure

3.12) The formation of **IIb** was supported by ^1H and ^{13}C NMR spectroscopy with resonances at 1.04 and -13.5 ppm respectively for the CH_2 protons consistent with the formation of the CH_2CN ligand. In addition, a crystal structure was also obtained, however, crystallisation was difficult due to the extreme low solubility of this complex in a suitable solvent to obtain crystals. As such, a cocrystallised derivative of **IIb** with $\text{K}[\text{PF}_6]$ was obtained (from a reaction attempted using KOH as a base). The metrics of the crystal structure of **IIb** is consistent with $[\{(\text{MesIm})_2\text{CH}_2\}\text{Pd}(\text{CH}_2\text{CN})_2]$ with $\text{Pd}-\text{C}_{\text{NHC}}$ distances of 2.023(9) and 2.037(10) Å and $\text{Pd}-\text{C}_{\text{CH}_2\text{CN}}$ distances of 2.116(10) and 2.122(10) Å (Table 3.1).



Scheme 3.9: Synthesis of $[\{(\text{MesIm})_2\text{CH}_2\}\text{Pd}(\text{CH}_2\text{CN})_2]$ (**IIb**).

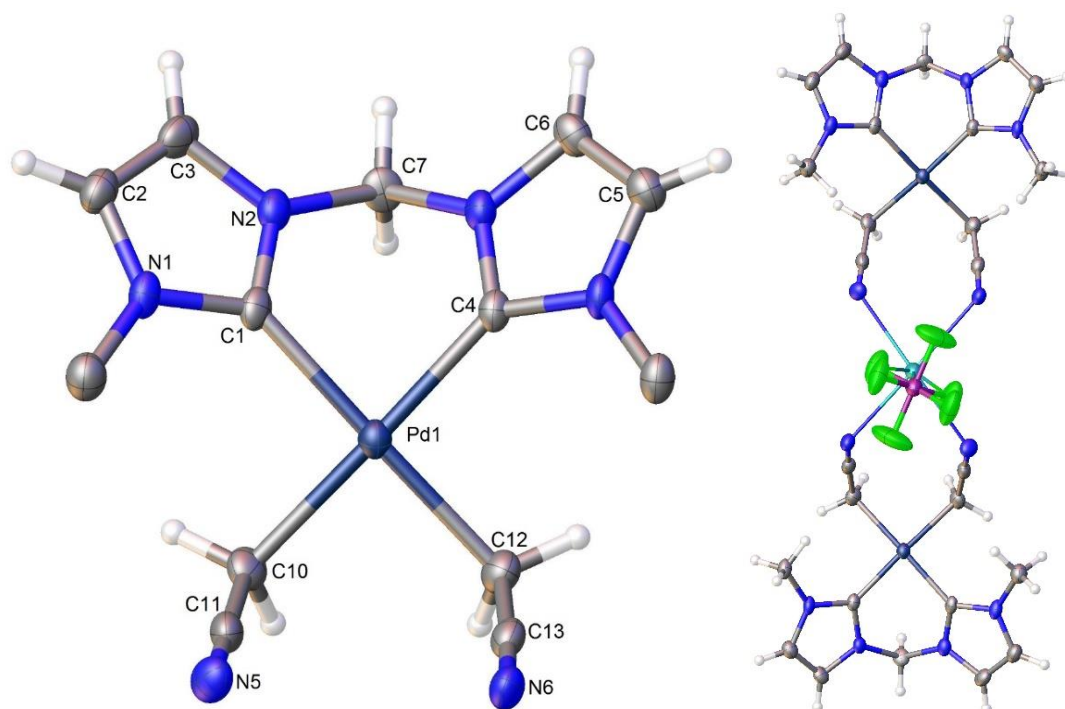


Figure 3.12: X-ray crystal structure of $[\{(\text{MeIm})_2\text{CH}_2\}\text{Pd}(\text{CH}_2\text{CN})_2]\cdot\text{K}[\text{PF}_6]$ **IIb**.

Thermal ellipsoids are shown at the 50% probability level. Left image $\text{K}[\text{PF}_6]$ molecule omitted for clarity, right image cocrystallised closest $\text{K}[\text{PF}_6]$ molecule shown in contact with **IIb**. All methyl hydrogen atoms removed for clarity. Selected bond lengths (Å) and angles (°): $\text{Pd}(1)\text{--C}(4)$ 2.023(9), $\text{Pd}(1)\text{--C}(1)$ 2.037(10), $\text{Pd}(1)\text{--C}(12)$ 2.116(10), $\text{Pd}(1)\text{--C}(10)$ 2.122(10), $\text{N}(6)\text{--K}(1)$ 2.801(9), $\text{N}(5)\text{--K}(1)$ 2.738(10), $\text{C}(4)\text{--Pd}(1)\text{--C}(1)$ 85.4(4), $\text{C}(4)\text{--Pd}(1)\text{--C}(12)$ 93.7(4), $\text{C}(1)\text{--Pd}(1)\text{--C}(10)$ 92.8(4), $\text{C}(12)\text{--Pd}(1)\text{--C}(10)$ 87.5(4).

During the synthesis of **IIb** an intermediate $[\{(\text{MeIm})_2\text{CH}_2\}\text{Pd}(\mu\text{-OH})_2][\text{PF}_6]_2$ was observed by ^1H NMR spectroscopy and X-ray crystallography. **1b** was reacted with NaOH in CD_3CN at room temperature in a J. Young NMR tube yielding $[\{(\text{MeIm})_2\text{CH}_2\}\text{Pd}(\mu\text{-OH})_2][\text{PF}_6]_2$. This intermediate was detected as the sole intermediate by ^1H NMR spectroscopy with no signals corresponding to $[\{(\text{MeIm})_2\text{CH}_2\}\text{Pd}(\mu\text{-CH}_2\text{CN})_2][\text{PF}_6]_2$ identified during the formation of

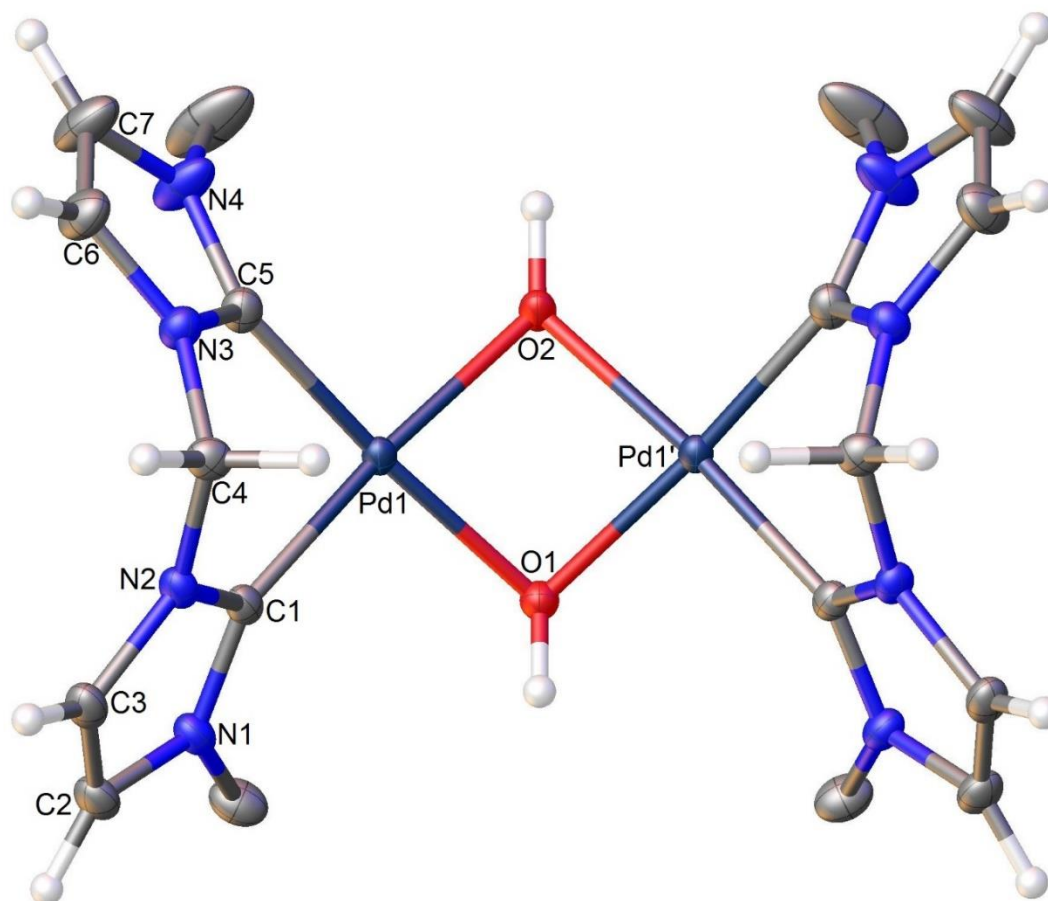
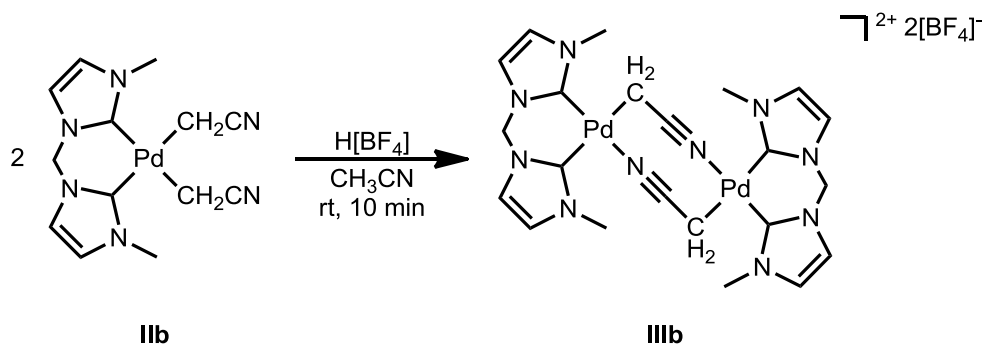


Figure 3.13: X-ray molecular structure of cation $[[[(\text{MeIm})_2\text{CH}_2]\text{Pd}(\mu\text{-OH})_2]_2]^{2+}$.

Thermal ellipsoids are shown at the 50% probability level. 2 $[\text{PF}_6]^-$ counter ions a Et_2O and a H_2O lattice solvent molecules omitted for clarity. All methyl hydrogen atoms removed for clarity. Selected bond lengths (\AA) and angles ($^\circ$): Pd(1)–O(2) 2.074(2), Pd(1)–C(5) 1.973(3), Pd(1)–C(1) 1.974(3), Pd(1)–O(1) 2.088(2), O(2)–Pd(1)–O(1) 78.15(9), C(5)–Pd(1)–O(2) 97.78(10), C(5)–Pd(1)–C(1) 84.92(11), C(5)–Pd(1)–O(1) 175.06(9), C(1)–Pd(1)–O(2) 174.63(10), C(1)–Pd(1)–O(1) 98.92(11), Pd(1)–O(2)–Pd(1) 87.42(11), Pd(1)–O(1)–Pd(1) 86.71(10).

$[(\text{Melm})_2\text{CH}_2\text{Pd}(\text{CH}_2\text{CN})_2]$ (Figure 3.13). The crystal structure has the methyl substituents with a *syn*-orientations with respect to the central Pd_2O_2 ring with Pd–O bond distances of 2.074(2) and 2.088(2) Å and Pd–C distances of 1.973(3) and 1.974(3) Å. This was consistent with the previously observed closely analogous methoxide dimer $[\{[(\text{Melm})_2\text{CH}_2]\text{Pd}(\mu\text{-OMe})\}_2][\text{PF}_6]_2$ which had Pd–O bond distances of 2.058(2)–2.978(2) Å and Pd–C distances of 1.966(3) and 1.979(3) Å.^[19] Due to the propensity for $[\{[(\text{Melm})_2\text{CH}_2]\text{Pd}(\mu\text{-OH})\}_2][\text{PF}_6]_2$ to react further to form **IIb** isolation and further characterisation was not possible.

$[\{[(\text{Melm})_2\text{CH}_2]\text{Pd}(\mu\text{-CH}_2\text{CN})\}_2][\text{BF}_4]_2$ (**IIIb**) was synthesised by reacting $[(\text{Melm})_2\text{CH}_2]\text{Pd}(\text{CH}_2\text{CN})_2$ (**IIb**) with $\text{H}[\text{BF}_4]$ in acetonitrile to gain further understanding of the *N*-mesityl system. The low yield observed (3 %) is likely due to the low solubility of **IIb** and could possibly be increased with further reaction time, however, the reaction was not repeated due to time constraints (Scheme 3.10).



Scheme 3.10: Synthesis of $[\{[(\text{Melm})_2\text{CH}_2]\text{Pd}(\mu\text{-CH}_2\text{CN})\}_2][\text{BF}_4]_2$ (**IIIb**).

The formation of **IIIb** was supported by ^1H NMR spectroscopy in CD_3CN with four inequivalent imidazol-2-ylidene peaks and two inequivalent CH_3 substituents. This is consistent with two different *trans* donating ligands. There is a resonance at 1.29 ppm consistent with the CH_2 from the formation of the CH_2CN ligand and two signals at 6.16 and 5.98 ppm consistent with the AB spin system of the methylene linker of the bis(NHC) ligand.

In contrast to the mesityl substituent, the ^1H NMR spectrum of **IIIb** in CD_3CN contains only one complex. To determine whether the complex observed was consistent with the formation of the previously discussed *N*-mesityl complexes A or B a DOSY NMR spectra was recorded of **IIIb** (Figure 3.14, red dots) with a capillary of $[\{(\text{Melm})_2\text{CH}_2\}\text{Pd}(\text{NCMe})_2][\text{PF}_6]_2$ (**1b**) (Figure 3.14, green dots). The capillary of **1b** in CD_3CN was used as a standard that would not impact the ^1H NMR spectrum of **IIIb**. Similar to the *N*-mesityl substituent, the molecular weight and thus diffusion coefficient of **1b** was similar to that of the $[\{(\text{Melm})_2\text{CH}_2\}\text{Pd}(\mu\text{-CH}_2\text{CN})]$ fragment within complex **IIIb**. The DOSY NMR spectrum shows the diffusion coefficients of **1b** and **IIIb** were found to be the same. This indicates that the species in solution had a similar molecular weight to **1b**, i.e. only complex B is observed (Scheme 3.11). This may be consistent with the observation that only **IIIb** was present in the reaction of **1b** with excess NaOH given the high level propensity for **IIIb** to dissociate in CH_3CN .

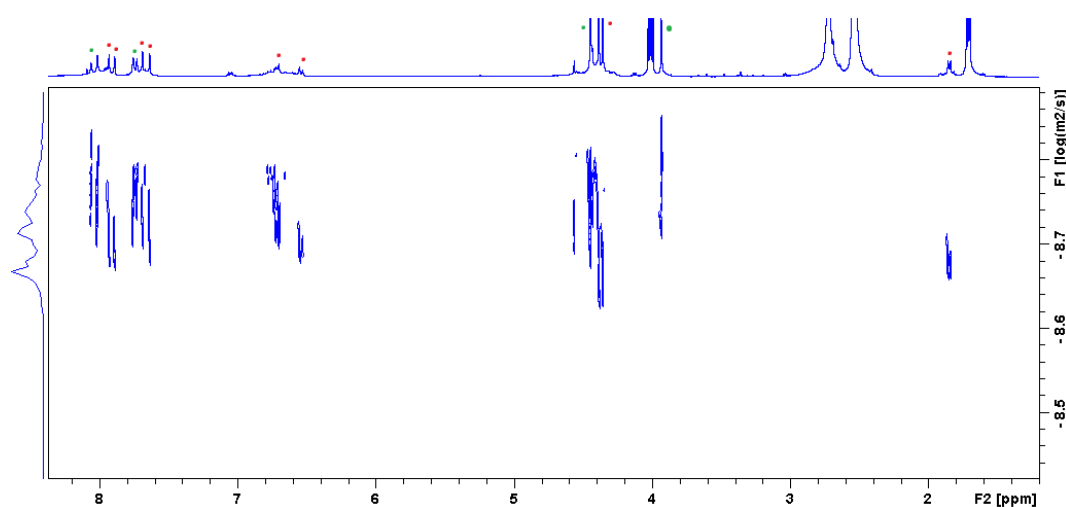
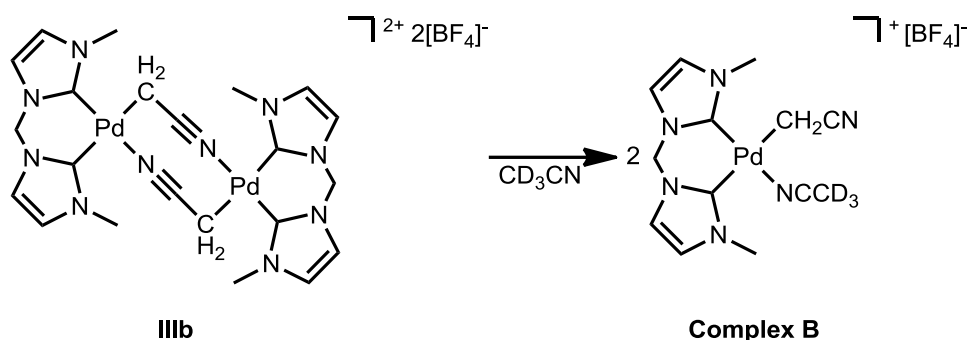


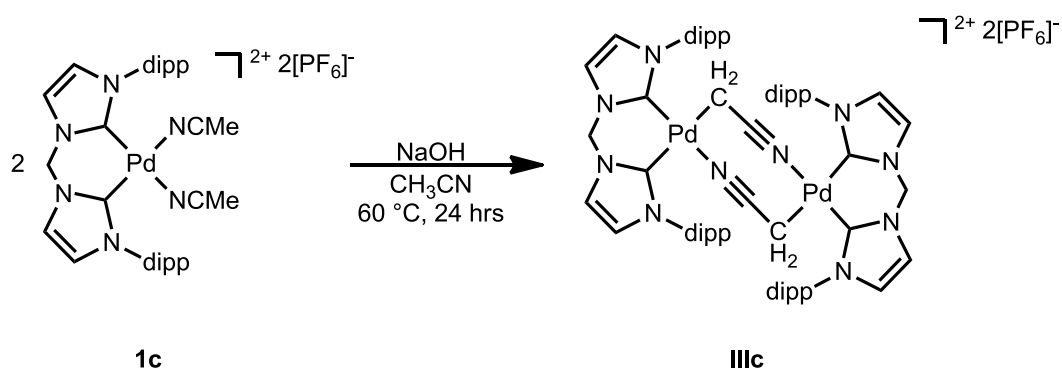
Figure 3.14: DOSY NMR spectra of a mixture of $[\{(\text{Melm})_2\text{CH}_2\}\text{Pd}(\text{NCMe})_2][\text{PF}_6]_2$ (**1b**, green dots) and $[\{(\text{Melm})_2\text{CH}_2\}\text{Pd}(\mu\text{-CH}_2\text{CN})_2][\text{BF}_4]_2$ (**IIIb**, red dots)



Scheme 3.11: Reaction of $\{[(\text{Melm})_2\text{CH}_2)\text{Pd}(\mu\text{-CH}_2\text{CN})_2][\text{BF}_4]_2$ in CD_3CN as observed by a DOSY NMR spectra.

3.2.3 Synthesis of $\{[(\text{Dipplm})_2\text{CH}_2)\text{Pd}(\mu\text{-CH}_2\text{CN})_2][\text{PF}_6]_2$:

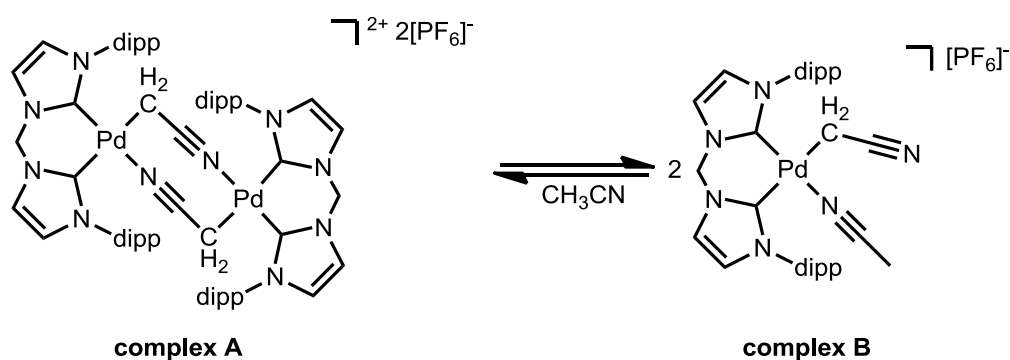
$\{[(\text{Dipplm})_2\text{CH}_2)\text{Pd}(\text{NCMe})_2][\text{PF}_6]_2$ (**1c**), Dipp = 2,6-diisopropylphenyl, was similarly reacted with NaOH in CH_3CN at 60°C for 24 h. Complex $\{[(\text{Dipplm})_2\text{CH}_2)\text{Pd}(\mu\text{-CH}_2\text{CN})_2][\text{PF}_6]_2$ (**IIIc**) was isolated while none of the 2:1 mono palladium complex was observed (Scheme 3.12, Figure 3.17). The formation of **IIIc** was supported by ^1H and ^{13}C NMR spectroscopy in $\text{DMSO-}d_6$ with resonances at 0.30 and -10.5 ppm respectively, consistent with the CH_2 from the formation of the $-\text{CH}_2\text{CN}$ ligand.



Scheme 3.12: Synthesis of $\{[(\text{Dipplm})_2\text{CH}_2)\text{Pd}(\mu\text{-CH}_2\text{CN})_2][\text{PF}_6]_2$ (**IIIc**).

The ^1H NMR spectrum was also recorded in CD_3CN , which indicated the presence of two complexes in solution analogous to that discussed above for the *N*-mesityl **IIIa** system. Extensive spectroscopic analysis of the two complexes in solution was

not performed due to the complicated overlapping nature of the resonances. A DOSY NMR spectrum was recorded of the sample indicating that the same equilibrium is present that was observed for **IIIa** (Scheme 3.13). Both the observation of the two diffusion rates and the large number of aromatic resonances supports the equilibrium proposed between complexes A and B (Figure 3.15 A trace contaminant was present in the NMR characterisation due to the difficulty to separate it from **IIIc**. This contaminant corresponds to another bis(NHC) complex and not **1c** or **IIc**).



Scheme 3.13: Proposed equilibrium of **IIIc** in NCMe.

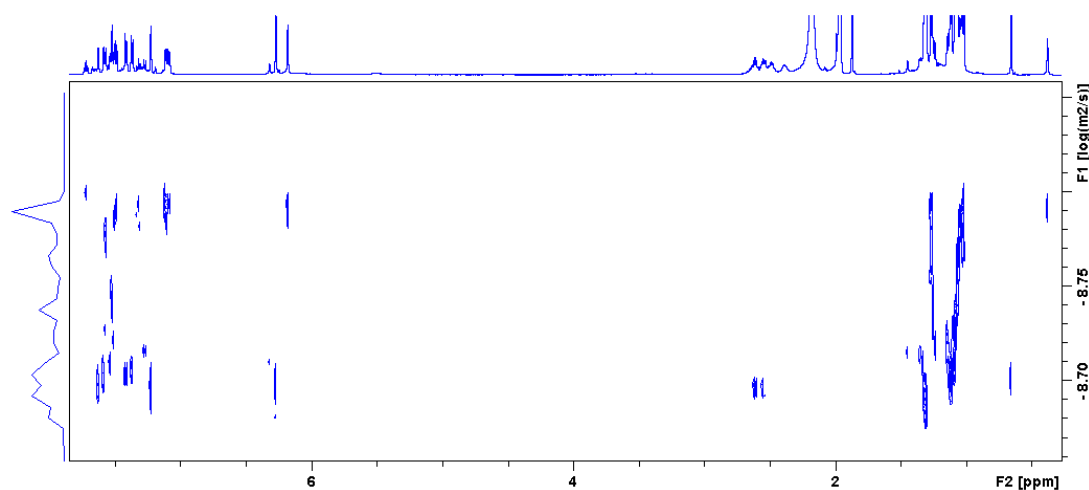


Figure 3.15: DOSY NMR spectra of **IIIc**.

A VT ^1H NMR was recorded of the sample from $-40\text{ }^\circ\text{C}$ to $70\text{ }^\circ\text{C}$. The characteristic methylene CH_2 resonances in the range of $6.15\text{--}6.30\text{ ppm}$ do not coalesce

indicating the presence of complexes A and B at all temperatures in a slow exchange on the NMR time scale. With a varying ratio of complexes A and B the ratio of complexes A:B at $-40\text{ }^{\circ}\text{C}$ was 1:2 while at $70\text{ }^{\circ}\text{C}$ it was 1.9:1 (Figure 3.16, blue dots).

The methylene CH_2 proton resonances of the bis(NHC) ligands between 6.15–6.30 ppm are equivalent at all temperatures. This is in contrast to **IIIa** which appear with a AB spin system at low temperature (Figure 3.16, blue dots). Similarly, the resonances between 0–1 ppm corresponding with the CH_2CN ligand do not observe an AB spin system at low temperatures in contrast to **IIIa** (Figure 3.16, green dots). In this case, there was no evidence that a third product was formed at low temperatures as was noted above for the analogous *N*-Mes system **IIIa**.

The fact that the Dipp substituent did not appear with the same AB spin system as was observed with the Mes substituent for the CH_2 peaks of the bis(NHC) ligand

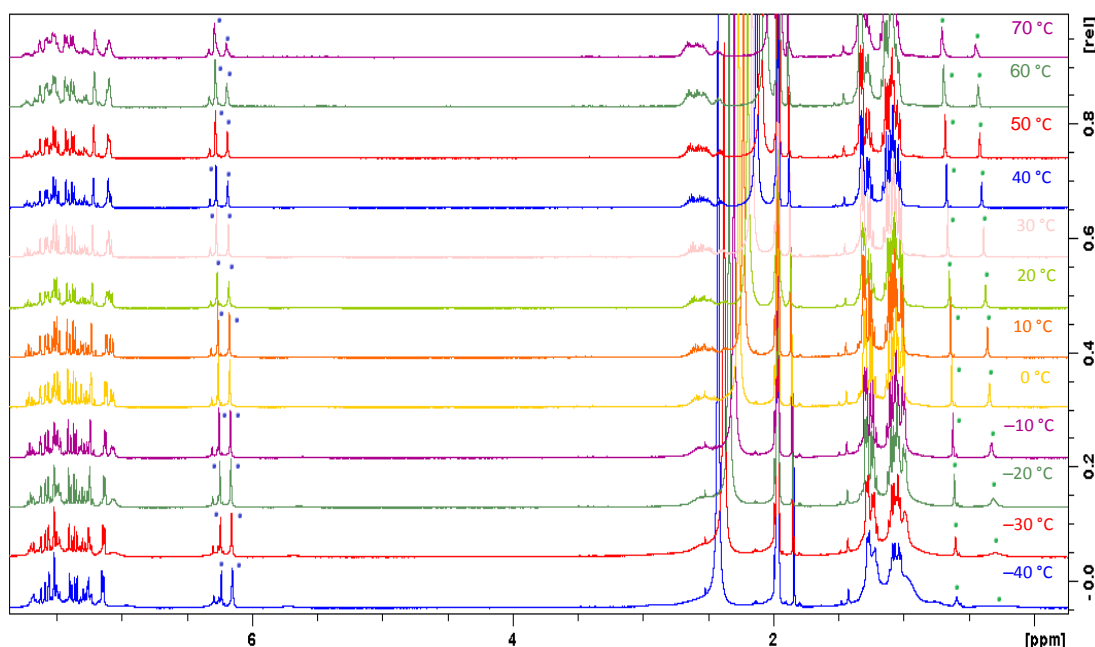


Figure 3.16: Overlay of the ^1H NMR spectra of **IIIc** in CD_3CN at temperatures from -40 to 70 °

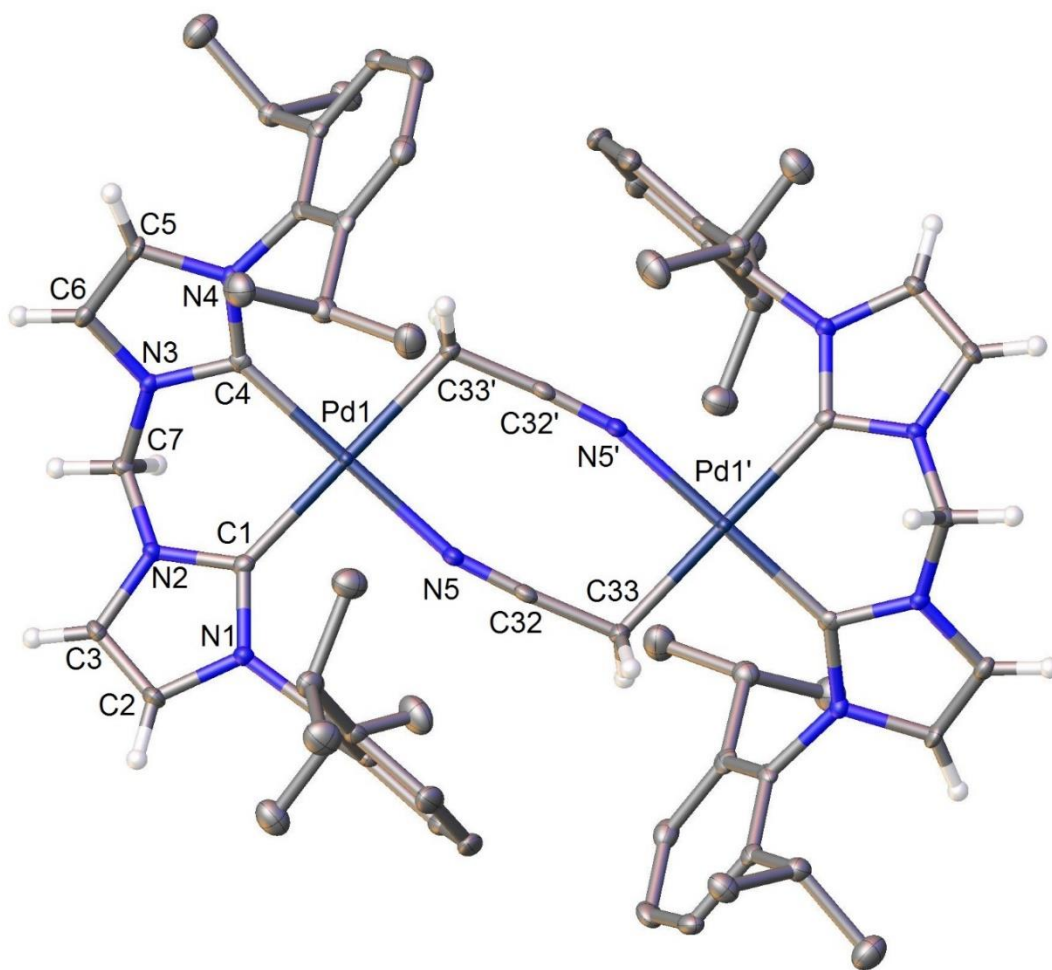


Figure 3.17: X-ray molecular structure of cation $\{([Dipplm]_2CH_2)Pd(\mu-CH_2CN)\}_2^{2+}$ of **IIIc**. Thermal ellipsoids are shown at the 50% probability level. 2 $[PF_6]^-$ counter ions and 2 Et_2O lattice solvent molecules omitted for clarity. All diisopropylphenyl hydrogen atoms removed for clarity. Selected bond lengths (Å) and angles ($^\circ$): Pd(1)–N(5) 2.038(3), Pd(1)–C(1) 2.065(3), Pd(1)–C(4) 2.013(3), Pd(1)–C(33) 2.126(3), N(5)–C(32) 1.146(4), C(32)–C(33) 1.433(4), N(5)–Pd(1)–C(1) 91.82(10), N(5)–Pd(1)–C(33) 88.37(10), C(4)–Pd(1)–C(1) 88.28(11), C(4)–Pd(1)–C(33) 91.77(11), C(32)–N(5)–Pd(1) 164.9(2), C(32)–C(33)–Pd(1) 110.7(2), N(5)–C(32)–C(33) 175.3(3).

was interesting due to the fact that the AB spin system is observed when solution phase fluctuation is restricted. This indicates that the steric hindrance of the mesityl

substituent for **IIIa** may be higher than that for the Dipp substituent of complex **IIIc**. The subsequent discussion of the comparison of the X-ray crystal structures of complexes **IIIa** and **IIIc** may account for this solution behaviour.

A crystal structure of $\{[(\text{DippIm})_2\text{CH}_2)\text{Pd}(\mu\text{-CH}_2\text{CN})_2][\text{PF}_6]_2$ (**IIIc**) was also obtained, containing metrics consistent with **IIIa** with Pd-C_{NHC} distances of 2.065(3) and 2.013(3) Å. The dimer has the same strained two CH₂CN ligands with a Pd–N≡C bond angle of 164.9(2) ° (Figure 3.17).

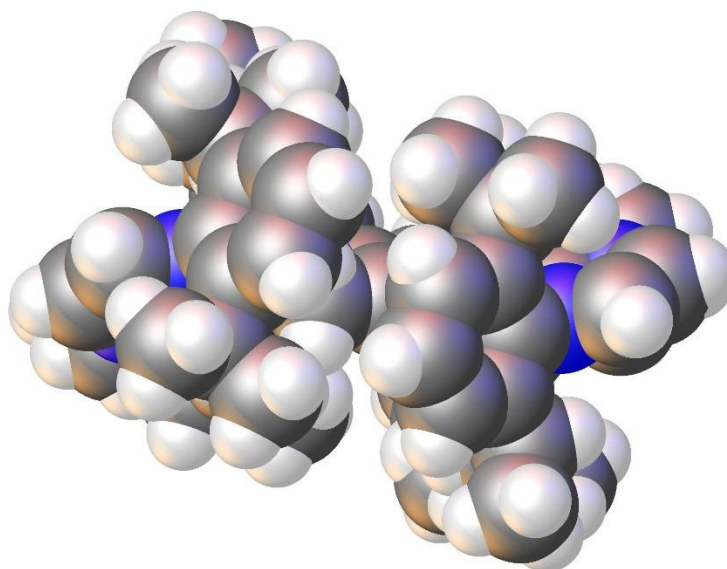
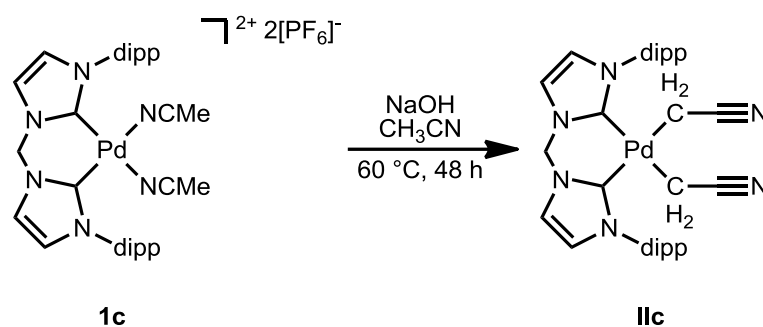


Figure 3.18: Spacefilling structure $\{[(\text{DippIm})_2\text{CH}_2)\text{Pd}(\mu\text{-CH}_2\text{CN})_2][\text{PF}_6]_2$ (**IIIc**) with *N*-diisopropyl substituents in the foreground.

$\{[(\text{DippIm})_2\text{CH}_2]\text{Pd}(\text{CH}_2\text{CN})_2$ (**IIc**) was synthesised by reacting $\{[(\text{DippIm})_2\text{CH}_2]\text{Pd}(\text{NCMe})_2][\text{PF}_6]_2$ (**1c**) with NaOH in CH₃CN for 48 h. The formation of the product was supported by ¹H and ¹³C NMR spectroscopy with resonances at 0.46 and –14.3 ppm respectively consistent with the CH₂ moiety within the CH₂CN ligand (Scheme 3.14). Unfortunately, due to the difficulty in acquiring large quantities of $\{[(\text{DippIm})_2\text{CH}_2]\text{Pd}(\text{CH}_2\text{CN})_2$ a crystal structure could not be obtained.



Scheme 3.14: Synthesis of $[\{(\text{DippIm})_2\text{CH}_2\}\text{Pd}(\text{CH}_2\text{CN})_2]$ (**11c**).

Analysis of the ^1H and ^{13}C NMR spectrum and X-ray crystal structures of the NCMe, CH_2CN and $\mu\text{-CH}_2\text{CN}$ ligated complexes for the *N*-Me, Mes and Dipp substituent reveals a trend around the strain observed for these complexes (Table 3.1).

The metrics of the crystal structures of the *N*-Mes substituted complexes $[\{(\text{MesIm})_2\text{CH}_2\}\text{Pd}(\text{NCMe})_2][\text{PF}_6]_2$ (**1a**) and $[\{(\text{MesIm})_2\text{CH}_2\}\text{Pd}(\text{CH}_2\text{CN})_2]$ (**11a**) are very similar for both the $\text{Im}/\text{PdC}_2\text{L}_2$ dihedral angles and the distance of the CH_2 from the PdC_2L_2 plane. The distance of the CH_2 from the PdC_2L_2 plane is a measure of the intra ligand *N*-substituent strain across the face of the chelating system.^[19] This is in contrast to $[\{([\text{MesIm}]_2\text{CH}_2)\text{Pd}(\mu\text{-CH}_2\text{CN})\}_2][\text{PF}_6]_2$ which has a lower dihedral angle and distance of the CH_2 from the PdC_2L_2 plane indicating higher strain on the molecule due to the steric influences from the second bis(NHC) ligand due to the dinuclear system.

Similarly the complexes with *N*-Me substituents $[\{(\text{MeIm})_2\text{CH}_2\}\text{Pd}(\text{NCMe})_2][\text{BF}_4]_2$ (**1b**) and $[\{(\text{MeIm})_2\text{CH}_2\}\text{Pd}(\text{CH}_2\text{CN})_2]$ (**11b**) have similar metrics and thus have similar strain on the molecules. However, comparing the metrics for the crystal structures for $[\{(\text{dippIm})_2\text{CH}_2\}\text{Pd}(\text{NCMe})_2][\text{PF}_6]_2$ (**1c**) and $[\{([\text{dippIm}]_2\text{CH}_2)\text{Pd}(\mu\text{-CH}_2\text{CN})\}_2][\text{PF}_6]_2$ (**111c**) it is important to note that although **1c** has a more strained geometry than the *N*-Mes equivalent **1a** the metrics of **111c** is close to that of **1c**. This indicates the presence of the strain observed in **111c** is primarily due to the steric influences within the bis(NHC) ligand of the diisopropylphenyl substituent rather than the interligand steric hindrance (Figure 3.19). This is highlighted by analysis of the space filling

representation of **IIIc** which doesn't appear to show an interaction between both bis(NHC) ligands (Figure 3.18). Despite the difference in the steric bulk of the ligands, the metrics of **IIIa** and **IIIc** are similar.

Comparing the ^1H and ^{13}C NMR spectra of all the compounds synthesised the values are consistent with those described in Chapter 1 for bonding mode **I** and **II** with all ^{13}C NMR resonances being in the region of -10.5 to -15.0 ppm. A trend emerges with **IIa**, **IIIa**, **IIb** and **IIIc** featuring an upfield ^1H NMR shift for the CH_2 resonances. In addition, although it unclear why both complexes **IIIb** and **IIIc** display ^1H NMR downfield shifts in comparison to the corresponding **II** complex. The ^{13}C NMR shift for the corresponding CH_2 carbon shifts upfield. Interestingly, the opposite is true for the *N*-Mes substituent.

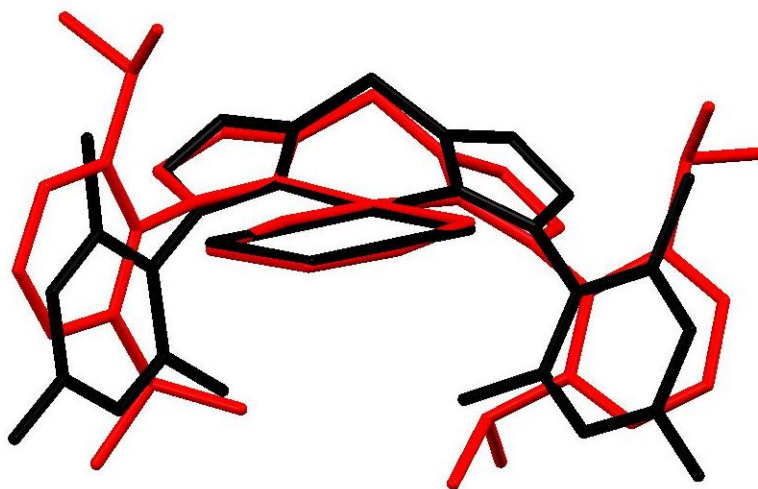


Figure 3.19: Structural overlay of $[[(\text{DippIm})_2\text{CH}_2)\text{Pd}(\mu\text{-CH}_2\text{CN})_2][\text{PF}_6]_2$ (red) and $[[(\text{MesIm})_2\text{CH}_2)\text{Pd}(\mu\text{-CH}_2\text{CN})_2][\text{PF}_6]_2$ (black) crystal structures. For clarity one bis(NHC) ligand is removed.

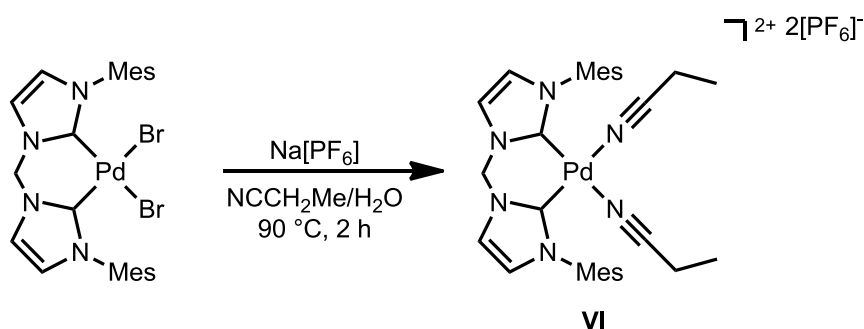
Comparing the steric bulk of the *N*-substituents a trend emerges around the selectivity between complex **II** and **III** (Figure 3.21, Table 3.1). Naota *et al.*^[20] postulated that the dinuclear complexes of type **III** are intermediates in the *N*- to *C*-bound isomerisation discussed in detail in the introduction. While all the reactions

were performed under similar equivalents of base, for *N*-Me only complex of **IIb** was observed, for *N*-Mes both complexes **IIa** and **IIIa** were observed while for *N*-Dipp only complex **IIIc** was observed after 24 h. Reacting **1c** with NaOH for 48 h the specificity of the product changed, forming **IIc** exclusively. In addition, when excess NaOH was added to the *N*-Mes complex **IIIa** it was converted to **IIa**. This indicates that the dinuclear product is an intermediate in the formation of the mononuclear product with the larger sterically hindered *N*-substituent complexes having a higher transition state energy for the formation of the second deprotonated acetonitrile ligand.

3.2.4 Synthesis of $[\{(MesIm)_2CH_2\}Pd(NCR)_2][PF_6]_2$:

Further work investigated increasing the scope of the reaction beyond acetonitrile to the more sterically hindered nitrile ligands to see whether the analogous α -deprotonated nitriles could be synthesised.

$[\{(MesIm)_2CH_2\}Pd(NCCH_2CH_3)_2][PF_6]_2$ (**VI**) was synthesised under analogous conditions to that previously published for the NCMe analogue $[\{(MesIm)_2CH_2\}Pd(NCMe)_2][PF_6]_2$ (**1a**) (Scheme 3.15, Figure 3.22).^[1] $[\{(MesIm)_2CH_2\}PdBr_2]$ was reacted with Na[PF₆] in a 1:1 mixture of propionitrile and H₂O at 90°C for 2 h forming the desired product. Unlike in the synthesis of **1a** where CH₃CN and H₂O are miscible, propionitrile and H₂O are immiscible and thus the reaction was stirred vigorously to afford a white solid in 42 % yield. The product



Scheme 3.15: Synthesis of $[\{(MesIm)_2CH_2\}Pd(NCCH_2CH_3)_2][PF_6]_2$ (**VI**).

identity was supported by both NMR spectroscopy and X-ray crystallography with ^1H NMR resonances at 2.45 and 1.14 ppm assigned to the propionitrile protons consistent with the coordination of propionitrile. The Pd–C_{NHC} distances of 1.983(4) and 1.992(4) Å are consistent with the previously reported **1a**.^[17]

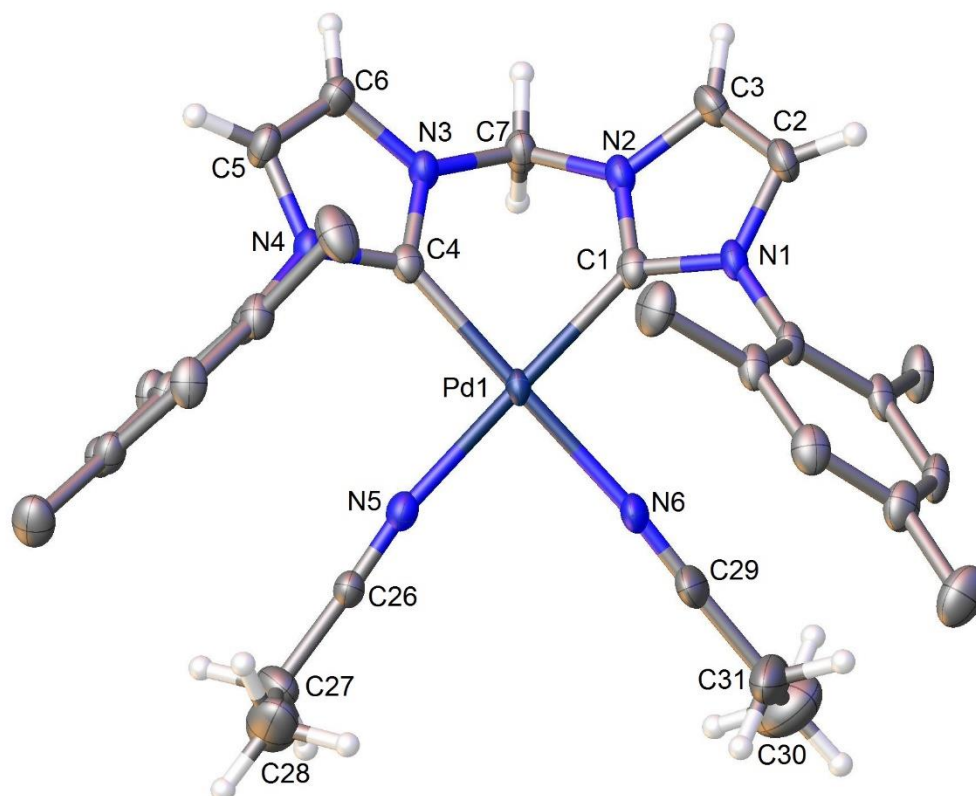
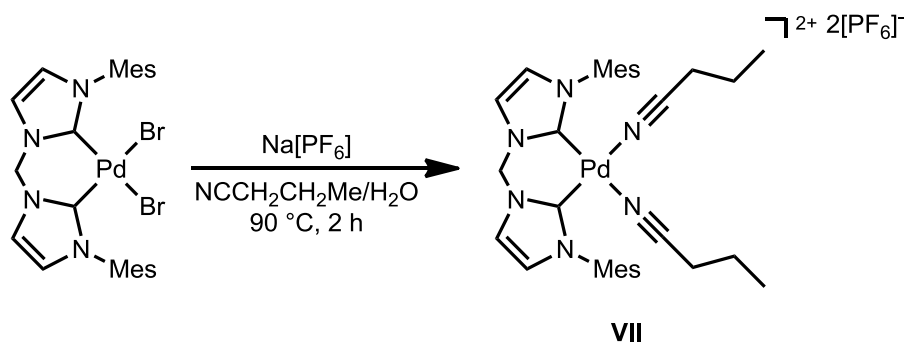


Figure 3.20: X-ray molecular structure of cation $[\{(\text{MesIm})_2\text{CH}_2\}\text{Pd}(\text{NCCH}_2\text{CH}_3)_2]^{2+}$ of **VI**. Thermal ellipsoids are shown at the 50% probability level. 2 $[\text{PF}_6]^-$ counter ions and a propionitrile lattice solvent molecule omitted for clarity. All mesityl hydrogen atoms removed for clarity. Selected bond lengths (Å) and angles (°): Pd(1)–N(5) 2.045(4), Pd(1)–N(6) 2.059(4), Pd(1)–C(1) 1.983(4), Pd(1)–C(4) 1.992(4), N(5)–Pd(1)–N(6) 85.92(15), C(1)–Pd(1)–N(6) 93.22(16), C(1)–Pd(1)–C(4) 85.66(18), C(4)–Pd(1)–N(5) 95.24(16).

Similarly $[\{(\text{MesIm})_2\text{CH}_2\}\text{Pd}(\text{NCCH}_2\text{CH}_2\text{CH}_3)_2][\text{PF}_6]_2$ (**VII**) was synthesised under analogous conditions to those previously published for

$[\{(MesIm)_2CH_2\}Pd(NCMe)_2][PF_6]_2$ (**1a**) (Scheme 3.16, Figure 3.21).^[1]

$[\{(MesIm)_2CH_2\}PdBr_2]$ was reacted with $Na[PF_6]$ in a 1:1 mixture of butyronitrile and H_2O at $90^\circ C$ for 2 h producing the desired product. As noted earlier, butyronitrile and H_2O are immiscible and thus the reaction was stirred vigorously to prepare the desired product in 45 % yield.



Scheme 3.16: Synthesis of $[\{(MesIm)_2CH_2\}Pd(NCCH_2CH_2CH_3)_2][PF_6]_2$ (**VII**).

Complex:	1a ^[1, 17]	VI	VII
Pd-C_{carbene} distance (Å)	1.983(4), 1.984(4)	1.983(4), 1.992(4)	1.969(6), 1.986(6)
C_{carbene}-Pd-C_{carbene} angle (°)	85.87(17)	85.66(18)	86.3(2)
C_{carbene}-N-R angle (°)	127.2(3), 128.1(4)	127.2(4), 129.5(4)	125.6(5), 128.8(5)
Av. distance from Im plane for C_N-substituent and Pd (Å)	0.045	0.0535	0.047
Im/PdC₂L₂ dihedral angle (°)	35.92(14), 37.7(2)	33.88(16), 37.63(16)	32.0(2), 37.50(19)
Distance of CH₂ from PdC₂L₂ plane (Å)	1.537(7)	1.448(7)	1.410(8)

Table 3.2: Key crystallographic data for $[\{(MesIm)_2CH_2\}Pd(NCMe)_2][PF_6]_2$ **1a**, $[\{(MesIm)_2CH_2\}Pd(NCCH_2CH_3)_2][PF_6]_2$ **VI** and $[\{(MesIm)_2CH_2\}Pd(NCCH_2CH_3)_2][PF_6]_2$ **VII**.

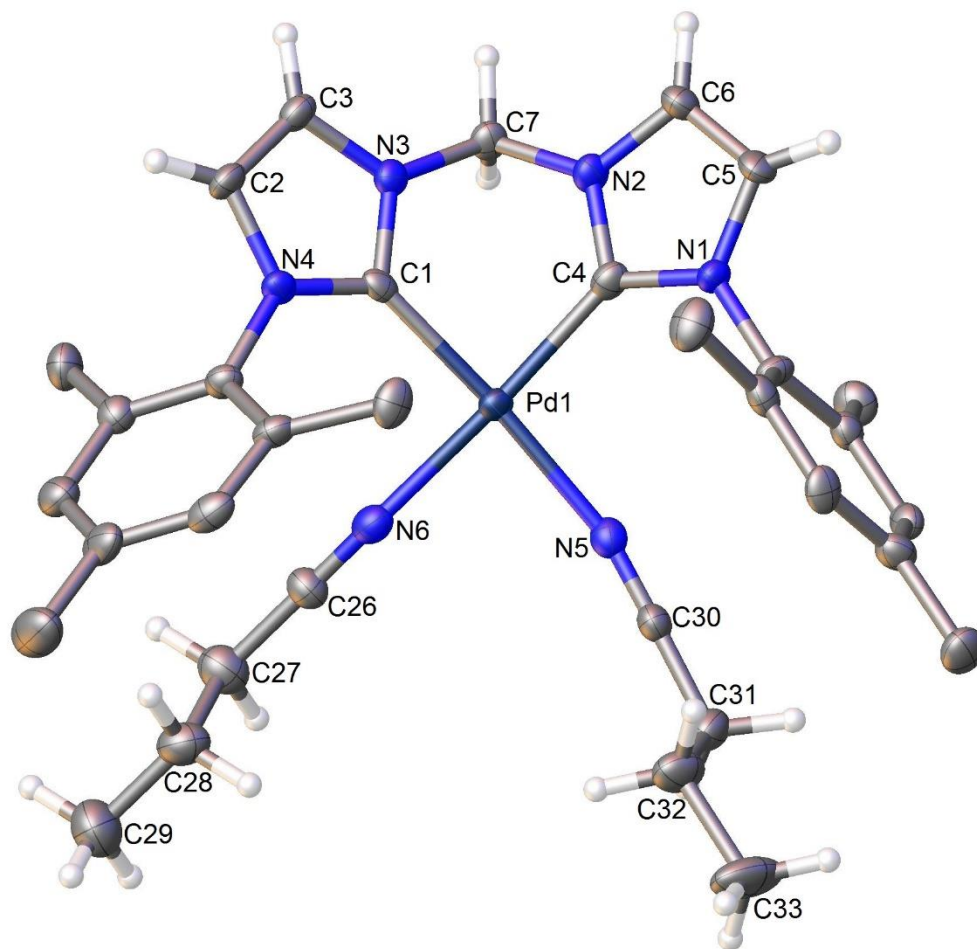


Figure 3.21: X-ray molecular structure of cation $[[(\text{MesIm})_2\text{CH}_2]\text{Pd}(\text{NCCH}_2\text{CH}_2\text{CH}_3)_2]^{2+}$ of **VII**. Thermal ellipsoids are shown at the 50% probability level. 2 $[\text{PF}_6]^-$ counter ions and a propionitrile lattice solvent molecule omitted for clarity. All mesityl hydrogen atoms removed for clarity. Selected bond lengths (Å) and angles ($^\circ$): Pd(1)–N(5) 2.060(5), Pd(1)–N(6) 2.051(5), Pd(1)–C(1) 1.969(6), Pd(1)–C(4) 1.986(6), N(6)–Pd(1)–N(5) 85.68(19), C(1)–Pd(1)–N(6) 91.0(2), C(1)–Pd(1)–C(4) 86.3(2), C(4)–Pd(1)–N(5) 97.3(2).

The formation of **VII** was supported by NMR spectroscopy and X-ray crystallography with ^1H NMR resonances at 2.46, 1.56 and 0.96 ppm assigned to the butyronitrile protons consistent with the coordination of the butyronitrile ligand. The X-ray crystal

structure metrics were consistent with **1a** and **VI** with Pd–C_{NHC} distances of 1.969(6) and 1.986(6) Å. Analysis of the change in metrics of the X-ray crystal structures of **1a**, **VI** and **VII** it can be seen that with the increase in length of the nitrile ligand there is increased strain within the molecule. This is observed with a decreasing of the Im/PdC₂L₂ dihedral angle and distance of the CH₂ from the PdC₂L₂ plane indicating a flattening of the bis(NHC) ligand to accommodate the increased steric bulk.

The synthesis of the corresponding α -cyanocarbanion complexes was attempted in an effort to understand the effect of the steric bulk of the nitrile on the complexes formed. Both **VI** and **VII** were treated with NaOH in the corresponding solvent in an attempt to form the desired α -cyanocarbanion complex, however, no reaction was observed.

3.3 Conclusion:

Syntheses of $[\{(\text{MesIm})_2\text{CH}_2\}\text{Pd}(\text{CH}_2\text{CN})_2]$ (**IIa**) and $[\{(\text{MesIm})_2\text{CH}_2\}\text{Pd}(\mu\text{-CH}_2\text{CN})\}_2][\text{PF}_6]_2$ (**IIIa**) were improved from the existing method developed in our group^[4] by reacting $[\{(\text{MesIm})_2\text{CH}_2\}\text{Pd}(\text{NCMe})_2][\text{PF}_6]_2$ (**1a**) with NaOH rather than NaOtBu. The use of NaOtBu led to an unintended side reaction, which was avoided by the former base, 3-aminocrotonitrile (**IV**) and 4-amino-2,6-dimethylpyrimidine (**V**) were synthesised by reacting NaOtBu in CH₃CN. Complex **IIa** and **IIIa** could be readily interconverted. Stirring **IIIa** with excess NaOH in CH₃CN yielded **IIa** and **IIa** was treated with one equivalent of H[BF₄] in CH₃CN affording **IIIa**.

The ¹H NMR spectrum of **IIIa** in CD₃CN shows an equilibrium that exists in solution. Through DOSY and NOESY NMR experiments it was suggested that an equilibrium between $[\{(\text{MesIm})_2\text{CH}_2\}\text{Pd}(\mu\text{-CH}_2\text{CN})\}_2][\text{PF}_6]_2$ and $[\{(\text{MesIm})_2\text{CH}_2\}\text{Pd}(\text{CH}_2\text{CN})(\text{NCMe})][\text{PF}_6]$ in solution occurs, which is slow on the NMR time scale at room temperature. VT ¹H NMR studies were performed to better understand the equilibrium at various temperatures. In each case, both complexes were present in solution at those temperatures utilised. When the solution was cooled below -15 °C a third product was also formed, however, the nature of this product was not determined due to the various products in solution.

To better understand the impact of steric hindrance on the above reaction two other bis(NHC) ligands were chosen, *N*-Me and *N*-Dipp. $[\{(\text{MeIm})_2\text{CH}_2\}\text{Pd}(\text{NCMe})_2][\text{PF}_6]_2$ was reacted with NaOH in CH₃CN yielding $[\{(\text{MeIm})_2\text{CH}_2\}\text{Pd}(\text{CH}_2\text{CN})_2]$ exclusively. An intermediate $[\{(\text{MeIm})_2\text{CH}_2\}\text{Pd}(\mu\text{-OH})\}_2][\text{PF}_6]_2$ was isolated which was the only intermediate observed when the reaction was performed on an NMR scale. $[\{(\text{MeIm})_2\text{CH}_2\}\text{Pd}(\text{CH}_2\text{CN})_2]$ was also reacted with H[BF₄] in CH₃CN forming $[\{(\text{MeIm})_2\text{CH}_2\}\text{Pd}(\mu\text{-CH}_2\text{CN})\}_2][\text{BF}_4]_2$ in low yield.

In comparison when $[\{(\text{DippIm})_2\text{CH}_2\}\text{Pd}(\text{NCMe})_2][\text{PF}_6]_2$ was reacted with NaOH in CH₃CN for 24 hours $[\{(\text{DippIm})_2\text{CH}_2\}\text{Pd}(\mu\text{-CH}_2\text{CN})\}_2][\text{BF}_4]_2$ (**IIIc**) was exclusively

formed. However, when the reaction was performed for 48 h $[\{(DippIm)_2CH_2\}Pd(CH_2CN)_2]$ (**IIc**) was formed exclusively, this is due to the increased steric hindrance requiring longer reaction time for complete conversion.

$[\{(MesIm)_2CH_2\}Pd(NCCH_2CH_3)_2][PF_6]_2$ and $[\{(MesIm)_2CH_2\}Pd(NCCH_2CH_2CH_3)_2][PF_6]_2$ were synthesised by reacting $[\{(MesIm)_2CH_2\}PdBr_2]$ and $Na[PF_6]$ in a 1:1 mixture of H_2O and the corresponding nitrile. However, reacting these complexes with $NaOH$ did not yield the α -cyanocarbanion complexes, which were anticipated to provide more information regarding the impact of the steric bulk of the nitrile on the complex and to expand the range of nitrile coupling reactions discussed in Chapter 5.

3.4 Experimental:

3.4.1 General Considerations:

All air sensitive reactions were performed under an atmosphere of high purity argon using standard Schlenk techniques. NMR scale reactions were prepared in a dry glove box (Innovative Technologies) under a nitrogen atmosphere with J Young's NMR tubes. Glassware was heated under vacuum and back-filled with argon to ensure the exclusion of oxygen and moisture in the reactions. The following chemicals were used as received: Na[PF₆] (Aldrich), dibromomethane (Aldrich), 2-methyl imidazole (Aldrich), Pd(OAc)₂ (Precious Metals On-Line Pty Ltd.), 2,4,6-trimethylaniline (Alfa Aesar), Glyoxal (VWR), [NH₄]Cl (Chem Supply), Orthophosphoric acid (85 % of an aqueous solution, Ajax), tetrafluoroboric acid (50 % of an aqueous solution, Riedel-de Haen), 2,6-diisopropylaniline (Fluka). NaOH was purchased from Chem Supply and dried under vacuum at 200 °C. NaOtBu was synthesised by a previous student and sublimed at 200 °C. For air sensitive reactions anhydrous DMSO was purchased from Sigma-Aldrich and stored in an ampoule over 3 Å molecular sieves, anhydrous CH₃CN was obtained by passage through an Innovative Technologies Solvent Purifier and stored in an ampoule over 3 Å molecular sieves. For air stable synthesis, solvents were of analytical grade and used as received. [{{(MesIm)₂CH₂}Pd(NCMe)₂][PF₆]₂^[11] (**1a**), [{{(MeIm)₂CH₂}Pd(NCMe)₂][PF₆]₂^[19] (**1b**), [{{(dipplm)₂CH₂}Pd(NCMe)₂][PF₆]₂^[18] (**1c**) and [{{(MesIm)₂CH₂}PdBr₂]^[11] were all synthesised according to literature procedures.

3.4.2 Instrumentation:

NMR spectroscopic studies were carried out on a Bruker Avance 3 HD 400 MHz Wide Bore Spectrometer with a 5 mm BBFO probe at room temperature (293 K) unless otherwise stated or a Bruker Avance III HD 600 MHz spectrometer with a 5 mm TCI-cyprobe at 300 K, in DMSO-*d*₆, CDCl₃ or CD₃CN. CDCl₃ was used as received, whereas CD₃CN and DMSO-*d*₆ were used as received except in air

sensitive NMR spectroscopy where they were distilled over calcium hydride and stored over 3 Å molecular sieves. ^1H NMR spectra were obtained at 399.58 or 600.07 MHz while ^{13}C NMR spectra were recorded at 100.47 or 150.89 MHz. ^1H NMR spectra were referenced to the residual ^1H resonance of the residual solvent peak while ^{13}C NMR spectra were referenced to a deuterated ^{13}C resonance.

Elemental analyses were conducted by Dr. Thomas Rodemann at the Central Science Laboratory at the University of Tasmania using a Carlo Erba EA1108 Elemental Analyser.

EI-MS studies were conducted on an Agilent Technologies 6850 GC with a 5975C VL MSD.

ESI-MS were conducted by Richard Wilson or Dr David Nichols at the Central Science Laboratory at the University of Tasmania using a LTQ-Orbitrap high resolution mass spectrometer (Thermo Fisher Scientific) by infusion at 5 $\mu\text{l}/\text{min}$ using Positive mode electrospray ionisation, with a voltage of 4 kV applied. Full scan data (m/z range 150-2000) was acquired at a resolution of 60,000 and reported values for $[\text{M}+\text{H}]$ or $[\text{M}+\text{Na}]$ ions were based on the averaged spectrum of 20 successive scans.

X-ray crystallographic data for **IIb** and $\{([\text{MeIm}]_2\text{CH}_2)\text{Pd}(\mu\text{-OH})_2\}_2[\text{PF}_6]_2$ were collected at $-173\text{ }^\circ\text{C}$ on crystals mounted on a Hampton Scientific cryoloop at the MX1 or MX2 beamlines of the Australian Synchrotron.^[21] Data completeness is limited by the single axis goniometer on the MX beamlines and the Australian synchrotron. Data for **IIIa**, **IIIc**, **VI** and **VII** were collected at $-173\text{ }^\circ\text{C}$ on crystals mounted on a Hampton Scientific cryoloop on a Bruker AXS D8 Quest with a Cu K α source. The structures were solved by direct methods with SHELXT, refined using full-matrix least-squares routines against F^2 with SHELXL-97,^[22] and visualised using Olex2.^[23] All non-hydrogen atoms were refined anisotropically. All hydrogen

atoms were placed in calculated positions and refined using a riding model with fixed C–H distances of 0.95 Å (sp^2 CH), 1.00 Å (sp^3 CH), 0.99 Å (CH₂), 0.98 Å (CH₃). The thermal parameters of all hydrogen atoms were estimated as $U_{iso}(H) = 1.2U_{eq}(C)$, except for CH₃ where $U_{iso}(H) = 1.5U_{eq}(C)$. Cif files available on request.

3.4.3 Preparation of [{{(MesIm)}₂CH₂}Pd(CH₂CN)₂] (IIa):

Method A: [{{(MesIm)}₂CH₂}Pd(NCMe)₂][2PF₆] (52.5 mg, 60.8 μmol) and NaOH (15.3 mg, 0.383 mmol) were combined in a predried Schlenk flask and then further dried under vacuum at 70 °C. CH₃CN (5.0 mL) was then added to the solid and the solution was stirred at 60 °C for 24 h. The solvent was removed under vacuum and the product was recrystallised by vapour diffusion of diethyl ether into a near saturated solution of CH₃CN. NMR spectroscopic analysis indicated that this compound was spectroscopically identical to equivalent data reported in the literature^[4]. (quantitative yield, 48.6 mg)

Method B: [{{([MesIm]₂CH₂)Pd(μ-CH₂CN)}₂][PF₆]₂ (104 mg, 76.6 μmol) and NaOH (66.1 mg, 1.65 mmol) were combined in a predried Schlenk flask and further dried under vacuum at 70 °C. The solid was dissolved in CH₃CN (5.0 mL) and stirred at 60 °C for 24 h. The solution was cooled to room temperature and the CH₃CN was removed under vacuum at 60 °C. The crude product was dissolved in H₂O and the pure product was collected via vacuum filtration and dried under vacuum for 72 h to provide the product as an off-white solid (75 % yield, 65.8 mg)

¹H NMR (400 MHz, CD₃CN): δ 7.50 (2H, d, $J = 2$ Hz, ImH), 7.02 (4 H, s, *m*-CH), 6.96 (2H, d, $J = 2$ Hz, ImH), 6.20 (2 H, bs, CH₂), 2.32 (6H, s, *p*-Me), 2.06 (12 H, s, *o*-Me), 0.36 ppm (4H, bs, Pd-CH₂).

MP: 233 °C (dec)

ESI-MS: m/z 588.2068 calculated for C₂₉H₃₆N₇Pd⁺ (IIa + NH₄) 588.2067

3.4.4 Preparation of $\{[(\text{MesIm})_2\text{CH}_2]\text{Pd}(\mu\text{-CH}_2\text{CN})_2\}[\text{PF}_6]_2$ (IIIa):

$\{[(\text{MesIm})_2\text{CH}_2]\text{Pd}(\text{NCMe})_2\}[\text{PF}_6]_2$ (71.1 mg, 82.4 μmol) and NaOH (11.4 mg, 0.285 mmol) were combined in a predried Schlenk and then further dried under vacuum at 70 °C. CH_3CN (5.0 mL) was then added to the solid and the solution was stirred at 60 °C for 24 h. The solvent was removed under vacuum and the product was recrystallised by vapour diffusion of diethyl ether into a near saturated solution of CH_3CN . The product was washed with a small quantity of CH_3CN . Only limited characterisation in CD_3CN was possible due to the low solubility and dissociation of the complex. (45 % yield, 25.3 mg)

^1H NMR (400 MHz, CD_3CN): δ (The complex dissociates partially in solution to form complex A and B in a 1.8:1 ratio) 7.62 (1H, d, $J = 1.9$ Hz, $\text{Im}_\text{B}\text{H}$), 7.60 (1H, d, $J = 1.8$ Hz, $\text{Im}_\text{B}\text{H}$), 7.59 (2H, d, $J = 1.8$ Hz, $\text{Im}_\text{A}\text{H}$) 7.56 (2H, d, $J = 1.8$ Hz, $\text{Im}_\text{A}\text{H}$), 7.23 (2H, bs, $\text{Ar}_\text{B}\text{H}$), 7.14 (1H, d, $J = 2.0$ Hz, $\text{Im}_\text{B}\text{H}$) 7.11–7.12 (3H, m, $\text{Im}_\text{B}\text{H}$ & ArH), 7.09 (2H, d, $J = 1.9$ Hz, $\text{Im}_\text{A}\text{H}$), 7.06 (3H, s, $\text{Ar}_\text{A}\text{H}$ & $\text{Ar}_\text{B}\text{H}$) 6.99 (2H, bs, $\text{Ar}_\text{A}\text{H}$), 6.82 (2H, bs, $\text{Ar}_\text{A}\text{H}$), 6.28 (2H, s, $\text{C}_\text{B}\text{H}_2$), 6.19 (4H, s, $\text{C}_\text{A}\text{H}_2$), 2.37 (9H, s, $\text{C}_\text{B}\text{H}_3$), 2.34 (3H, s, $\text{C}_\text{B}\text{H}_3$), 2.30 (6H, s, $\text{C}_\text{B}\text{H}_3$), 2.11 (12H, s, $\text{C}_\text{A}\text{H}_3$), 2.02 (12H, s, $\text{C}_\text{A}\text{H}_3$), 1.77–1.91 (12H, s, $\text{C}_\text{A}\text{H}_3$), 0.52 (4H, bs, $\text{C}_\text{A}\text{H}_2\text{CN}$), 0.06 ppm (2H, bs, $\text{C}_\text{B}\text{H}_2\text{CN}$).

^{13}C NMR (150 MHz, CD_3CN): δ 172.5 ($\text{Im}_\text{B}\text{-Pd}$), 168.5 (b, $\text{Im}_\text{A}\text{-Pd}$), 160.2 ($\text{Im}_\text{B}\text{-Pd}$), 158.8 (b, $\text{Im}_\text{A}\text{-Pd}$), 140.5 ($\text{Ar}_\text{B}\text{C}$), 140.0 ($\text{Ar}_\text{B}\text{C}$), 129.8 ($\text{Ar}_\text{A}\text{H}$), 129.7 ($\text{Ar}_\text{B}\text{H}$), 129.4 (ArH), 129.1 ($\text{Ar}_\text{A}\text{H}$), 128.9 ($\text{Ar}_\text{A}\text{H}$), 124.8 ($\text{Im}_\text{B}\text{H}$), 124.7 (ArH), 123.8 ($\text{Im}_\text{A}\text{H}$), 123.0 ($\text{Im}_\text{A}\text{H}$ & $\text{Im}_\text{B}\text{H}$), 122.2 ($\text{Im}_\text{B}\text{H}$), 122.1 ($\text{Im}_\text{A}\text{H}$), 63.7 ($\text{C}_\text{B}\text{H}_2$), 63.5 ($\text{C}_\text{A}\text{H}_2$), 20.9 ($\text{C}_\text{B}\text{H}_3$), 20.8 ($\text{C}_\text{B}\text{H}_3$), 20.7 ($\text{C}_\text{B}\text{H}_3$), 17.5 (b, $\text{C}_\text{A}\text{H}_3$), -12.3 ($\text{C}_\text{B}\text{H}_2\text{CN}$), -15.0 ppm ($\text{C}_\text{A}\text{H}_2\text{CN}$).

^1H NMR (400 MHz, $\text{DMSO-}d_6$, 120 °C): δ 7.86 (2H, s, NCHCHN), 7.79 (2H, s, NCHCHN), 7.41 (2H, s, NCHCHN), 7.34 (2H, s, NCHCHN), 7.15 (4H, s, $m\text{-CH}$), 6.89 (4H, s, $m\text{-CH}$), 6.44 (4H, s, NCH_2N), 2.36 (6H, s, $p\text{-CH}_3$), 2.28 (6H, s, $p\text{-CH}_3$), 2.04 (12H, s, $o\text{-CH}_3$), 1.83 (12H, s, $o\text{-CH}_3$), 0.31 ppm (4H, s, CH_2CN).

^{13}C NMR (100.47 MHz, DMSO- d_6): δ 167.1 (Ar), 157.5 (Ar), 139.9 (Ar), 138.9 (Ar), 136.1 (Ar), 135.7 (Ar), 135.5 (Ar), 135.1 (Ar), 134.7 (Ar), 134.3 (Ar), 133.1 (Ar), 129.7 (*m*-CH), 129.3 (*m*-CH), 129.0 (*m*-CH), 128.5 (*m*-CH), 124.7 (NCHCHN), 124.0 (NCHCHN), 123.3 (NCHCHN), 122.3 (NCHCHN), 62.9 (NCH₂N), 21.1 (*p*-CH₃), 21.0 (*p*-CH₃), 18.6 (*o*-CH₃), 17.9 (*o*-CH₃), 17.6 (*o*-CH₃), 17.4 (*o*-CH₃), -12.4 ppm (CH₂CN).

ESI-MS: *m/z* 530.1512 calc. for PdN₅C₂₇H₃₀ (M⁺ broken between Pd-N bonds) 530.1531

Elemental composition: Calculated: Pd₂N₁₀C₅₄H₆₀P₂F₁₂: C 47.98, N 10.36; H 4.47%; Found: C 48.04; N 11.01; H 4.70%

MP: 194 °C (dec)

3.4.5 Preparation of [({[MesIm]₂CH₂})Pd(μ -CH₂CN)]₂[BF₄]₂:

[({[MesIm]₂CH₂})Pd(CH₂CN)₂] (61.8 mg, 0.108 mmol), H[BF₄] (50 % in H₂O, 13.8 μ L, 0.108 mmol) and CH₃CN (5.0 mL) were combined in a round-bottom flask and stirred at room temperature for 5 min. The CH₃CN was removed under vacuum and the solid was washed with H₂O to provide a white solid with NMR spectroscopic analysis indicated that this compound was spectroscopically identical to equivalent data reported for the [PF₆] analogue **IIIa** (97 % yield, 64.7 mg).

^1H NMR (400 MHz, CD₃CN): δ 7.64-7.59 (4H, m, ImH), 7.57 (2H, d, *J* = 1.6 Hz, ImH), 7.23 (2H, bs, ArH), 7.14 (1H, d, *J* = 1.8 Hz, ImH), 7.12 (4H, s, ArH), 7.09 (2H, d, *J* = 1.7 Hz, ImH), 7.06 (3H, s, ArH), 6.99 (2H, bs, ArH), 6.83 (2H, bs, ArH), 6.29 (2H, s, CH₂), 6.20 (4H, s, CH₂), 2.37 (9H, s, CH₃), 2.34 (3H, s, CH₃), 2.30 (6H, s, CH₃), 2.106-2.12 (12H, m, CH₃), 2.03 (12H, s, CH₃), 1.78-1.89 (12H, s, CH₃), 0.53 (2H, bs, CH₂CN), 0.08 ppm (2H, bs, CH₂CN).

3.4.6 Preparation of 3-Aminocrotonitrile (IV) and 4-Amino-2,6-dimethylpyrimidine (V): NaOtBu (61 mg, 0.635 mmol) and CH₃CN (10 mL) were combined in a predried Schlenk flask and stirred at 70 °C for 16 h. The solid was filtered through a plug of celite[®] and the CH₃CN was removed under vacuum. The products were separated via flash column chromatography eluting with 70% EtOAc/hexanes yielding **IV** as a 1:0.6 mixture of *Z*- & *E*-isomers (81.3 mg, 0.990 mmol).

¹H NMR (400 MHz, CDCl₃): δ 4.99 (2H_a, bs, NH₂), 4.85 (2H_b, bs, NH₂), 4.03 (1H_b, s, CH), 3.70 (1H_a, s, CH), 2.02 (3H_b, s, CH₃), 1.86 ppm (3H_a, s, CH₃).

¹³C NMR (151 MHz, CDCl₃): δ 162.3 (C-NH₂), 161.7 (C-NH₂), 122.0 (C≡N), 120.0 (C≡N), 63.7 (CH), 61.6 (CH), 21.1 (CH₃), 19.4 ppm (CH₃).

EI-MS: *m/z* 82 (M⁺)

IR: 3327 (N-H), 2858 (C-H), 2781 (C-H), 2217 (C≡N), 1658 (C≡N/ C=C), 1652 (C≡N/ C=C), 1612 (C≡N/ C=C), 1562, 1413, 1375, 1201, 945, 924, 874, 722 cm⁻¹.

The second product was eluted with 10% MeOH/CH₂Cl₂ to provide an off-white solid of **V**. (77.5 mg, 0.629 mmol) NMR spectroscopic analysis indicated that this compound was spectroscopically identical to equivalent data reported in the literature.^[9]

¹H NMR (400 MHz, DMSO-*d*₆): δ 6.07 (1H, s, CH), 2.25 (3H, s, CH₃), 2.14 ppm (3H, s, CH₃).

3.4.7 Preparation of [{{(MeIm)₂CH₂}Pd(CH₂CN)₂] (IIb):

[{{(MeIm)₂CH₂}Pd(NCMe)₂][2PF₆] (53.6 mg, 81.6 μmol) and NaOH (30.6 mg, 0.765 mmol) were combined in a predried Schlenk flask and then further dried under vacuum at 70 °C. CH₃CN (5.0 mL) was then added to the solid and the

solution was stirred at 60 °C for 24 h. The solvent was removed under vacuum and the product was recrystallised via slow evaporation of CH₃CN. (76 % yield, 21.0 mg)

¹H NMR (400 MHz, CD₃CN): δ 7.24 (2H, d, *J* = 1.7 Hz, 1mH), 6.98 (2H, d, *J* = 1.7 Hz, 1mH), 6.08 (1H, d, *J* = 13.1 Hz, CH₂), 5.84 (1H, d, *J* = 13.2 Hz, CH₂), 3.77 (6H, s, CH₃), 1.12 (2H, d, *J* = 13.5 Hz, CH₂CN), 1.04 ppm (2H, d, *J* = 13.6 Hz, CH₂CN).

¹³C NMR (100.47 MHz, CD₃CN): δ 180.0 (C-Pd), 130.3 (C≡N), 121.7 (1mH), 120.6 (1mH), 63.1 (CH₂), 36.8 (CH₃), -13.5 ppm (CH₂CN).

ESI-MS: 322.0306 calculated for C₁₃H₁₆N₆Pd⁺ (**IIb** - CH₂CN) 322.0284 and 381.0674 calculated for C₁₃H₁₉N₆OPd⁺ (**IIb** + H₃O⁺) 381.0655

MP: 282 °C (dec)

3.4.8 Preparation of [({(MeIm)₂CH₂)Pd(μ-CH₂CN)₂][BF₄]₂ (**IIb**):

[{(MeIm)₂CH₂Pd(CH₂CN)₂] (52.5 mg, 0.145 mmol), H[BF₄] (50 % in H₂O, 18.5 μL, 0.147 mmol) and CH₃CN (7 mL) were stirred in a round bottom flask at rt for 10 minutes. The CH₃CN was removed under vacuum and the solid was washed with water. The solid was redissolved in CH₃CN, filtered and the CH₃CN was removed under vacuum forming a white solid (3 % yield, 1.5 mg)

¹H NMR (600 MHz, CD₃CN): δ 7.37 (1H, s, 1mH), 7.33 (1H, s, 1mH), 7.13 (1H, s, 1mH), 7.08 (1H, s, 1mH), 6.15 (1H, d, *J* = 13.4 Hz, CH₂), 5.98 (1H, d, *J* = 13.0 Hz, CH₂), 3.83 (3H, s, Me), 3.80 (3H, s, Me), 1.26–1.32 ppm (2H, m, CH₂CN).

¹³C NMR (150 MHz, CD₃CN): δ 171.7 (Pd-C, found by HMBC), 161.1 (Pd-C, found by HMBC), 127.6 (C≡N, found by HMBC), 123.1 (1mH), 122.3 (1mH), 122.1 (1mH), 121.1 (1mH), 62.9 (CH₂), 37.3 (Me), 37.2 (Me), -14.1 (CH₂CN) ppm.

ESI-MS: 322.0297 calc for C₂₂H₂₈N₁₀Pd₂²⁺ 322.0279

3.4.9 Preparation of $[\{(\text{Dipplm})_2\text{CH}_2\}\text{Pd}(\mu\text{-CH}_2\text{CN})_2\][\text{PF}_6]_2$ (IIIc):

$[\{(\text{dipplm})_2\text{CH}_2\}\text{Pd}(\text{NCMe})_2][\text{PF}_6]_2$ (0.107 g, 0.113 mmol) and NaOH (49 mg, 1.23 mmol) were combined in a predried Schlenk flask and then further dried under vacuum at 70 °C. CH_3CN (5.0 mL) was then added to the solid and the solution was stirred at 60 °C for 24 h. The solvent was removed under vacuum and the product was recrystallised by vapour diffusion of Et_2O into a near saturated solution of CH_3CN to provide colourless crystals (25 % yield, 21.2 mg)

^1H NMR (400 MHz, $\text{DMSO-}d_6$): δ 7.88 (2H, d, $J=2.0$ Hz, 1mH), 7.80 (2H, d, $J=1.8$ Hz, 1mH), 7.72 (2H, t, $J=7.8$ Hz, $p\text{-CH}$), 7.55 (4H, t, $J=1.7$ Hz, 1mH), 7.51 (4H, d, $J=7.8$ Hz, $m\text{-CH}$), 7.29 (2H, t, $J=7.8$ Hz, $m\text{-CH}$), 7.05 (4H, d, $J=7.7$ Hz, $p\text{-H}$), 6.45 (4H, s, CH_2), 2.26 (8H, bs, $i\text{Pr CH}$), 1.20 (12H, d, $J=6.8$ Hz, $i\text{Pr CH}_3$), 1.05 (12H, d, $J=6.7$ Hz, $i\text{Pr CH}_3$), 1.00 (12H, d, $J=6.8$ Hz, $i\text{Pr CH}_3$), 0.99 (12H, bs, $i\text{Pr CH}_3$), 0.30 ppm (4H, s, CH_2CN).

^{13}C NMR (100.47 MHz, $\text{DMSO-}d_6$): δ 167.4 (Pd-C), 154.9 (Pd-C), 145.0 (Ar), 135.4 (Ar), 135.0 (Ar), 133.5 ($\text{C}\equiv\text{N}$), 131.5 ($p\text{-H}$), 130.6 ($m\text{-H}$), 127.7 (1mH), 126.5 (1mH), 125.0 ($m\text{-H}$), 123.7 ($p\text{-H}$), 123.0 (1mH), 121.7 (1mH), 28.3 ($i\text{Pr CH}$), 25.5 ($i\text{Pr CH}_3$), 25.3 ($i\text{Pr CH}_3$), 23.5 ($i\text{Pr CH}_3$), 23.4 ($i\text{Pr CH}_3$), -10.5 ppm (CH_2CN).

MP: 218 °C (dec)

Anal. Calc. for $\text{C}_{66}\text{N}_{10}\text{H}_{84}\text{Pd}_2\text{P}_2\text{F}_{12}$: C, 52.14; H, 5.57; N, 9.21; Found: C, 51.88; H, 5.65; N, 8.82 %

3.4.10 Preparation of $[\{(\text{Dipplm})_2\text{CH}_2\}\text{Pd}(\text{CH}_2\text{CN})_2]$ (IIc):

$[\{(\text{Dipplm})_2\text{CH}_2\}\text{Pd}(\text{NCMe})_2][\text{PF}_6]_2$ (47.1 mg, 49.7 μmol) and NaOH (23 mg, 0.575 mmol) were combined in a predried Schlenk flask and further dried under vacuum at 70 °C. To the CH_3CN (5 mL) was added and the solution was stirred at 60 °C for 48 hours. The CH_3CN was removed under vacuum and the solid was washed with H_2O isolating a white solid (91 % yield, 29.6 mg).

¹H NMR (400 MHz, CD₃CN): δ 7.53 (2H, d, *J* = 1.8 Hz, 1mH), 7.51 (2H, t, *J* = 7.8 Hz, *p*-CH), 7.35 (4H, d, *J* = 7.8 Hz, *m*-CH), 7.09 (2H, d, *J* = 1.9 Hz, 1mH), 6.21 (2H, s, CH₂), 2.65 (4H, sep, *J* = 6.8 Hz, *i*Pr CH), 1.30 (12H, d, *J* = 6.8 Hz, *i*Pr CH₃), 1.07 (12H, d, *J* = 6.8 Hz, *i*Pr CH₃), 0.46 ppm (4H, s, CH₂CN).

¹³C NMR (150 MHz, CD₃CN): δ 179.5 (Pd-C), 145.6 (*o*-C), 136.1 (N-C), 130.0 (*p*-CH), 129.3 (CN), 125.4 (1mH), 124.0 (*m*-CH), 120.2 (1mH), 63.1 (CH₂), 28.1 (*i*Pr CH), 24.5 (*i*Pr CH₃), 22.6 (*i*Pr CH₃), -14.3 ppm (CH₂CN).

ESI-MS: 614.2515 calculated for C₃₃H₄₂N₅Pd⁺ (**IIc** - CH₂CN) 614.2475 and 673.2891 calculated for C₃₅H₄₇N₆OPd⁺ (**IIc** + H₃O⁺) 673.2846

3.4.11 Preparation of [((MesIm)₂CH₂)Pd(NCCH₂CH₃)₂][PF₆]₂ (**VI**):

[((MesIm)₂CH₂)PdBr₂] (0.142 g, 0.218 mmol) and NaPF₆ (0.721 g, 4.30 mmol), H₂O (10 mL) and propionitrile (10 mL) were combined in a round-bottom flask. This solution was stirred vigorously (800 rpm) and heated to 90 °C for 2 h. The solvents were removed via rotary evaporation. The solid was washed with water and recrystallization was achieved via layering of diethyl ether on a near saturated propionitrile solution (42 % yield, 81.9 mg).

¹H NMR (400 MHz, DMSO-*d*₆): δ 8.00 (2H, d, *J* = 2.0 Hz, 1mH), 7.58 (2H, d, *J* = 2.0 Hz, 1mH), 7.11 (4H, s, *m*-CH), 6.63 (2H, s, CH₂), 2.45 (4H, q, *J* = 7.6 Hz, NCCH₂), 2.33 (6H, s, *p*-CH₃), 2.07 (12H, s, *o*-CH₃), 1.14 ppm (6H, t, *J* = 7.6 Hz, NCCH₂CH₃).

¹³C NMR (100.47 MHz, DMSO-*d*₆): δ 145.5 (Pd-C), 139.6 (Ar-C), 135.0 (Ar-C), 134.6 (Ar-C), 129.5 (*m*-CH), 126.0 (1mH), 123.3 (1mH), 122.2 (N≡C), 62.8 (CH₂), 21.0 (*p*-CH₃), 18.7 (*o*-CH₃), 10.6 (NCCH₂CH₃), 10.4 ppm (NCCH₂).

Anal. Calc. for Pd₁N₆C₃₁H₃₈P₂F₁₂; C 41.79, N 9.43, H 4.30; Found: C 41.66, N 9.34, H 4.32%.

MP: 225 °C (dec)

3.4.12 Preparation of $[\{(\text{MesIm})_2\text{CH}_2\}\text{Pd}(\text{NCCH}_2\text{CH}_2\text{CH}_3)_2][\text{PF}_6]_2$ (VII):

$[\{(\text{MesIm})_2\text{CH}_2\}\text{PdBr}_2]$ (0.118 g, 0.181 mmol) and NaPF_6 (0.595 g, 3.54 mmol), H_2O (10 mL) and butyronitrile (10 mL) were combined in a round-bottom flask. This solution was stirred vigorously (800 rpm) and heated to 90 °C for 2 h. The solvents were removed via rotary evaporation. The solid was washed with water and recrystallised via layering of hexanes on a near saturated butyronitrile solution. (45 % yield, 74.8 mg).

^1H NMR (400 MHz, $\text{DMSO}-d_6$): δ 8.01 (2H, d, $J = 1.7$ Hz, ImH), 7.60 (2H, d, $J = 1.6$ Hz, ImH), 7.12 (4H, s, *m*-CH), 6.64 (2H, s, CH_2), 2.46 (4H, t, $J = 7.0$, NCCH_2), 2.33 (6H, s, *p*- CH_3), 2.07 (12H, s, *o*- CH_3), 1.56 (4H, sex, $J = 7.2$ Hz, $\text{CH}_2\text{CH}_2\text{CH}_3$), 0.96 ppm (6H, t, $J = 7.4$ Hz, CH_3).

^{13}C NMR (100.47 MHz, $\text{DMSO}-d_6$): δ 145.5 (Pd-C), 139.6 (Ar-C), 135.0 (Ar-C), 134.6 (*o*-C), 129.5 (*m*-CH), 126.0 (ImH), 123.3 (ImH), 121.1 ($\text{N}\equiv\text{C}$), 62.8 (CH_2), 21.0 (*p*- CH_3), 19.0 ($\text{CH}_2\text{CH}_2\text{CH}_3$), 18.7 (*o*- CH_3), 18.4 (NCCH_2), 13.5 ppm (CH_3).

Anal Calc for $\text{Pd}_1\text{N}_6\text{C}_{33}\text{H}_{42}\text{P}_2\text{F}_{12}$: C 43.13, N 9.14, H 4.61; Found C 43.27, N 9.06, H 4.48.

MP: 176 °C (dec)

3.5 References:

- [1] M. G. Gardiner, W. A. Herrmann, C.-P. Reisinger, J. Schwarz, M. Spiegler, *J. Organomet. Chem.* **1999**, *572*, 239–247.
- [2] E. Drent, W. P. Mul, A. A. Smaardijk, in *Encyclopedia of Polymer Science and Technology* (Ed.: I. John Wiley & Sons), **2001**.
- [3] P. D. Boyd, A. J. Edwards, M. G. Gardiner, C. C. Ho, M. H. Lemee-Cailleau, D. S. McGuinness, A. Riapanitra, J. W. Steed, D. N. Stringer, B. F. Yates, *Angew. Chem. Int. Ed.* **2010**, *49*, 6315–6318.
- [4] M. Tucker, Honours Thesis, University of Tasmania (Hobart Tasmania), **2014**.
- [5] S. Chakraborty, Y. J. Patel, J. A. Krause, H. Guan, *Angew. Chem. Int. Ed.* **2013**, *52*, 7523–7526.
- [6] F. G. Bordwell, *Acc. Chem. Res.* **1988**, *21*, 456–463.
- [7] R. G. Pearson, R. L. Dillon, *J. Am. Chem. Soc.* **1953**, *75*, 2439–2443.
- [8] K. Yoshizawa, S. Toyota, F. Toda, *Green Chem.* **2002**, *4*, 68–70.
- [9] I. R. Baxendale, S. V. Ley, *J. Comb. Chem.* **2005**, *7*, 483–489.
- [10] N. R. Smyrl, R. W. Smithwick, *J. Heterocyclic Chem.* **1982**, *19*, 493–496.
- [11] A. R. Ronzio, W. B. Cook, *Org. Synth.* **1944**, *24*, 6.
- [12] H. Takaya, T. Naota, S.-I. Murahashi, *J. Am. Chem. Soc.* **1998**, *120*, 4244–4245.
- [13] J. Tehranchi, P. J. Donoghue, C. J. Cramer, W. B. Tolman, *Eur. J. Inorg. Chem.* **2013**, 4077–4084.
- [14] D. M. Tellers, J. C. M. Ritter, R. G. Bergman, *Inorg. Chem.* **1999**, *38*, 4810–4818.

- [15] V. Y. Kukushkin, A. J. L. Pombeiro, *Inorg. Chim. Acta* **2005**, 358, 1–21.
- [16] W. Herrmann, T. Scherg, S. Schneider, G. Frey, J. Schwarz, E. Herdtweck, *Synlett*. **2006**, 2006, 2894–2907.
- [17] M. G. Gardiner, C. C. Ho, F. M. Mackay, D. S. McGuinness, M. Tucker, *Dalton Trans.* **2013**, 42, 7447–7457.
- [18] A. Riapanitra, Masters Thesis, University of Tasmania (Hobart Tasmania), **2009**.
- [19] C. C. Ho, PhD Thesis, University of Tasmania (Hobart Tasmania), **2014**.
- [20] a) T. Naota, A. Tanna, S. Kamuro, S.-I. Murahashi, *J. Am. Chem. Soc.* **2002**, 124, 6842–6843; b) T. Naota, A. Tanna, S. Kamuro, M. Hieda, K. Ogata, S. Murahashi, H. Takaya, *Chem. Eur. J* **2008**, 14, 2482–2498.
- [21] T. M. McPhillips, S. E. McPhillips, H. J. Chiu, A. E. Cohen, A. M. Deacom, P. J. Ellis, E. Garman, A. Gonzalez, N. K. Sauter, R. P. Phizackerly, S. M. Soltis, P. Kuhn, *Synchrotron Radiat.* **2009**, 9, 401.
- [22] G. M. Sheldrick, in *SHELX97, Programs for Crystal Structure Analysis*, Universität Göttingen: Germany, **1998**.
- [23] O. V. Dolomanov, L. J. Bourhis, R. J. Gildea, J. A. K. Howard, H. Puschmann, *J. Appl. Cryst.* **2009**, 42, 339–341.

Chapter 4: Synthesis of NHC Containing Pincer Complexes

4.1 Introduction to NHC Containing Pincer Complexes:

NHC based pincer complexes were first synthesised in 2001.^[1] The vast majority of those synthesised since that time fall in two main classes: CEC and C[^]E[^]C complexes where E = C or N (Figure 4.1). The C[^]E[^]C complexes differ from the CEC complexes with the presence of a methylene linker leading to a characteristic C₂ twisted conformation. The two wingtip NHCs for the methylene linked complex project out of the coordination plane in opposite directions (average imidazole-PdL₄ dihedral angle of 39 °^[2]), while in comparison CEC complexes have a flat geometry (average imidazole-PdL₄ dihedral angle of 2 °^[3]).^[4] The square planar geometry is distorted for CEC complexes with an average C–M–C angle 155(6) ° for the CCC complexes due to the strained 5 membered Pd–C–N–C–C ring. This is in contrast to the C[^]C[^]C species which have an average angle of 172(2) ° due to the 6 membered Pd–C–N–C–C–C ring.^[5] While a large portion of the CEC and C[^]E[^]C complexes are of group 10 metals the majority of those published have focussed on E = N complexes while the synthesis of few CCC and C[^]C[^]C species have been reported. This is with the exception of a body of work focusing on CCC platinum complexes which have potential applications as light-emitting complexes.^[5]

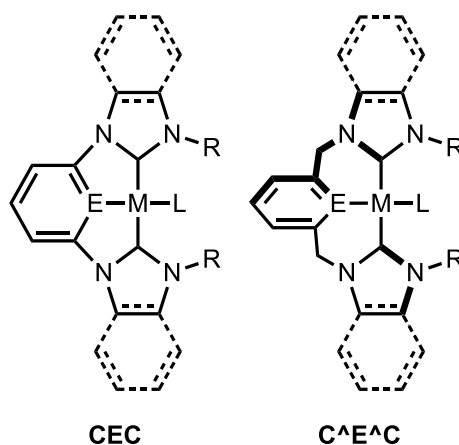
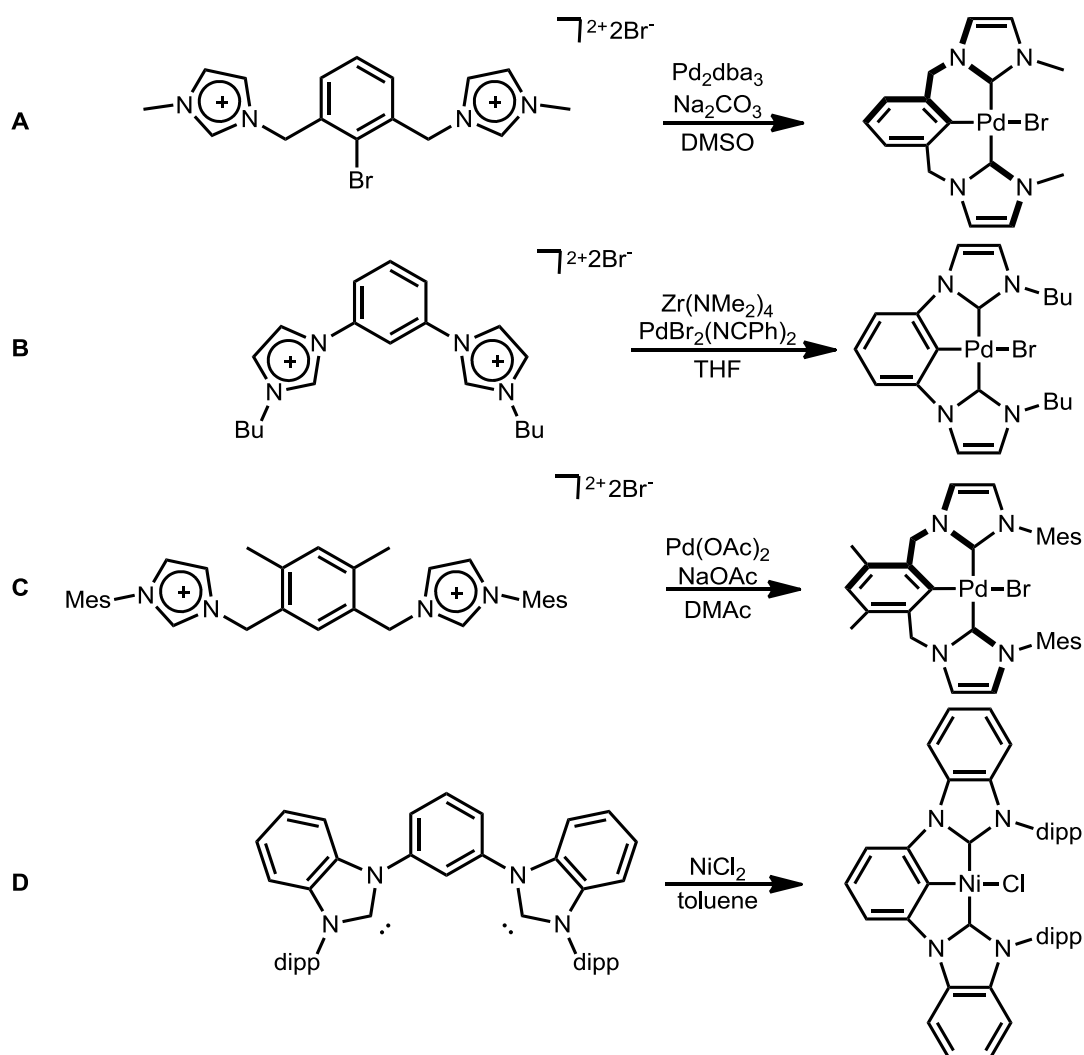


Figure 4.1: The two types of NHC containing pincer complexes: CEC and C[^]E[^]C

Pd CNC and C[∧]N[∧]C complexes are typically synthesised by reacting the NHC pro-ligand with Pd(OAc)₂.^[1, 6] However, the synthesis of CCC and C[∧]C[∧]C pincer complexes provide a more difficult reaction pathway due to the three C–H bond activations required. Initial reactions with Pd(OAc)₂ failed to form the three Pd–C bonds.^[7] Since then, a number of synthetic pathways have been developed that allow for the synthesis of various CCC and C[∧]C[∧]C complexes. One method involves prefunctionalisation to the corresponding aryl bromide, which then reacts with the desired metal *via* oxidative addition^[8] (Scheme 4.1, A). The second method involves the synthesis of a zirconium intermediate complex followed by the transmetalation



Scheme 4.1: Various synthetic methods for group 10 NHC containing CCC and C[∧]C[∧]C pincer complexes

with the desired metal (Scheme 4.1, B).^[9] In addition, a modified ligand with methyl substituents on the aryl ring was reacted with a mixture of Pd(OAc)₂ and NaOAc yielding the desired complex (Scheme 4.1, C).^[10] These complexes have also been synthesised by the reaction of free carbenes developed *in situ* with NiCl₂ (Scheme 4.1, D).^[11]

Various catalytic applications have been discovered for NHC containing pincer complexes including C-C bond formation through Mizoroki–Heck reactions^[1, 12] and hydroamination.^[13] Additionally these complexes have shown applications as photo sensitisers^[14] and as light-emitting complexes.^[15]

The applications of NHC pincer complexes in the synthesis of α -cyanocarbanion compounds were explored due to their similarities to the POCOP complexes described by Guan and co-workers.^[16] As NHC pincer complexes exhibited many of the key characteristics identified in the DFT calculations in Chapter 2 and due to the successful synthesis of [{{(RIm)₂CH₂}Pd(CH₂CN)₂] complexes in Chapter 3 these complexes may observe the same reactivity. As NHCs represent established alternatives to phosphine ligands these complexes may provide enhanced or complementary reactivity to the related POCOP complexes. Pincers with the C[^]C[^]C and CCC motif contain a strong *trans* donor ligand at the active catalyst site, which DFT calculations suggest is crucial in lowering the activation energy of the reaction as discussed in Chapter 2. Pincers of type CEC contain the same flat geometry as the POCOP ligand, however, it is unclear whether this will affect the activation energy. It should also be noted that the charge on CNC complexes is different to POCOP complexes. As NHC pincer complexes have different geometry to the POCOP complexes it was unclear what effect the steric bulk of the N-substituent would have on the reactivity and, thus, ligands with different N-substituents were investigated. Complexes of the following type will be discussed in this Chapter:

1. The synthesis of $[(\text{CNC}^{\text{R}})\text{PdBr}]$ from a published method and the reaction of this complex to form the $-\text{NCMe}$ and $-\text{CH}_2\text{CN}$ analogues to test in the catalytic formation of β -hydroxynitriles.
2. The synthesis of $[(\text{C}^{\wedge}\text{C}^{\text{R}})\text{PdBr}]$ from a published method and the reaction of this to form the $-\text{NCMe}$ analogue as well as attempts to form other potentially catalytically active analogues including $-\text{CH}_2\text{CN}$ and $-\text{OH}$ complexes.
3. A number of synthetic pathways were investigated for the formation of $[(\text{CCC}^{\text{R}})\text{PdBr}]$ with a number of different ligands synthesised including the NCMe analogue.
4. The use of the new synthetic method developed for the synthesis of $[(\text{CCC}^{\text{R}})\text{PdBr}]$ was then extended to the other metals in group 10 as they may also show the same activity.

Many of the complexes synthesised in this Chapter will be discussed again in Chapter 5 as they will be tested for their catalytic activity in the formation of β -hydroxynitriles.

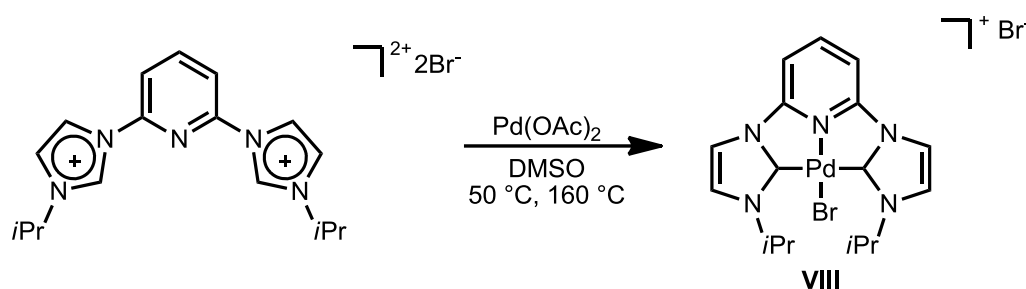
4.2 Results and Discussion:

4.2.1 Synthesis of $[(\text{CNC}^{\text{iPr}})\text{Pd}(\text{CH}_2\text{CN})][\text{SbF}_6]$:

Complexes of the type $[(\text{CNC}^{\text{R}})\text{Pd}(\text{CH}_2\text{CN})]$ were synthesised due to their structural similarities to $[\{2,6-(\text{iPr}_2\text{PO})_2\text{C}_6\text{H}_3\}\text{Ni}(\text{CH}_2\text{CN})]^{[16]}$ and as a comparison to the later synthesised $[(\text{CCC}^{\text{R}})\text{PdL}]$ complexes due to its lack of a strong *trans* donation ligand. $\text{R} = \text{iPr}$ was chosen due its small steric demand and its availability as there was pro-ligand available from a previous researcher.

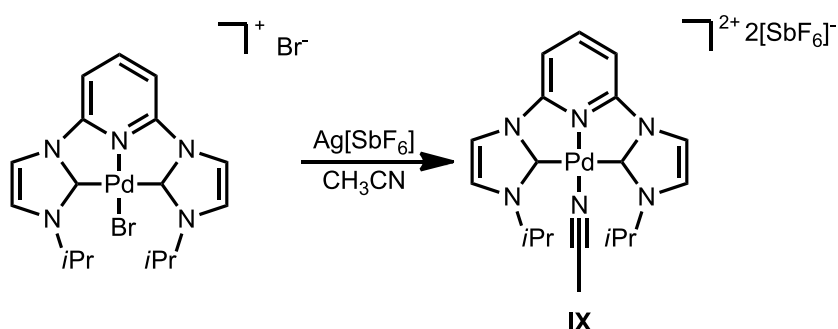
$[(\text{CNC}^{\text{iPr}})\text{PdBr}]\text{Br}$ (**VIII**) was synthesised by reacting $[(\text{iPrImH})_2\text{Py}]\text{Br}_2$ with $\text{Pd}(\text{OAc})_2$ in DMSO under conditions analogous to those used by Crabtree and co-workers

(Scheme 4.2).^[1] The product was purified *via* column chromatography and the formation of the desired product was supported by ¹H NMR spectroscopy which was consistent with previous literature reports of the compound with loss of the characteristic downfield imidazolium C2 proton resonances at 10.38 ppm consistent with the formation of the Pd–C bonds.^[17]



Scheme 4.2: Synthesis of [(CNC^{iPr})PdBr]Br (**VIII**)

[(CNC^{iPr})Pd(NCMe)][SbF₆]₂ (**IX**) was synthesised by reacting [(CNC^{iPr})PdBr]Br with Ag[SbF₆] in CH₃CN. The complex was then purified *via* recrystallisation by vapour diffusion of Et₂O into a solution in CH₃CN giving the desired product in a 34 % yield (Scheme 4.3). The formation of the product was supported by ¹H and ¹³C NMR spectroscopy. With signals in the ¹H NMR spectrum at 2.08 ppm and ¹³C NMR spectrum 1.6 ppm consistent with the CH₃ from the coordinated acetonitrile ligand.



Scheme 4.3: Synthesis of [(CNC^{iPr})Pd(NCMe)][SbF₆]₂ (**IX**)

Analysis of the X-ray crystal structure reveals the bond lengths and angles are consistent with the previously published [(CNC^{iPr})Pd(NCMe)][PF₆]₂.^[17] The complex has a flat geometry of the CNC ligand with the largest deviating from the least

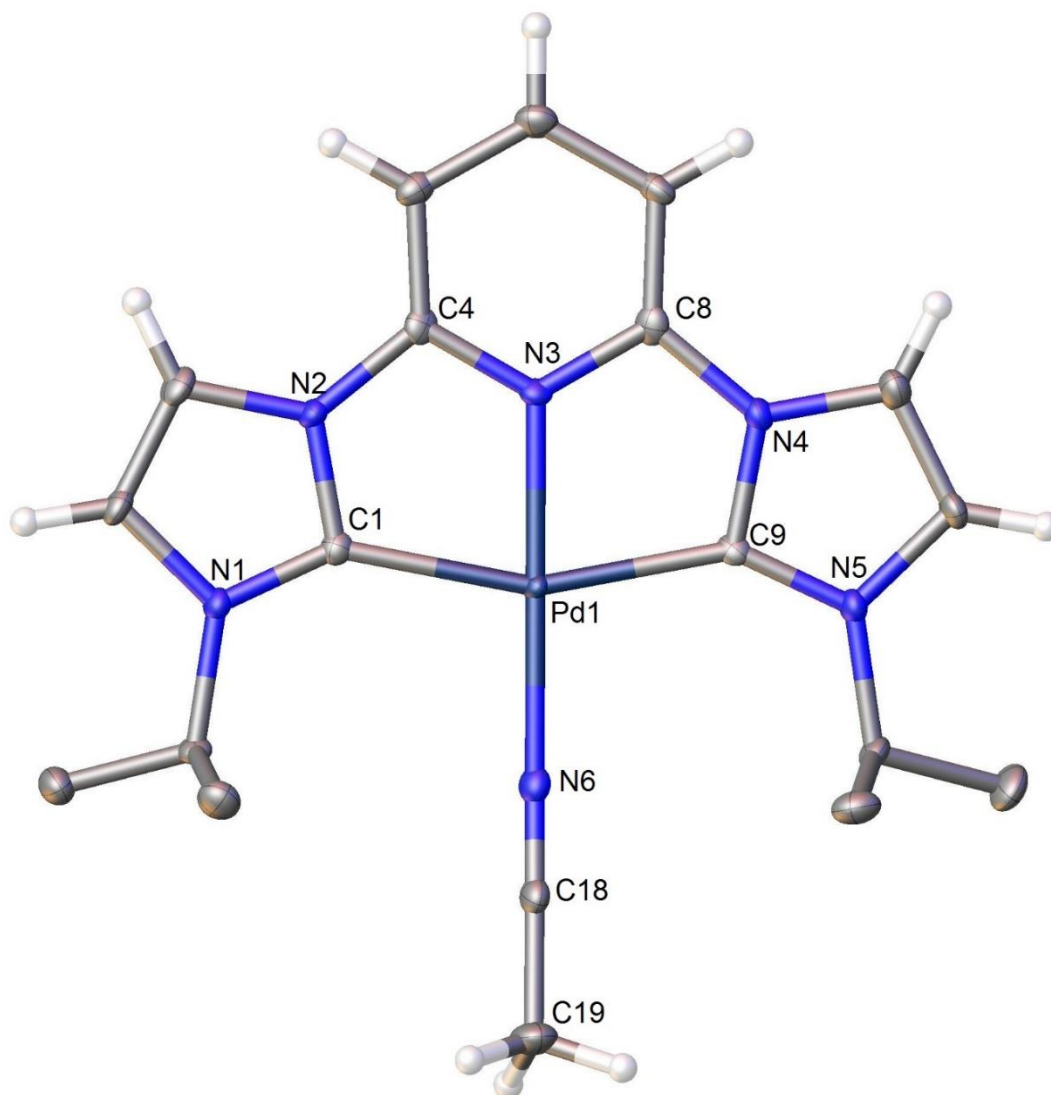
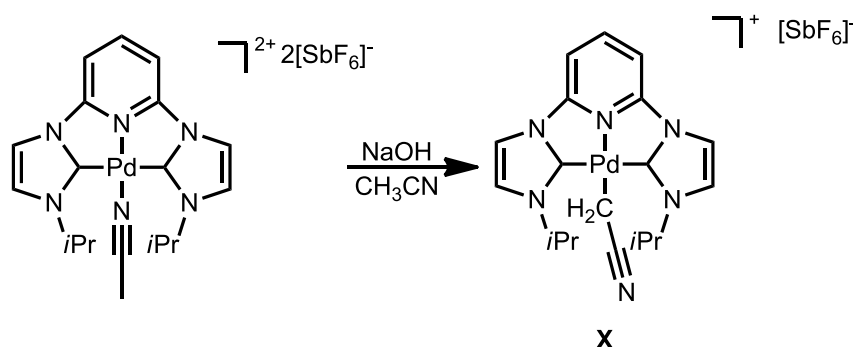


Figure 4.2: X-ray molecular structure of cation $[(\text{CNC}^{\text{Pr}})\text{Pd}(\text{NCMe})]^{2+}$ of **IX**. Thermal ellipsoids are shown at the 50% probability level. 2 $[\text{SbF}_6]^-$ counter ions and a CH_3CN lattice solvent molecule omitted for clarity. All isopropyl hydrogen atoms removed for clarity. Selected bond lengths (\AA) and angles ($^\circ$): Pd(1)–C(1) 2.040(4), Pd(1)–C(9) 2.031(4), Pd(1)–N(3) 1.956(3), Pd(1)–N(6) 1.999(4), N(6)–C(18) 1.134(6), C(18)–C(19) 1.450(6), N(3)–Pd(1)–N(6) 178.88(15), N(3)–Pd(1)–C(1) 79.24(15), N(3)–Pd(1)–C(9) 79.36(15), N(6)–Pd(1)–C(1) 100.70(15), N(6)–Pd(1)–C(9) 100.70(15), C(9)–Pd(1)–C(1) 158.60(16), C(18)–N(6)–Pd(1) 172.6(4), N(6)–C(18)–C(19) 179.5(5).

square plane being 0.046(4) Å for C(2) and imidazole-PdL₄ dihedral angles of 2.16(16) and 2.00(18) °. The complex observes a distorted square planar geometry, with the main deviation being a non-linear C–Pd–C angle (158.60(16) °) arising from the C₂N₂Pd 5-membered chelate rings (Figure 4.2).

[(CNC^{*i*Pr})Pd(NCMe)][SbF₆]₂ was then reacted with NaOH in CH₃CN to synthesise the α-cyanocarbanion complex [(CNC^{*i*Pr})Pd(CH₂CN)][SbF₆] (Scheme 4.4). The reaction was performed under analogous conditions to those described for the synthesis of the bis(NHC) complexes in Chapter 3. The formation of the desired complex was supported by the upfield shift of the ¹³C NMR resonance of the CH₂ protons of the CH₂CN ligand (–10.0 ppm), which is consistent with similar complexes of bonding mode I discussed in Chapter 1.



Scheme 4.4: Synthesis of [(CNC^{*i*Pr})Pd(CH₂CN)][SbF₆] (**X**)

Analysis of the X-ray crystal structure for **X** reveals similar bond distances to complex **IX**. [(CNC^{*i*Pr})Pd(CH₂CN)][SbF₆] (**X**) has a flat CNC ligand geometry (largest deviation from the least square plane of 0.308(15) Å), small imidazole-PdL₄ dihedral angles (2.19(16) & 2.01(18) °) and a distorted square planar geometry of the palladium (C(9)–Pd(1)–C(1) 156.9(4) °). One difference between **IX** and **X** is the elongation of the Pd(1)–N(3) bond length by 0.066 Å. This elongation is consistent with the increase in *trans*-donation effect from the change in ligation from an N-bound to C-bound donor ligand.

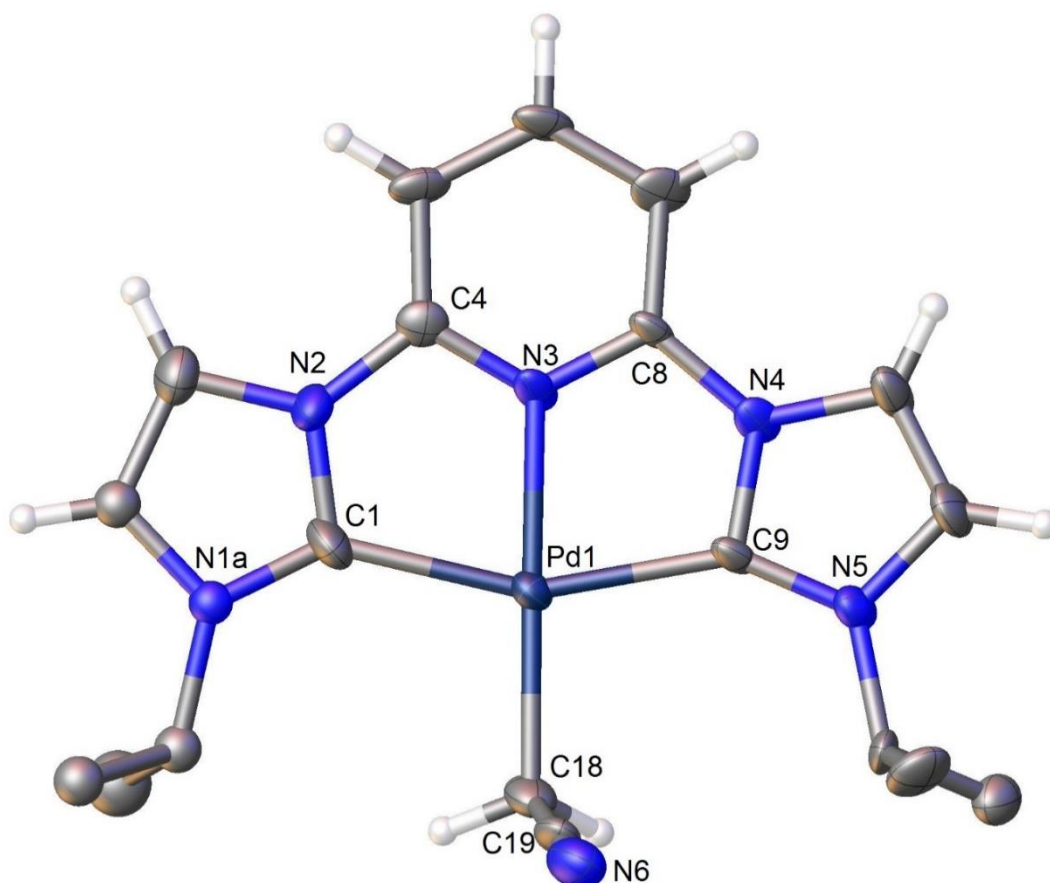


Figure 4.3: X-ray molecular structure of cation $[(\text{CNC}^{\text{Pr}})\text{Pd}(\text{CH}_2\text{CN})]^+$ of **X**. Thermal ellipsoids are shown at the 50% probability level. 1 $[\text{SbF}_6]^-$ counter ion molecule omitted for clarity. Disorder in one of the NHC rings and corresponding isopropyl substituent removed for clarity (N1B, C2B, C12B-C14B), discussed further below. All isopropyl hydrogen atoms removed for clarity. Selected bond lengths (Å) and angles (°): Pd(1)–N(3) 2.022(8), Pd(1)–C(1) 2.086(11), Pd(1)–C(9) 2.067(10), Pd(1)–C(18) 2.070(10), C(18)–C(19) 1.417(17), N(6)–C(19) 1.151(15), N(3)–Pd(1)–C(1) 77.9(4), N(3)–Pd(1)–C(9) 79.0(3), N(3)–Pd(1)–C(18) 177.9(4), C(9)–Pd(1)–C(1) 156.9(4), C(9)–Pd(1)–C(18) 100.2(4), C(18)–Pd(1)–C(1) 102.9(4), C(19)–C(18)–Pd(1) 107.7(7), N(6)–C(19)–C(18) 177.3(12).

The CH₂CN ligand has a C–C bond length of 1.417(17) Å, an N–C bond length of 1.151(15) Å a Pd–C–C bond angle of 107.7(7) ° and a N–C–C angle of 177.3(12) °.

These bond angles and distances are consistent with the dominant resonance form of CH₂CN consistent with bonding mode I as discussed in Chapter 1 (Figure 4.3).

The crystal structure of [(CNC^{iPr})Pd(CH₂CN)][SbF₆] included disorder in one of the NHC rings where there was some electron density above and below the plane. This was modelled with a refined ~0.56 occupancy for those modelled with continuous bonds and ~0.44 with dashed bonds. This disorder was modelled with isotropic atoms in this area as, although electron density was clearly observed, modelling this disorder anisotropically was not stable. (Figure 4.3, 4.4)

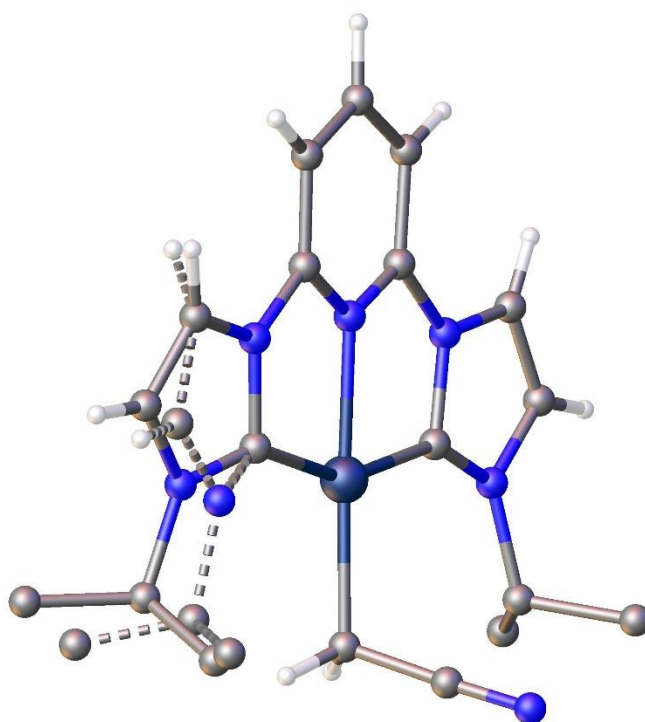


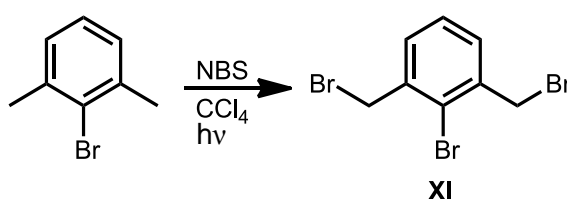
Figure 4.4: X-ray molecular structure of cation [(CNC^{iPr})Pd(CH₂CN)]⁺ of X. Ball and stick diagram showing disorder modelled for NHC ring (dashed bonds).

4.2.2 Synthesis of [(C^{Ar}C^{Me})Pd(NCMe)][SbF₆]:

[(C^{Ar}C^R)PdL] complexes were synthesised as the central aryl carbon's strong *trans* donating ability make them strong candidates as catalysts. Although these

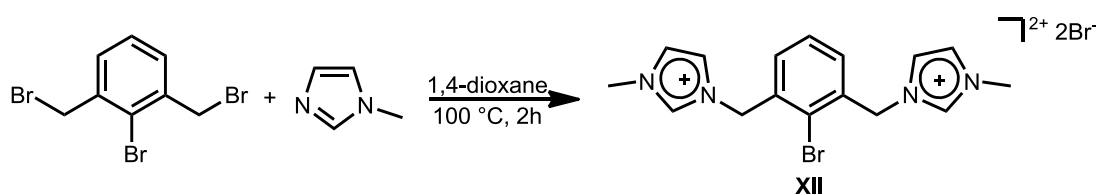
complexes do not have the same flat geometry to $[\{2,6-(iPr_2PO)_2C_6H_3\}Ni(CH_2CN)]$ it is unclear whether this geometry is crucial for catalysis. Given successful previous work by Crabtree and co-workers synthesising $[(C^*C^*C^{Me})PdBr]$ this was chosen as the desired backbone.^[8]

2,6-(BrCH₂)₂-1-BrPh was synthesised by reacting bromo-*m*-xylene with *N*-bromosuccinimide in CCl₄ while irradiated with a 23 W compact fluorescent light bulb.^[18] The desired product was isolated in a 28 % yield. No reaction was observed in the absence of visible light irradiation and when the reaction was attempted with a benzoyl peroxide catalyst a complex mixture of products were formed. The ¹H NMR spectrum of the product was consistent with that previously reported for the target compound with resonances at 4.65 ppm consistent with the CH₂ signal from the downfield shift due to coupling of the Br.^[19]



Scheme 4.5: Synthesis of 2,6-(BrCH₂)₂-1-BrPh (**XI**).

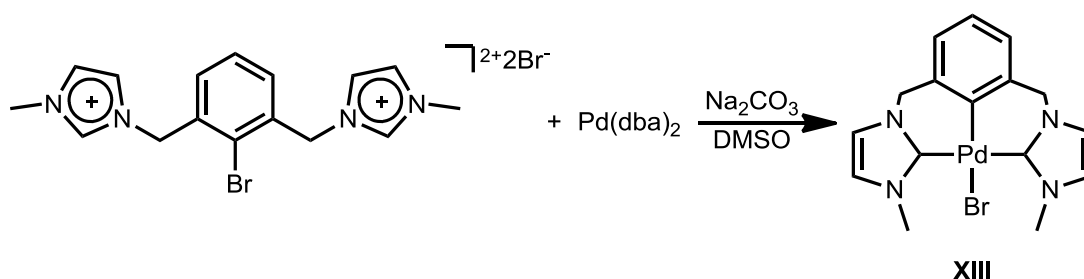
$[2,6-(MeImHCH_2)_2-1-BrPh]Br_2$ was then synthesised from the tribromide **XI** by reaction with 1-methylimidazole in 1,4-dioxane for 2 h in a 83 % yield.^[8] The ¹H NMR spectrum of the product was consistent with that previously reported for the compound with a C2 proton resonance at 9.21 ppm consistent with the formation of



Scheme 4.6: Synthesis of $[2,6-(MeImHCH_2)_2-1-BrPh]Br_2$ (**XII**).

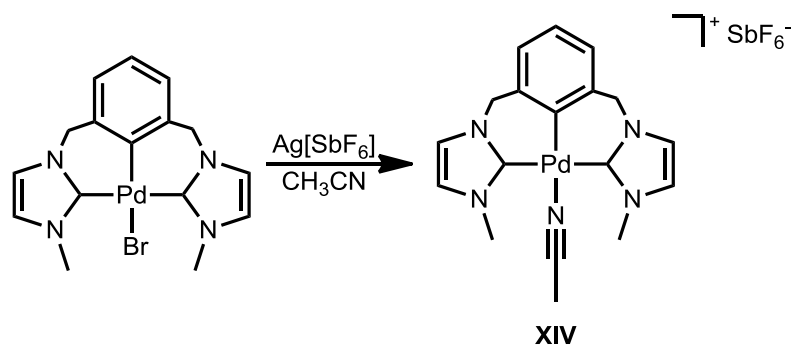
the imidazolium.^[8]

$[(C^{\wedge}C^{\wedge}Me)PdBr]$ was synthesised in a 27 % yield by reacting $[2,6-(MeImHCH_2)_2-1-BrPh]Br_2$ with $Pd(dba)_2$ and Na_2CO_3 in DMSO following a modified literature procedure replacing $Pd_2(dba)_3$ with the more accessible $Pd(dba)_2$.^[8] The reaction was also performed using $Pd_2(dba)_3 \cdot CHCl_3$ however, the yield observed was comparable. The 1H NMR spectrum of **XIII** was consistent with that previously reported^[8] with the characteristic loss of the imidazolium resonances at 9.21 ppm due to the newly formed Pd–C bonds.



Scheme 4.7: Synthesis of $[(C^{\wedge}C^{\wedge}Me)PdBr]$ (**XIII**).

$[(C^{\wedge}C^{\wedge}Me)Pd(NCMe)][SbF_6]$ was subsequently synthesised by reacting $[(C^{\wedge}C^{\wedge}Me)PdBr]$ with $Ag[SbF_6]$ in CH_3CN in a 77% yield (Scheme 4.8). The formation of the product was supported by the presence of resonances in the 1H & ^{13}C NMR spectrum at 2.09 and 1.77 ppm respectively consistent with the CH_3 group of the acetonitrile ligand. The X-ray crystal structure of the product indicates a



Scheme 4.8: Synthesis of $[(C^{\wedge}C^{\wedge}Me)Pd(NCMe)][SbF_6]$ (**XIV**)

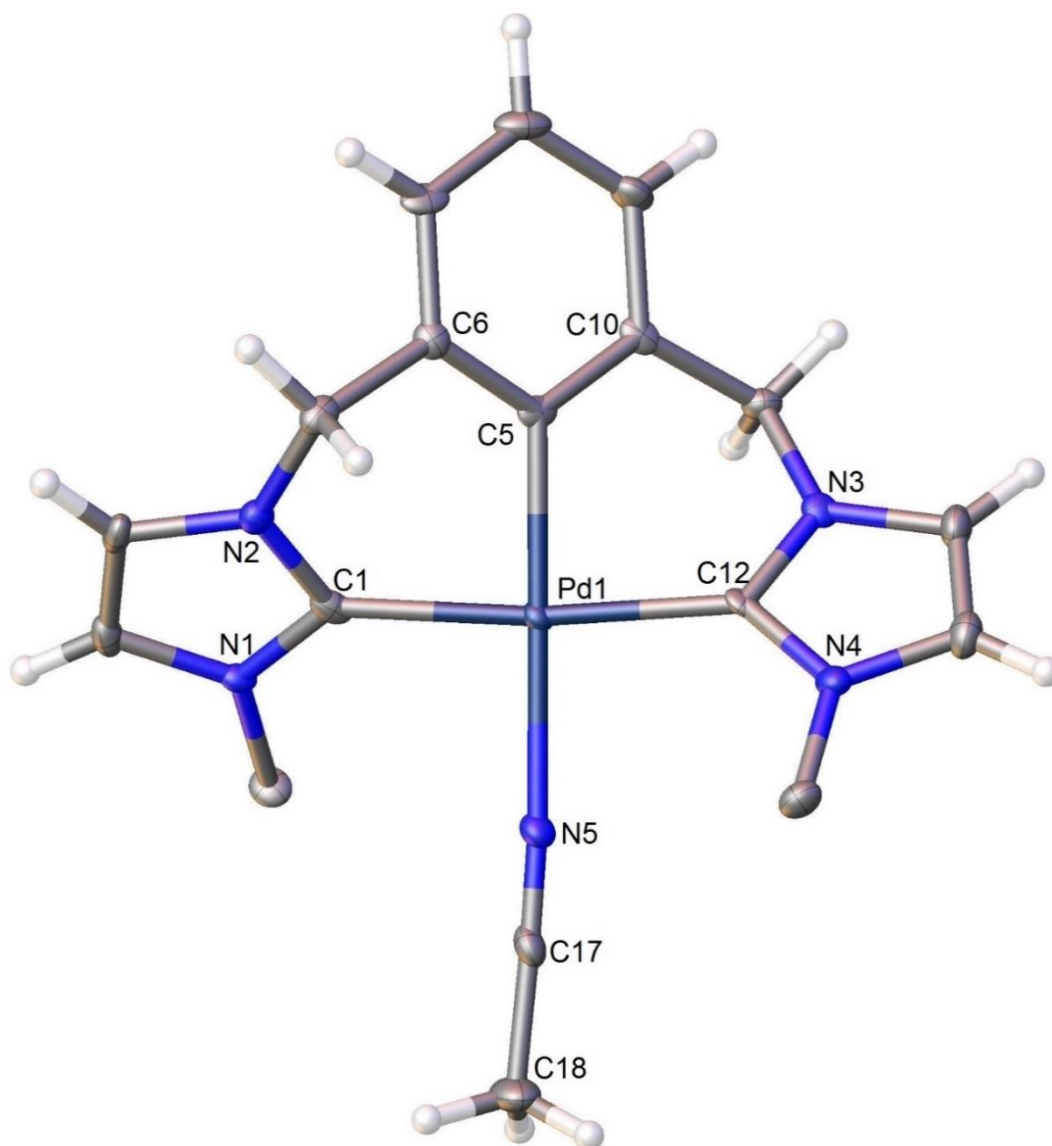


Figure 4.5: X-ray molecular structure of cation $[(C^C^C^{Me})Pd(NCMe)]^+$ of **XIV**.

Thermal ellipsoids are shown at the 50% probability level. 1 $[SbF_6]^-$ counter ion and an CH_3CN solvent molecule omitted for clarity. All methyl hydrogen atoms removed for clarity. Selected bond lengths (\AA) and angles ($^\circ$): Pd(1)–N(5) 2.103(5), Pd(1)–C(1) 2.040(6), Pd(1)–C(5) 2.007(6), Pd(1)–C(12) 2.031(6), N(5)–C(17) 1.134(7), C(17)–C(18) 1.465(8), C(1)–Pd(1)–N(5) 92.4(2), C(5)–Pd(1)–C(1) 87.3(2), C(5)–Pd(1)–C(12) 86.5(2), C(12)–Pd(1)–N(5) 93.9(2), C(12)–Pd(1)–C(1) 173.7(2), N(5)–C(17)–C(18) 178.0(7), C(17)–N(5)–Pd(1) 176.2(5).

twisted geometry of the C[^]C[^]C ligand consistent with the corresponding Br complex with NHC ring-PdL₄ dihedral angles of 39.17(19) and 40.3(2) ° (Figure 4.6).^[8] The C(1)–Pd(1)–C(12) angle of 173.7(2) ° is closer to the ideal linear angle in comparison to the CNC analogue due to the presence of the methylene linker creating the 6-membered C₄NPd chelate ring. The Pd–N bond length for **XIV** is 2.103(5) Å in contrast to 1.99(4) Å for [(CNCⁱPr)Pd(NCMe)][SbF₆]₂ and is consistent with the stronger *trans* donation of the central aryl carbon of the C[^]C[^]C ligand (Figure 4.5).

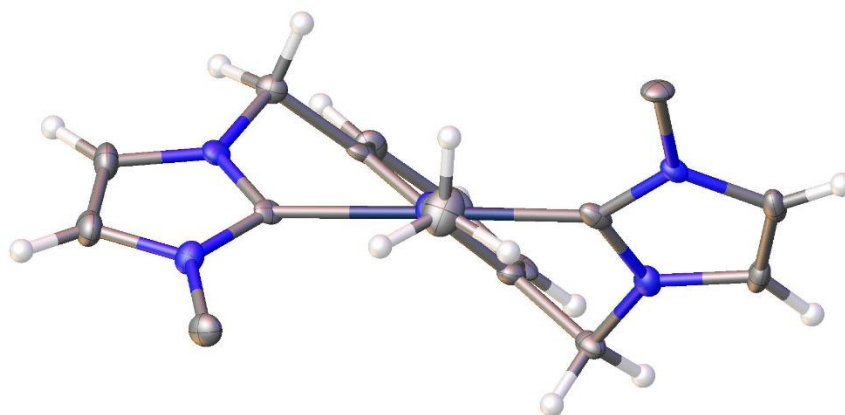


Figure 4.6: Side on view of the molecular structure of cation [(C[^]C[^]C^{Me})Pd(NCMe)]⁺ of **XIV** highlighting the twisted geometry of the NHC rings-PdL₄ dihedral angle.

The synthesis of [(C[^]C[^]C^{Me})Pd(CH₂CN)] was attempted by the reaction of **XIV** with NaOH in CH₃CN, however various products were observed by ¹H NMR spectroscopy and were inseparable by chromatography or crystallisation. Given the difficulty in the formation of the CH₂CN complex, the synthesis of [(C[^]C[^]C^{Me})Pd(OH)] was attempted as it may feature the same reactivity given the OH-ligated complex was observed as an intermediate in the formation of [(MeIm)₂CH₂}Pd(CH₂CN)₂]. The synthesis of [(C[^]C[^]C^{Me})Pd(OH)] was attempted following a method developed for a PdPCP complex.^[20] [(C[^]C[^]C^{Me})PdBr] was reacted with AgNO₃ in THF yielding [(C[^]C[^]C^{Me})Pd(ONO₂)] which was then reacted

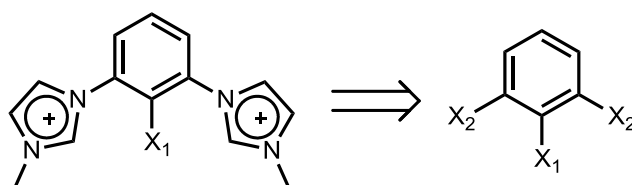
with NaOH in THF to provide $[(C^{\wedge}C^{\wedge}C^{Me})Pd(OH)]$. However, due to difficulties in purification it was unclear whether the desired product was formed.

4.2.3 Synthesis Attempt for CCC Complex Using Unsubstituted Ligand:

$[(CCC^R)PdL]$ complexes were synthesised as these have the same geometry and *trans* donating ability as $[\{2,6-(iPr_2PO)_2C_6H_3\}Ni(CH_2CN)]$ and thus may find useful applications in catalysis.

As discussed at the start of this Chapter, very few successful synthetic methods have been established for complexes of the type $[(CCC)ML]$. When the CCC pro-ligand $[1,3-(RImH)_2Ph]X_2$ was treated with $Pd(OAc)_2$ the product formed contained only two of the Pd–C bonds as assigned by NMR spectroscopy.^[7] Successful synthetic pathways for complexes of the type CCC have involved the use of a zirconium transmetallation reagent before treating the solution with the desired metal salt.^[9] This is in contrast to complexes of the type $C^{\wedge}C^{\wedge}C$ which are commonly synthesised by the use of a brominated aryl ligand allowing oxidative addition of palladium(0) (as discussed in 4.2.2).^[8] Another report claims to have made the complex, however, no experimental information or characterisation was provided.^[21]

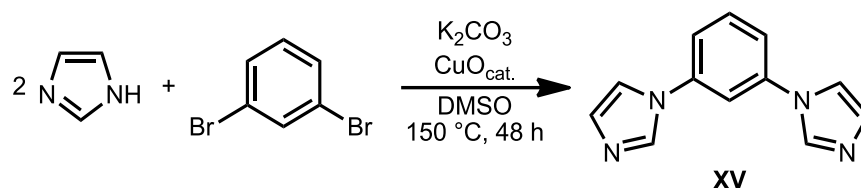
However, the same synthetic pathway cannot be used for the synthesis of the CCC complexes as was used for **XII**. One of the intermediates in the synthesis of the pro-ligand for **XII** is 2,6-(BrCH₂)₂-1-BrPh and with the absence of the methylene linker in the CCC pro-ligand the specificity for the addition of imidazole cannot be achieved for a tribromobenzene (i.e. $X_1=X_2=Br$). Thus an alternative method was required. Initially the 3x C–H activation pathway was attempted, i.e. $X_1 = H$, $X_2 = Br$ (Scheme



Scheme 4.9: Retrosynthetic analysis for the synthesis of the CCC pro-ligands.

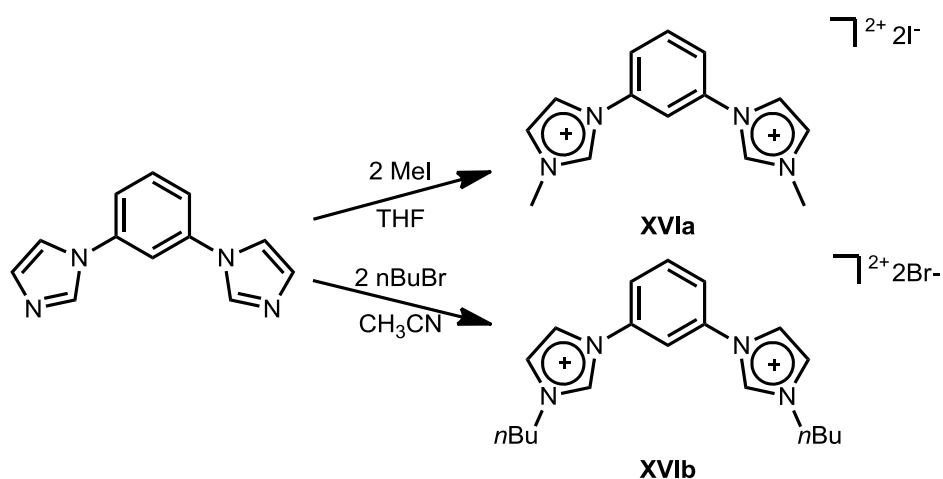
4.9).

1,3-Im₂Ph was synthesised following a modified published procedure.^[22] Imidazole was reacted with 1,3-dibromobenzene in DMSO in the presence of K₂CO₃ and CuO and was purified by eluting on a silica plug in a 44 % yield (Scheme 4.10). The product was spectroscopically consistent to the literature.^[23]



Scheme 4.10: Synthesis of 1,3-Im₂Ph (**XV**).

From this compound [1,3-(MelmH)₂Ph]₂ (**XVIa**) and [1,3-(nBulmH)₂Ph]Br₂ (**XVIb**) could both be synthesised under very similar conditions in a pressure tube. The NMR spectroscopic data for these compounds were consistent with the literature with the presence of downfield ¹H NMR resonances at 9.88 for **XVIa** and 11.33 ppm for **XVIb** consistent with the formation of the imidazolium C2-protons (Scheme 4.11).^[23-24]



Scheme 4.11: Synthesis of [1,3-(MelmH)₂Ph]₂ (**XVIa**) and [1,3-(nBulmH)₂Ph]Br₂ (**XVIb**).

A number of reactions were attempted with **XVIa** and **XVIb** to synthesise the desired $[(CCC^R)PdX]$ complex. Initially, the ligand **XVIa** was treated with $Pd(OAc)_2$ under identical conditions for the synthesis of complex **VIII**. The 1H NMR spectrum indicated a mixture of products were formed. The crude product was then treated with $Ag[SbF_6]$ in acetonitrile and a crystal structure of the product was obtained. The crystal structure shows a binuclear palladium complex with two bridging NHC ligands. Each palladium also has one water and one DMSO ligand. The DMSO is likely to be present from the $Pd(OAc)_2$ reaction while the water may have been present from the subsequent reaction in acetonitrile or during the recrystallisation process. The Pd–C bond distances between 2.038(8) – 2.055(8) Å are consistent with the Pd–C distances for the NHC ring distances observed for $[(C^C^C^{Me})Pd(NCMe)][SbF_6]$ (Figure 4.7). Similar Cu, Ag and Au metallated complexes have previously been synthesised due to their application in photoluminescence.^[25]

The formation of this product indicates the lack of the desired three C–H deprotonation and metalation steps as expected. $[1,3-(nBulmH)_2Ph]Br_2$ (**XVIb**) was treated with $Pd(OAc)_2$ giving a mixture of products by 1H NMR spectroscopy. Attempting this reaction again with the addition NaOAc also yielding an inseparable mixture. **XVIb** was also treated with Ag_2O in CH_2Cl_2 in an attempt to form the silver salt intermediate before treating with $[PdBr_2(COD)]$. However, an inseparable mixture was formed and further reaction with NaOAc to promote the formation of the complex did not give the desired result.

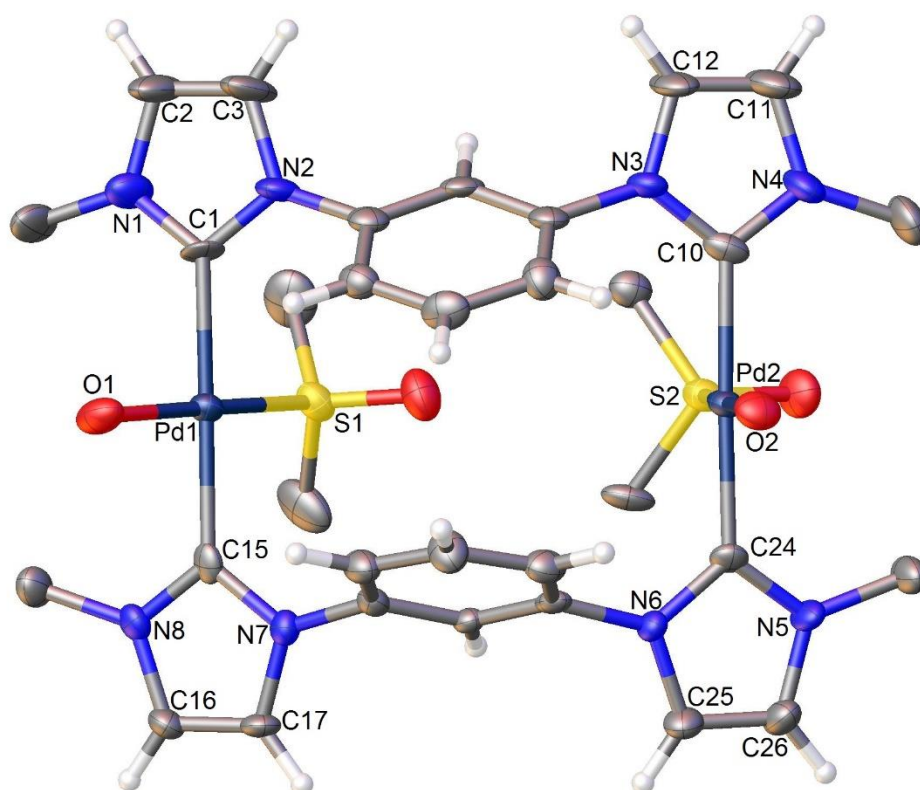


Figure 4.7: X-ray molecular structure of the product formed from the reaction of [1,3-(MelmH)₂Ph]₂ (**XVIa**) and Pd(OAc)₂. Thermal ellipsoids are shown at the 50% probability level. 4 [SbF₆]⁻ counter ions modelled, 1 of these modelled via solvent mask, omitted for clarity. 4 DMSO solvent molecule omitted for clarity. All ligated DMSO hydrogen atoms and methyl hydrogen atoms removed for clarity. Selected bond lengths (Å) and angles (°): Pd–S 2.215(2) – 2.225(2), Pd–O 2.057(7) – 2.059(6), Pd(1)–C(1) 2.055(8), Pd(1)–C(15) 2.043(9), Pd(2)–C(10) 2.042(8), Pd(2)–C(24) 2.038(8), O–Pd–S 175.73(19) – 177.7(2), C–Pd–S 89.7(2) – 90.6(3), C–Pd–O 90.1(3) – 90.3(3), C–Pd–S 89.0(2) – 89.6(2), C–Pd–O 89.4(3) – 91.1(3), C–Pd–C 177.8(3) – 179.3(4).

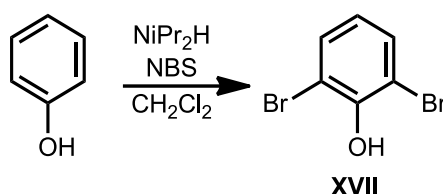
To try to replicate the successfully synthesised CCC complex using Zr(NMe₂)₄ an alternative zirconium transmetallation agent was used which would have synthetic advantages due to its lower cost.^[9] Zr(NEt₂)₄^[26] was treated with both **XVIa** and **XVIb**

however none of the desired complex was observed. Due to the high cost of $\text{Zr}(\text{NMe}_2)_4$ and the low atom economy of the formation of $[(\text{CCC}^{\text{R}})\text{PdX}]$, an alternative method was further investigated.

4.2.4 Attempted Synthesis of CCC Complex using Triflate Functionality on Central Carbon:

Due to the difficulty in synthesising $[(\text{CCC}^{\text{R}})\text{PdX}]$ using the 3 x C–H activation pathway an alternative synthesis method was needed. Thus the use of an $\text{X}_1 = \text{OTf}$ substituent while $\text{X}_2 = \text{Br}$ (Scheme 4.9) would allow synthesis by the oxidative addition pathway pioneered by Crabtree's work for the $\text{C}^{\wedge}\text{C}^{\wedge}\text{C}$ complex.

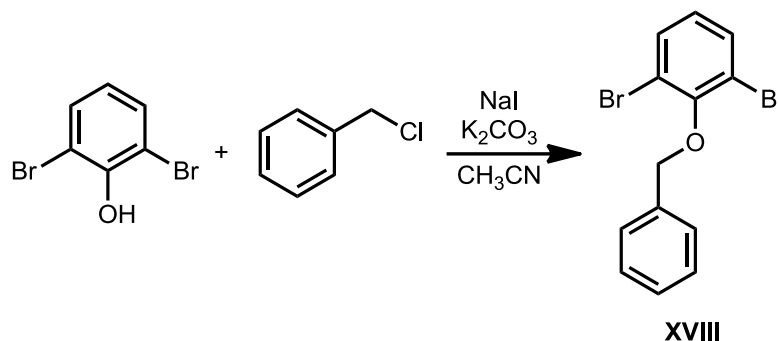
2,6-Dibromophenol was synthesised by the reaction of phenol with *N*-bromosuccinimide in the presence of diisopropylamine following a modified literature procedure.^[27] In addition to the formation of 2,6-dibromophenol in a 67 % yield, 2,4,6-tribromophenol was also observed by ^1H NMR spectroscopy. The ^1H NMR spectrum was consistent with that previously reported (Scheme 4.12).^[27]



Scheme 4.12: Synthesis of 2,6-dibromophenol (**XVII**).

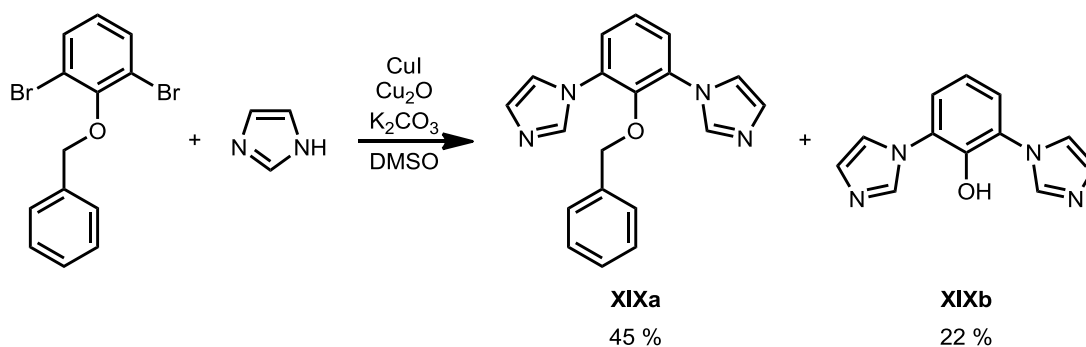
2,6-Dibromophenol was treated with imidazole in the presence of a CuO catalyst however, various products were observed in an inseparable mixture. This was in contrast to a previous literature report which successfully coupled imidazole to 2-bromophenol using a copper catalyst.^[27] To prevent unwanted side reactions,^[27] 2,6-dibromophenol was protected with a benzyl protecting group by treating it with benzylchloride and a catalytic quantity of NaI forming the desired product in 94 % yield (Scheme 4.13).^[29] The formation of 2,6- Br_2 -1-OBnPh was supported by ^1H

NMR spectroscopy with resonances equivalent to that published in the literature including those at 5.06 ppm consistent with the CH₂ benzyl protons.^[29]



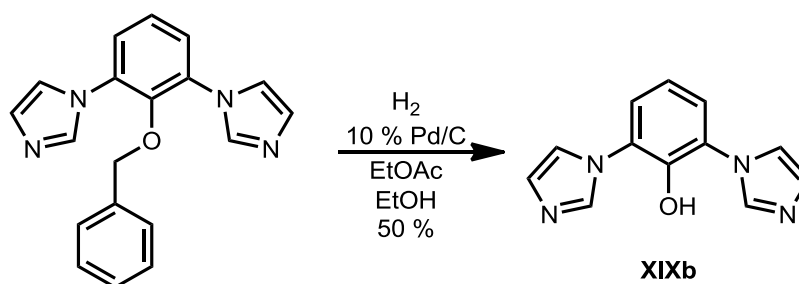
Scheme 4.13: Synthesis of 2,6-Br₂-1-OBnPh (**XVIII**).

Initial coupling reactions to form 2,6-Im₂-1-OBnPh followed the identical synthetic method used for **XV** by treating 2,6-Br₂-1-OBnPh with imidazole in the presence of a CuO catalyst. However, ¹H NMR spectroscopy indicated the intermediate 2-Br-6-Im-1-OBnPh was synthesised. To promote complete conversion the more reactive CuI and Cu₂O were used as coupling catalysts. Both have been used for similar couplings previously.^[30] 2,6-Br₂-1-OBnPh and imidazole were heated in DMSO in the presence of CuI and Cu₂O and K₂CO₃ yielding both 2,6-Im₂-1-OBnPh (**XIXa**) and 2,6-Im₂-1-OHPh (**XIXb**) which were separated on a basic alumina plug (Scheme 4.14). ¹H and ¹³C NMR, IR spectroscopy and mass spectrometry supported the formation of **XIXa** with ¹H NMR resonances at 8.03, 7.58 and 7.44 ppm consistent with the imidazole resonances supporting coupling of the two imidazoles. **XIXb** displayed ¹H NMR resonances at 8.21, 7.48, 6.89 ppm consistent with the imidazole resonances and absence of the signal at 5.32 ppm for the benzyl protons. The formation of **XIXb** is possibly due to a copper mediated debenzylolation reaction.



Scheme 4.14: Synthesis of 2,6-Im₂-1-OBnPh (**XIXa**) and 2,6-Im₂-1-OHPH (**XIXb**).

The benzyl protected product 2,6-Im₂-1-OBnPh was then converted to the alcohol by the reaction of **XIXa** with 10 % Pd/C in a H₂ atmosphere yielding **XIXb** (Scheme 4.15).



Scheme 4.15: Synthesis of 2,6-Im₂-1-OHPH (**XIXb**) from **XIXa**.

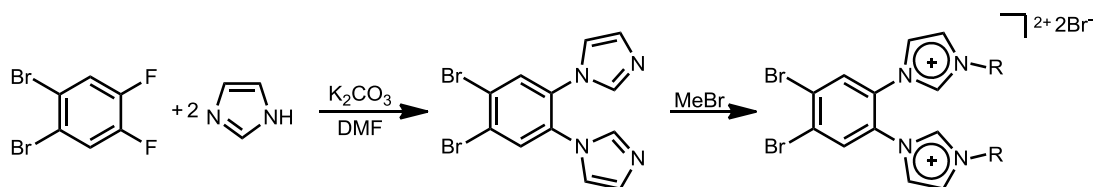
The last two steps to form the desired ligand involved the triflation and methylation of **XIXa** or **XIXb** and these steps could occur in either order. For the desired formation of the triflate, **XIXb** was treated with triflic anhydride with various bases in CH₂Cl₂. Similarly, *N*-methylation of both **XIXa** and **XIXb** were attempted with CH₃I in toluene. Both are described together below in Table 4.1. As neither the triflation nor the *N*-methylation reaction proceeded, the formation of desired triflate based CCC pro-ligand became unfeasible and thus an alternative ligand pathway was pursued for the synthesis of [(CCC^R)PdBr].

Reaction Conditions	Product Formed
XIXb + Tf ₂ O + Pyridine + CH ₂ Cl ₂	No triflate formed, likely protonated imidazolium as shifts are consistent with XIXb + HCl
XIXb + Tf ₂ O + DMAP + CH ₂ Cl ₂	Product unclear, impossible to separate from DMAP
XIXb + Tf ₂ O + NaH + CH ₂ Cl ₂	No triflate formed, ESI-MS indicated major ion 227 i.e. protonated product
XIXb + CH ₃ I + Toluene, 62 h, 110 °C	Mixture of products, unclear whether correct product was formed.
XIXa + CH ₃ I + Toluene, 24 h, 110 °C	Mixture of products, unclear whether correct product was formed.

Table 4.1: Synthesis attempts for the formation of the desired triflate CCC pro-ligand.

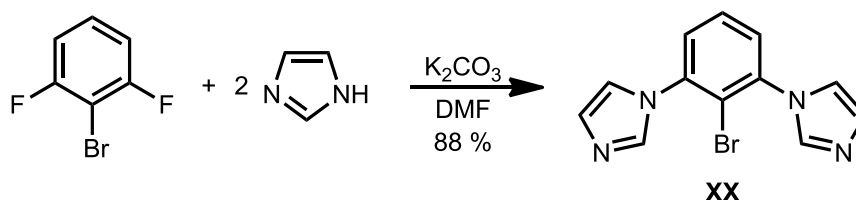
4.2.5 Synthesis of [2,6-(ImHR)₂1-BrPh]X₂:

Due to the difficulty in synthesising the desired ligand with a triflate functionality on the central carbon, an alternative synthetic method was sought. Strassner and co-workers treated 1,2-dibromo-4,5-difluorobenzene with imidazole and K₂CO₃ in DMF yielding (3,4-dibromo-1,2-phenylene)bisimidazole. This intermediate was successfully treated with MeBr to form the desired imidazolium salt (Scheme 4.16).^[31]



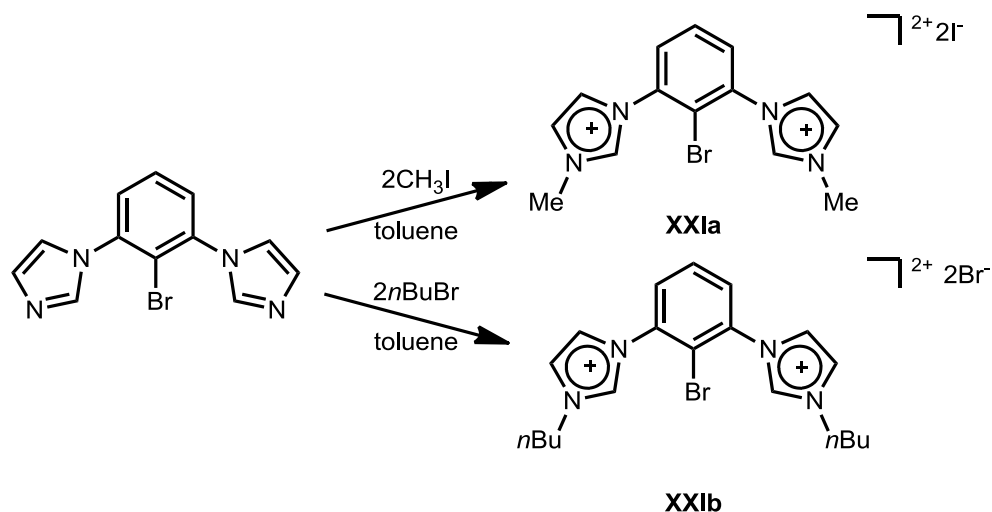
Scheme 4.16: Synthesis of (3,4-dibromo-1,2-phenylene)bisimidazole by Strassner and co-workers.^[31]

Given the success of Strassner and co-workers and their ability to synthesise the desired imidazolium salt a mixed halide synthesis method was pursued where $X_1 = \text{Br}$ and $X_2 = \text{F}$ (Scheme 4.9). Anticipating the same results could be used to achieve selective addition of imidazole, 1-bromo-2,6-difluorobenzene was used as a starting material for the synthesis of the pro-ligand (Scheme 4.9). 1-Bromo-2,6-difluorobenzene was treated with imidazole and K_2CO_3 in DMF giving 2,6- Im_2 -1-BrPh in 88 % yield (Scheme 4.17). The formation of the product was supported by NMR spectroscopy with ^1H NMR resonances at 7.70, 7.23 and 7.16 ppm consistent with the imidazole protons and the formation of the product. This yield is higher than that observed for the synthesis of 1,3- Im_2 Ph (**XV**, 44 %). In addition, this method does not require a CuO catalyst and thus the use of 1,3-difluorobenzene may be a better synthetic method for **XV** but this was not attempted due to time constraints.



Scheme 4.17: Synthesis of 2,6- Im_2 -1-BrPh (**XX**).

The desired ligands can then easily be synthesised from **XX** under varying conditions. 2,6- Im_2 -1-BrPh was treated with iodomethane or 1-bromobutane in toluene yielding the desired corresponding ligands $[2,6-(\text{MeImH})_2-1-\text{BrPh}]_2$ (**XXIa**) and $[2,6-(n\text{BuImH})_2-1-\text{BrPh}]\text{Br}_2$ (**XXIb**) (Scheme 4.18). The formation of these ligands were supported by ^1H and ^{13}C NMR spectroscopy with ^1H NMR resonances at 9.61 and 9.73 ppm respectively consistent with the formation of the C2 proton imidazolium. An X-ray crystal structure was obtained for both ligands with a Br–C bond length of 1.884(7) Å for **XXIa** and 1.890(2) Å for **XXIb** (Figure 4.8 and 4.9).



Scheme 4.18: Synthesis of [2,6-(ImH)₂-1-BrPh]₂ (**XXIa**) and [2,6-(nBuImH)₂-1-BrPh]Br₂ (**XXIb**)

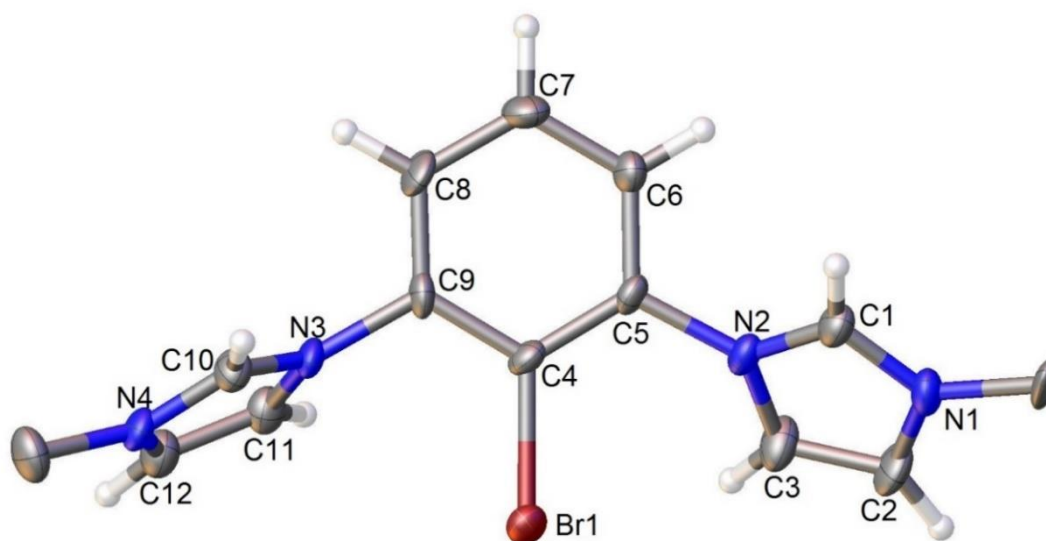


Figure 4.8: X-ray molecular structure of cation [2,6-(ImHCH₃)₂-1-BrPh]²⁺ of **XXIa**.

Thermal ellipsoids are shown at the 50% probability level. two I⁻ counter anions and all methyl hydrogen atoms omitted for clarity. Selected bond length (Å): Br(1)–C(4) 1.884(7).

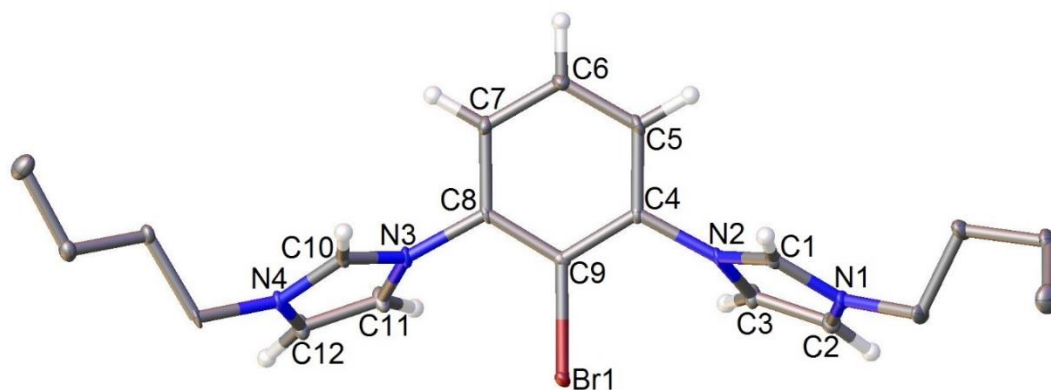
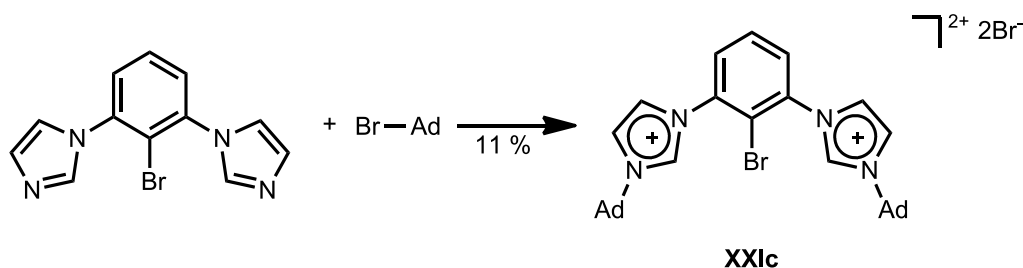


Figure 4.9: X-ray molecular structure of cation $[2,6-(n\text{BuImH})_2-1\text{-BrPh}]^{2+}$ of **XXIb**.

Thermal ellipsoids are shown at the 50% probability level. two Br^- counter anion and a methanol lattice solvent molecule omitted for clarity. All *n*butyl hydrogen atoms omitted for clarity. Selected bond length (Å): $\text{Br}(1)\text{-C}(9)$ 1.890(2).

For the *N*-adamantyl ligand $[2,6\text{-}(\text{AdImH})_2\text{-1-BrPh}]\text{Br}_2$, the synthesis was more difficult due to the increased steric hindrance of the *N*-substituent in comparison to **XXIb**. Following the method used for the synthesis of the analogous ligand without the 1-Br substituent,^[32] solid 2,6- $\text{Im}_2\text{-1-BrPh}$ **XX** and 1-bromoadamantane were stirred at 170 °C for 24 hours forming the desired ligand in 7 % yield. This was compared to a 77 % yield recorded for the analogue without the 1-Br substituent under identical conditions.^[32] The yield was increased slightly to 11 % when the reaction was stirred at 170 °C for 48 hours. Perhaps, the increased steric hindrance or electron withdrawing effects of the Br-substituent makes 2,6- $\text{Im}_2\text{-1-BrPh}$ more stable than 1,3- Im_2Ph and, thus, less reactive. In addition, 1-bromoadamantane was observed to sublime and crystallise on the side of the pressure tube during the reaction and, although steps were taken to minimise this, it may have reduced the yield (Scheme 4.19, Figure 4.10).



Scheme 4.19: Synthesis of [2,6-(AdImH)₂-1-BrPh]Br₂ (**XXIc**).

Analysis of the three pro-ligands indicates **XXIc** in comparison to the other ligands has an increase in the C–Br distance and the distance from the Ph plane of the Br substituent. This is likely due to the increased steric demand of the *N*-adamantyl substituents forcing the Br to sit slightly out of plane and may also contribute to the

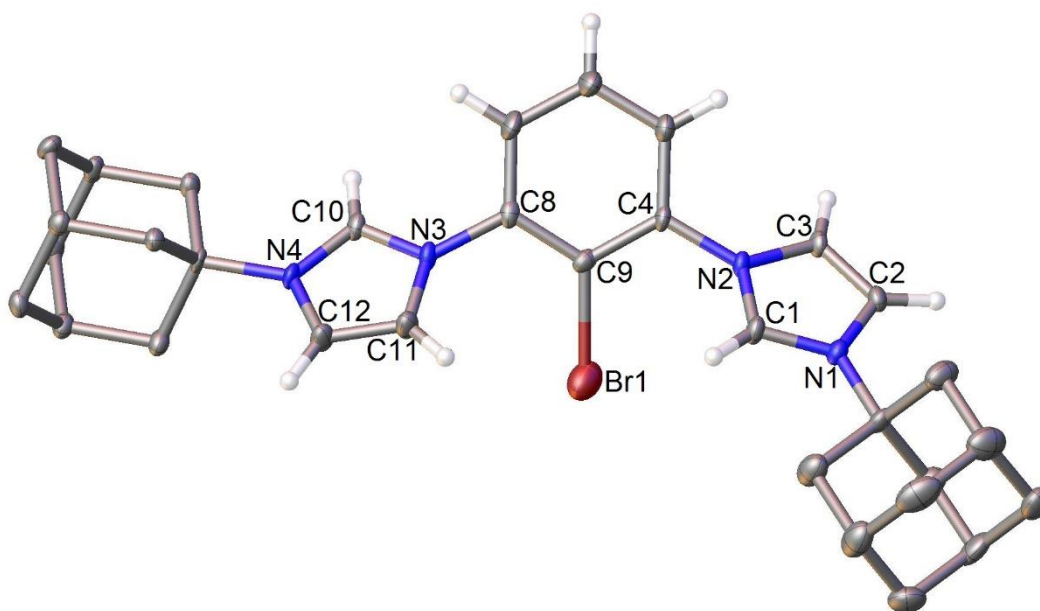


Figure 4.10: X-ray molecular structure of cation [2,6-(AdImH)₂-1-BrPh]²⁺ of **XXIc**.

Thermal ellipsoids are shown at the 50% probability level. Only one of the two **XXIc** cations in the asymmetric unit is displayed for clarity. two Br⁻ counter anions and a Et₂O lattice solvent molecule omitted for clarity. All N-adamantyl hydrogen atoms omitted for clarity. Selected bond length (Å): Br–C 1.909(5), 1.922(5).

lower yield of **XXIc** observed (Table 4.2).

<i>N</i> -substituent	<i>N</i> -Me	<i>N</i> -Butyl	<i>N</i> -Adamantyl
C-Br distance (Å)	1.884(7)	1.890(2)	1.909(5), 1.922(5)
Distance from Ph plane to the Br substituent (Å)	0.0811(12)	0.104(4)	0.425(10), 0.433(9)

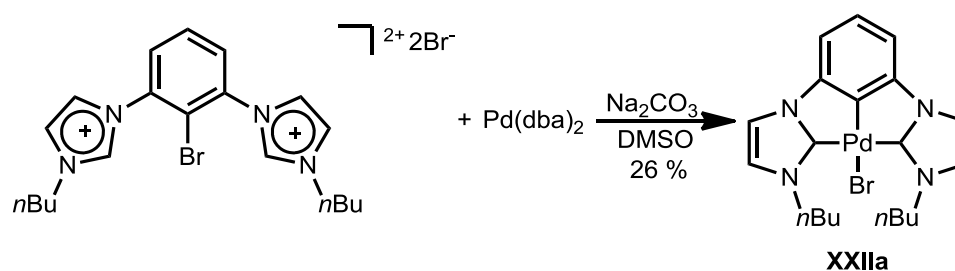
Table 4.2: Comparison of the strain on the Br substituent for the three pro-ligands **XXIa-c**.

4.2.6 Synthesis of [(CCC^R)Pd(NCMe)][SbF₆]:

The synthesis of complexes of the type [(CCC^R)PdBr] followed a modified procedure for the synthesis of the equivalent [(C[^]^C^{Me})PdBr] complex developed by Crabtree and co-workers.^[8]

[2,6-(MelmH)₂-1-BrPh]₂ was treated with Pd(dba)₂ and Na₂CO₃ in DMSO in an attempt to synthesise the complex [(CCC^{Me})PdX], X=Br/I. Due to the poor solubility of the final product, the multiple species observed by ¹H NMR spectroscopy and the difficulty in purification the focus moved on to [(CCC^{nBu})PdBr] which had previously been synthesised using a zirconium transfer agent.^[9b]

[2,6-(*n*BulmH)₂-1-BrPh]Br₂ was treated with Pd(dba)₂ and Na₂CO₃ in DMSO giving



Scheme 4.20: Synthesis of [CCC^{nBu}PdBr] (**XXIIa**).

[(CCC^{nBu})PdBr], spectroscopically identical to that previously published (Scheme 4.20).^[9b] Although the yield was slightly lower than the previously published method (26 % vs 40 %) the better atom economy, air stable starting materials and the advantage of not having to use an expensive zirconium transfer agent makes this synthesis method superior.

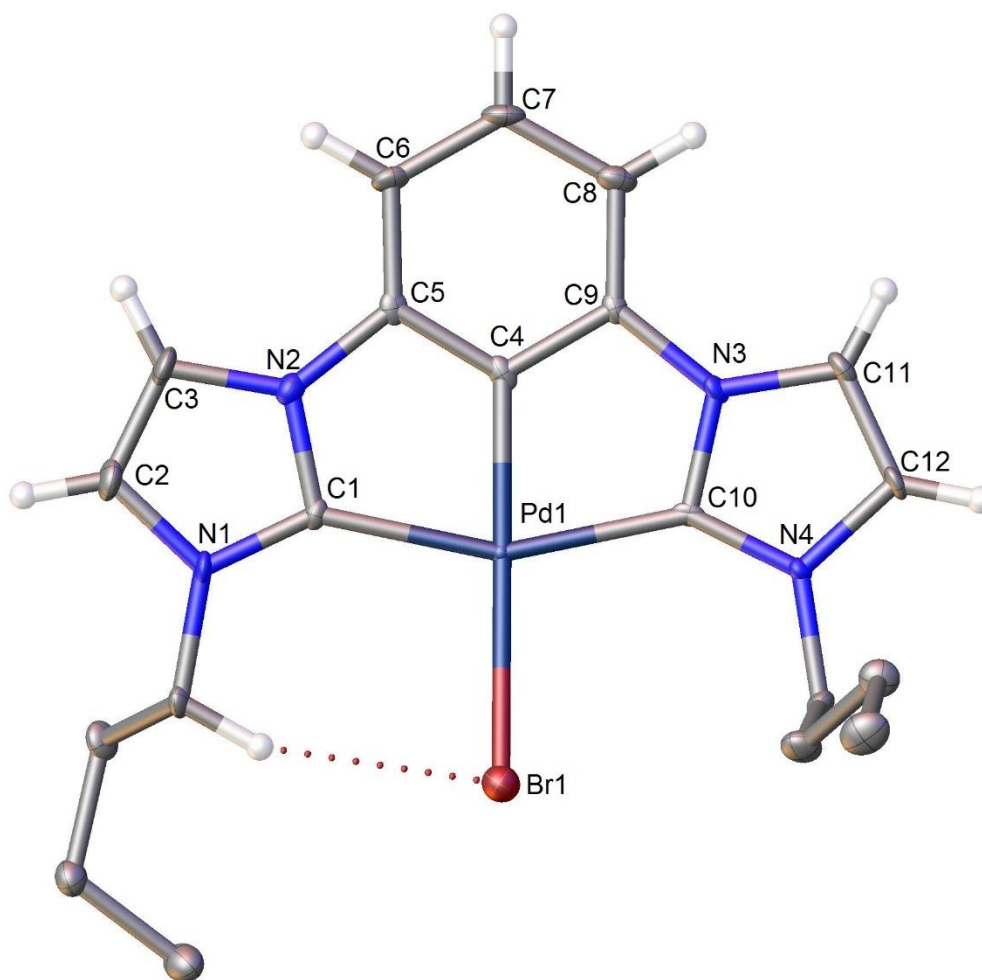
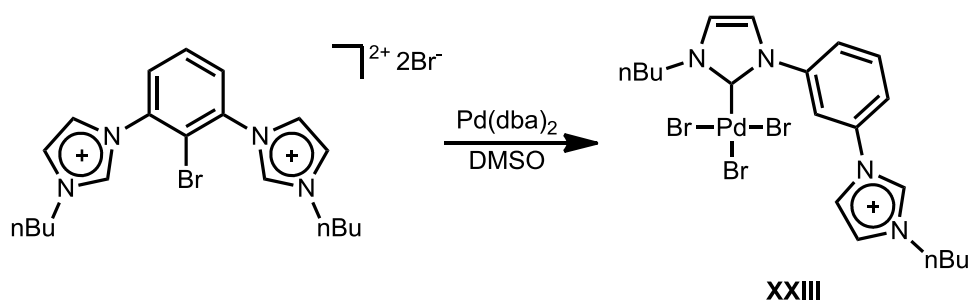


Figure 4.11: X-ray molecular structure of [(CCC^{nBu})PdBr] **XXIIa**. Thermal ellipsoids are shown at the 50% probability level. All nbutyl hydrogen atoms removed for clarity. Selected bond lengths (Å) and angles (°): Pd(1)–Br(1) 2.4979(10), Pd(1)–C(1) 2.058(7), Pd(1)–C(4) 1.940(7), Pd(1)–C(10) 2.054(7), C(1)–Pd(1)–Br(1) 101.48(19), C(4)–Pd(1)–Br(1) 177.5(2), C(4)–Pd(1)–C(1) 78.2(3), C(4)–Pd(1)–C(10) 78.5(3), C(10)–Pd(1)–Br(1) 101.78(18), C(10)–Pd(1)–C(1) 156.7(3).

The crystal structure of **XXIIa** is consistent with similar CCC metal complexes.^[15] The imidazolium rings, aryl and palladium square planar ligand plane are all on the same plane with the palladium having a distorted square planar geometry. The C(1)–Pd(1)–C(10) angle is 156.7(3) ° due to the 5 membered PdC₃N ring which is comparable to the angle observed for [(CNC^{Pt})Pd(NCMe)][SbF₆]₂ (**IX**) (158.60(16) °). In addition the dihedral angle of the imidazolium to palladium ligand plane are 3.7(3) and 5.2(3) ° slightly higher than those observed for **IX** (2.19(16) and 2.01(18) °) (Figure 4.11).

The oxidative addition intermediate prior to the NHC coordination was trapped in an attempt to learn more about the synthesis of [(CCC^{nBu})PdBr] due to the moderate yield for the synthesis of the complex.

The first attempt to isolate the oxidative addition intermediate yielded unexpected results. [2,6-(*n*BulmH)₂-1-BrPh]Br₂ was treated with Pd(dba)₂ in DMSO and the solution was stirred at room temperature for 19 h, however, to remove the DMSO the solution was heated to 140 °C. Upon characterisation of the product the ¹H and ¹³C NMR spectroscopy, X-ray crystal structure and ESI-MS were all consistent with the formation [(3-(*n*BulmH)-1-(*n*BulmPdBr₃)Ph)] (**XXIII**) (Scheme 4.21, Figure 4.10). The ¹H NMR spectrum had inequivalent *N*-butyl chains and an imidazolium C2 proton resonance remaining at 9.96 ppm supporting one Pd–NHC bond. In addition, a ESI-MS with a *m/z* of 588.9617 was consistent with the proposed product with the loss of a Br atom. Due to the low solubility of **XXIII** and a high number of



Scheme 4.21: Synthesis of [(3-(*n*BulmH)-1-(*n*BulmPdBr₃)Ph)] (**XXIII**).

inequivalent peaks, incomplete ^{13}C NMR spectroscopy characterisation was possible. The crystal structure had large thermal ellipsoids due to larger R_1 (10.39 %) and R_{int} (8.41 %) factors as the crystals obtained were small (20x 10x 10 μm) and were collected on the MX2 beamline at the Australian Synchrotron. The Pd–Br distances of between 2.4337(14)–2.4848(14) Å are consistent with [(3-(cylmH)-1-(cylmPdBr₃)Py)] of 2.429–2.483 Å with a C–Pd distance of 1.994(9) Å longer than 1.957 Å observed for the literature compound.^[17]

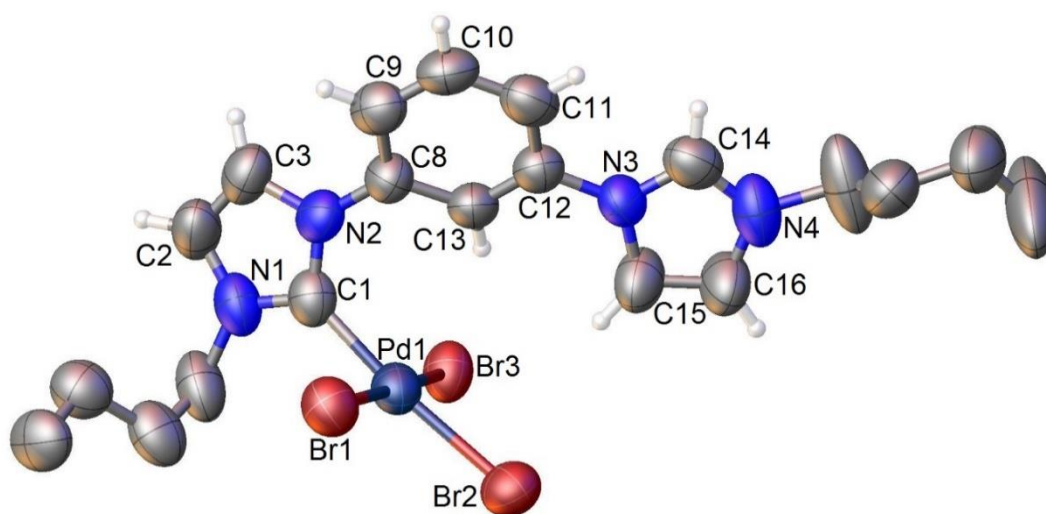
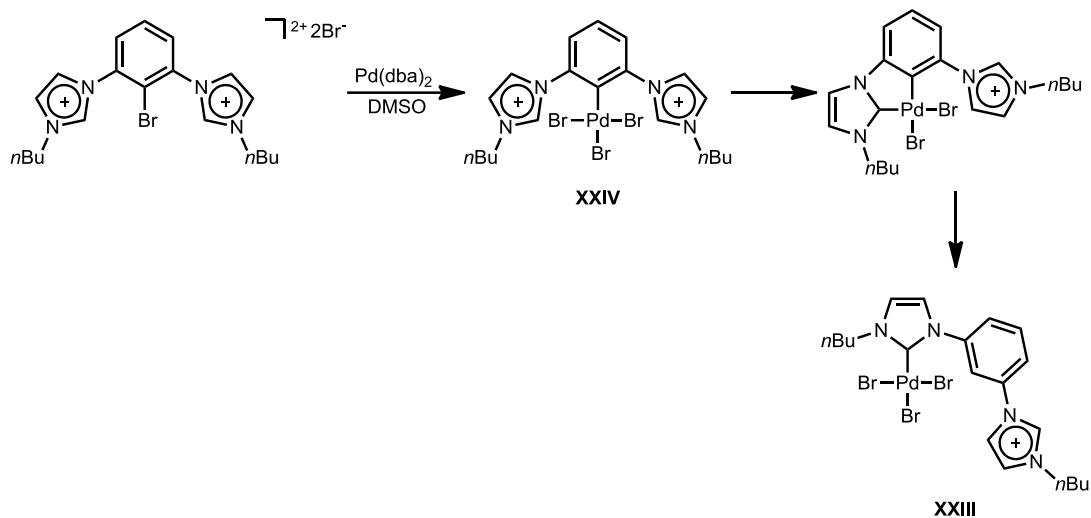


Figure 4.12: X-ray molecular structure of [(3-(*n*BulmH)-1-(*n*BulmPdBr₃)Ph)] **XXIII**.

Thermal ellipsoids are shown at the 50% probability level. All *n*-butyl hydrogen atoms removed for clarity. Selected bond lengths (Å) and angles (°): Pd(1)–Br(1) 2.4337(14), Pd(1)–Br(2) 2.4542(14), Pd(1)–Br(3) 2.4848(14), Pd(1)–C(1) 1.994(9), Br(1)–Pd(1)–Br(3) 92.17(5), Br(2)–Pd(1)–Br(3) 92.18(5), C(1)–Pd(1)–Br(1) 87.3(3), C(1)–Pd(1)–Br(2) 88.9(3).

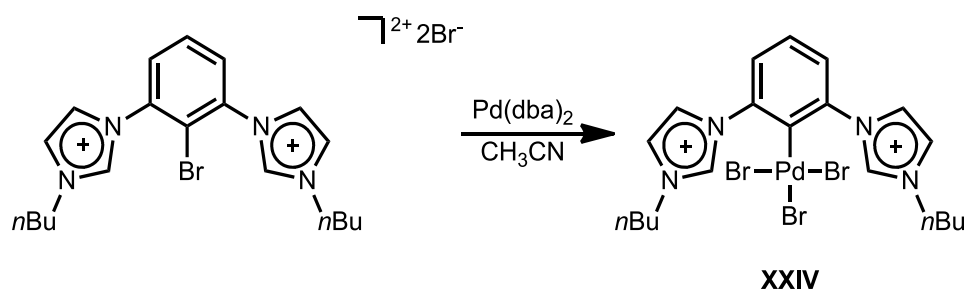
A postulated mechanism for the formation of **XXIII** began with the anticipated oxidative addition of Pd(0) to the C–Br to an aryl bond. As the solution was heated during the removal of the DMSO, this heat facilitated the coordination of the NHC

carbon to the palladium and the decoordination of the Pd–C to aryl bond yielding **XXIII** (Scheme 4.22).



Scheme 4.22: Proposed mechanism for the synthesis of [(3-(*n*BulmH)-1-(*n*BulmPdBr₃)Ph)] (**XXIII**).

The reaction was repeated in acetonitrile as this polar solvent could be removed at room temperature and would hopefully trap the desired oxidative addition intermediate. [2,6-(*n*BulmH)₂-1-BrPh]Br₂ was treated with Pd(dba)₂ in CH₃CN and the solution was stirred at room temperature for 17 hours. The expected oxidative addition product [(2,6-(*n*BulmH)₂Ph)PdBr₃] was isolated. The identity of the product was supported by ¹H NMR spectroscopy with the presence of the C2 proton imidazolium resonance at 9.67 ppm and symmetrical *n*Bu substituent. In addition, the ¹³C NMR spectroscopy, ESI-MS and X-ray crystallography all supported the



Scheme 4.23: Synthesis of [(2,6-(*n*BulmH)₂Ph)PdBr₃] (**XXIV**).

formation of **XXIV**. The Pd–Br bond lengths of 2.4370(12) and 2.5499(18) Å and Pd–C bond length of 1.991(14) Å are consistent with those observed with **XXIII**. With a yield of 18 % for the isolation of **XXIV**, the reaction of this isolated product with Na₂CO₃ will not lead to an increase in the yield of [(CCCⁿBu)PdBr] as the one step reaction described previously had a yield of 26 % (**XXIIa**) (Scheme 4.23).

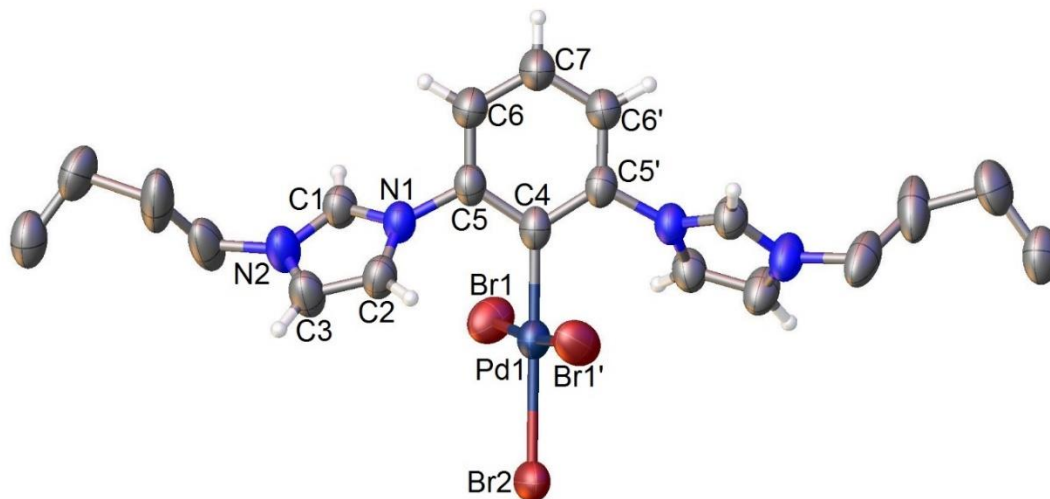


Figure 4.13: X-ray molecular structure of [(2,6-(*n*BulmH)₂Ph)PdBr₃] **XXIV**. Thermal ellipsoids are shown at the 50% probability level. All *n*-butyl hydrogen atoms removed for clarity. Disorder in *n*-butyl chain (C10B and C11B) omitted for clarity, see cif for details. Selected bond lengths (Å) and angles (°): Pd(1)–Br(1) 2.4370(12), Pd(1)–Br(2) 2.5499(18), Pd(1)–C(4) 1.991(14), Br(1)–Pd(1)–Br(1) 173.61(8), Br(1)–Pd(1)–Br(2) 93.19(4), 93.20(4), C(4)–Pd(1)–Br(1) 86.80(4), 86.81(4).

[(CCCⁿBu)PdBr] **XXIIa** was treated with Ag[SbF₆] in acetonitrile to form the desired acetonitrile complex [(CCCⁿBu)Pd(NCMe)][SbF₆] (**XXIIIa**, Scheme 4.24). This was supported by X-ray crystallography and ¹H NMR spectroscopy with a peak at 2.10 ppm consistent with the coordination of an acetonitrile ligand.

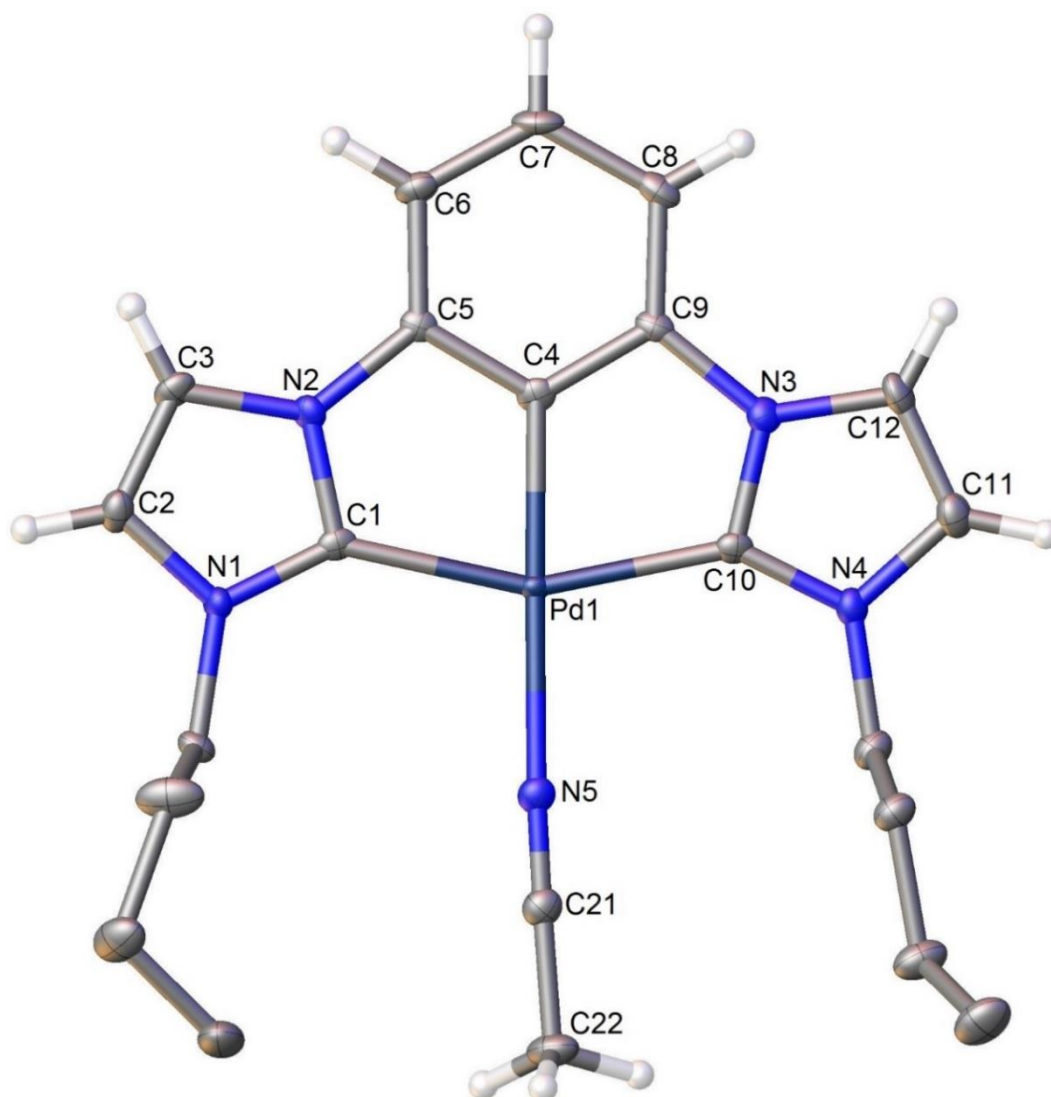
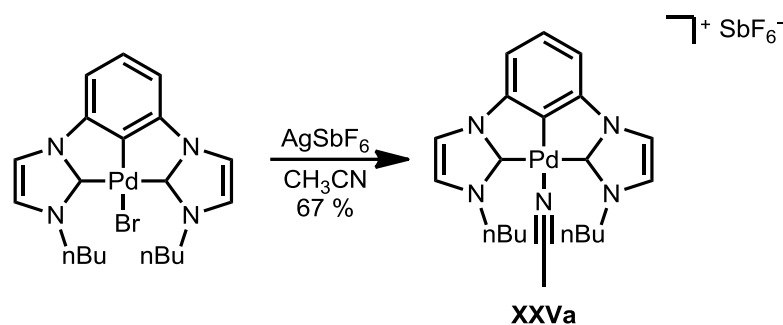


Figure 4.12: X-ray molecular structure of cation $[(CCC^{nBu})Pd(NCMe)]^+$ of **XXVa**.

Thermal ellipsoids are shown at the 50% probability level. Only one complex shown for clarity, $[SbF_6]^-$ counter ion omitted for clarity. All *N*-butyl hydrogen atoms removed for clarity. Selected bond lengths (Å) and angles (°): Pd–N 2.101(4), 2.103(4), Pd–C_{NHC} 2.043(4) – 2.059(4), Pd–C_{aryl} 1.943(4), 1.951(4), N≡C 1.132(6), 1.141(6), C–C α 1.454(6), 1.468(7), C_{NHC}–Pd–N 100.69(16) – 102.73(16), C_{aryl}–Pd–N 177.43(16), 178.53(15), C_{aryl}–Pd–C_{NHC} 77.98(18) – 78.62(17), C_{NHC}–Pd–C_{NHC} 156.80(17), 156.23(17), C≡N–Pd 176.1(4), 177.0(4), N≡C–C α 178.3(6), 178.7(5).

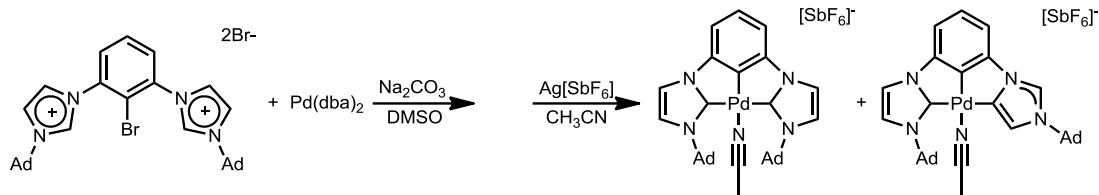


Scheme 4.24: Synthesis of $[(CCC^{nBu})Pd(NCMe)][SbF_6]$ (**XXVa**).

$[(CCC^{nBu})Pd(NCMe)][SbF_6]$ has similar bond angles and distances to $[(CCC^{nBu})PdBr]$ with a Pd–N distance bond of 2.101(4) and 2.103(4) Å consistent with the Pd–N distance observed for $[(C^{\wedge}C^{\wedge}C^{Me})Pd(NCMe)][SbF_6]$.

Only two NHC containing CCC complexes with adamantyl *N*-substituents have previously been recorded, both of which are iridium complexes. A nNHC-nNHC (normal NHC-normalNHC) iridium complex was observed for a benzimidazole based ligand with a square pyramidal geometry.^[33] Similarly a mixed nNHC-aNHC (normalNHC-abnormal NHC) iridium complex was observed with an octahedral geometry under similar reaction conditions.^[32] While normal NHC complexes bond via the C2 carbon, with increased steric bulk or substitution, coordination can occur via the C4 carbon and are classed as abnormal carbenes.^[34]

$[2,6-(AdImH)_2-1-BrPh]Br_2$ was treated with $Pd(dba)_2$ and Na_2CO_3 in DMSO. Due to a range of products being observed by 1H NMR spectroscopy and difficulty in separating the compounds at this stage the crude reaction product was treated with $Ag[SbF_6]$ in CH_3CN . Despite difficulties in separating the products, two different pincer complexes were observed by X-ray crystallography. These are the first examples of metal containing CCC complexes with adamantyl *N*-substituents in distorted square planar geometries (Scheme 4.25).



Scheme 4.25: Synthesis of [(CCC^{Ad})Pd(NCMe)][SbF₆] and [(CCC_a^{Ad})Pd(NCMe)][SbF₆].

[(CCC^{Ad})Pd(NCMe)][SbF₆], one of the products observed is the expected product, consistent with that observed for [(CCCⁿBu)Pd(NCMe)][SbF₆]. However, the X-ray crystallographic data indicates the complex is highly strained. Additionally, there is a disorder of the NCMe ligand below and above the plane with distances of the nitrogen from the PdL₃ plane of 0.802814(18) and 0.662617(15) Å (Figure 4.15). The spacefill diagram highlights the strain in [(CCC^{Ad})Pd(NCMe)][SbF₆] (Figure 4.17). The strain can be observed through the elongated Pd–N bond of 2.14(5) and 2.18(4) Å compared to 2.101(4) and 2.103(4) Å for **XXIIIa**, a distorted C_{aryl}–Pd–N angle (168.7(3), 170.5(3) °) and Pd–N≡C angle (159.5(6), 162.7(7) °) (Scheme 4.25, Figure 4.16, Table 4.3).

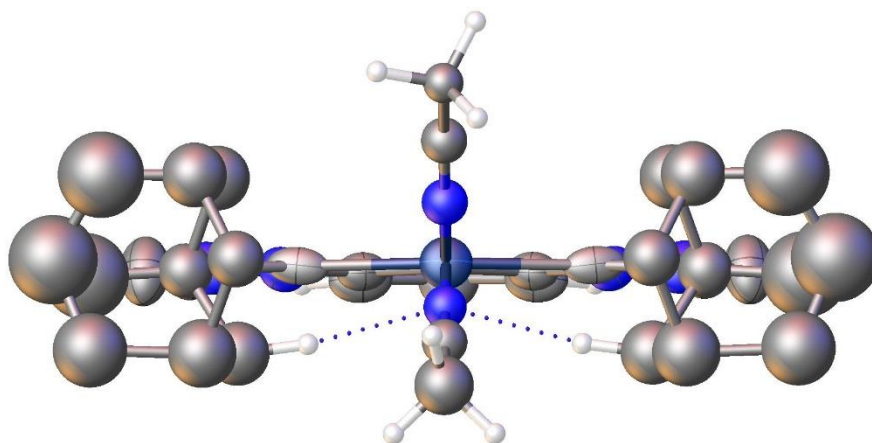


Figure 4.15: X-ray molecular structure of cation [(CCC^{Ad})Pd(NCMe)]⁺ showing distortion and disorder of NCMe ligand from the palladium ligand

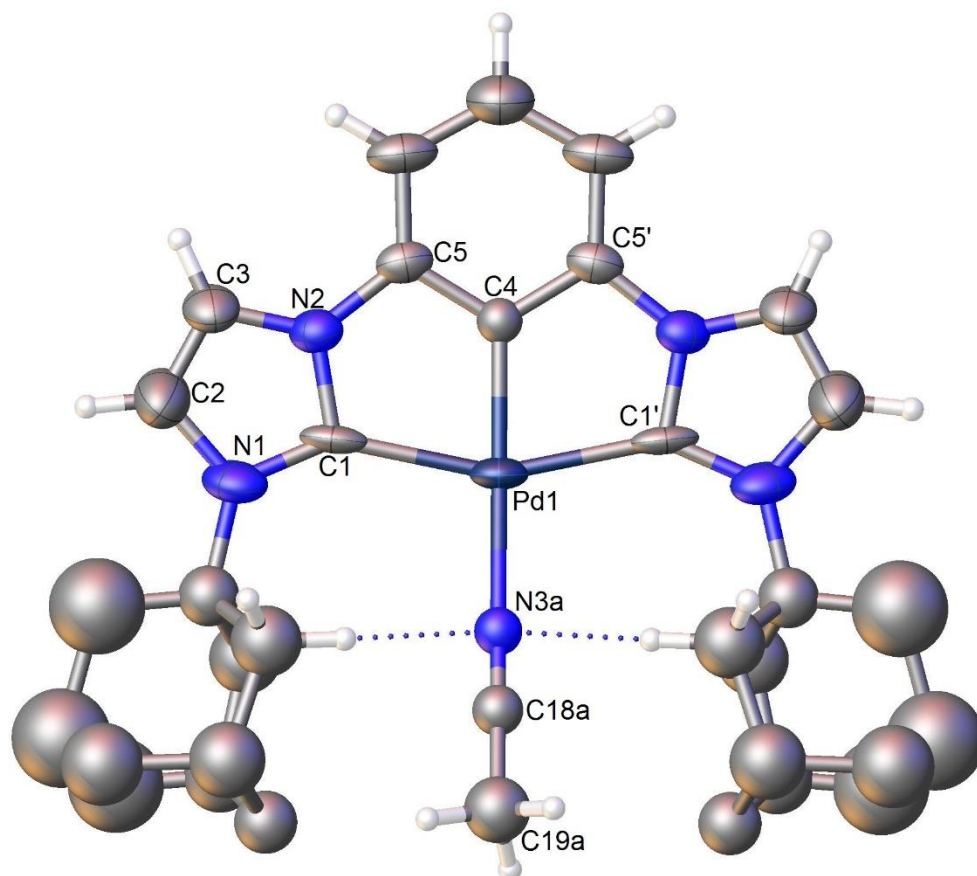


Figure 4.16: X-ray molecular structure of $[(CCC^{Ad})Pd(NCMe)]^+$. Thermal ellipsoids are shown at the 50% probability level. $[SbF_6]^-$ counter ion and NCMe ligand disorder (N(3B), C(18B), C(19B)) omitted for clarity, see cif for details. All adamantyl hydrogen atoms removed for clarity except for that with a close distance to N(3A). Selected bond lengths (Å) and angles (°): Pd(1)–C(1) 2.11(2), Pd(1)–C(4) 1.91(2), Pd(1)–N(3) 2.14(5), 2.18(4), N(3)–C(18) 1.15(7), 1.20(6), C(18)–C(19) 1.45(10), 1.49(6), C(1)–Pd(1)–C(1) 157.0(8), C(1)–Pd(1)–N(3) 100.7(4), 100.9(4), C(4)–Pd(1)–C(1) 78.5(4), C(4)–Pd(1)–N(3) 159.2(13), 161.2(14), C(18)–N(3)–Pd(1) 157(4), 172(5), N(3)–C(18)–C(19) 167(5), 180(7).

The X-ray crystal structure data has poor data quality ($R_1 = 16.02\%$ $R_{int} = 7.51\%$) this is partially due to the difficulty to model a partial acetonitrile molecule in the lattice and large thermal motion of the adamantyl ligands (Figure 4.16).

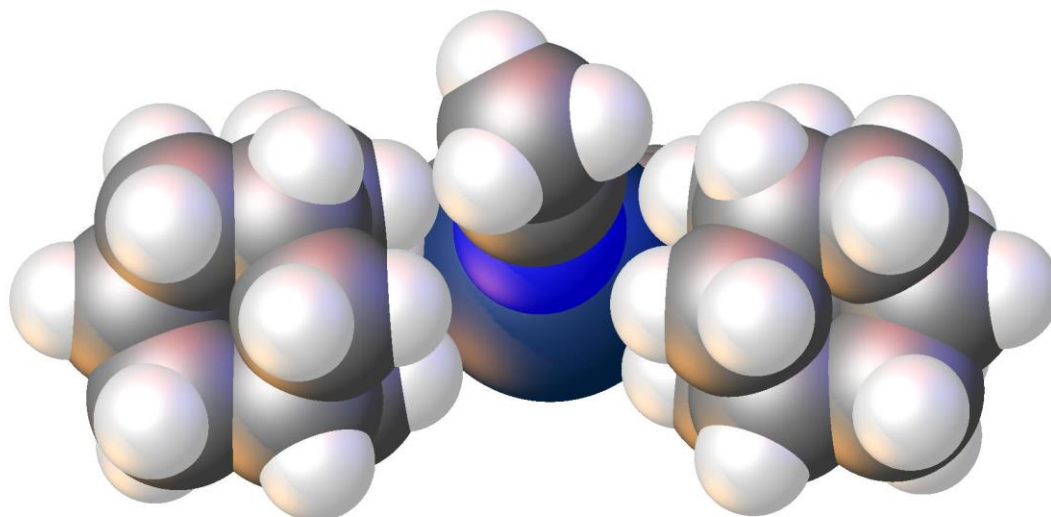


Figure 4.17: Spacefill diagram of $[(CCC^{Ad})Pd(NCMe)][SbF_6]$ showing steric hindrance of adamantyl substituent on the NCMe ligand, one NCMe ligand shown for clarity.

The second product observed was $[(CCC_a^{Ad})Pd(NCMe)][SbF_6]$. This is consistent with the previously reported product for the identical ligand on iridium.^[32] As has been previously reported for bis(NHC) complexes the reason for the formation of mixed normalNHC-abnormalNHC complexes is due to the increased steric hindrance effectively blocking the attack on the normal carbon with the abnormal carbene proton becoming the next most acidic proton for attack.^[35] Analysis of the X-ray crystal structure data indicates that the product, while more strained than the *n*-butyl substituent is less strained than $[(CCC^{Ad})Pd(NCMe)][SbF_6]$ (Scheme 4.25, Figure 4.18, Table 4.3).

Analysis of Table 4.3 shows both $[(CCC^{Ad})Pd(NCMe)][SbF_6]$ and $[(CCC_a^{Ad})Pd(NCMe)][SbF_6]$ have a distorted $-NCMe$ ligand while $[(CCC_a^{Ad})Pd(NCMe)][SbF_6]$ has alleviated some of the steric strain as the adamantyl ligand is pointing away from the $-NCMe$ coordination area.

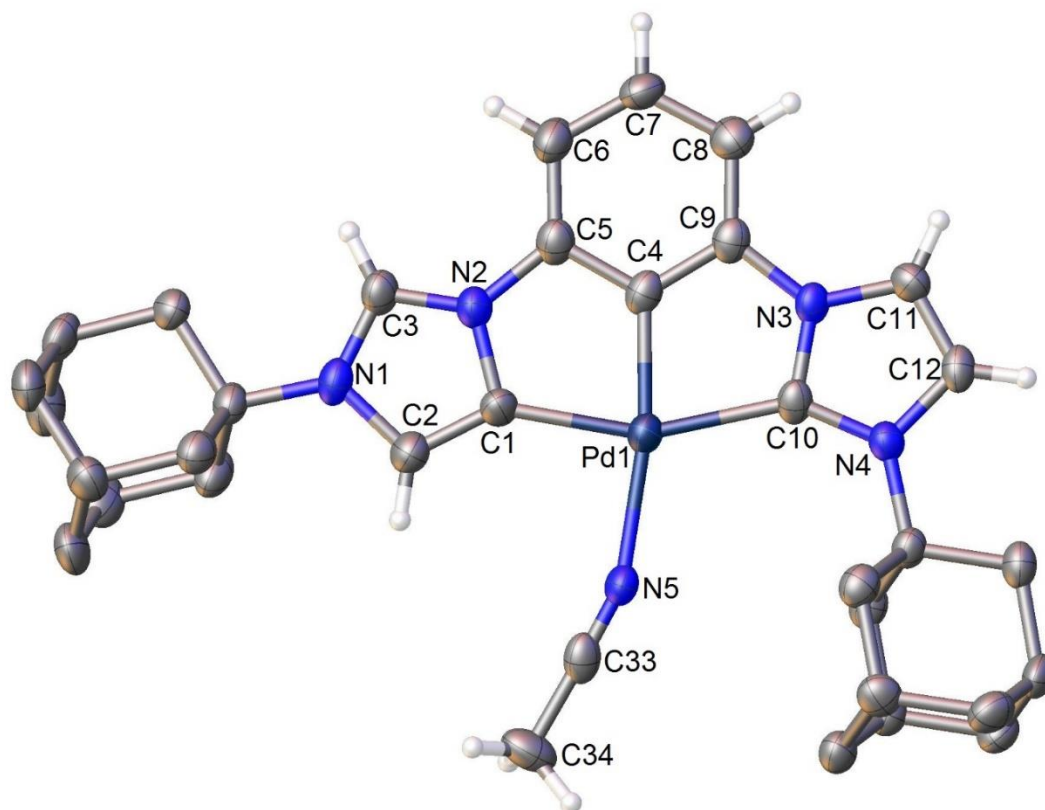


Figure 4.18: X-ray molecular structure of cation $[(\text{CCC}_a^{\text{Ad}})\text{Pd}(\text{NCMe})]^+$. Thermal ellipsoids are shown at the 50% probability level. Only one of the three $[(\text{CCC}_a^{\text{Ad}})\text{Pd}(\text{NCMe})]^+$ complexes in the asymmetric unit is displayed, two DBU co-crystallisation molecules, two $[\text{SbF}_6]^-$ counter ion and a CH_3CN solvent molecule omitted for clarity. All adamantyl hydrogen atoms removed for clarity. Selected bond lengths (\AA) and angles ($^\circ$): Pd(1)–N(5) 2.094(7), 2.095(6), Pd(1)–C(1) 2.026(7), 2.033(7), Pd(1)–C(4) 1.925(8), Pd(1)–C(10) 2.082(8), 2.091(7), N(5)–C(33) 1.138(10), 1.144(10), C(33)–C(34) 1.448(12), 1.453(11), C(1)–Pd(1)–N(5) 91.2(3), 92.0(3), C(1)–Pd(1)–C(10) 158.0(3), 158.4(3), C(4)–Pd(1)–N(5) 168.7(3), 170.5(3), C(4)–Pd(1)–C(1) 79.4(3), C(4)–Pd(1)–C(10) 79.0(3), 78.7(3), C(10)–Pd(1)–N(5) 109.4(3), 110.7(3), C(33)–N(5)–Pd(1) 159.5(6), 162.7(7), N(5)–C(33)–C(34) 177.4(9), 177.5(10).

Complex	[(CCC ^{nBu})Pd(NCMe)][SbF ₆]	[(CCC ^{Ad})Pd(NCMe)][SbF ₆]	[(CCC _a ^{Ad})Pd(NCMe)][SbF ₆]
Pd–C _{NHC} distance	2.043(4) - 2.059(4)	2.11(2)	2.026(7), 2.033(7) (abnormal), 2.082(8), 2.091(7) (normal)
Pd–C _{aryl} distance	2.056(4), 2.059(4)	1.91(2)	1.925(8)
Pd–N distance	2.101(4), 2.103(4)	2.14(5), 2.18(4)	2.094(7), 2.095(6)
C _{aryl} –Pd–N angle	177.43(16), 178.53(15)	159.2(13), 161.2(14)	168.7(3), 170.5(3)
Pd–N≡C angle	176.1(4), 177.0(4)	157(4), 172(5),	159.5(6), 162.7(7)
N≡C–C angle	178.3(6), 178.7(5)	167(5), 180(7)	177.4(9), 177.5(10)
Distance of N from Pd C–C–C plane	0.006, 0.052	0.66(6), 0.81(6)	0.061(16), 0.261(15)

Table 4.3: Various X-ray crystallographic data for the complexes of type [(CCC^R)Pd(NCMe)][SbF₆].

The X-ray crystal structure data for $[(CCC_a^{Ad})Pd(NCMe)][SbF_6]$ shows strain in the NCMe ligand with C(4)–Pd(1)–N(5) angles of 168.7(3) and 170.5(3) ° and C(33)–N(5)–Pd(1) angles of 159.5(6) and 162.7(7) °. This is distorted from the near linear angles observed for $[(CCC^{nBu})Pd(NCMe)][SbF_6]$. (Figure 4.18)

4.2.7 Synthesis of $[(CCC^{nBu})PdL]$ Complexes:

The synthesis of various complexes of the type $[(CCC^{nBu})PdL]$ were attempted from **XXIIa** that were seen as potential catalysts for the formation of β -hydroxynitriles. Given the success of Guan and co-workers, initial work focussed in the synthesis of the CH_2CN complexes.

The synthesis of $[(CCC^{nBu})Pd(CH_2CN)]$ was attempted by treating $[(CCC^{nBu})Pd(NCMe)][SbF_6]$ with NaOH in CH_3CN , however, various products were observed. $[(CCC^{nBu})Pd(CN)Pd(CCC^{nBu})]$ was isolated from this reaction mixture. This product is likely the result of the decomposition of the –NCMe ligand by C–C activation, similar to previous reactivity as outlined in Chapter 1.^[36]

The X-ray crystal structure of $[(CCC^{nBu})Pd(CN)Pd(CCC^{nBu})]$ is modelled with a C and N atom with half occupancy for the CN ligand as the complex was modelled with half a molecule occupying an asymmetric unit (Figure 4.19). The Pd(1)–N(5)/C(21) bond length is 2.064(9) Å, with a N(5)–C(21) 1.122(19) Å bond length consistent with a CN triple bond.

The synthesis of $[(CCC^{nBu})Pd(CH_2CN)]$ was also attempted by treating $[(CCC^{nBu})Pd(NCMe)]$ with $[LiN(SiMe_3)_2]$ in THF following a synthetic method described by Guan *et al.*^[16] However, ¹H NMR spectroscopic analysis showed that a number of products were formed and separation was not possible.

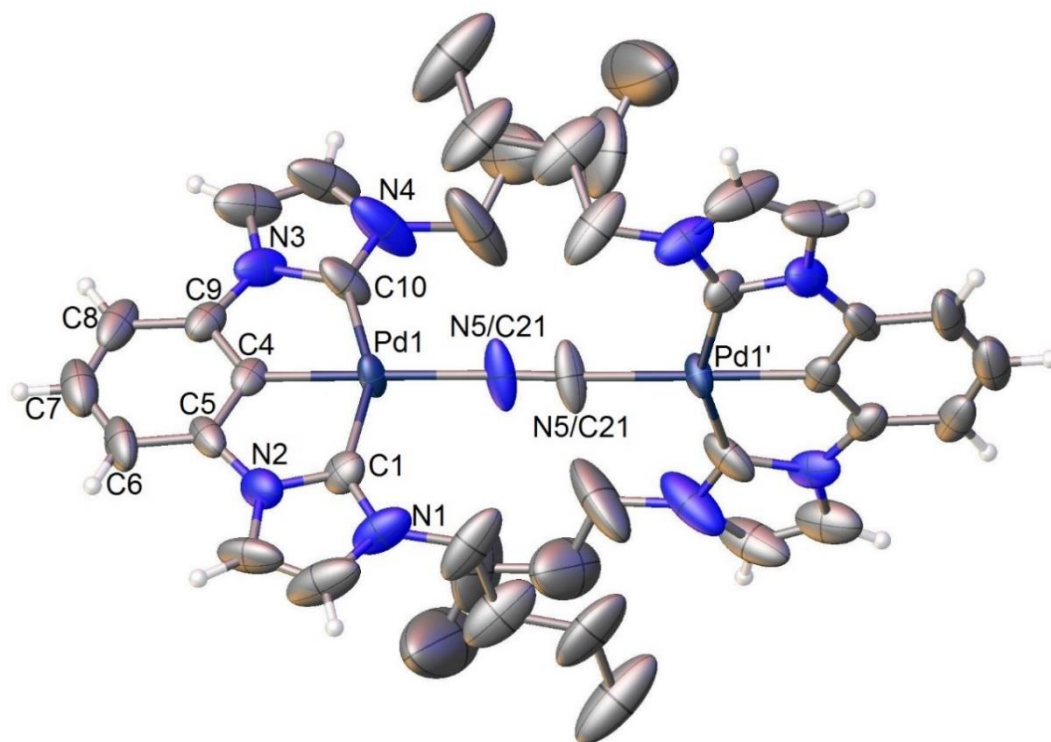
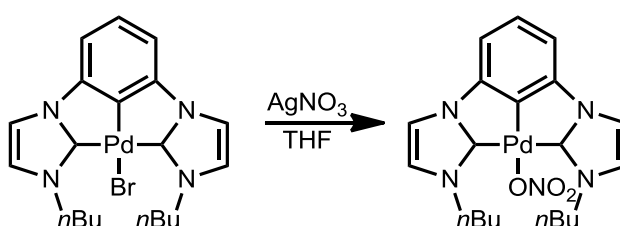


Figure 4.19: X-ray molecular structure of $[(\text{CCC}^{n\text{Bu}})\text{Pd}(\text{CN})\text{Pd}(\text{CCC}^{n\text{Bu}})]$. Thermal ellipsoids are shown at the 50% probability level. $[\text{SbF}_6]^-$ counter ion omitted for clarity. All *n*-butyl hydrogen atoms removed for clarity. Selected bond lengths (Å) and angles (°): Pd(1)–C(1) 2.050(10), Pd(1)–C(4) 1.971(9), Pd(1)–C(10) 2.039(12), Pd(1)–N(5)/C(21) 2.064(9), N(5)/C(21)–N(5)/C(21) 1.122(19), C(1)–Pd(1)–N(5)/C(21) 101.9(4), C(4)–Pd(1)–C(1) 77.3(4), C(4)–Pd(1)–C(10) 77.7(5), C(4)–Pd(1)–N(5)/C(21) 179.1(4), C(10)–Pd(1)–C(1) 155.0(5), C(10)–Pd(1)–N(5)/C(21) 103.1(5), N(5)/C(21)–N(5)/C(21)–Pd(1) 178.1(19).

Similarly, $[(\text{CCC}^{n\text{Bu}})\text{PdBr}]$ was also treated with a solution of *n*BuLi and CH_3CN in THF in an attempt to yield $[(\text{CCC}^{n\text{Bu}})\text{Pd}(\text{CH}_2\text{CN})]$ following a previously published method.^[16] However, although one major product was observed by ^1H NMR

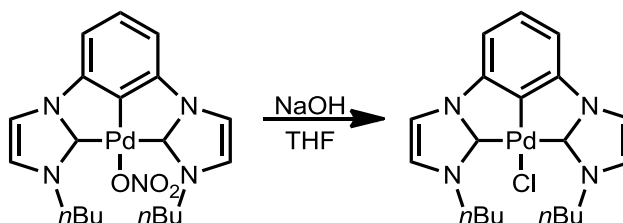
spectroscopy, there were no peaks in the -1 to 1 ppm region consistent with the formation of a $-\text{CH}_2\text{CN}$ ligand.

Given the difficulty in preparing $[(\text{CCC}^{n\text{Bu}})\text{Pd}(\text{CH}_2\text{CN})]$, synthesis of $[(\text{CCC}^{n\text{Bu}})\text{Pd}(\text{OH})]$ was attempted as it may exhibit similar catalytic activity as outlined previously. $[(\text{CCC}^{n\text{Bu}})\text{PdBr}]$ was treated with AgNO_3 in THF yielding $[(\text{CCC}^{n\text{Bu}})\text{Pd}(\text{ONO}_2)]$ which was supported by ^1H and ^{13}C NMR spectroscopy (Scheme 4.26).



Scheme 4.26: Synthesis of $[(\text{CCC}^{n\text{Bu}})\text{Pd}(\text{ONO}_2)]$ (**XXVI**)

When $[(\text{CCC}^{n\text{Bu}})\text{Pd}(\text{ONO}_2)]$ was treated with NaOH in THF an unexpected product was observed. The workup required the use of dichloromethane due to the insolubility of the product in other solvents, however both the X-ray crystal structure and ^1H NMR spectroscopic analysis indicate that the product was $[(\text{CCC}^{n\text{Bu}})\text{PdCl}]$.^[9b] The formation of this product is likely due to the reaction of the initial hydroxide product with the dichloromethane in solution (Scheme 4.27).



Scheme 4.27: Synthesis of $[(\text{CCC}^{n\text{Bu}})\text{PdCl}]$ (**XXIIb**).

The crystal structure of $[(\text{CCC}^{n\text{Bu}})\text{PdCl}]$ exhibits the same flat geometry of $[(\text{CCC}^{n\text{Bu}})\text{PdBr}]$ with similar bond distances and angles with a Pd–Cl distance of 2.4123(17) Å (Figure 4.20).

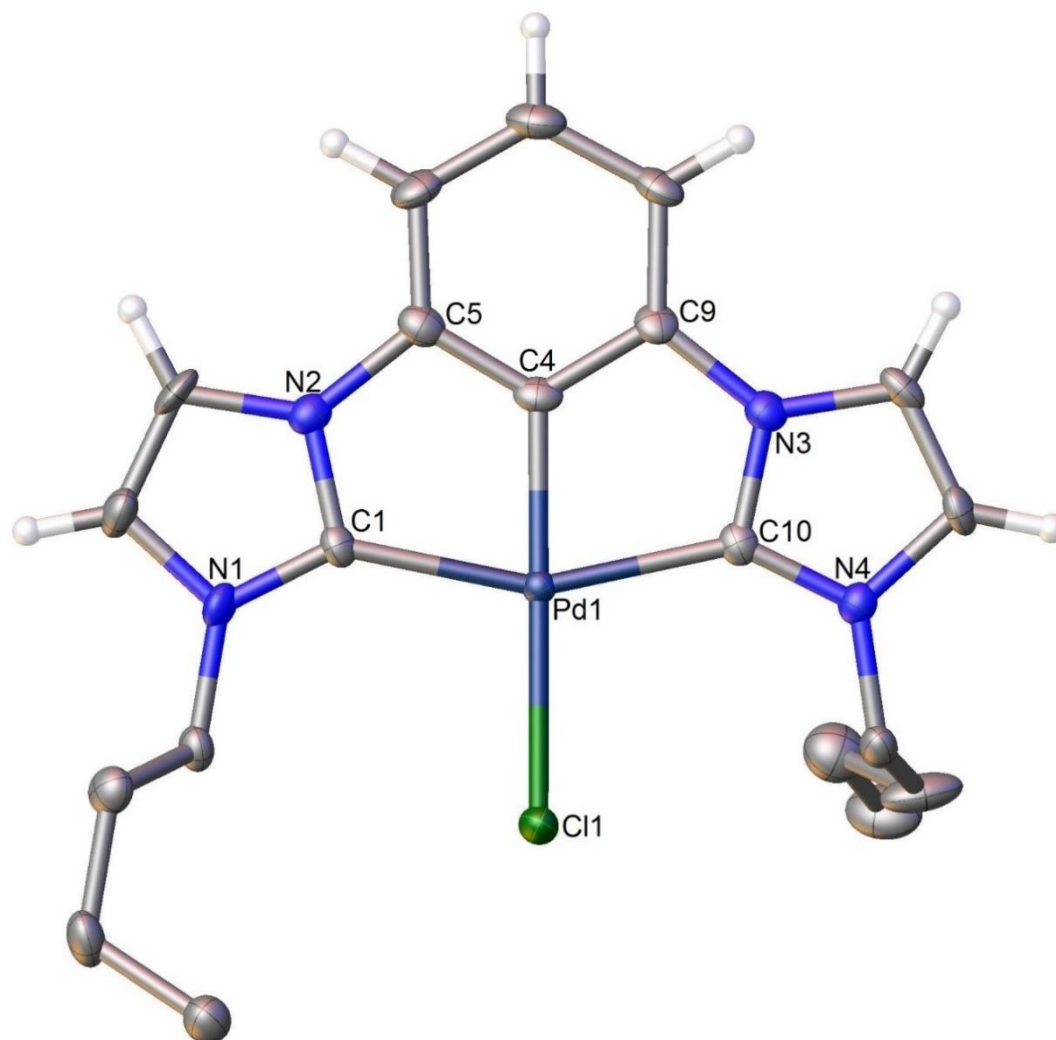
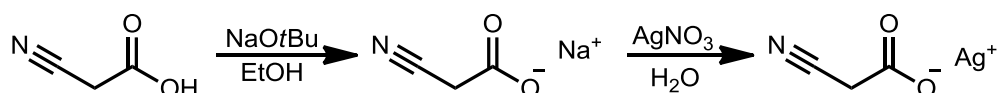


Figure 4.20: X-ray molecular structure of $[(\text{CCC}^{n\text{Bu}})\text{PdCl}]$ **XXIIb**. Thermal ellipsoids are shown at the 50 % probability level. All *n*-butyl hydrogen atoms removed for clarity. Selected bond lengths (Å) and angles (°): Pd(1)–Cl(1) 2.4123(17), Pd(1)–C(1) 2.067(6), Pd(1)–C(4) 1.941(7), Pd(1)–C(10) 2.064(6), C(1)–Pd(1)–Cl(1) 101.46(19), C(4)–Pd(1)–Cl(1) 179.0(2), C(4)–Pd(1)–C(1) 78.3(3), C(4)–Pd(1)–C(10) 78.2(3), C(10)–Pd(1)–Cl(1) 102.12(19), C(10)–Pd(1)–C(1) 156.4(3).

Synthesis of the cyanoacetate complex $[(CCC^{nBu})Pd(O_2CCH_2CN)]$ was also attempted as a potential pre-catalyst for the synthesis of β -hydroxynitriles. Previous work has shown that cyanoacetate ligands decarboxylate under catalytically relevant conditions making them candidates for the formation of α -cyanocarbanions.^[37]

$[NaO_2CCH_2CN]$ was synthesised by treating 2-cyanoacetic acid with $NaOtBu$ in ethanol.^[37b] $[AgO_2CCH_2CN]$ was then synthesised by treating $[NaO_2CCH_2CN]$ with $AgNO_3$ in H_2O . The low yield of 5 % observed is likely due to the decomposition of the final product *via* decarboxylation (Scheme 4.28). **XXVIII** was treated with $[(CCC^{nBu})PdBr]$ in an attempt to form $[(CCC^{nBu})Pd(O_2CCH_2CN)]$, however, no reaction was observed.



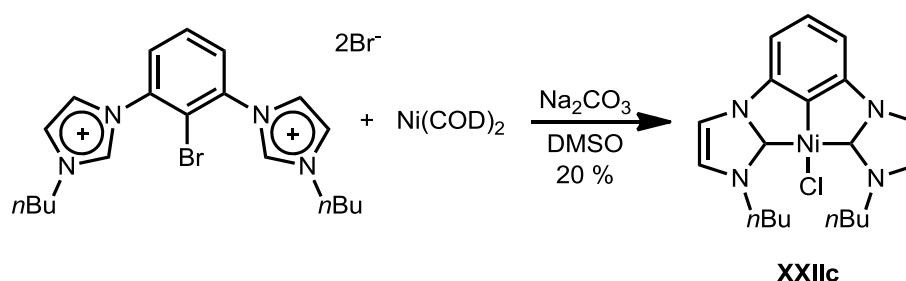
Scheme 4.28: Synthesis of $[NaO_2CCH_2CN]$ (**XXVII**) and $[AgO_2CCH_2CN]$ (**XXVIII**).

4.2.8 Synthesis of Other $[(CCC^{nBu})M(NCMe)][SbF_6]$ Group 10 Metal Complexes:

To extend the scope of the synthesis of $[(CCC^{nBu})PdBr]$ beyond palladium and to generate a larger range of catalysts, the synthesis of equivalent complexes of platinum and nickel was attempted. This was also of particular interest due to the applications of platinum CCC complexes as light emitting complexes.^[9b, 15] When the ligand $[2,6-(nBuImH)_2-1-BrPh]Br_2$ was treated with $[Pt(PPh_3)_4]$ and Na_2CO_3 in DMSO a mixture of products was obtained which were inseparable by column chromatography. Thus, the synthesis of the platinum complex was not pursued further due to time constraints.

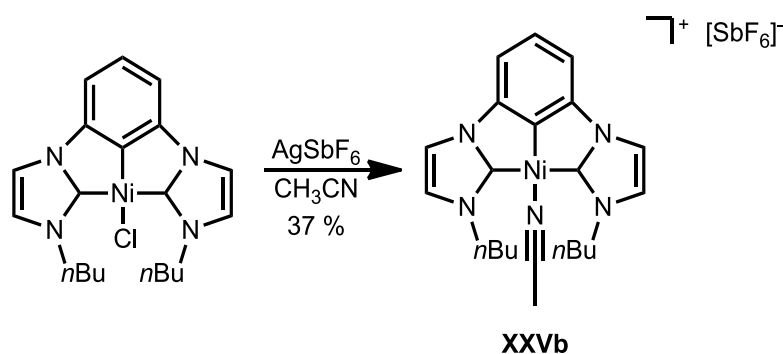
$[(CCC^{nBu})NiCl]$ was synthesised by treating $[2,6-(nBuImH)_2-1-BrPh]Br_2$ with $[Ni(COD)_2]$ and Na_2CO_3 in DMSO in a 20 % yield. The reaction was initially performed in a J. Youngs tube, by monitoring the reaction by 1H NMR spectroscopy

an optimum heating regime could be determined. This meant the solution was heated at 25 °C for 3 h followed by 180 °C for 18 h giving a complete loss of the imidazolium proton signal at 9.73 ppm. The X-ray crystal structure was consistent with the formation of $[(\text{CCC}^{n\text{Bu}})\text{NiCl}]$ however NMR spectroscopic analysis was unclear due to similar ^1H and ^{13}C NMR shifts for both $[(\text{CCC}^{n\text{Bu}})\text{NiCl}]$ and $[(\text{CCC}^{n\text{Bu}})\text{NiBr}]$.^[9b] Elemental analysis also supported the formation of $[(\text{CCC}^{n\text{Bu}})\text{NiCl}]$ exclusively. The change in the co-ligand from the expected Br to Cl is likely to have occurred in the workup when dichloromethane was used as a solvent for purification *via* column chromatography (Scheme 4.29).



Scheme 4.29: Synthesis of $[(\text{CCC}^{n\text{Bu}})\text{NiCl}]$ (**XXIIc**).

The crystal structure of **XXIIc** has shorter bond distances including the metal in comparison to $[(\text{CCC}^{n\text{Bu}})\text{PdCl}]$ with a Ni(1)–Cl(1) distance of 2.2520(7) Å, Ni(1) to NHC bound C distance of 1.960(3) and 1.968(3) Å and a Ni(1)–C(4) distance of 1.862(3) Å (Figure 4.21).



Scheme 4.30: Synthesis of $[(\text{CCC}^{n\text{Bu}})\text{Ni}(\text{NCMe})][\text{SbF}_6]$ (**XXVb**)

$[(\text{CCC}^{n\text{Bu}})\text{Ni}(\text{NCMe})][\text{SbF}_6]$ was synthesised by treating $[(\text{CCC}^{n\text{Bu}})\text{NiCl}]$ with $\text{Ag}[\text{SbF}_6]$ in CH_3CN in a 37 % yield. The formation of the product was supported by ^1H and

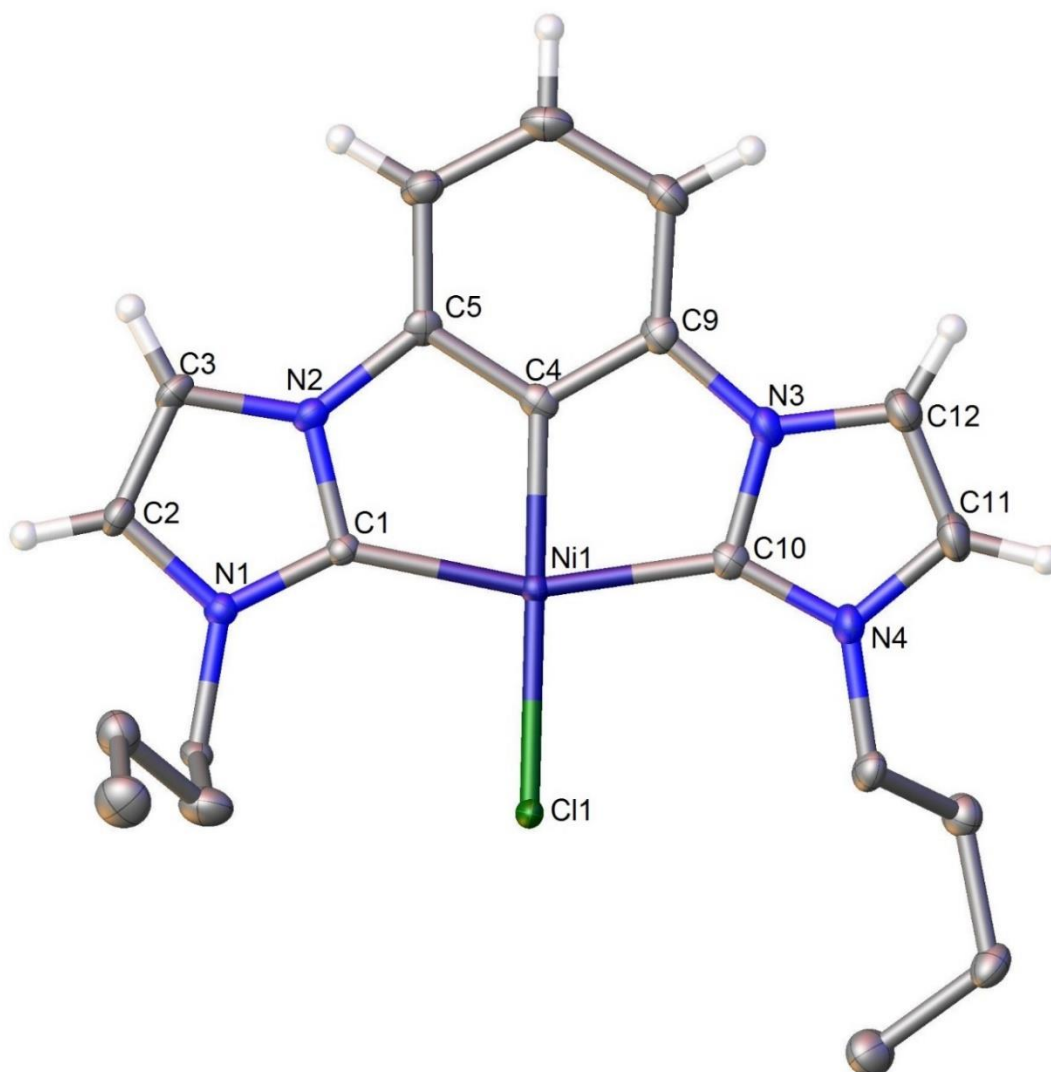


Figure 4.21: X-ray molecular structure of $[(\text{CCC}^{n\text{Bu}})\text{NiCl}]$ **XXIIc**. Thermal ellipsoids are shown at the 50% probability level. All *n*-butyl hydrogen atoms removed for clarity. Selected bond lengths (Å) and angles (°): Ni(1)–Cl(1) 2.2520(7), Ni(1)–C(10) 1.968(3), Ni(1)–C(4) 1.862(3), Ni(1)–C(1) 1.960(3), C(10)–Ni(1)–Cl(1) 99.54(8), C(4)–Ni(1)–Cl(1) 177.31(9), C(4)–Ni(1)–C(10) 80.61(12), C(4)–Ni(1)–C(1) 79.68(11), C(1)–Ni(1)–Cl(1) 100.09(8), C(1)–Ni(1)–C(10) 160.26(11).

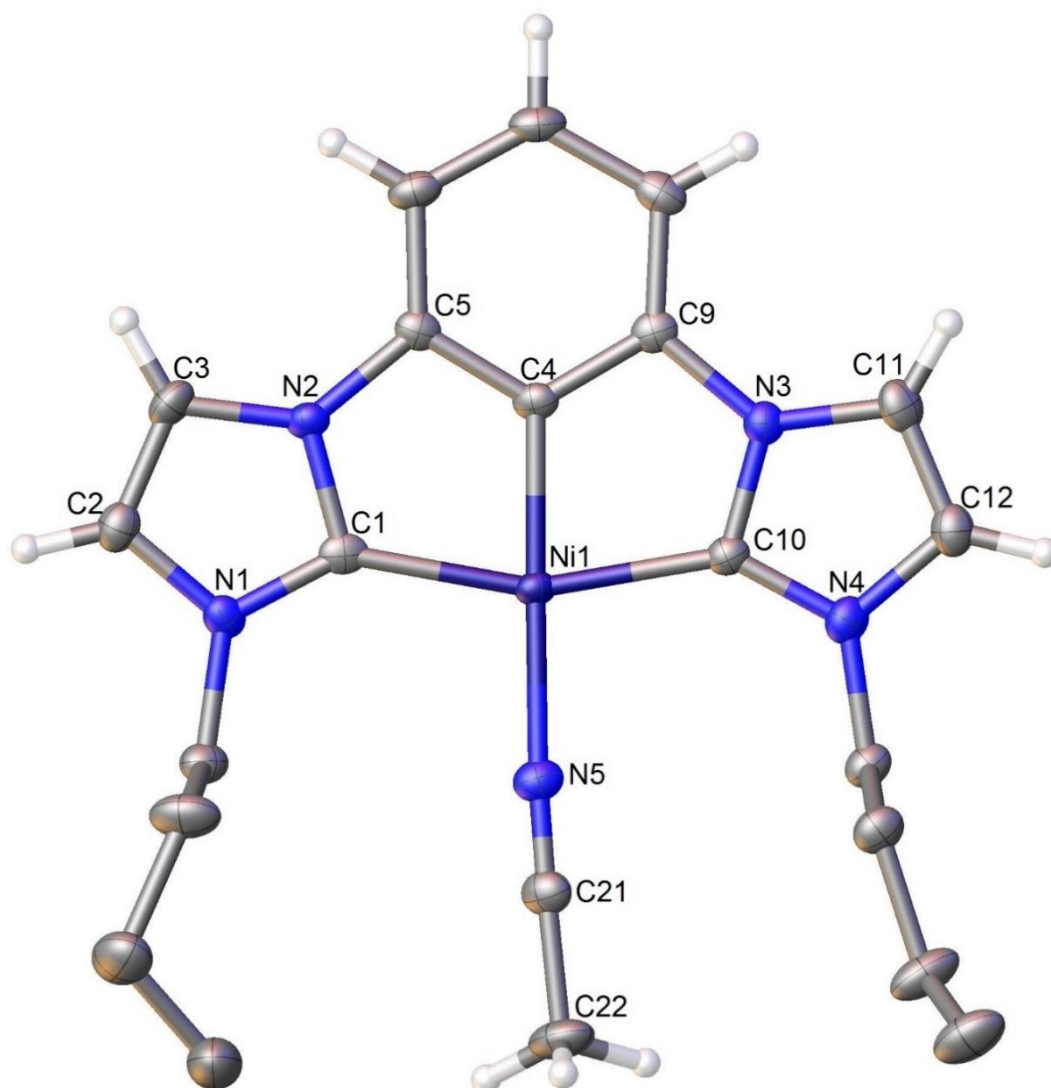


Figure 4.22: X-ray molecular structure of cation $[(CCC^{nBu})Ni(NCMe)]^+$ of **XXVb**.

Thermal ellipsoids are shown at the 50% probability level. Only one of the two $[(CCC^{nBu})Ni(NCMe)]$ complexes in the asymmetric unit is displayed, $[SbF_6]^-$ counter ion omitted for clarity. All *n*-butyl hydrogen atoms removed for clarity. Selected bond lengths (Å) and angles (°): Ni–N 1.906(4), 1.916(4), Ni–C_{NHC} 1.938(5) – 1.951(5), Ni–C_{aryl} 1.854(5), 1.866(5), N≡C 1.126(6), 1.141(6), C–C_α 1.465(7), 1.469(7), N–Ni–C_{NHC} 98.88(18) – 101.04(18), C_{NHC}–Ni–C_{NHC} 159.84(19), 160.3(2), C_{aryl}–Ni–C_{NHC} 79.7(2) – 80.7(2), C≡N–Ni 176.4(4), 177.9(4), N≡C–C_α 177.7(6), 178.3(6).

^{13}C NMR spectroscopy with ^1H NMR resonances at 2.12 ppm consistent with the CH_3 from the coordination of the NCMe ligand. The bond distances and angles are consistent with **XXIc** with Ni(1)–N(5) bond lengths of 1.906(4) and 1.926(4) Å (Scheme 4.30, Figure 4.22).

In an attempt to synthesise the α -cyano carbanion, $[(\text{CCC}^{n\text{Bu}})\text{Ni}(\text{NCMe})][\text{SbF}_6]$ was reacted with $[\text{LiN}(\text{SiMe}_3)_2]$ in THF following a previously published method for the synthesis of $[\{2,6-(i\text{Pr}_2\text{PO})_2\text{C}_6\text{H}_3\}\text{Ni}(\text{CH}_2\text{CN})]$.^[16] However the ^1H NMR spectrum of the product did not indicate the presence of a $-\text{CH}_2\text{CN}$ ligand. Due to time constraints of the PhD project this was not pursued further.

4.3 Conclusion:

A range of CEC and C[^]C[^]C complexes were synthesised as target catalysts and pre-catalysts for the synthesis of β-hydroxynitriles which is discussed in Chapter 5.

The desired CNC palladium complex [(CNC^{Pr})Pd(CH₂CN)][SbF₆] (**X**) was synthesised from the corresponding NMe ligated complex **IX** using analogous reaction conditions to that designed in Chapter 3 for the corresponding bis(NHC) complexes. The C[^]C[^]C complex [(C[^]C[^]C^{Me})Pd(NCMe)][SbF₆] (**XIV**) was successfully prepared by modifying a previously reported synthesis of the corresponding Br complex.^[8] Attempts to access other catalytically useful complexes with the corresponding hydroxide and CH₂CN ligand were not fruitful.

A number of different approaches were explored for the synthesis of the CCC complex. The first strategy used ligands [1,3-((R)ImH)₂Ph]X₂ (**XVIa** and **XVIb**) in an attempt to form the desired palladium complex. However, due to the need for the deprotonation of three C–H bonds this synthetic pathway was not successful. Thus an alternative method was investigated based on that used for [(C[^]C[^]C^{Me})PdBr] utilising an oxidative addition pathway. The initial pathway focused on the synthesis of the corresponding ligand using a OTf on the central aryl carbon but was unfruitful due to difficulties in methylating or forming the desired triflate from either **XIXa** or **XIXb**.

An alternative synthetic method for the desired CCC ligand was developed using 2-bromo-1,3-difluorobenzene allowing oxidative addition on the aryl carbon. The desired pro-ligands **XXIa** and **XXIb** were prepared by reacting **XX** with the corresponding alkyl halide in toluene while the more sterically hindered adamantyl ligand **XXIc** was synthesised by reacting **XX** with bromoadamantane neat, albeit in a low yield. [(CCC^{nBu})PdBr] (**XXIIa**) was successfully obtained from the corresponding ligand **XXIb** in a good yield providing an alternative synthetic pathway to that previously developed by Hollis and co-workers.^[9b] This new

synthesis method has higher atom efficiency, uses air stable starting materials and avoids the zirconium transfer reagent which makes this method advantageous despite the lower yield under minimally optimised conditions. Oxidative addition intermediate **XXIV** was isolated in similar yields to the final product and thus a stepwise synthesis method would not prove fruitful to increase the yield of the reaction. A number of catalytically relevant related complexes were prepared. $[(\text{CCC}^{n\text{Bu}})\text{Pd}(\text{NCMe})][\text{SbF}_6]$ (**XXVa**) was synthesised from $[(\text{CCC}^{n\text{Bu}})\text{PdBr}]$ **XXIIa**, however attempted formation of the CH_2CN , OH and $\text{O}_2\text{CCH}_2\text{CN}$ ligated complexes were not successful.

$[2,6\text{-}(\text{AdImH})_2\text{-BrPh}]\text{Br}_2$ **XXIc** was similarly treated with $\text{Pd}(\text{dba})_2$ in an attempt to form the desired palladium complex. Both $[(\text{CCC}^{\text{Ad}})\text{Pd}(\text{NCMe})][\text{SbF}_6]$ and $[(\text{CCC}_a^{\text{Ad}})\text{Pd}(\text{NCMe})][\text{SbF}_6]$ were observed which are the first square planar metal complexes with a CCC adamantyl ligand. The geometry observed for the nNHC/nNHC isomer was highly distorted due to the steric hindrance of the adamantyl group.

$[(\text{CCC}^{n\text{Bu}})\text{NiCl}]$ (**XXIIc**) was synthesised by treating the corresponding ligand **XXIb** with $[\text{Ni}(\text{COD})_2]$. Again providing a viable alternative to that previously reported by Hollis and co-workers.^[9b] The Cl ligand forms *via* exchange in CH_2Cl_2 during the workup, **XXVb** was prepared by the reaction of **XXIIc** with $\text{Ag}[\text{SbF}_6]$ in CH_3CN .

4.4 Experimental:

4.4.1 General Considerations:

All air sensitive reactions were performed under an atmosphere of high purity argon using standard Schlenk techniques. NMR scale reactions were prepared in a dry glove box (Innovative Technologies) under a nitrogen atmosphere with J. Young's NMR tubes. Glassware was heated under vacuum and back-filled with argon to ensure the exclusion of oxygen and moisture in the reactions. $[(iPrIm)_2Py]Br_2^{[38]}$ was obtained from Dr David S. McGuinness. The following chemicals were used as received: $Ag[SbF_6]$ (Sigma Aldrich), *N*-bromosuccinimide (Sigma Aldrich), 1,3-dibromobenzene (Combi-Blocks), 2-bromo-*m*-xylene (Combi-Blocks) 1-bromoadamantane (Combi-Blocks), imidazole (Koch-light), *n*BuLi (1.6 M in hexanes, Aldrich), $Li(NSiMe_3)_2$ (1.0 M in THF, Aldrich), Cu_2O (Aldrich), CuO (BDH), NaI (BDH), MeI (BDH), $MgSO_4$ (Scharlau), CuI (Merck), $Pd(OAc)_2$ (Precious Metals On-Line Pty Ltd.), phenol (Griffin), HCl (36 % of an aqueous solution, RCI Labscan), benzyl chloride (Hopkin & Williams), 2-cyanoacetic acid (Acros Organics), $AgNO_3$ (Chem Supply), 1-bromobutane (Fluka), and diisopropylamine (Fluka). Na_2CO_3 was purchased from Ajax, dried under vacuum at 200 °C and stored in a vacuum desiccator. NaOH was purchased from Chem Supply and dried under vacuum at 200 °C. K_2CO_3 was purchased from Strem and stored in an oven 150 °C. For air sensitive reactions anhydrous DMSO was purchased from Sigma-Aldrich and stored in an ampoule over 3 Å molecular sieves, anhydrous CH_3CN was obtained by passage through an Innovative Technologies Solvent Purifier and stored in an ampoule over 3 Å molecular sieves. All other anhydrous solvents were obtained by passage through an Innovative Technologies Solvent Purifier and stored in an ampoule over a mirror of sodium. For air stable synthesis, solvents were of analytical grade and used as received. $LiNEt_2^{[39]}$ $Zr(NEt_2)_4^{[26]}$ $Pd(dba)_2^{[40]}$

$\text{Pd}_2(\text{dba})_3 \cdot \text{CHCl}_3$ ^[40] and $[\text{Ni}(\text{COD})_2]$ ^[41] were all synthesised according to literature procedure.

4.4.2 Instrumentation:

NMR spectroscopic studies were carried out on a 400 MHz Bruker Avance 3 HD 400 MHz Wide Bore Spectrometer with a 5 mm BBFO probe at room temperature (298 K) or 120 °C where stated or a 600 MHz Bruker Avance III HD 600 MHz spectrometer with a 5 mm TCI-cyproprobe at 300 K, in $\text{DMSO}-d_6$, CDCl_3 or CD_3CN . CD_3Cl_3 was used as received, whereas CD_3CN and $\text{DMSO}-d_6$ were used as received except in air sensitive NMR spectroscopy where they were distilled over calcium hydride and stored over 3 Å molecular sieves. ^1H NMR spectra were obtained at 399.58 or 600.07 MHz while ^{13}C NMR spectra were recorded at 100.47 or 150.89 MHz. ^1H NMR spectra were referenced to the residual ^1H resonance of the residual solvent peak while ^{13}C NMR spectra were referenced to a deuterated ^{13}C resonance, assignments were supported by COSY, HSQC and HMBC NMR spectra.

Elemental analyses were conducted by Dr. Thomas Rodemann at the Central Science Laboratory at the University of Tasmania using a Carlo Erba EA1108 Elemental Analyser.

ESI-MS were conducted by Richard Wilson at the Central Science Laboratory at the University of Tasmania using a LTQ-Orbitrap high resolution mass spectrometer (Thermo Fisher Scientific) by infusion at 5 $\mu\text{l}/\text{min}$ using Positive mode electrospray ionisation, with a voltage of 4 kV applied. Full scan data (m/z range 150-2000) was acquired at a resolution of 60,000 and reported values for $[\text{M}+\text{H}]$ or $[\text{M}+\text{Na}]$ ions were based on the averaged spectrum of 20 successive scans.

X-ray crystallography data for **XXIII**, **XXIV** and $[(\text{CCC}_a^{\text{Ad}})\text{Pd}(\text{NCMe})][\text{SbF}_6]$ were collected at -173 °C on crystals mounted on a Hampton Scientific cryoloop at the

MX1 or MX2 beamlines of the Australian Synchrotron.^[42] Data completeness is limited by the single axis goniometer on the MX beamlines and the Australian synchrotron. Data for **IX**, **X**, **XIV**, reaction of **XVIa** and Pd(OAc)₂, **XXIa**, **XXIb**, **XXIc**, **XXIIa**, **XXVa**, [(CCC^{Ad})Pd(NCMe)][SbF₆], [(CCC^{nBu})Pd(CN)Pd(CCC^{nBu})], **XXIIb**, **XXIIc** and **XXVb** were collected at -173 °C on crystals mounted on a Hampton Scientific cryoloop on a Bruker AXS D8 Quest with a Cu K α source. The structures were solved by direct methods with SHELXT, refined using full-matrix least-squares routines against F² with SHELXL-97,^[43] and visualised using Olex2.^[44] All non-hydrogen atoms were refined anisotropically. All hydrogen atoms were placed in calculated positions and refined using a riding model with fixed C–H distances of 0.95 Å (*sp*²CH), 1.00 Å (*sp*³CH), 0.99 Å (CH₂), 0.98 Å (CH₃). The thermal parameters of all hydrogen atoms were estimated as $U_{\text{iso}}(\text{H}) = 1.2U_{\text{eq}}(\text{C})$, except for CH₃ where $U_{\text{iso}}(\text{H}) = 1.5U_{\text{eq}}(\text{C})$. Cif files available on request.

4.4.3: Preparation of [(CNC^{Pr})PdBr]Br (**VIII**):

The synthesis followed a modified published procedure.^[1] [(*i*PrIm)₂Py]Br₂ (0.2100 g, 0.459 mmol) and Pd(OAc)₂ (0.1085 g, 0.483 mmol) were combined in a predried Schlenk flask and further dried under vacuum at 70 °C. DMSO (5 mL) was then added and the solution was stirred at room temperature for 3 h and then heated to 50 °C for 18 h and 160 °C for 1 h. DMSO was removed under reduced pressure at 160 °C. A column was run of the product, first eluting with CH₂Cl₂ then 10 % MeOH in CH₂Cl₂. The product was recrystallised by vapour diffusion of Et₂O onto a near saturated solution of MeOH forming an orange solid (20 % yield, 51.6 mg). NMR spectroscopic analysis indicated that this compound was spectroscopically identical to equivalent data reported in the literature.^[17]

¹H NMR (400 MHz, DMSO-*d*₆): δ 8.59 (1H, t, $J = 8.2$ Hz, *p*-CH), 8.54 (2H, d, $J = 2.2$ Hz, ImH), 8.02 (2H, d, $J = 8.2$ Hz, *m*-CH), 7.98 (2H, d, $J = 2.2$ Hz, ImH), 5.79 (2H, sep, $J = 6.7$ Hz, *i*Pr CH), 1.46 ppm (12H, d, $J = 6.8$ Hz, *i*Pr CH₃).

^{13}C NMR (100.47 MHz, DMSO- d_6): δ 165.2 (C-Pd), 150.7 (*o*-C), 147.0 (*p*-CH), 120.8 (ImH), 119.3 (ImH), 109.2 (*m*-CH), 52.5 (*i*Pr CH), 22.8 ppm (*i*Pr CH₃).

M.P.: 182 °C (dec)

4.4.4 Preparation of [(CNC^{*i*Pr})Pd(NCMe)][SbF₆]₂ (IX):

[(CNC^{*i*Pr})PdBr]Br (51.6 mg, 91.9 μmol), Ag[SbF₆] (72.6 mg, 0.211 mmol) and CH₃CN (8 mL) were combined in a round bottom flask and allowed to stir at room temperature for 17 h with the exclusion of light. The solution was filtered through a plug of celite[®] and the solvent was removed under vacuum. The product was then recrystallised with the vapour diffusion of diethyl ether onto a near saturated solution in acetonitrile (34 % yield, 28.5 mg).

^1H NMR (400 MHz, DMSO- d_6): δ 8.62 (1H, t, J = 8.2 Hz, *p*-CH), 8.55 (2H, d, J = 1.6 Hz, ImH), 8.06 (2H, d, J = 1.6 Hz, ImH), 8.01 (2H, d, J = 8.2 Hz, *m*-CH), 4.70–4.73 (2H, m, *i*Pr CH), 2.08 (6H, s, NCCH₃), 1.53 ppm (12H, d, J = 6.6 Hz, *i*Pr CH₃).

^{13}C NMR (100.47 MHz, DMSO- d_6): δ 164.4 (Pd-C), 151.4 (*o*-C), 148.0 (*p*-CH), 120.9 (ImH), 119.8 (ImH), 118.6 (NC), 109.6 (*m*-CH), 52.3 (*i*Pr CH), 23.0 (*i*Pr CH₃), 1.6 ppm (NCCH₃).

M.P.: 276 °C (dec)

4.4.5 Preparation of [(CNC^{*i*Pr})Pd(CH₂CN)][SbF₆] (X):

[(CNC^{*i*Pr})Pd(NCMe)][SbF₆]₂ (27.2 mg, 29.7 μmol) and NaOH (14.5 mg, 0.363 mmol) were combined in a predried Schlenk flask which was further dried under vacuum. To this CH₃CN (5 mL) was added and they were allowed to stir at 60 °C for 18 h. The solvent was removed under reduced pressure. The product was recrystallised via vapour diffusion of Et₂O into a near saturated solution in CH₃CN. (44 % yield, 8.9 mg)

¹H NMR (400 MHz, DMSO-*d*₆): δ 8.52–8.54 (3H, m, ImH & *m*-CH), 7.98–8.00 (4H, m, ImH & *p*-CH), 4.74 (2H, sep, *J* = 6.64 Hz, *i*Pr CH), 2.12 (2H, s, PdCH₂), 1.54 ppm (12H, d, *J* = 6.64 Hz, *i*Pr CH₃).

¹³C NMR (100.47 MHz, DMSO-*d*₆): δ 170.2 (Pd-C_{im}), 149.7 (*o*-C), 146.7 (*m*-CH), 126.6 (C≡N), 120.9 (ImH), 119.5 (ImH), 109.1 (*p*-CH), 52.8 (*i*Pr CH), 23.3 (*i*Pr CH₃), –10.0 ppm (Pd-CH₂).

M.P.: 216 °C (dec)

4.4.6 Preparation of 2,6-(CH₂Br)₂-1-BrPh (XI):

Synthesis followed a modified published procedure.^[18] 2-bromo-*m*-xylene (3.0 mL, 22.5 mmol), *N*-bromosuccinimide (8.99 g, 50.5 mmol) and CCl₄ (25 mL) were combined in a round bottom flask and stirred at reflux overnight irradiated by a 23 W compact fluorescent light bulb. The solution was cooled to room temperature and filtered. The solvent was removed under vacuum from the filtrate and the product was recrystallised from hot hexanes giving **XI** as a white solid (28 % yield, 2.161 g). NMR spectroscopic analysis indicated that this compound was spectroscopically identical to equivalent data reported in the literature.^[19]

¹H NMR (400 MHz, CDCl₃): δ 7.42 (2H, d, *J* = 7.6 Hz, *m*-CH), 7.29 (1H, t, *J* = 7.6 Hz, *p*-CH), 4.65 ppm (4H, s, CH₂).

4.4.7 Preparation of [2,6-(MeImHCH₂)₂-1-BrPh]Br₂ (XII):

Synthesis followed a modified published procedure.^[8] 2,6-(CH₂Br)₂-1-BrPh (0.360 g, 1.05 mmol), 1-methylimidazole (280 μL, 3.51 mmol) and 1,4-dioxane (15 mL) were combined in a round bottom flask and stirred at 100 °C for 2 h. The solution was cooled to room temperature and the product was collected via vacuum filtration and washed with 1,4-dioxane and Et₂O giving a white powder (83 % yield, 0.4394 g). NMR spectroscopic analysis indicated that this compound was spectroscopically identical to equivalent data reported in the literature.^[8]

¹H NMR (400 MHz, DMSO): δ 9.21 (2H, s, 1mH), 7.78 (2H, s, 1mH), 7.76 (2H, s, 1mH), 7.55 (1H, t, $J = 7.6$ Hz, *p*-CH), 7.38 (2H, d, $J = 7.7$ Hz, *m*-CH), 5.58 (4H, s, CH₂), 3.89 ppm (6H, s, CH₃).

4.4.8 Preparation of [(C[^]C[^]C^{Me})PdBr] (XIII):

Synthesis followed a modified published procedure.^[8] [2,6-(MelmHCH₂)₂-1-BrPh]Br₂ (1.104 g, 2.18x10 mmol), Pd(dba)₂ (1.256 g, 2.78 mmol) and Na₂CO₃ (0.939 g, 8.86 mmol) were combined in a predried Schlenk flask and further dried under vacuum. These were dissolved in DMSO (30 mL) and the solution was stirred at room temperature for 6 h. The solution was then heated to 125 °C 17 h. The solution was cooled to room temperature, brine (270 mL) was added and it was separated with CH₂Cl₂ (3x100 mL). The organic layers were combined, washed with brine, dried with MgSO₄, filtered and the solvent was removed under vacuum. The product was purified via column chromatography, first eluting with CH₂Cl₂ followed by 40 % acetone/60 % CH₂Cl₂ forming the desired product as a white powder (27 % yield, 0.268 g) NMR spectroscopic analysis indicated that this compound was spectroscopically identical to equivalent data reported in the literature.^[8]

¹H NMR (400 MHz, CDCl₃): δ 7.01 (2H, d, $J = 7.4$ Hz, *m*-CH), 6.97 (2H, d, $J = 1.6$ Hz, 1mH), 6.89 (1H, t, $J = 7.3$ Hz, *p*-CH), 6.72 (2H, d, $J = 1.6$ Hz, 1mH), 5.47 (2H, d, $J = 13.6$ Hz, CH₂), 4.65 (2H, d, $J = 13.7$ Hz, CH₂), 4.09 (6H, s, CH₃).

4.4.9 Preparation of [(C[^]C[^]C^{Me})Pd(NCMe)][SbF₆] (XIV):

[(C[^]C[^]C^{Me})PdBr] (0.268 g, 0.594 mmol), Ag[SbF₆] (0.233 g, 0.679 mmol) and CH₃CN (5 mL) were combined in a round bottom flask and stirred for 2 h at room temperature with the exclusion of light. The solution was filtered through a celite[®] plug and the solvent was evaporated under reduced pressure. The product was then recrystallised via vapour diffusion of Et₂O into a near saturated solution in CH₃CN giving colourless crystals (77 % yield, 0.297 g)

¹H NMR (600 MHz, DMSO-*d*₆): δ 7.53 (2H, d, *J* = 1.38 Hz, 1*m*H), 7.26 (2H, s, 1*m*H), 7.01 (2H, d, *J* = 7.38 Hz, *m*-CH), 6.86 (1H, t, *J* = 7.32 Hz, *p*-CH), 5.23 (2H, s, CH₂), 4.99 (2H, s, CH₂), 3.83 (6H, s, N-CH₃), 2.09 ppm (3H, s, NCCH₃).

¹³C NMR (150 MHz, DMSO-*d*₆): δ 175.5 (1*m*-Pd), 144.4 (Ph-Pd), 141.4 (*o*-C), 125.9 (*m*-CH), 123.4 (*p*-CH), 122.4 (1*m*), 121.8 (1*m*), 118.5 (NCCH₃), 57.2 (CH₂), 37.3 (N-CH₃), 1.7 ppm (NCCH₃).

M.P.: 168 °C (dec).

Anal. Calc. for C₁₈N₅H₂₀PdSbF₆.NCMe: C, 34.83; H, 3.36; N, 12.19; Found: C, 34.72; H, 3.22; N, 12.10 %.

4.4.10 Preparation of 1,3-1*m*₂Ph (XV):

The synthesis followed a modified published procedure.^[22] 1,3-dibromobenzene (2.00 mL, 16.5 mmol), imidazole (2.847 g, 41.8 mmol), K₂CO₃ (5.728 g, 41.4 mmol), CuO (0.156 g, 1.95 mmol) and DMSO (25 mL) were combined in a round bottom flask and allowed to stir at 150 °C for 48 h. The reaction was confirmed to have been completed by TLC. The DMSO was removed under vacuum at 150 °C. The product was then eluted through a plug of silica with 10% MeOH in CH₂Cl₂. The product was recrystallised via slow evaporation of MeOH yielding a light yellow solid. NMR spectroscopic analysis indicated that this compound was spectroscopically identical to equivalent data reported in the literature.^[23] (44 % yield, 1.539 g).

¹H NMR (400 MHz, CDCl₃): δ 7.88 (2H, s, 1*m*H), 7.57 (1H, t, *J* = 8.0 Hz, Ph₅H), 7.41 (1H, d, *J* = 1.8 Hz, Ph₂H), 7.37 (2H, dd, *J* = 8.0, 2.0 Hz, Ph_{4&6}H), 7.30 (2H, s, 1*m*H), 7.19 ppm (2H, s, 1*m*H).

¹³C NMR (100.47 MHz, CDCl₃): δ 138.8 (Ph_{1&3}), 135.6 (1*m*H), 131.6 (Ph₅H), 131.0 (1*m*H), 120.2 (Ph_{4&6}H), 118.2 (1*m*H), 114.6 (Ph₂H) ppm.

4.4.11 Preparation of [1,3-(MeImH)₂Ph]I₂ (XVIa):

1,3-Im₂Ph (0.445 g, 2.12 mmol), CH₃I (1.25 mL, 20.1 mmol) and THF (5.0 mL) were combined in a pressure tube and stirred at reflux for 18 h. The white solid was collected via vacuum filtration and washed with both THF and Et₂O (91 % yield, 0.953 g). NMR spectroscopic analysis indicated that this compound was spectroscopically identical to equivalent data reported in the literature.^[23]

¹H NMR (400 MHz, DMSO-*d*₆): δ 9.88 (2H, s, ImH), 8.38 (2H, s, ArH), 8.31 (1H, s, ArH), 8.03 (2H, s, ArH), 7.97-8.01 (3H, m, ArH), 4.00 ppm (6H, s, CH₃).

4.4.12 Preparation of [1,3-(*n*BulmH)₂Ph]Br₂ (XVIb):

The synthesis followed a modified published procedure.^[15] 1,3-Im₂Ph (0.483 g, 2.30 mmol), 1-bromobutane (1.00 mL, 9.25 mmol) and CH₃CN (9 mL) were combined in a pressure tube and allowed to reflux for 68 h. The CH₃CN was removed under vacuum and the solution was dissolved in acetone. The solid was collected via vacuum filtration and washed with acetone, Et₂O and toluene forming an off white solid (64 % yield, 0.835 g). NMR spectroscopic analysis indicated that this compound was spectroscopically identical to equivalent data reported in the literature.^[24]

¹H NMR (400 MHz, DMSO-*d*₆): δ 11.33 (2H, s, ImH), 9.05 (2H, s, ArH), 8.95 (1H, s, ArH), 8.30 (2H, d, *J* = 8.0 Hz, ArH), 7.60-7.67 (3H, m, ArH), 4.45 (4H, t, *J* = 7.2 Hz, N-CH₂), 2.01 (4H, p, *J* = 7.4 Hz, N-CH₂CH₂), 1.42 (4H, sex, *J* = 7.4 Hz, N-CH₂CH₂CH₂), 0.97 ppm (6H, t, *J* = 7.3 Hz, N-CH₂CH₂CH₂CH₃).

4.4.13 Preparation of 2,6-Br₂1-OHPh (XVII):

The synthesis followed a modified published procedure.^[27] Phenol (3.088 g, 32.81 mmol) and CH₂Cl₂ (20 mL) were combined in a round bottom flask. To this NN'-diisopropylamine (0.88 mL, 6.28 mmol) was added. *N*-Bromosuccinimide (11.48 g, 64.6 mmol) and CH₂Cl₂ (300 mL) were combined and added via a

dropping funnel over 1 h. The solution was then stirred at rt for 1 h and the reaction was confirmed to be completed by TLC. The solution was then acidified by the addition of HCl (50 mL, 1 molL⁻¹) and the organic layer was separated, washed with H₂O (100 mL), dried with MgSO₄ and filtered. The solvent was removed under reduced pressure. The product was then filtered through a plug of silica with hexanes yielding a white solid. (67 % yield, 5.542 g). NMR spectroscopic analysis indicated that this compound was spectroscopically identical to equivalent data reported in the literature.^[27]

¹H NMR (400MHz, CDCl₃): δ 7.44 (2H, d, *J* = 8.0 Hz, *m*-CH), 6.70 (1H, t, *J* = 8.0 Hz, *p*-CH), 5.89 ppm (1H, s, OH).

4.4.14 Preparation of 2,6-Br₂1-OBnPh (XVIII):

The synthesis followed a modified published procedure.^[29] 2,6-Br₂1-OHPh (5.542 g, 22.0 mmol), benzyl chloride (2.60 mL, 22.6 mmol), K₂CO₃ (4.565 g, 33.0 mmol), NaI (0.398 g, 2.65 mmol) and CH₃CN (30 mL) were combined in a round bottom flask with a reflux condenser attached and allowed to reflux for 5 h. At this time a TLC was run to confirm that reaction was complete. The solution was cooled to room temperature and H₂O (100 mL) was added to the solution. The product was extracted with Et₂O (3x 100 mL). The organic layer was washed with brine (100 mL), dried with MgSO₄ and filtered. The Et₂O was removed under rotary evaporation and filtered through a plug of silica with hexanes giving **XVIII** as a white solid (94 % yield, 7.038 g). NMR spectroscopic analysis indicated that this compound was spectroscopically identical to equivalent data reported in the literature.^[29]

¹H NMR (400 MHz, CDCl₃): δ 7.64 (2H, d, *J* = 6.9 Hz, BnH), 7.55 (2H, d, *J* = 8.0 Hz, Ph_{3,5}H), 7.37-7.46 (3H, m, BnH), 6.91 (1H, t, *J* = 8.0 Hz, Ph₄H), 5.06 ppm (2H, s, CH₂).

4.4.15 Preparation of 2,6-Im₂1-OBnPh (XIXa) and 2,6-Im₂1-OHPH (XIXb):

The synthesis followed a modified published procedure.^[30] 2,6-Br₂1-OBnPh (6.390 g, 18.7 mmol), Imidazole (7.674 g, 0.113 mol), CuI (3.424 g, 4.77 mmol), Cu₂O (0.678 g, 4.75 mmol) and K₂CO₃ (15.614 g, 0.113 mol) were combined evenly in three predried Schlenk flasks and then further dried under vacuum. DMSO (60 mL) was added and the solution was heated to 150 °C for 4 days. The DMSO was removed under vacuum at 140 °C. The solid was dissolved in EtOAc and filtered through celite®. The solvent was removed under vacuum and the compound was purified via filtration through a basic plug of alumina first washing with CH₂Cl₂, then 10% MeOH in CH₂Cl₂ giving **XIXa** as a brown solid (45 % yield, 2.689 g).

¹H NMR (400 MHz, DMSO-*d*₆, 120 °C): δ 8.03 (2H, s, ImH), 7.58 (2H, s, ImH), 7.44 (2H, s, ImH), 7.18 (2H, d, *J* = 7.8 Hz, *p*-CH), 7.00 (10H, s, Ph), 6.60 (1H, t, *J* = 7.8 Hz, *m*-CH), 5.32 ppm (2H, bs, O-CH₂).

¹³C NMR (100.47 MHz, DMSO-*d*₆): δ 153.3 (Ar), 137.9 (b, ImH), 135.7 (b, ImH), 129.1 (Ar), 127.9 (Ph), 123.7 (*p*-CH), 122.2 (b, Ph), 120.5 (b, ImH), 115.8 (Ar), 112.1 (*m*-CH), 50.0 ppm (O-CH₂).

ESI-MS: *m/z* 316 (M⁺) calc for C₁₉H₁₆N₄O 316

IR (nujol mull): 2951 (C-H), 2948 (C-H), 2923 (C-H), 2853 (C-H), 1721, 1454 (C-H), 1377, 1216 (C-O-C), 722 cm⁻¹.

MP: 156 °C (dec)

XIXb was isolated by washing the basic alumina plug with MeOH as a purple solid (22 % yield, 0.926 g).

¹H NMR (400 MHz, DMSO-*d*₆): δ 8.21 (2H, s, ImH), 7.48 (2H, s, ImH), 6.94 (2H, d, *J* = 7.7 Hz, *m*-CH), 6.89 (2H, s, ImH), 5.96 ppm (1H, t, *J* = 8.2 Hz, *p*-CH).

^{13}C NMR (100.47 MHz, DMSO- d_6): δ 158.3 (O-C), 137.8 (ImH), 128.7 (*o*-C), 127.2 (ImH), 122.1 (*m*-CH), 120.1 (ImH), 105.5 ppm (*p*-CH).

ESI-MS: m/z 226.08514 calc for $\text{C}_{12}\text{H}_{10}\text{N}_4\text{O}$ 226.08546

IR: 3312 (OH), 3117 (CH), 3030 (CH), 2927 (CH), 1503, 1325, 1064, 827, 743 cm^{-1} .

M.P.: 72 °C (dec)

4.4.16 Preparation of 2,6-Im₂-1-OHPH (XIXb):

2,6-Im₂-1-OBnPh (2.689 g, 8.50 mmol), 10 % Pd/C (92.4 mg, 0.868 mmol), EtOAc (35 mL) and EtOH (35 mL) were combined in a 2-neck round bottom flask under a balloon of H₂. The solution was stirred for 16 h and filtered through celite[®]. The solvent was removed under vacuum with the product crystallising out of the crude oil (50 % yield, 0.954 g) NMR spectroscopic analysis indicated that this compound was spectroscopically identical to that synthesised in 4.3.15.

4.4.17 Preparation of 2,6-Im₂-1-BrPh (XX):

This experiment followed a modified published procedure.^[31] 2-Bromo-1,3-difluorobenzene (1.0 mL, 8.86 mmol), Imidazole (1.852 g, 27.2 mmol), K₂CO₃ (7.43 g, 53.8 mmol) and DMF (40 mL) were combined in a round bottom flask and was stirred at 140 °C for 43 h. The DMF was removed under reduced pressure at 140 °C yielding an orange powder. The solid was dissolved in H₂O (75 mL) and extracted with CH₂Cl₂ (3x 75 mL). The organic layers were combined, washed with brine (20 mL) and dried with MgSO₄. The solution was filtered through a scintered glass funnel and the CH₂Cl₂ removed under vacuum. The crude product was then recrystallised via layering of hexanes onto a near saturated solution in CH₂Cl₂ forming colourless crystals (88 % yield, 2.248 g)

^1H NMR (400 MHz, CDCl₃): δ 7.70 (2H, s, ImH), 7.56 (1H, t, J = 8.4 MHz, *p*-CH), 7.45 (2H, d, J = 8.0 MHz, *m*-CH), 7.23 (2H, s, ImH), 7.16 ppm (2H, s, ImH).

^{13}C NMR (100.47 MHz, CDCl_3): δ 138.7 (C-N), 137.5 (ImH), 129.8 (ImH), 128.9 (*p*-CH), 128.5 (*m*-CH), 120.5 (ImH), 119.4 ppm (C-Br).

ESI-MS: m/z 288.00100 calculated for $\text{C}_{12}\text{H}_9\text{N}_4\text{Br}$ 288.0106

IR: 3120 (C-H), 3101 (C-H), 1610 (C=C), 1600 (C=C), 1498 (C=C), 1483 (C=C), 1312, 1298, 1249, 1106, 1065, 1059, 1001, 880, 814, 798, 771, 746, 725, 690, 652 cm^{-1} .

MP: 118 – 130 °C

4.4.18 Preparation of [2,6-(MelmH)₂1-BrPh]I₂ (XXIa):

2,6-Im₂1-BrPh (107.8 mg, 0.373 mmol), CH_3I (150 μL , 2.40 mmol) and toluene (5 mL) were combined in a pressure tube and stirred at reflux for 17 h. The solution was then cooled to room temperature, the solvent was decanted off and the solid was dissolved in MeOH and recrystallised via vapour diffusion of Et_2O into a near saturated solution in MeOH giving a light yellow solid (81 % yield, 173.9 mg).

^1H NMR (400 MHz, $\text{DMSO}-d_6$): δ 9.61 (2H, s, ImH), 8.05–8.08 (6H, m, 2 x ImH and *m*-CH), 7.95–7.99 (1H, m, *p*-CH), 4.02 ppm (6H, s, CH_3).

^{13}C NMR (150 MHz, $\text{DMSO}-d_6$): δ 138.6 (ImH), 136.0 (*o*-C), 131.6 (*m*-CH), 130.7 (*p*-CH), 124.7 (ImH), 124.5 (ImH), 119.1 (C-Br), 36.9 ppm (CH_3).

IR: 3067 (C-H), 2959 (C-H), 2872 (C-H), 1567 (C=C), 1547 (C=C), 1470 (C=C), 1273, 1221, 1174, 1117, 1107, 1075, 837, 804, 712 cm^{-1} .

MP: 242 °C (dec)

ESI-MS: m/z 160.0222 calculated for $\text{C}_{14}\text{H}_{15}\text{N}_4\text{Br}^{2+}$ 160.0224

4.4.19 Preparation of [2,6-(*n*BulmH)₂1-BrPh]Br₂ (XXIb):

2,6-Im₂1-BrPh (1.289 g, 4.46 mmol), 1-bromobutane (2.6 mL, 24 mmol) and toluene (15 mL) were combined a pressure tube and heated to 120 °C for 24 h. The solution

was cooled to room temperature and the solvent was removed under reduced pressure. Recrystallisation the desired product was achieved by layering Et₂O on a near saturated solution of [2,6-(*n*BulmH)₂1-BrPh]Br₂ in CH₂Cl₂ yielding a white powder (48 % yield, 1.203 g).

¹H NMR (400 MHz, DMSO-*d*₆): δ 9.73 (2H, d, *J* = 6.0 Hz, ImH), 8.16 (2H, d, *J* = 1.4 MHz, ImH), 8.12-8.13 (4H, m, ImH & *m*-CH), 7.99 (1H, t, *J* = 8.0 MHz, *p*-CH), 4.35 (4H, t, *J* = 7.1 MHz, NCH₂), 1.89 (4H, p, *J* = 7.3 MHz, NCH₂CH₂), 1.33 (4H, sex, *J* = 7.5 MHz, NCH₂CH₂CH₂), 0.95 ppm (6H, t, *J* = 7.4 MHz, NCH₂CH₂CH₂CH₃).

¹³C NMR (150 MHz, DMSO-*d*₆): δ 138.1 (ImH), 136.0 (*o*-C), 131.7 (*m*-CH), 130.6 (*p*-CH), 124.8 (ImH), 123.5 (ImH), 119.3 (C-Br), 49.7 (NCH₂), 31.7 (NCH₂CH₂), 19.2 (NCH₂CH₂CH₂), 13.8 ppm (NCH₂CH₂CH₂CH₃).

ESI-MS: *m/z* 202.0694 calculated for C₂₀N₄H₂₇Br²⁺ 202.0694

IR: 3064 (C-H), 2962 (C-H), 2869 (C-H), 1567 (C=C), 1547 (C=C), 1470 (C=C), 1273, 1219, 1173, 1107, 1075, 839, 802, 712 cm⁻¹.

MP: 214-220 °C.

4.4.20 Preparation of [2,6-(AdImH)₂1-BrPh]Br₂ (XXIc):

2,6-Im₂1-BrPh (0.503 g, 1.74 mmol) and 1-bromoadamantane (3.78 g, 17.6 mmol) were combined in a screw cap vial and stirred at 170 °C for 48 h. The solution was cooled to room temperature and the solid was washed with THF to remove the excess 1-bromoadamantane. The solid was recrystallised via layering of Et₂O onto a near saturated solution in MeOH forming an off-white solid (11 % yield, 0.140 g)

¹H NMR (600 MHz, CDCl₃): δ 10.78 (2H, s, ImH), 8.16 (2H, s, ImH), 7.84 (2H, d, *J* = 8.0 Hz, *m*-CH), 7.69 (1H, t, *J* = 8.0 Hz, *p*-CH), 7.54 (2H, s, ImH) 2.30-2.31 (6H, m, Ad CH), 2.24 (12H, d, *J* = 2.2 Hz, Ad CH₂), 1.75 ppm (12H, s, Ad CH₂).

¹³C NMR (150 MHz, CDCl₃): δ 136.8 (ImH), 135.2 (*o*-C), 130.7 (*m*-CH), 130.1 (*p*-CH), 124.3 (ImH), 120.6 (C-Br confirmed by HMBC), 118.5 (ImH), 61.9 (N-C), 42.9 (Ad CH₂), 35.2 (Ad CH₂), 29.5 (Ad CH)

ESI-MS: m/z 280.1161 calculated for C₃₂N₄H₃₉Br²⁺ 280.1162

4.4.21 Preparation of [(CCC^{*n*Bu})PdBr] (XXIIa):

The experiment followed a modified published procedure.^[8] [2,6-(*n*BulmH)₂1-BrPh]Br₂ (1.001 g, 1.78 mmol) and [Pd(dba)₂] (1.042 g, 1.81 mmol) were combined in a predried Schlenk flask and further dried under vacuum at approx. 70 °C. To this DMSO (20 mL) was added and this was allowed to stir at room temperature for 2 h. Na₂CO₃ (0.767 g, 7.23 mmol) was added and the solution was heated to 120 °C for 19 h. The DMSO was removed under vacuum at 140 °C and the solid was dissolved in CH₂Cl₂ and filtered through a plug of celite[®]. The solvent was removed under vacuum and the dba was removed via dissolving in Et₂O and filtering. The solid was collected and was purified via column chromatography with an eluent of CH₂Cl₂ yielding the desire complex as an off-white solid (26 % yield, 0.237 g). NMR spectroscopic analysis indicated that this compound was spectroscopically identical to equivalent data reported in the literature.^[9b]

¹H NMR (400 MHz, CDCl₃): δ 7.34 (2H, d, *J* = 1.8 Hz, ImH) 7.15 (1H, t, *J* = 7.8 Hz, *p*-CH), 6.93 (2H, d, *J* = 1.8 Hz, ImH), 6.90 (2H, d, *J* = 7.8 Hz, *m*-CH), 4.79 (4H, t, *J* = 7.3 Hz, N-CH₂), 1.90 (4H, p, *J* = 7.5 Hz, N-CH₂CH₂), 1.50 (4H, sex, *J* = 7.5 Hz, N-CH₂CH₂CH₂), 0.99 ppm (6H, t, *J* = 7.4 Hz, N-CH₂CH₂CH₂CH₃).

¹³C NMR (150 MHz, CDCl₃): 177.2 (Im-Pd), 146.1 (*o*-C), 144.5 (Pd-C), 124.9 (*p*-CH), 119.9 (ImH), 114.2 (ImH), 107.9 (*m*-CH), 49.6 (N-CH₂), 33.8 (N-CH₂CH₂), 19.8 (N-CH₂CH₂CH₂), 13.9 ppm (N-CH₂CH₂CH₂CH₃).

4.4.22 Preparation of [(3-(*n*Bulm_aH),1-(*n*Bulm_bPdBr₃)Ph)] (XXIII):

[2,6-(*n*BulmH)₂1-BrPh]Br₂ (0.1035 g, 0.214 mmol) and [Pd(dba)₂] (0.1040 g, 0.181 mmol), were combined in a predried Schlenk flask and further dried under vacuum. To this DMSO (5 mL) was added and the solution was stirred at room temperature for 19 h. The DMSO was removed under vacuum at 140 °C. The solid was dissolved in MeOH and filtered through a plug of celite®. The MeOH was removed under vacuum and the solid was washed with Et₂O. The solid was recrystallised via vapour diffusion of Et₂O into a near saturated solution in MeOH yielding orange crystals. (17 % yield, 24.3 mg). Incomplete NMR spectroscopic characterisation was possible due to low solubility.

¹H NMR (600 MHz, DMSO-*d*₆): δ 9.96 (1H, s, C_{2a}H), 8.37-8.45 (2H, m, Im_aH & ArH), 8.12 (1H, s, Im_aH), 7.95 (2H, s, ArH), 7.90 (1H, s, Im_bH), 7.77 (1H, bs, Im_bH), 4.51 (2H, t, *J* = 7.4 Hz, N_b-CH₂), 4.28 (2H, t, *J* = 7.2 Hz, N_a-CH₂), 2.07 (2H, p, *J* = 7.5 Hz, N_b-CH₂CH₂), 1.91 (2H, p, *J* = 7.4 Hz, N_a-CH₂CH₂), 1.41-1.44 (2H, m, N_b-CH₂CH₂CH₂), 1.36 (2H, sex, *J* = 7.5 Hz, N_a-CH₂CH₂CH₂), 0.99 (3H, t, *J* = 7.4 Hz, N_b-CH₂CH₂CH₂CH₃), 0.95 ppm (3H, t, *J* = 7.4 Hz, N_a-CH₂CH₂CH₂CH₃).

¹³C NMR (150 MHz, DMSO-*d*₆): δ 141.1 (Im_b-Pd, found by HMBC), 140.7 (ArC), 136.0 (C_{2a}H), 135.4 (ArC, found by HMBC), 131.5 (ArC), 126.1 (126.1, found by HSQC), 124.6 (Im_bH), 124.2 (Im_bH, found by HSQC), 124.1 (ArC), 121.5 (Im_aH), 51.1 (N_b-CH₂), 49.8 (N_a-CH₂), 31.7 (N_b-CH₂CH₂), 31.5 (N_a-CH₂CH₂), 19.8 (N_b-CH₂CH₂CH₂), 19.3 (N_a-CH₂CH₂CH₂), 14.1 (N_b-CH₂CH₂CH₂CH₃), 13.8 ppm (N_a-CH₂CH₂CH₂CH₃).

ESI-MS: *m/z* calc for PdN₄C₂₀H₂₇Br₂ (M⁺-Br as consistent with other literature reports^[43]): 588.9611. Found: 588.9617.

MP: 214 °C (dec)

4.4.23 Preparation of [(2,6-(*n*BulmH)₂Ph)PdBr₃] (XXIV):

[2,6-(*n*BulmH)₂1-BrPh]Br₂ (0.103 g, 0.182 mmol) and Pd(dba)₂ (0.106 g, 0.184 mmol) were combined in a predried Schlenk flask and further dried under vacuum. To this CH₃CN (5 mL) was added and the solution was stirred at 25 °C for 17 h. The CH₃CN was removed under vacuum at 25 °C and the solid was washed with Et₂O, dissolved in CH₂Cl₂ and filtered through a plug of celite[®]. The solid was recrystallised via layering of Et₂O onto a solution in CH₂Cl₂ giving orange crystals (18 % yield, 22.1 mg).

¹H NMR (400 MHz, DMSO-*d*₆): δ 9.67 (2H, s, 1mH), 8.38 (2H, s, 1mH), 8.04 (2H, s, 1mH), 7.47 (2H, d, *J* = 7.8 Hz, *m*-CH), 7.32 (1H, t, *J* = 7.8 Hz, *p*-CH), 4.32 (4H, t, *J* = 6.9 Hz, N-CH₂), 1.88 (4H, p, *J* = 7.2 Hz, N-CH₂CH₂), 1.37 (4H, sex, *J* = 7.5 Hz, N-CH₂CH₂CH₂), 0.93 ppm (6H, t, *J* = 7.3 Hz, N-CH₂CH₂CH₂CH₃).

¹³C NMR (150 MHz, DMSO-*d*₆): δ 141.3 (*o*-C), 136.8 (1mH), 136.0 (Pd-C, found in HMBC), 126.3 (*p*-CH), 125.8 (*m*-CH), 124.3 (1mH), 122.3 (1mH), 49.3 (N-CH₂), 32.0 (N-CH₂CH₂), 19.3 (N-CH₂CH₂CH₂), 13.8 ppm (N-CH₂CH₂CH₂CH₃).

ESI-MS: *m/z* 588.9617 calculated for C₂₀H₂₇Br₂N₄Pd (M+-Br as consistent with other literature reports^[43]) 588.9611.

MP: 186 – 192 °C

4.4.24 Preparation of [(CCC^{*n*Bu})Pd(NCMe)][SbF₆] (XXVa):

[(CCC^{*n*Bu})PdBr] (0.140 g, 0.276 mmol), Ag[SbF₆] (0.112 g, 0.326 mmol) and CH₃CN (10 mL) were combined in a round-bottom flask and stirred at room temperature for 2.5 h with the exclusion of light. The solution was filtered through a plug of celite[®] and the solvent was removed under vacuum. The product was recrystallised by vapour diffusion of Et₂O into a near saturated solution in CH₃CN forming white needles (67 % yield, 0.130 g).

¹H NMR (400 MHz, DMSO-*d*₆): δ 8.12 (2H, s, 1mH), 7.59 (2H, s, 1mH), 7.25 (3H, s, ArH), 4.26 (4H, t, *J* = 6.5 Hz, N-CH₂), 2.10 (3H, s, NCCH₃), 1.83 (4H, p, *J* = 7.4 Hz, N-CH₂CH₂), 1.33 (4H, sex, *J* = 7.4 Hz, N-CH₂CH₂CH₂), 0.94 ppm (6H, t, *J* = 7.4 Hz, CH₃).

¹³C NMR (150 MHz, DMSO-*d*₆): δ 175.3 (1m-Pd), 146.0 (Ar), 139.7 (Ar, found by HMBC), 126.7 (ArH), 121.9 (1mH), 118.7 (NCCH₃), 116.9 (1mH), 109.8 (ArH), 49.1 (N-CH₂), 33.0 (N-CH₂CH₂), 19.5 (N-CH₂CH₂CH₂) 14.0 (CH₃), 1.65 ppm (NCCH₃).

MP: 228 °C (dec)

Anal. Calc. for C₂₂N₅H₂₈PdSbF₆: C, 37.50; H, 4.00; N, 9.94; Found: C, 37.52; H, 3.98; N, 9.81 %

4.4.25 Preparation of [(CCC^{*n*}Bu)Pd(ONO₂)] (XXVI):

[(CCC^{*n*}Bu)PdBr] (0.0390 g, 76.8 μmol), AgNO₃ (0.0212 g, 12.5 mmol) and THF (7 mL) were combined in a round-bottom flask and stirred at room temperature for 48 h. The THF was removed under vacuum and the solid was dissolved in CH₃CN and filtered through a plug of celite[®]. The CH₃CN was removed under vacuum and the product was used crudely in the following reaction.

¹H NMR (400 MHz, CDCl₃): δ 7.35 (2H, d, *J* = 1.8 Hz, 1mH), 7.14 (1H, t, *J* = 8.0 Hz, *p*-CH), 6.94 (2H, d, *J* = 1.8 Hz, 1mH), 6.87 (2H, d, *J* = 8.0 Hz, *m*-CH), 4.18 (4H, t, *J* = 7.3 Hz, N-CH₂), 1.86 (4H, p, *J* = 7.5 Hz, N-CH₂CH₂), 1.41-1.47 (4H, m, N-CH₂CH₂CH₂), 0.98 ppm (6H, t, *J* = 7.4 Hz, N-CH₂CH₂CH₂CH₃).

¹³C NMR (150 MHz, CDCl₃): δ 175.7 (1m-Pd), 144.4 (*o*-C), 139.4 (Pd-C), 123.7 (*p*-CH), 118.0 (1m-H), 112.8 (1m-H), 106.4 (*m*-CH), 48.1 (N-CH₂), 31.6 (N-CH₂CH₂), 17.9 (N-CH₂CH₂CH₂), 11.8 ppm (N-CH₂CH₂CH₂CH₃).

4.4.26 Preparation of [(CCCⁿBu)PdCl] (XXIIb):

[(CCCⁿBu)Pd(ONO₂)] (76.8 μmol), NaOH (0.0686g, 1.72 mmol) and THF (5 mL) were sonicated for 5 h. The THF was removed under vacuum. The solid was dissolved in CH₂Cl₂ and filtered through a plug of celite[®]. The CH₂Cl₂ was removed under vacuum yielding the desired crude product (quantitative yield, 38.8 mg). NMR spectroscopic analysis indicated that this compound was spectroscopically identical to equivalent data reported in the literature.^[9b]

¹H NMR (400 MHz, CDCl₃): δ 7.35 (d, 2H, *J* = 2.0 Hz, 1mH), 7.14 (t, 1H, *J* = 7.8 Hz, *p*-CH), 6.93 (d, 2H, *J* = 2.0 Hz, 1mH), 6.90 (d, 2H, *J* = 7.8 Hz, *m*-CH), 4.73 (t, 4H, *J* = 7.3 Hz, N-CH₂), 1.90 (p, 4H, *J* = 7.5 Hz, N-CH₂CH₂), 1.49 (sex, 4H, *J* = 7.6 Hz, N-CH₂CH₂CH₂) 0.99 ppm (t, 6H, *J* = 7.4 Hz, N-CH₂CH₂CH₂CH₃).

¹³C NMR (150 MHz, CDCl₃): δ 177.2 (Pd-1m), 146.2 (*o*-C), 144.6 (Pd-C), 124.9 (*p*-CH), 119.9 (1mH), 114.1 (1mH), 107.9 (*m*-CH), 49.7 (N-CH₂), 33.8 (N-CH₂CH₂), 19.8 (N-CH₂CH₂CH₂), 13.9 ppm (N-CH₂CH₂CH₂CH₃).

4.4.27 Preparation of [NaO₂CCH₂CN] (XXVII):

The experimental followed a modified published procedure.^[37b] 2-cyanoacetic acid (3.422 g, 40.2 mmol) and EtOH (40 mL), were combined in a 2 neck round bottom flask. To this NaOtBu (3.866 g, 40.2 mmol) dissolved in EtOH (80 mL) was added *via* a pressure equalising dropping funnel over 30 min. The solution was then stirred for a further 1 h at room temperature. The volume was then reduced to approx. 20 mL via rotary evaporation and Et₂O (50 mL) was added. The solid was collected *via* vacuum filtration and washed with Et₂O (2x 10 mL) and EtOH (2x 5 mL). The desired product was dried under vacuum giving a white powder (91 % yield, 3.924 g). NMR spectroscopic analysis indicated that this compound was spectroscopically identical to equivalent data reported in the literature.^[37b] CH₂ resonances were invisible in the ¹H and ¹³C NMR spectrum due to H-D exchange.

¹³C NMR (100.47 MHz, D₂O): 170.1 (COO⁻), 117.9 ppm (C≡N).

4.4.28 Preparation of [AgO₂CCH₂CN] (XXVIII):

[NaO₂CCH₂CN] (0.228 g, 2.13 mmol) and H₂O (10 mL) were combined in a conical flask and separately AgNO₃ (0.342 g, 2.01 mmol) was dissolved in H₂O (4 mL) and added to the solution of [NaO₂CCH₂CN]. This solution was stirred at room temperature for 1 h with the exclusion of light. The solution was collected *via* vacuum filtration and was dried under vacuum yielding a grey solid (5 % yield, 19.6 mg).

4.4.29 Preparation of [(CCC^{nBu})NiCl] (XXIIc):

[2,6-(*n*BulmH)₂-BrPh]Br₂ (0.2136 g, 0.379 mmol) and [Ni(COD)₂] (0.108 g, 0.393 mmol) were added to a predried Schlenk and further dried under vacuum. The solid was dissolved in DMSO (5 mL) and stirred at room temperature for 3 h. The Na₂CO₃ (0.154 g, 1.46 mmol) was added and the solution was heated to 180 °C for 18 h. The solution was cooled to room temperature and the DMSO was removed under vacuum at 140 °C. The solid was dissolved in CH₂Cl₂ and filtered through a plug of celite[®]. The solvent was removed under vacuum and a column was then run of the product eluting with CH₂Cl₂ giving the desired product as orange crystals (20 % yield, 31.0 mg). NMR spectroscopic analysis indicated that this compound was spectroscopically identical to equivalent data reported in the literature.^[9b]

¹H NMR (400 MHz, CDCl₃): δ 7.24 (2H, bs, ArH), 7.04 (1H, t, *J* = 7.4 Hz, *p*-CH) 6.80 (2H, bs, ArH), 6.71 (2H, bs, ArH), 4.66 (4H, bs, N-CH₂), 1.88 (4H, bs, N-CH₂CH₂), 1.40-1.52 (4H, m, N-CH₂CH₂CH₂), 0.99 ppm (6H, t, *J* = 7.0 Hz, N-CH₂CH₂CH₂CH₃).

Anal. Calc. for C₂₀N₄H₂₅NiCl: C, 57.80; H, 6.06; N, 13.48; Found: C, 57.30; H, 6.31; N, 13.14 %

4.4.30 Preparation of [(CCC^{nBu})Ni(NCMe)][SbF₆] (XXVb):

[(CCC^{nBu})NiCl] (20.3 mg, 48.8 μmol), Ag[SbF₆] (17.7 mg, 51.5 μmol) and CH₃CN (5 mL) were combined in a round bottom flask and stirred at room temperature for 22 h with the exclusion of light. The solution was filtered through a plug of celite[®] and the CH₃CN was removed under vacuum. The solid was recrystallised via vapour diffusion of diethyl ether into a near saturated solution in CH₃CN yielding red needles (37 % yield, 11.8 mg).

¹H NMR (600 MHz, DMSO-*d*₆): δ 7.97 (2H, d, *J* = 1.8 Hz, 1mH), 7.44 (2H, d, *J* = 1.7 Hz, 1mH), 7.11 (1H, t, *J* = 7.7 Hz, *p*-CH), 7.01 (2H, d, *J* = 7.7 Hz, *m*-CH), 4.10 (4H, t, *J* = 7.0 Hz, N-CH₂), 2.12 (3H, s, NCCH₃), 1.80 (4H, p, *J* = 7.2 Hz, NCH₂CH₂), 1.33 (4H, sep, *J* = 7.4 Hz, NCH₂CH₂CH₂), 0.96 ppm (6H, t, *J* = 7.4 Hz, NCH₂CH₂CH₂CH₃)

¹³C NMR (150 MHz, DMSO-*d*₆): δ 171.6 (C2), 147.1 (*o*-C), 141.8 (Ni-C), 126.5 (*p*-CH), 123.0 (1mH), 119.4 (NCCH₃), 115.9 (1mH), 108.4 (*m*-CH), 48.3 (N-CH₂), 33.0 (N-CH₂CH₂), 19.4 (N-CH₂CH₂CH₂), 13.9 (N-CH₂CH₂CH₂CH₃), 1.7 ppm (NCCH₃).

MP: 196–224 °C

Anal. Calc. for C₂₂N₅H₂₈NiSbF₆: C, 40.22; H, 4.30; N, 10.66; Found: C, 40.02; H, 4.10; N, 10.34 %

4.5 References:

- [1] E. Peris, J. Mata, J. A. Loch, R. H. Crabtree, *Chem. Commun.* **2001**, 201–202.
- [2] a) S. Gründemann, A. Kovacevic, M. Albrecht, J. W. Faller Robert, H. Crabtree, *Chem. Commun.* **2001**, 2274–2275; b) D. Serra, P. Cao, J. Cabrera, R. Padilla, F. Rominger, M. Limbach, *Organometallics* **2011**, *30*, 1885–1895.
- [3] a) W. J. Lin, A. R. Naziruddin, Y. H. Chen, B. J. Sun, A. H. Chang, W. J. Wang, W. S. Hwang, *Chem. Asian J.* **2015**, *10*, 728–739; b) D. J. Nielsen, A. M. Magill, B. F. Yates, K. J. Cavell, B. W. Skelton, A. H. White, *Chem. Commun.* **2002**, 2500–2501.
- [4] Values was calculated from data obtained from the CCDC
- [5] R. E. Andrew, L. Gonzalez-Sebastian, A. B. Chaplin, *Dalton Trans.* **2016**, *45*, 1299–1305.
- [6] A. A. D. Tulloch, A. A. Danopoulos, G. J. Tizzard, S. J. Coles, M. B. Hursthouse, R. S. Hay-Motherwell, W. B. Motherwell, *Chem. Commun.* **2001**, 1270–1271.
- [7] A. M. Magill, D. S. McGuinness, K. J. Cavell, G. J. P. Britovsek, V. C. Gibson, A. J. P. White, D. J. Williams, A. H. White, B. W. Skelton, *J. Organomet. Chem.* **2001**, 546–560.
- [8] S. Grundemann, M. Albrecht, J. A. Loch, J. W. Faller, R. H. Crabtree, *Organometallics* **2001**, *20*, 5485–5488.
- [9] a) R. J. Rubio, G. T. S. Andavan, E. B. Bauer, T. K. Hollis, J. C. F. S. Tham, B. Donnadieu, *J. Organomet. Chem.* **2005**, *690*, 5353–5364; b) T. K. Hollis, X. Zhang, *Air-stable, Blue Light Emitting Chemical Compounds, US9029804B2*, **2010**.

- [10] A. A. Danopoulos, M. B. Hursthouse, A. A. D. Tulloch, S. Winston, G. Eastham, *Dalton Trans.* **2002**, 1009–1015.
- [11] E. M. Matson, G. Espinosa Martinez, A. D. Ibrahim, B. J. Jackson, J. A. Bertke, A. R. Fout, *Organometallics* **2015**, *34*, 399–407.
- [12] T. Tu, J. Malineni, X. Bao, K. H. Dötz, *Adv. Synth. Catal.* **2009**, *351*, 1029–1034.
- [13] a) J. Houghton, G. Dyson, R. E. Douthwaite, A. C. Whitwood, B. M. Kariuki, *Dalton Trans.* **2007**, 3065–3073; b) P. Cao, J. Cabrera, R. Padilla, D. Serra, F. Rominger, M. Limbach, *Organometallics* **2012**, *31*, 921–929.
- [14] a) S. U. Son, K. H. Park, Y.-S. Lee, B. Y. Kim, C. H. Choi, M. S. Lah, Y. H. Jang, D. Jang, Y. K. Chung, *Inorg. Chem.* **2004**, *43*, 6896–6898; b) L. A. Fredin, M. Papai, E. Rozsalyi, G. Vanko, K. Warnmark, V. Sundstrom, P. Persson, *J. Phys. Chem. Lett.* **2014**, *5*, 2066–2071; c) L. H. Chung, H. S. Lo, S. W. Ng, D. L. Ma, C. H. Leung, C. Y. Wong, *Sci. Rep.* **2015**, *5*, 15394.
- [15] X. Zhang, A. M. Wright, N. J. DeYonker, T. K. Hollis, N. I. Hammer, C. E. Webster, E. J. Valente, *Organometallics* **2012**, *31*, 1664–1672.
- [16] S. Chakraborty, Y. J. Patel, J. A. Krause, H. Guan, *Angew. Chem. Int. Ed.* **2013**, *52*, 7523–7526.
- [17] G. A. Andrade, J. L. DiMeglio, E. T. Guardino, G. P. A. Yap, J. Rosenthal, *Polyhedron* **2017**, *135*, 134–143.
- [18] H. Fujihara, J. Chiu, N. Furukawa, *Chem. Lett.* **1991**, 141–144.
- [19] H. J. R. d. Boer, F. J. J. d. Kanter, O. S. Akkerman, F. Bickelhaupt, *Main Group Met. Chem.* **2001**, *24*, 841–844.

- [20] J. Cámpora, P. Palma, D. d. Río, E. Álvarez, *Organometallics* **2004**, *23*, 1652–1655.
- [21] X. Hou, Y. Wang, I. Göttker-Schnetmann, *Organometallics* **2011**, *30*, 6053–6056.
- [22] J. Cho, T. K. Hollis, E. J. Valente, J. M. Trate, *J. Organomet. Chem.* **2011**, *696*, 373–377.
- [23] V. C. Vargas, R. J. Rubio, T. K. Hollis, M. E. Salcido, *Org. Lett.* **2003**, *5*, 4847–4849.
- [24] W. D. Clark, J. Cho, H. U. Valle, T. K. Hollis, E. J. Valente, *J. Organomet. Chem.* **2014**, *751*, 534–540.
- [25] a) T. P. Pell, B. D. Stringer, C. Tubaro, C. F. Hogan, D. J. D. Wilson, P. J. Barnard, *Eur. J. Inorg. Chem.* **2017**, 3661–3674; b) M. Monticelli, C. Tubaro, M. Baron, M. Basato, P. Sgarbossa, C. Grai, G. Accorsi, T. P. Pell, D. J. D. Wilson, P. J. Barnard, *Dalton Trans.* **2016**, *45*, 9540–9552.
- [26] D. C. Bradley, K. J. Chivers, *J. Chem. Soc. A.* **1968**, 1967–1969.
- [27] H. R. M. Aitken, D. P. Furkert, J. G. Hubert, J. M. Wood, M. A. Brimble, *Org. Biomol. Chem.* **2013**, *11*, 5147–5155.
- [28] L. Zhu, L. Cheng, Y. Zhang, R. Xie, J. You, *J. Org. Chem.* **2007**, *72*, 2737–2743.
- [29] M. C. Young, A. M. Johnson, A. S. Gamboa, R. J. Hooley, *Chem. Commun.* **2013**, *49*, 1627–1629.
- [30] a) V. Diachenko, M. J. Page, M. R. D. Gatus, M. Bhadbhade, B. A. Messerle, *Organometallics* **2015**, *34*, 4543–4552; b) S. Matsumoto, E. Batmunkh, M. Akazome, Y. Takata, M. Tamano, *Org. Biomol. Chem* **2011**, *9*, 5941–5944.

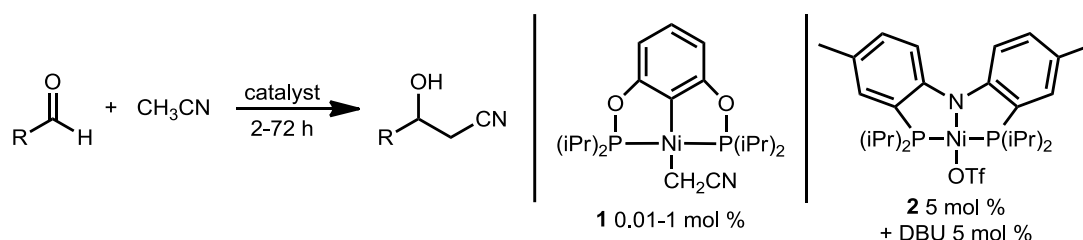
- [31] D. Munz, A. Poethig, A. Tronnier, T. Strassner, *Dalton Trans.* **2013**, *42*, 7297–7304.
- [32] W. Zuo, P. Braunstein, *Organometallics* **2012**, *31*, 2606–2615.
- [33] A. R. Chianese, S. E. Shaner, J. A. Tendler, D. M. Pudalov, D. Y. Shopov, D. Kim, S. L. Rogers, A. Mo, *Organometallics* **2012**, *31*, 7359–7367.
- [34] R. H. Crabtree, *Coord. Chem. Rev.* **2013**, *257*, 755–766.
- [35] S. Saha, T. Ghatak, B. Saha, H. Doucet, J. K. Bera, *Organometallics* **2012**, *31*, 5500–5505.
- [36] M. E. Evans, T. Li, W. D. Jones, *J. Am. Chem. Soc.* **2010**, *132*, 16278–16284.
- [37] a) J. Li, G. N. Khairallah, V. Steinmetz, P. Maitred, R. A. J. O’Hair, *Dalton Trans.* **2015**, *44*, 9230–9240; b) R. Shang, D. S. Ji, L. Chu, Y. Fu, L. Liu, *Angew. Chem. Int. Ed.* **2011**, *50*, 4470–4474; c) Y. S. Feng, Z. Q. Xu, L. Mao, F. F. Zhang, H. J. Xu, *Org. Lett.* **2013**, *15*, 1472–1475.
- [38] D. S. McGuinness, V. C. Gibson, J. W. Steed, *Organometallics* **2004**, *23*, 6288–6292.
- [39] S.-J. Chen, H. Cai, Z.-L. Xue, *Organometallics* **2009**, *28*, 167–171.
- [40] M. Schlosser, *Organometallics in Synthesis: a Manual, 2nd ed.*, Wiley, Chichester, West Sussex, England ; New York, **2002**.
- [41] D. J. Krysan, P. B. Mackenzie, *J. Org. Chem.* **1990**, *55*, 4229–4230.
- [42] T. M. McPhillips, S. E. McPhillips, H. J. Chiu, A. E. Cohen, A. M. Deacom, P. J. Ellis, E. Garman, A. Gonzalez, N. K. Sauter, R. P. Phizackerly, S. M. Soltis, P. Kuhn, *Synchrotron Radiat.* **2009**, *9*, 401.
- [43] G. M. Sheldrick, in *SHELX97, Programs for Crystal Structure Analysis*, Universität Göttingen: Germany, **1998**.

- [44] O. V. Dolomanov, L. J. Bourhis, R. J. Gildea, J. A. K. Howard, H. Puschmann, *J. Appl. Cryst.* **2009**, *42*, 339–341.
- [45] M. T. Zamora, M. J. Ferguson, R. McDonald, M. Cowie, *Dalton Trans.* **2009**, 7269–7287.

Chapter 5: Catalytic Synthesis of β -Hydroxynitriles

5.1 Introduction:

The synthesis of 3-hydroxy-3-phenylpropionitrile was first achieved under base-free conditions by Guan and co-workers using $[\{2,6\text{-}(\text{iPr}_2\text{PO})_2\text{C}_6\text{H}_3\}\text{Ni}(\text{CH}_2\text{CN})]$ (**1**) low catalyst loadings at room temperature (discussed in more detail in Chapters 1.4.4 and 2, Scheme 5.1).^[1] Prior to this, similar reactions were achieved with a Ni(PNP) catalyst (**2**) in the presence of the base DBU at 45 °C. Longer reaction times and higher catalyst loadings were required in comparison to catalyst **1**. Notably, the equivalent Ni(PNP)CH₂CN complex did not react.^[2]



Scheme 5.1: Synthesis of various β -hydroxynitriles *via* Ni(POCOP) and Ni(PNP) catalysts.

The formation of 3-hydroxy-3-phenylpropionitrile has previously been observed in the presence of DBU without a transition metal catalyst, albeit in a low yield.^[2] While many reports investigating the synthesis of β -hydroxy and β -aminonitriles using transition metal catalysts undertook a background reaction, these reactions contained only the organic compound and solvent. But they had not considered the fact that the catalyst precursors used featured basic ligands such as $-\text{CH}_2\text{CN}$, $-\text{OMe}$ or $-\text{OAc}$ {e.g. $[\text{Rh}(\text{OMe})(\text{cod})]_2$, $\text{Pd}(\text{OAc})_2$ }.^[1, 3] Therefore, to make sure that the catalytic reactions performed were the result of the proposed complex, the reaction should have also been reported with the corresponding transition metal precursor.

5.2 Results and Discussion:

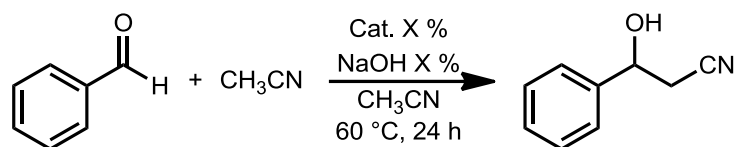
For the synthesis of 3-hydroxy-3-phenylpropionitrile from benzaldehyde various catalysts were employed. Where possible $-\text{CH}_2\text{CN}$ ligated complexes were used in the reaction. However, in some cases, due to the difficulty in isolating the $\text{M}-\text{CH}_2\text{CN}$ complex the $\text{M}-\text{NCMe}$ complex was used. In these instances, NaOH was added as an external base due to requirement for the formation of the active $-\text{NCCH}_2$ catalyst *in situ* as determined by DFT calculations (Chapter 2.1.1, Table 5.1 & 5.2). When the reactions were attempted at room temperature no reaction was observed. Subsequent reactions were performed at 60 °C as this was consistent with the temperature employed for the synthesis of CH_2CN complexes from their corresponding NCMe complex outlined in Chapter 3.

As noted in Chapter 2 the synthesis of $[\{2,6-(i\text{Pr}_2\text{PO})_2\text{C}_6\text{H}_3\}\text{Ni}(\text{CH}_2\text{CN})]$ (**1**) was not possible. Consequently, the related $[\{2,6-(i\text{Pr}_2\text{PO})_2\text{C}_6\text{H}_3\}\text{Ni}(\text{NCMe})][\text{SbF}_6]$ **I** was used in the presence of NaOH for benchmarking purposes.

As discussed in Chapter 2 the characteristics of the Ni(POCOP) catalyst that promoted the desired reactivity were determined by the DFT calculations:

- a) The C-bound CH_2CN isomer is not the active catalyst instead the N-bound $-\text{NCCH}_2$ ligated complex is the active catalyst.
- b) The *trans* donor effect of the phenyl ring is important in lowering the energy of the transition state of the intramolecular isomerisation and the 5-coordinate transition state.

Due to the presence of the 5-coordinate transition state, increasing the steric bulk to $[\{2,6-(t\text{Bu}_2\text{PO})_2\text{C}_6\text{H}_3\}\text{Ni}(\text{CH}_2\text{CN})]$ prevents the reaction from proceeding.



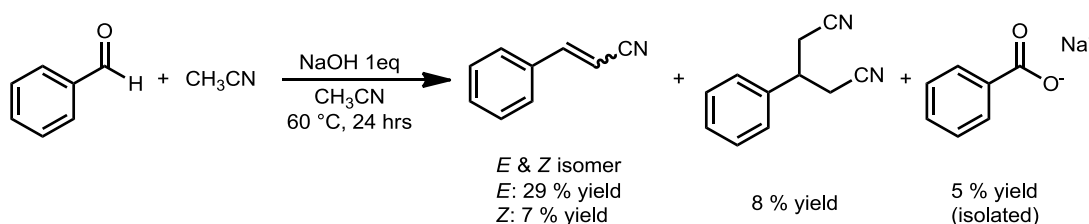
	Catalyst	Catalyst (mol %)	Base (mol %)	Temp (°C)	Time (h)	Yield (%)
1	none	0	0	60	24	0
2	none	0	5	25	20	0
3 [†]	none	0	9	60	24	20
4 [†]	none	0	12	60	24	42
5 ^[1]	[[2,6-(<i>i</i> Pr ₂ PO) ₂ C ₆ H ₃]Ni(CH ₂ CN)] (1) (lit)	1	0	25	6	91
6 ^[1]	[[2,6-(<i>i</i> Pr ₂ PO) ₂ C ₆ H ₃]Ni(CH ₂ CN)] (1) (lit)	0.01	0	25	72	83

Table 5.1: Background reactions for the synthesis of 3-hydroxy-3-phenylpropionitrile from benzaldehyde. Yields determined by GC with the aid of a calibrated internal standard. [†]Yield determined by NMR spectroscopy with the aid of an internal standard.

Control reactions were performed by treating benzaldehyde with substoichiometric quantities of NaOH in acetonitrile. Preliminary screening revealed that when the reaction was performed at 25 °C no reaction occurred (Table 5.1, entry 2). However, when the reaction temperature was raised to 60 °C, 3-hydroxy-3-phenylpropionitrile was formed in a 20 % yield with a 9 % loading of NaOH and 42 % yield (12 % NaOH loading) (Table 5.1, entries 3 & 4). The yield of this reaction was lower than that observed by Guan and co-workers using catalyst **1** at 25 °C in the absence of base (Table 5.1, entries 5 & 6). While the formation of 3-hydroxy-3-phenylpropionitrile in the presence of NaOH was perhaps not unexpected, the relatively high yield obtained was somewhat surprising. Indeed, it

has been reported that the synthesis of 3-hydroxy-3-phenylpropionitrile can be promoted by DBU in a 13 % yield at 60 °C.^[2]

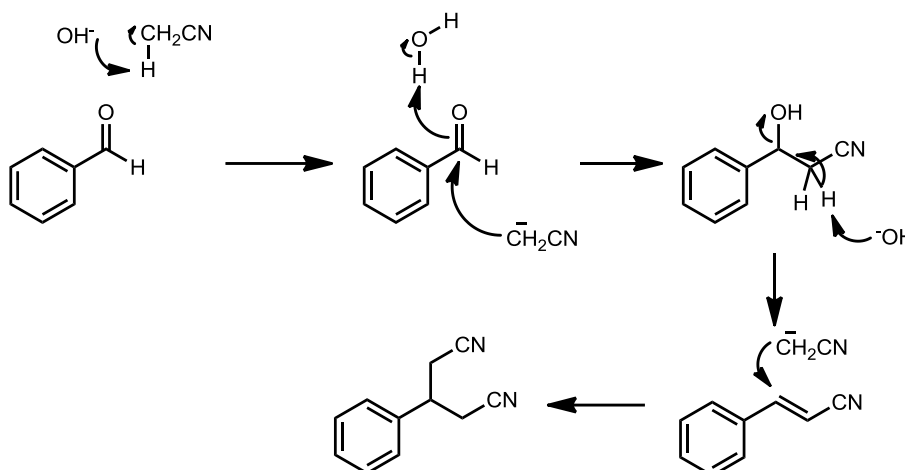
When benzaldehyde was treated with one equivalent of NaOH in acetonitrile a number of products were formed (Scheme 5.3). With the exception of sodium benzoate, the yields of all products were determined by NMR spectroscopy. The formation of sodium benzoate is likely due to the Cannizzaro reaction.^[4] This product is most commonly observed in concentrated solutions in H₂O, and, thus, the formation of this product from a reaction in a dilute CH₃CN solution was surprising. The other three products observed are both (*E*)- and (*Z*)-cinnamionitrile and 3-phenylpentanedinitrile. The formation of (*E*)- and (*Z*)-cinnamionitrile both involve the addition of an acetonitrile to benzaldehyde while 3-phenylpentanedinitrile involves the addition of two acetonitrile molecules to benzaldehyde (Scheme 5.3).



Scheme 5.3: Synthesis of various products from a 1:1 mixture of benzaldehyde and NaOH.

A possible mechanism for the synthesis of (*E*)- and (*Z*)-cinnamionitrile and 3-phenylpentanedinitrile may involve the intermediate 3-hydroxy-3-phenylpropionitrile, which was observed when the reaction was performed with a catalytic amount of NaOH (Scheme 5.4).

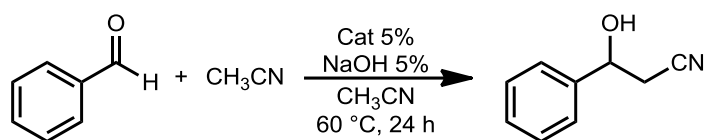
The benchmarking reactions were performed by treating benzaldehyde with [{2,6-(*i*Pr₂PO)₂C₆H₃}Ni(NCMe)][SbF₆] (**I**) as a catalyst in CH₃CN. When the reaction was performed in the absence of NaOH no reaction was observed (Table 5.2, entry 1). Similarly, when the reaction was performed with NaOH at room temperature no



Scheme 5.4: Possible mechanism for the synthesis of (*E*)- and (*Z*)-cinnamionitrile and 3-phenylpentanedinitrile from the reaction observed when benzaldehyde was treated with one equivalent of NaOH.

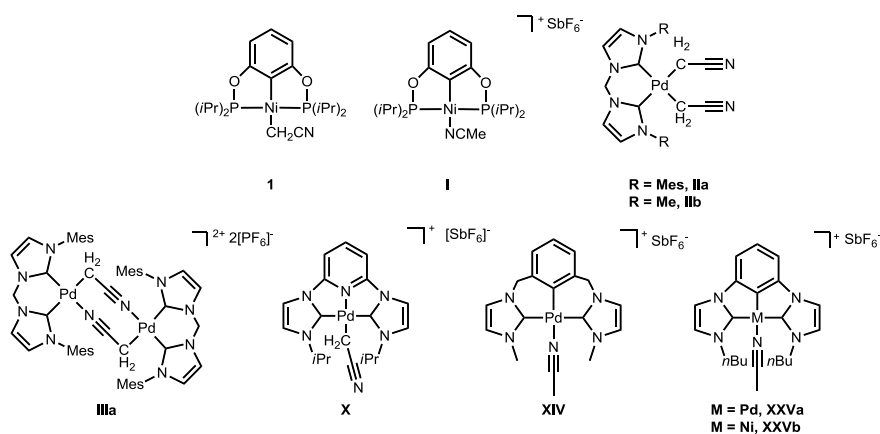
reaction was observed (Table 5.2, entry 2). However, heating the reaction mixture at 60 °C gave a yield of 35 % (Table 5.2, entry 3). This is comparable to results obtained in the absence of the catalyst indicating that this was due to the background reaction.

A range of different complexes were screened in an attempt to find an effective catalyst which had the best activity in the synthesis of 3-hydroxy-3-phenylpropionitrile. No reaction occurred when the bis(NHC) catalysts [((MesIm)₂CH₂)Pd(CH₂CN)₂] (**IIa**), [((MeIm)₂CH₂)Pd(CH₂CN)₂] (**IIb**), and [((MesIm)₂CH₂)Pd(μ-CH₂CN)₂][PF₆]₂ (**IIIa**) were used (Table 5.2, entries 4 – 6). It is unclear why these complexes are not active in catalysis. The POCOP catalyst has one active site and these systems potentially have two. Thus, complexes were synthesised which had a geometry closer to the POCOP catalyst consistent with the DFT calculations performed.



	Catalyst	Cat. load. (mol %)	Base load. (mol %)	Temp (°C)	Time (h)	Con. (%)	Yield (%)
1	[[2,6-(<i>i</i> Pr ₂ PO) ₂ C ₆ H ₃]Ni(NCMe)][SbF ₆] (I)	4.91	0	rt/60 [^]	48	0	0
2	[[2,6-(<i>i</i> Pr ₂ PO) ₂ C ₆ H ₃]Ni(NCMe)][SbF ₆] (I)	4.91	5	25	22	0	0
3*	[[2,6-(<i>i</i> Pr ₂ PO) ₂ C ₆ H ₃]Ni(NCMe)][SbF ₆] (I)	4.91	5	60	24	43	35 [†]
4 [†]	[(MesIm) ₂ CH ₂]Pd(CH ₂ CN) ₂ (IIa)	4.1	0	60	24	0	0
5	[[([MesIm) ₂ CH ₂]Pd(μ-CH ₂ CN)) ₂][PF ₆] ₂ (IIIa)	2.5	0	60	24	0	0
6	[(MeIm) ₂ CH ₂]Pd(CH ₂ CN) ₂ (IIb)	5.3	0	60	24	0	0 [□]
7	[(CNC ^{<i>Pr</i>})Pd(CH ₂ CN)][SbF ₆] (X)	4.90	0	rt/60 [^]	48	0	0
8	[(C [^] C [^] C ^{Me})Pd(NCMe)][SbF ₆] (XIV)	5.1	5	rt/60 [^]	48	0	0
9	[(CCC ^{<i>n</i>Bu})Pd(NCMe)][SbF ₆] (XXVa)	4.9	10	rt	20	0	0
10 [†]	[(CCC ^{<i>n</i>Bu})Pd(NCMe)][SbF ₆] (XXVa)	5.4	22	60	24		40
11	[(CCC ^{<i>n</i>Bu})Pd(NCMe)][SbF ₆] (XXVa)	5.0	5.0 [‡]	rt/60 [^]	48	0	0
12	[(CCC ^{<i>n</i>Bu})Pd(NCMe)][SbF ₆] (XXVa)	5.2	5.61 [#]	rt/60 [^]	48	0	0
13 [†]	[(CCC ^{<i>n</i>Bu})Ni(NCMe)][SbF ₆] (XXVb)	4.8	13	60	24	0	0

Table 5.2: Synthesis of 3-hydroxy-3-phenylpropionitrile from benzaldehyde. Yields determined by GC with the aid of a calibrated internal standard. [†]Yield determined by NMR spectroscopy with the aid of an internal standard. *reaction as previous mixture heated ^the solution was stirred at rt for 24 h followed by 60 °C for 24 h, * uncalibrated yield, [□] benzoic acid was observed instead, [‡] DBU used instead of NaOH, [#] NaO₂CCH₂CN used instead of NaOH.



As discussed in Chapter 4 a group of complexes of the type CEC and C^EC were synthesised due to their structural similarities to POCOP complexes and the ability to tailor both the electronic and steric properties of the complex independently. Complexes of the type CNC exhibit the same flat ligand skeleton geometry as POCOP complexes, but do not have the same *trans* donating ability as the C atom of the POCOP complex, which was shown to be crucial using DFT. Unfortunately, the reaction of complex [(CNC^{*i*Pr})Pd(CH₂CN)][SbF₆] (**X**) with benzaldehyde in acetonitrile did not yield any product (Table 5.2, entry 7).

Complexes of the type C^AC were also tested in catalysis. They exhibit the same *trans* donation of a central aryl carbon as the POCOP ligand, however, the twisted geometry created by the methylene linker (discussed in Chapter 4) may affect that catalysis. When the reaction was catalysed by [(C^AC^{Me})Pd(NCMe)][SbF₆] (**XIV**) in the presence of a catalytic amount of NaOH in CH₃CN no reaction was observed (Table 5.2, entry 8). Unfortunately, the corresponding –CH₂CN or –OH complex, which may have displayed better reactivity could not be synthesised.

The CCC complex exhibits the desired *trans* donating ability and flat geometry, which is similar to the POCOP complex. The reaction of benzaldehyde was catalysed by [(CCC^{*n*Bu})Pd(NCMe)][SbF₆] (**XXVa**) in the presence of a catalytic amount of NaOH in CH₃CN, however, the yield was comparable to the background reaction, which indicates that the catalyst did not facilitate this reaction (Table 5.2, entry 10). The reaction was also attempted using **XXVa** and two alternative bases due to their increased solubility in CH₃CN. Specifically benzaldehyde was treated with **XXVa** and DBU, however no reactivity was observed (Table 5.2, entry 11). Similarly, NaO₂CCH₂CN was also used as the acetate may decarboxylate on the metal to form the desired –CH₂CN complex *in situ* (Table 5.2, entry 12). Unfortunately, this was also not successful.

As the previous work by Guan and co-workers focussed on a nickel catalyst, the transformation was also attempted by treating benzaldehyde with $[(\text{CCC}^{n\text{Bu}})\text{Ni}(\text{NCMe})][\text{SbF}_6]$ (**XXVb**) and NaOH. However, no reaction was observed (Table 5.2, entry 13).

5.3 Conclusion:

A significant background reaction was observed when treating benzaldehyde with a catalytic amount of NaOH in CH_3CN yielding 3-hydroxy-3-phenylpropionitrile.

When the reaction was performed using a 1:1 mixture of NaOH and benzaldehyde in CH_3CN , a number of products were formed, including sodium benzoate. This compound is the likely result of a Cannizzaro reaction. In addition, (*E*)- and (*Z*)-cinnamionitrile and 3-phenylpentanedinitrile were obtained.

Various bis(NHC) and NHC containing CNC $-\text{CH}_2\text{CN}$ complexes were tested in catalysis. Unfortunately, in all cases, no reaction was observed. NHC-containing CCC and C[^]C[^]C pincer $-\text{NCMe}$ complexes in the presence of NaOH were tested in catalysis, however, only the background reaction was observed. While no desired reactivity was observed for any of the catalysts screened, those described in Chapter 4 to likely have the best success *i.e.* the $-\text{CH}_2\text{CN}$ ligated CCC and C[^]C[^]C complexes could not be synthesised. Therefore, if these complexes could be prepared in future they may facilitate the desired transformation.

5.4 Experimental:

5.4.1 General Considerations:

All air sensitive reactions were performed under an atmosphere of high purity argon using standard Schlenk techniques. Catalysis reactions were prepared in a dry glove box (Innovative Technologies or MBraun) under a nitrogen atmosphere in a 4 mL scintillation vial. Glassware was heated under vacuum and back-filled with argon to ensure the exclusion of oxygen and moisture in the reactions. NaOH was purchased from Chem Supply and dried under vacuum at 200 °C. Benzaldehyde and tridecane were purchased from Sigma Aldrich dried with MgSO_4 and distilled. For air sensitive reactions anhydrous CH_3CN was obtained by passage through an Innovative Technologies Solvent Purifier and stored in an ampoule over 3 Å molecular sieves.

5.4.2 Instrumentation:

NMR spectroscopic studies were carried out on a 400 MHz Bruker Avance 3 HD 400 MHz Wide Bore Spectrometer with a 5 mm BBFO probe at room temperature (293 K) or a 600 MHz Bruker Avance III HD 600 MHz spectrometer with a 5 mm TCI-cyprobeat 300 K, in CDCl_3 . CDCl_3 was used as received. ^1H NMR spectra were obtained at 399.58 or 600.07 MHz. ^1H NMR spectra were referenced to the residual ^1H resonance of the residual solvent peak.

GC-FID studies were conducted on a Shimadzu GC-2014.

GC-MS studies were conducted on an Agilent Technologies 6850 GC with a 5975C VL MSD.

5.4.3 Synthesis of β -hydroxynitriles and other by-products:

For GC analysed reactions: Benzaldehyde (25.5 μL , 2.50×10^{-4} mol), catalyst (1.25×10^{-5} mol), NaOH (0.5 mg, 1.25×10^{-5} mol), tridecane (15.2 μL , 6.25×10^{-5} mol) and CH_3CN (3.0 mL) were combined in a scintillation vial under an atmosphere of

N₂. The solution was stirred at 60 °C for 24 h. it was cooled to room temperature and a 300 µL aliquot was taken for GC-FID analysis and where relevant GC-MS analysis. The yield was calculated using a calibrated internal standard (tridecane).

For ¹H NMR spectra analysed reactions: Benzaldehyde (25.5 µL, 2.50x10⁻⁴ mol), catalyst (1.25x10⁻⁵ mol), NaOH (0.5 mg, 1.25x10⁻⁵ mol) and CH₃CN (3.0 mL) were combined in a scintillation vial under an atmosphere of N₂. The solution was stirred at 60 °C for 24 h. it was cooled to room temperature and the CH₃CN was removed under vacuum the solid was dissolved in a solution of 1,3,5-trioxane (2.50x10⁻⁴ mol) in CDCl₃ (0.4 mL). The yield of 3-hydroxy-3-phenylpropionitrile was then calculated by ¹H NMR analysis of the reaction mixture using an internal standard (1,3,5-trioxane).^[5]

For 1:1 benzaldehyde:NaOH reaction: Benzaldehyde (25.5 µL, 2.50x10⁻⁴ mol), NaOH (10.0 mg, 2.50x10⁻⁴ mol) and CH₃CN (3.0 mL) were combined in a scintillation vial under an atmosphere of N₂. The solution was stirred at 60 °C for 24 h. it was cooled to room temperature and the CH₃CN was removed under vacuum the solid was dissolved in a solution of 1,3,5-trioxane (2.50x10⁻⁴ mol) in CDCl₃ (0.4 mL). The yield was then calculated by ¹H NMR spectra analysis with comparison of the integration ratio of 1,3,5-trioxane and the integrations of (*E*).^[6] and (*Z*)-cinnamionitrile^[7] and 3-phenylpentanedinitrile.^[8] To determine the yield of sodium benzoate the CDCl₃ was removed under vacuum, the solid was washed with CH₂Cl₂, and dissolved in MeOH. The MeOH was removed under vacuum yielding sodium benzoate. This allowed the isolated yield of sodium benzoate to be determined.

5.5 References

- [1] S. Chakraborty, Y. J. Patel, J. A. Krause, H. Guan, *Angew. Chem. Int. Ed.* **2013**, *52*, 7523–7526.
- [2] L. Fan, O. V. Ozerov, *Chem. Commun.* **2005**, 4450–4452.
- [3] a) A. Goto, K. Endo, Y. Ukai, S. Irle, S. Saito, *Chem. Commun.* **2008**, 2212–2214; b) D. Sureshkumar, V. Ganesh, N. Kumagai, M. Shibasaki, *Chem. Eur. J.* **2014**, *20*, 15723–15726; c) G. Wang, A. Zhou, J. Wang, R. Hu, S. Yang, *Org Lett.* **2013**, *15*, 5270–5273.
- [4] a) S. Cannizzaro, *Ann.* **1853**, *88*, 129–130; b) K. List, H. Limpricht, *Ann.* **1854**, *90*, 190–210
- [5] T. Itoh, Y. Takagi, S. Nishiyama, *J. Org. Chem.* **1991**, *56*, 1521–1524
- [6] J. Ruan, X. Li, O. Saidi, J. Xiao, *J. Am. Chem. Soc.* **2008**, *130*, 2424–2425
- [7] S. Kojima, T. Fukuzaki, A. Yamakawa, Y. Murai, *Org. Lett.* **2004**, *6*, 3917–3920
- [8] Y. Duan, P. Yao, J. Ren, C. Han, Q. Li, J. Yuan, J. Feng, Q. Wu, D. Zhu, *Sci. China Chem.* **2014**, *57*, 1164–1171